IMPROVED PROCEDURES FOR THE DESIGN OF SLENDER STRUCTURAL CONCRETE COLUMNS

Ryan W. Jenkins, PhD
Robert J. Frosch, PhD, PE, FACI

August 2015
Purdue University
West Lafayette, Indiana

ACKNOWLEDGMENTS

We are very grateful for the donors, which made this project a reality. We would like to thank the Concrete Reinforcing Steel Institute (CRSI), the Precast/Prestressed Concrete Institute (PCI), ACI Foundation's Concrete Research Council (CRC), and The Concrete Industry Foundation of New York for their funding support. We would also like to thank Gerdau Long Steel of North America and Spancrete for their material donations.

TABLE OF CONTENTS

Page

Page

Page

Page

LIST OF TABLES

LIST OF FIGURES

Figure Page

Figure Page

Figure Page

ABSTRACT

Jenkins, Ryan William. Ph.D., Purdue University, August 2015. Improving the Design of Slender, Concrete Columns. Major Professor: Robert J. Frosch.

With the greater availability and affordability of high-strength concrete, designers have been able to reduce concrete column cross-sections, leading to in an increase in the prevalence of slender columns in building construction. In spite of this trend, provisions for the design of slender columns have not changed significantly since the provisions were first introduced 1971. Improved understanding of as well as improved design provisions for slender, concrete columns can allow for further use while maintaining safety. The objective of this research is to better understand the behavior and limits of slender, concrete columns and, from the results, develop improved design procedures for incorporation into building codes. The research program consisted of experimental testing coupled with computational modeling. The experimental testing was designed to expand the boundaries of practical column design while maintaining realistic service conditions. Additionally, the columns tests were designed to simulate theoretical conditions, which correspond better to code provisions and simplified computational analysis. The columns were tested with equal end eccentricities, braced against sidesway, and used pinned-pinned loading conditions. A computational model was further developed from a previous study. It incorporated commonly assumed material properties, simple mechanics, and structural analysis. The results of the experimental tests were used to evaluate and calibrate the computational model. With increased confidence, the computational model was used to develop design methods through analysis and parametric evaluation. Based on the results, design equations and recommendations are recommended for the short-term and long-term loading of nonprestressed and prestressed, slender, concrete columns.

CHAPTER 1 INTRODUCTION

1.1 Problem Statement

With the greater availability and affordability of high-strength concrete, designers have been able to reduce concrete column cross-sections, leading to in an increase in the prevalence of slender columns in building construction. At the same time, the provisions in the Building Code Requirements for Structural Concrete (ACI Committee 318 2014) regarding slender concrete columns have remained mostly unchanged since their introduction in 1971 (MacGregor, Breen, and Pfrang 1970). Improvements to ACI 318 can further advance the use of slender columns as well as better account for modern building materials such as high-strength concrete and high-yield reinforcement.

1.2 Background

The behavior of concrete columns can be divided into two components: long-term and short-term effects. Short-term effects are caused by relatively sudden application of axial load such as initial loading due to removal of falsework, construction loading, and live loading. Long-term effects are caused by the application of sustained loads. These loads are primarily due to gravity loads and dead loads but can also be caused by prestressing.

Slenderness in compression members, which affects both short-term and long-term behavior, leads to second-order effects (increases in demand to the structure due to the deflection of the structure). These effects can be significant, and designers must account for them when designing compression members. Figure 1.1 shows the two types of second-order effects: global effects ($P\Delta$) and member effects ($P\delta$). Global effects are most commonly associated with sway effects, where deflection of the end points of members cause increased second order effects. Member effects, on the other hand, are usually associated with non-sway effects, where deflection between the member endpoints causes increased demands.

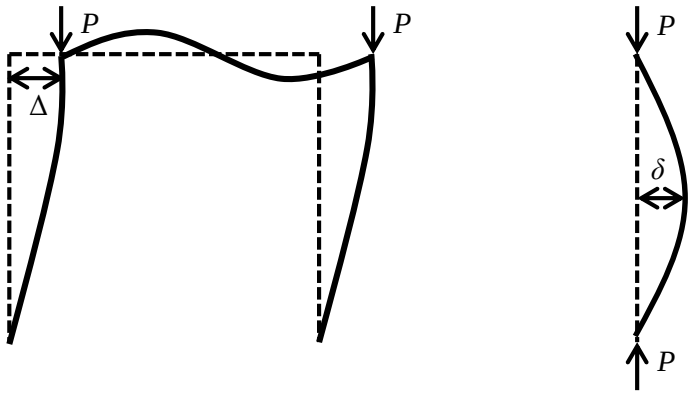

Figure 1.1 – Second Order Effects

When slender, concrete columns are subject to sustained loads, there are typically three phases of behavior, as illustrated in Figure 1.2. In the first phase, under initial loading, the short-term stiffness governs the behavior of the column. As shown, the moment demand for a slender column is greater than the moment demand for a short column under the same load and applied eccentricity, the result of second-order effects. In the second phase, when columns are subject to sustained loads, creep effects in the concrete decrease the column's stiffness thus increasing second-order effects. As a result, the moment demand of a column increases without an increase in axial load. Lastly, typical columns do not generally fail under sustained load, and in the third phase, these columns have some amount of post-sustained load residual capacity.

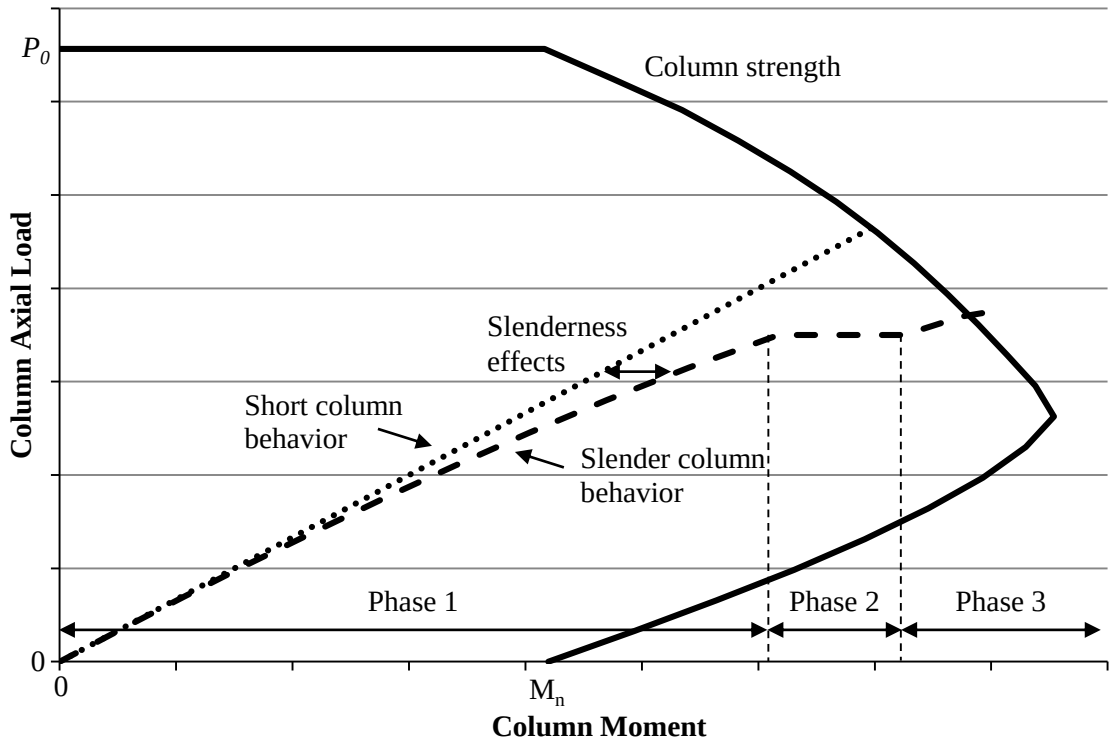

Figure 1.2 – Typical Column Behavior

1.3 Current Design Methodology

ACI 318 is the governing standard for the design of columns for use in buildings. The Code permits the use of three methods for the analysis of slenderness effects in compression members.

1. Nonlinear second-order analysis
2. Elastic second-order analysis
3. Moment magnification procedure

Nonlinear analysis is generally not used due to vague and complex requirements, but the elastic analysis is typically used in the form of a system level computational analysis. In general, elastic second-order analysis is widely used by designers for most types of frames and columns, but these methods typically ignore moment magnification between the ends of columns, the $P\delta$ effect. Including moment magnification between the ends results in a significant increase in computational cost and, importantly, is generally not consistent with code approaches.

Consequently, designers commonly employ second-order analysis on a global scale to determine $P\Delta$ effects and rely on code provisions to determine $P\delta$ effects.

Of particular interest for research are columns that are part of non-sway frames, where $P\delta$ effects are most significant. For analysis of these effects, ACI 318 provides a design methodology known as the moment magnification procedure and prescribed as follows in Equations 1.1 to 1.3. As shown, the procedure estimates the amplified moment with a magnification factor applied to the end moment of a column. The magnification factor is derived from theoretical, stability analysis, simplified for small deflections, and the factor includes the Euler, critical buckling load. It should be noted that the equations are simplified for non-sway, pinned columns with equal end eccentricities.

$$M_c = \delta M \qquad \text{(Eq. 1.1)}$$

$$\delta = \frac{1}{1 - \frac{P}{0.75P_c}} \qquad \text{(Eq. 1.2)}$$

$$P_c = \frac{\pi^2 EI}{l_u^2} \qquad \text{(Eq. 1.3)}$$

where:

EI = flexural stiffness of compression member, in.^{2}-lb
l_u = unsupported length of compression member, in.
M = end moment of compression member, in.-lb
M_c = moment amplified for the effects of member curvature, in.-lb
P = axial force, lb
P_c = critical buckling load, lb.
δ = moment magnification factor for the effect of member curvature

1.4 Problems with Current Design Methods

First introduced to ACI 318 in 1971, the moment magnification procedure is based on stability theory, and because of its sound basis, has remained mostly unchanged. The method, however, relies on certain estimations to which researchers have introduced modifications and additions over the years, most notably in the estimation of the flexural stiffness. MacGregor et al. (1970), Mirza (1990), and Khuntia and Ghosh (2004) have proposed equations for the short-term stiffness

of slender, concrete columns which have been introduced to and modified in ACI 318 to various degrees over the years. These methods, however, tend to have significant limits. The older approaches are very simple and very conservative while the newer approaches are too complex for use in typical design (Jenkins 2011).

In addition to the estimation of short-term stiffness, the long-term stiffness is required for design. The current method in ACI 318 uses an approach developed by MacGregor et al. (1970) which reduces the stiffness of columns subjected to sustained loads. To develop the method, the researchers used results from 11 experimental tests and limited analytical research. Furthermore, the authors provide little reasoning for the method of reduction and state "this factor has been chosen to give the correct trend when compared to analyses and test of columns under sustained loads." Later, ACI Committee 318 replaced the original method of using the sustained moment ratio with a similar method using the sustained load ratio, also without much basis. Neither case directly considers creep of the concrete, which, along with the factors that affect it, is important for the reduction of stiffness caused by sustained loads.

Beginning in 2008, ACI Committee 318 introduced a limit on second-order effects to 40% of first-order effects. This limit was introduced to simplify the code by eliminating the requirement of a stability analysis. The analytical research on which this limit is based, however, focused on sway frames. As such, traditional stability analysis and the newer second-order limit typically result in similar designs for columns in sway frames. This limit, though, may be unwarranted and overly limiting for columns in non-sway frames, which rely on other structural members for global stability.

While ACI 318 provides considerable guidance on the design of nonprestressed columns, it provides little guidance on the design of prestressed columns. In particular, no provisions exist for slender, prestressed columns. As a result, most designers rely on the PCI Design Handbook (2010) for guidance. Because prestressed columns have less than the ACI 318 minimum required mild steel for columns, the PCI Handbook suggests the design of slender, prestressed columns should use elastic second-order analysis. For reasons mentioned previously, this analysis does not typically evaluate $P\delta$ effects. Alternatively, the PCI Committee on Prestressed Concrete Columns (1988) provides a method to estimate the stiffness of prestressed columns for use with the moment magnification procedure of ACI 318. It notes that the stiffness of prestressed

concrete columns differs greatly from that of reinforced concrete columns, which necessitated the alternative method to determine stiffness.

1.5 Objective and Scope

The objective of this research is to improve the understanding of the behavior of slender, non-sway, concrete columns. Supported by a better understanding, several portions of the slender column provisions in ACI 318 are of interest for advancement.

1. Current design methods to estimate the short-term stiffness of non-sway, slender, concrete columns are inadequate; these equations are either overly conservative or too complex to use in design (Jenkins 2011). Though recent research has attempted to address this problem (Khuntia and Ghosh 2004; Jenkins 2011), experimental research including modern materials and realistic service conditions will improve recent analytical work and provide confidence in improving existing design procedures.
2. The reduction factor for sustained loads on non-sway, slender, concrete columns has remained relatively unchanged for many years and lacks a strong experimental research foundation. An analytical study coupled with experimental research can improve design procedures for this complex phenomenon.
3. In 2008, to simplify the code, ACI 318 introduced a limit on second-order effects to remove the requirement for a direct stability analysis. Since this change, however, designers have indicated that this limit is restricting the ability to design and use slender columns, particularly columns in non-sway frames. Further experimental research and analytical modeling will allow reexamination of this limit when applied to non-sway frames.
4. ACI 318 does not address slender, prestressed concrete column design. While there is considerable use of these members, very limited design guidance exists. Further experimental research and analytical modeling will evaluate current design procedures and improve them, if necessary. With increased confidence, these procedures can be proposed for inclusion to the ACI 318 Building Code.

CHAPTER 2 ANALYTICAL MODELING

2.1 Introduction

Because of the complexity of slender, concrete columns, particularly under sustained loads, experimental tests are essential to understand their behavior. Due to time and cost restrictions, it would be unreasonable, however, to test a wide range of concrete columns, especially those that are commonly used by the industry because of their large scale. Accordingly, analytical modeling is crucial in the development of improved design procedures. A computational model was developed to estimate the behavior of slender, concrete columns. The model estimates both short-term and long-term effects of nonprestressed and prestressed concrete columns. It used common material properties, and simple mechanics and structural analysis. In subsequent chapters, the model is compared against experimental tests and calibrated when necessary. Finally, with improved confidence in the model, it is used to develop improved design procedures and equations.

2.2 Analysis Methodology

The computational model was a progression of a model developed during a previous analytical study (Jenkins 2011) and computes a deflection profile of an eccentrically loaded, concrete column. The methodology of the model was identical to that developed in the previous study, but the model was optimized and modified to include the effect of prestressing steel. To maintain simplicity, the model was limited to equal end eccentricities and non-sway columns bent in single curvature, and when applicable, all values were linearly interpolated. The general methodology of the computational model and the model optimizations are as follows.

To compute the entire behavior of a column, an initial axial load was selected as a small ratio of the expected nominal strength. The analysis was conducted, and the resulting maximum deflection was recorded. Next, the axial load was incrementally increased until the column failed, continuing to record corresponding axial load and deflection values. This was continued

until the column theoretically failed. All values were saved and used to illustrate the theoretical behavior of the column.

2.2.1 Moment-Area

The model computed column profiles and deflections using the moment-area method. Given an axial load (P) and applied load eccentricity (e), a moment profile was computed along the length of the column at 101 equally spaced, discrete points. During the first iteration, the moment along the length of the column was equal to the end moment (Pe). Using a moment-curvature relationship discussed later, a corresponding curvature profile (φ) was computed, from which a deflection profile (δ) was then calculated using the moment-area method. Given the updated column profile, a new moment profile was computed considering the deflected shape ($M = P\,(e + \delta)$). At all iterations, the maximum moment in the column was compared against the maximum moment of the respective moment-curvature relationship (M_n) to detect column failure. This process was repeated until the consecutive change in maximum column moments was less than a threshold ($\Delta M_{max} \leq Pe/10^6$), at which point the column was considered to be in equilibrium. The flow logic for the model is shown below.

1. Assume a column with a zero deflection profile
2. Calculate the first order moment along the column ($M = Pe$)
3. Calculate the curvature along the column (φ)
4. Calculate the deflection along the column (δ)
5. Calculate the moment along the column ($M = P\,(e + \delta)$)
    a. If $M_{max} < M_n$, proceed to step 6
    b. Else, end the algorithm (the column has failed)
6. Compare the maximum moment against the maximum moment of the previous iteration
    a. If $\Delta M_{max} > Pe/10^6$, proceed to Step 3
    b. Else, end the algorithm (the column is in equilibrium)

2.2.2 Moment-Curvature

The moment-curvature relationship was computed using cross-sectional strain compatibility and simple static analysis, consistent with the approach used by ACI 318 (2014). The model assumed that plane-sections remained plane. Each moment-curvature relationship is valid for exactly one axial load, and as such, the moment-curvature relationship was recalculated for different axial

loads. A maximum strain on the compressive side of the column was assumed (ε_{max}), and for the first iteration, the strain was assumed to be 3000 με (0.003), which is defined as concrete failure in accordance with ACI 318. A distance to the neutral axis was assumed (c), and for the first iteration, the distance was assumed to be half of the column depth (h/2). Then, the cross-sectional forces (F) were computed using material stress-strain relationships discussed later. Equilibrium was checked between the cross-sectional forces and the applied load (P). The distance to the neutral axis was varied until equilibrium was satisfied, which was defined when the sum of cross-sectional forces was less than a threshold ($P/10^6$). Once equilibrium was achieved, the cross-sectional moment (M) and cross-sectional curvature ($\varphi = \varepsilon_{max} / c$) were computed at the corresponding strain and distance to the neutral axis. The moment, distance to the neutral axis, and cross-sectional curvature were recorded. The maximum strain was decreased by 30 με, and the iteration was repeated. The flow logic for the model is shown below.

1. Assume an initial maximum strain (ε_{max}) of 3000 με
2. Assume an initial distance to the neutral axis (c) of h/2
3. Calculate the sum of all cross-sectional forces (F)
4. Check equilibrium with applied load
    a. If $abs(F - P) > P/10^6$, adjust c, proceed to Step 3
    b. Else, proceed to Step 5
    5. Calculate and record cross-sectional moment (M) and curvature (φ) and record the distance to the neutral axis (c)
6. Decrease the maximum strain (ε_{max}) by 30 με
    a. If $\varepsilon_{max} > 0$, proceed to Step 3
    b. Else, end the algorithm

2.3 Material Stress-Strain Relationships

2.3.1 Concrete

The stress-strain relationship for concrete was a modified Hognestad's relationship, as shown in Equation 2.1, which is commonly used to model concrete (Lin and Burns 1981).

$$f_c = f_c^{'}\left[\frac{2\varepsilon}{\varepsilon_0} - \left(\frac{\varepsilon}{\varepsilon_0}\right)^2\right] \quad \text{(Eq. 2.1)}$$

where:

f_c = concrete stress, psi

$f_c^{'}$ = compressive strength of concrete, psi

ε = concrete strain, in./in.

ε_0 = Hognestad's constant, in./in.

As mentioned previously, the relationship was used with a maximum permitted concrete strain of 3000 με. Hognestad's constant was determined by matching the secant modulus of the equation to the modulus of elasticity of the concrete. When the measured value of the modulus was not available, the modulus was computed as shown in Equation 2.2, in accordance with ACI 318. It should be noted that the equation assumes normal-weight concrete. Hognestad's constant was computed as shown in Equations 2.3 and 2.4.

$$E_c = 57{,}000\sqrt{f_c^{'}}, \text{ psi} \quad \text{(Eq. 2.2)}$$

$$\varepsilon_0 = \frac{f_c^{'}\left(1+\sqrt{1-x}\right)}{E_c} \quad \text{(Eq. 2.3)}$$

$$x = 0.5 + \frac{f_c^{'} - 3000 \text{ psi}}{70{,}000 \text{ psi}} \quad \text{(Eq. 2.4)}$$

where:

E_c = modulus of elasticity of concrete, psi

x = factor to adjust for concrete strength

The equations for the constant were developed to adjust for higher-strength concrete. They were not derived from any study but were created after examining stress-strain relationships for varying strengths of concrete. The concrete was assumed to provide tensile strength if the maximum tensile strain the concrete was less than the modulus of rupture ($f_r = 7.5\sqrt{f_c^{'}}$, psi), which would indicate the concrete was uncracked. If the concrete was uncracked, the concrete stress was computed as a linear relationship between the modulus of elasticity and the concrete strain.

2.3.2 Reinforcing Bar

The stress-strain relationship for reinforcing steel was a linear elastic-plastic curve, as shown in Equation 2.5. The relationship was computed with the defined modulus of elasticity, regardless of the measured value.

$$f_s = \begin{cases} E_s \varepsilon & \text{if } \varepsilon < \varepsilon_y \\ f_y & \text{else} \end{cases} \qquad \text{(Eq. 2.5)}$$

where:

E_s = 29,000,000 ksi = modulus of elasticity of steel, ksi
f_s = steel stress, ksi
f_y = yield strength of steel, ksi
ε = steel strain, in./in.
$\varepsilon_y = f_y / E_s$ = yield strain of steel, in./in.

2.3.3 Prestressing Steel

The stress-strain relationship for prestressing steel, as shown in Equations 2.6 and 2.7, was a modified version of an equation from the PCI Design Handbook. The relationship was computed with the defined modulus of elasticity, regardless of the measured value. The constant (ε_0) adjusted Equation 2.6 to the tensile strength of the steel and matched the equations at 90% of the tensile strength.

$$f_{ps} = \begin{cases} E_{ps} \varepsilon & \text{if } \varepsilon < 0.9 f_{pu} / E_{ps} \\ f_{pu} - \dfrac{0.04}{\varepsilon - \varepsilon_0} & \text{else} \end{cases} \qquad \text{(Eq. 2.6)}$$

$$\varepsilon_0 = \frac{9 f_u^2 - 4 E_{ps}}{10 f_u E_{ps}} \qquad \text{(Eq. 2.7)}$$

where:

E_{ps} = 29000 ksi = modulus of elasticity of steel, ksi
f_{ps} = steel stress, ksi
f_{pu} = tensile strength of steel, ksi
ε = steel strain, in./in.
ε_0 = constant to adjust for tensile strength of steel

2.4 Definition of Nominal Strength

When computing the behavior of a column under increasing axial load, a state must be defined to indicate theoretical column failure. This can be defined in two ways: moment-limited or curvature-limited. Figure 2.1 illustrates the difference between these two methods using a representative moment-curvature relationship. Curves are shown for two different axial loads: a moderate load and a high load with the maximum moments indicated with an X. For moderate and low axial loads, the maximum moment occurs at a maximum curvature and thus maximum strain. For these axial loads, the moment-limited and curvature-limited strengths are equal. When computing the relationship for columns under high axial loads, however, the maximum moment may not occur at the maximum curvature. This is due to the fact that Hognestad's relationship does not peak at the maximum strain. If the analysis was allowed to extend to the end of the curve, the column would have a theoretically higher failure deflection but a lower axial load strength. Because a post-failure analysis was not necessary for this study, the moment-limited control was used by ignoring the post-peak portion of the moment-curvature relationships.

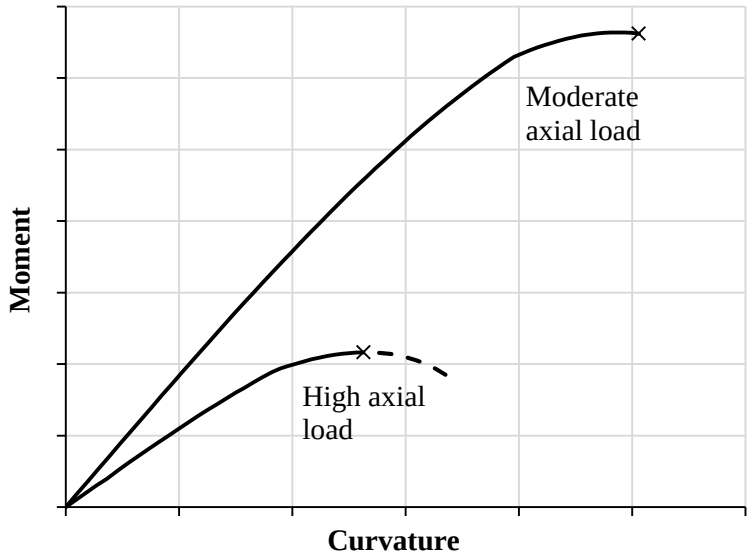

Figure 2.1 – Representative Moment-Curvature Relationship

Many of the figures in this study show the load-moment relationship of the columns, also known as an interaction diagram. To improve clarity, the computed nominal strength is also included on these figures, an example of which is shown in Figure 2.2. This nominal strength was not directly used to compute column failures but was plotted to provide qualitative illustration. Simply, any

load and moment combination for a given column that falls within the nominal strength curve is safe, while combinations falling outside of the curve would indicate failure. Based on experimental results, the computed nominal strength was typically conservative, and the columns' behavior usually extended beyond the nominal strength before failing.

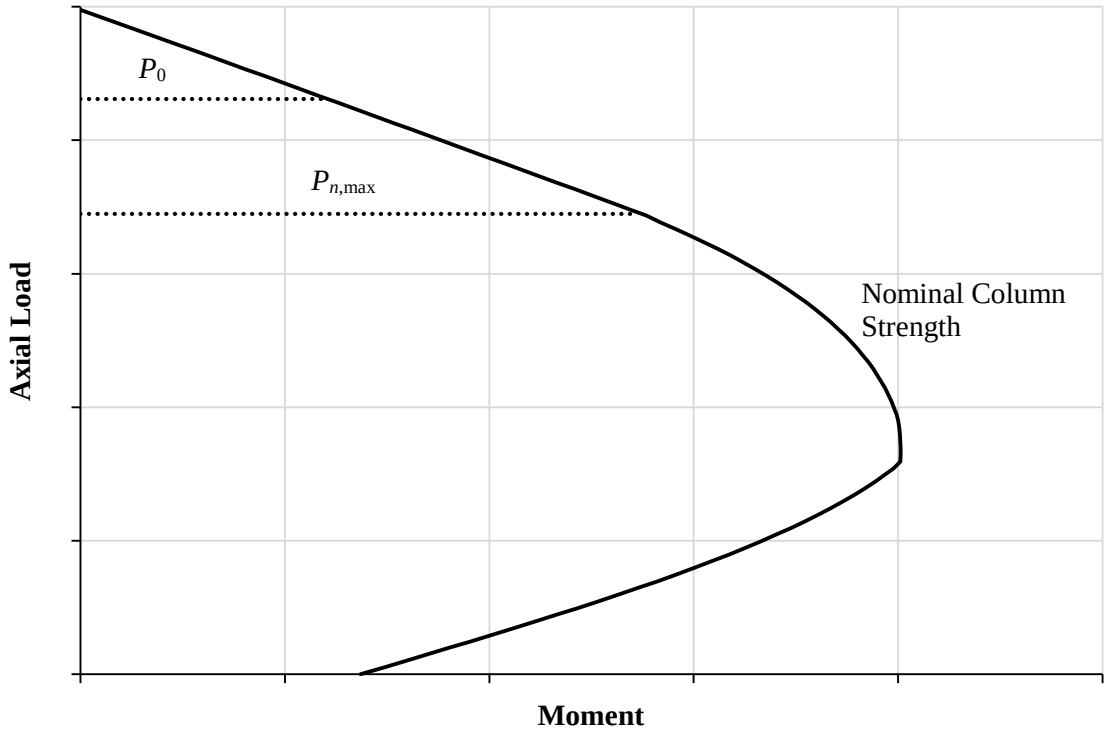

Figure 2.2 – Representative Nominal Strength Interaction Diagram

The figure also includes ACI 318 design values, further detailed in Equations 2.8 and 2.9. It should be noted that these equations are representative of nonprestressed columns with tie reinforcement. The nominal axial strength (P_0) is based on the ACI 318 design strength, which is more conservative than the nominal strength calculation used by the computational model because it limits the concrete compressive stress to 85% of the concrete strength. Subsequent interaction diagram figures in this study will limit the nominal strength by truncating the computed nominal strength to the ACI 318 limit (P_0) to be consistent with the code. Additionally, Figure 2.2 includes the maximum allowable axial load ($P_{n.\max}$), which ACI 318 applies to account for unintended eccentricities. Because this study is evaluating true behavior, this limit is ignored and omitted from subsequent figures.

$$P_0 = 0.85 f_c^{'} \left(A_g - A_{st} \right) + f_y A_{st} \quad \text{(Eq. 2.8)}$$

$$P_{n,\max} = 0.80 P_0 \quad \text{(Eq. 2.9)}$$

where:

A_g = gross area of concrete section, in.^{2}

A_{st} = total area of nonprestressed longitudinal reinforcement, in.^{2}

$f_c^{'}$ = compressive strength of concrete, psi

f_y = yield strength of reinforcement, psi

P_0 = nominal axial strength at zero eccentricity, lb

$P_{n,\max}$ = maximum allowable axial load, lb

2.5 Prestressed Concrete Columns

For prestressed columns, the computational model was adjusted to account for the effect of the prestressing. When computing cross-sectional strains, an effective prestressing strain (ε_{si}) was added to the effective cross-sectional strain, adjusting for certain prestressing losses. To determine this strain, consider Figure 2.3, which shows the effect of prestressing at three different stages. Detailed calculations for a representative example are provided in Appendix A.

The prestressing steel is stressed to an initial amount (f_{si}) before being released into the concrete, which has zero stress. After release, the stress from the prestressing steel is imparted onto the concrete while maintaining strain compatibility. Known as elastic shortening losses, this leads to a stress in the concrete (f_{cir}) balanced with a resultant stress in the prestressing steel ($f_{s,\mathrm{ES}}$). Due to time dependent losses including concrete creep, concrete shrinkage, and steel relaxation, the stresses in the concrete and steel decrease over time. After total losses, the resulting stress in the concrete (f_{ce}) and prestressing steel (f_{se}) are balanced. Due to steel relaxation, the strains are not necessarily compatible after total losses. Additionally, the modulus of elasticity of the concrete changes over time, compounding the differences in stresses and strains.

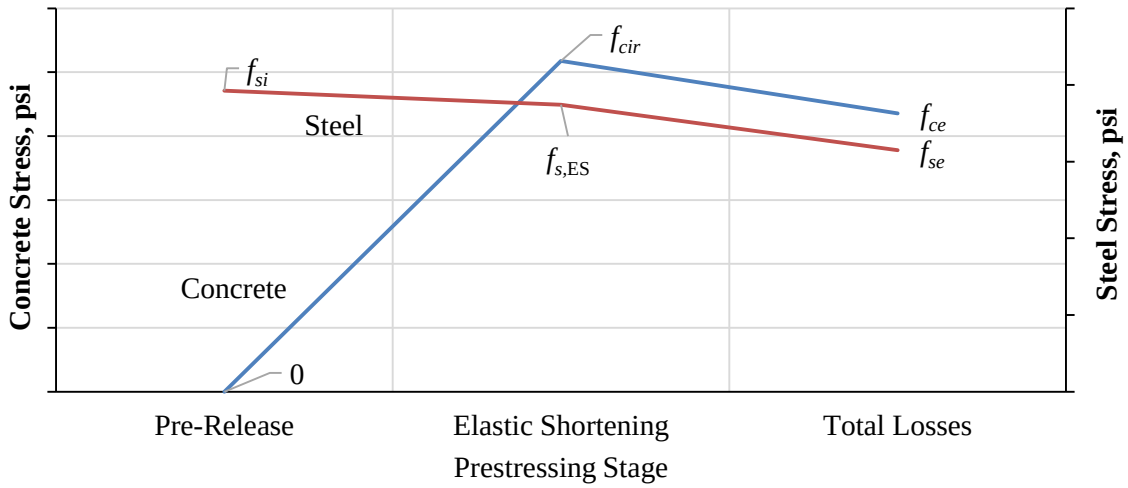

Figure 2.3 – Prestressing Effect over Time

To provide consistency, an approach was developed to include prestressing effects in the computational model. The primary goal was to maintain the effective concrete and steel stresses after total losses, and this was determined based on the modulus elasticity of the concrete (E_c) for the day of interest. The effective prestressing stress after losses (f_{se}) was determined through calculations or strain measurements and was used as a basis for the approach.

Considering force equilibrium, an effective concrete stress after total losses (f_{ce}) was calculated according to Equation 2.10. In the moment-curvature analysis, all strains are referenced at zero concrete stress. As a result, an effective prestressing strain (ε_{si}) was calculated according to Equation 2.11 and added to the cross-sectional strain to yield the correct prestressing strain and thus prestressing stress. The effective prestressing strain was assumed to be uniform along the length of the column, regardless of the transfer length.

$$f_{ce} = \frac{A_{ps} f_{se}}{A_g - A_{ps}} \qquad \text{(Eq. 2.10)}$$

$$\varepsilon_{si} = \frac{f_{se}}{E_{ps}} + \frac{f_{ce}}{E_c} \qquad \text{(Eq. 2.11)}$$

where:

A_{ps} = total area of prestressed longitudinal reinforcement, in.^{2}

CHAPTER 3 EXPERIMENTAL PROGRAM

3.1 Introduction

The experimental program was developed to test a range of variables contributing to slender column behavior. The parameters were selected to be practical and realistic but advance the current boundaries of design. In addition, the program was tailored to represent current building materials and methods, as opposed to many previous studies that relied on materials that would now be considered substandard such as low strength reinforcing steel and low strength concrete.

3.2 Experimental Program

Nearly all column parameters affect column behavior. Geometric and loading parameters to note include column slenderness, axial load eccentricity, axial load level, presence of sustained load, cross-sectional dimensions, and reinforcement configuration. Material parameters include concrete compressive strength, concrete stiffness, reinforcement type (nonprestressed or prestressed), and reinforcement strength. Because of the numerous parameters, only those deemed most important were evaluated. Furthermore, the loading method was simplified to allow for tests that represented theoretical conditions, which correspond better to code provisions and simplified computational analysis. The testing setup was developed to simulate the following assumptions: equal end eccentricities, columns braced against sidesway, and pinned-pinned loading conditions. These parameters are further discussed in Sections 3.2.2 and 3.5.

First, to reduce the variables to a manageable amount, column cross-section size and concrete strength were kept constant. Accordingly, the main parameters of interest were chosen to be slenderness ratio, eccentricity ratio, reinforcement, prestressing, presence of sustained loading, and, to a lesser extent, sustained load ratio. Most column types were tested using both short-term and long-term loading.

Due primarily to laboratory limitations, a column cross-section of 6-1/8 in. square was chosen. This resulted in columns that were approximately one-half to one-third scale. Any scaling effects

concerning construction, experimental testing, column behavior, and analysis will be discussed later. All materials were selected to be representative of current construction.

In addition to slender columns, several short columns were tested under long-term loading. These columns were designed similarly to the slender columns, but because they were short, they were not subject to slenderness effects. The results of these tests allowed better understanding of behavior under long-term loading by removing the additional factor of slenderness effects. Particularly, these columns were important in the development of the computational analysis of creep behavior in concrete sections discussed in Section 2.3.

3.2.1 Testing Matrix

Table 3.1 presents a summary of the slender column tests. The parameters tested included five steel configurations, two slenderness ratios (40 and 70), two eccentricity ratios (10% and 25%), and two loading types (short-term and long-term). The ratio values listed are nominal, and exact dimensions are discussed in Section 3.2.2. The columns were identified using system shown by Figure 3.1, which is used as shorthand when referring to the experimental tests. A few additional columns were retested under slightly different loading conditions, and these will be discussed in subsequent chapters.

Reinforcement – Slenderness – Eccentricity – Loading Type

Reinforcement:	R - Nonprestressed followed by bar size P - Prestressed followed by number of wires PL – Plain Concrete
Slenderness:	kl_u/r
Eccentricity:	e/h, %
Loading Type:	ST - Short-term loading LT - Long-term loading S - Shrinkage

Figure 3.1 – Column ID Key

Table 3.1 – Slender Column Testing Matrix

Column ID	Reinforcement	Slenderness Ratio, kl_u / r	Eccentricity Ratio, e / h	Loading Type
R3-40-10-ST	4 – #3s	40	10%	Short-term
R3-40-10-LT				Long-term
R3-40-25-ST			25%	Short-term
R3-40-25-LT				Long-term
R3-70-10-ST		70	10%	Short-term
R3-70-10-LT				Long-term
R3-70-25-ST			25%	Short-term
R3-70-25-LT				Long-term
R5-40-10-ST	4 – #5s	40	10%	Short-term
R5-40-10-LT				Long-term
R5-40-25-ST			25%	Short-term
R5-40-25-LT				Long-term
R5-70-10-ST		70	10%	Short-term
R5-70-10-LT				Long-term
R5-70-25-ST			25%	Short-term
R5-70-25-LT				Long-term
P2-40-10-ST	2 – Prestressing Wires	40	10%	Short-term
P2-40-25-ST			25%	
P2-70-10-ST		70	10%	
P2-70-25-ST			25%	
P4-40-10-ST	4 – Prestressing Wires	40	10%	Short-term
P4-40-10-LT			25%	Long-term
P4-40-25-ST		70	10%	Short-term
P4-40-25-LT			25%	Long-term
P4-70-10-ST		40	10%	Short-term
P4-70-10-LT			25%	Long-term
P4-70-25-ST		70	10%	Short-term
P4-70-25-LT			25%	Long-term
P6-40-10-ST	6 – Prestressing Wires	40	10%	Short-term
P6-40-25-ST			25%	
P6-70-10-ST		70	10%	
P6-70-25-ST			25%	

As mentioned previously, all parameters were selected to represent practical columns but extend current design boundaries. The nonprestressed columns used typical, deformed, reinforcing bars: four #3s ($A_{st}/A_g \approx 1.2\%$) and four #5s ($A_{st}/A_g \approx 3.3\%$). ACI 318 (2014) requires reinforcement ratios in nonprestressed columns to be between 1% and 8%. Due to practical limitations, however, reinforcement ratios above 3% to 4% are unlikely; thus, the reinforcement ratios chosen represent the practical minimum and maximum range. For the prestressed columns, preliminary calculations and available prestressing wire controlled the design. The columns satisfied ACI 318 provisions for minimum prestressing force, which eliminates minimum longitudinal reinforcement requirements.

For columns braced against sidesway and with equal end moments, ACI 318 permits slenderness effects to be neglected if the slenderness ratio (kl_u/r) is equal to or less than 22. Considering this, any column with a slenderness ratio equal to or less than 22 is considered short, which is the terminology used hereafter. Columns with a slenderness ratio of just greater than 22, though effects cannot be neglected for design, do not exhibit significant slenderness effects for the purpose of this project. Based on preliminary calculations, a lower slenderness ratio of 40 was chosen as a length that begins to show significant effects. The higher value of 70 was chosen as a practical maximum.

Eccentricity ratios ($M/Ph = e/h$) of 10% and 25% were selected. ACI 318 requires the use of a minimum eccentricity to account for out-of-straightness and unknown end conditions. The minimum eccentricity approaches 3% for larger columns but is closer to 6% to 8% for typically sized columns. Based on this, a smaller value of 10% was selected. The higher eccentricity was selected based on a few reasons. First, the eccentricity was selected to be outside of the kern, which introduces tensile stresses in a cross-section immediately upon loading, but the value should not be exceedingly high and thus unlikely to occur in service conditions. Upon consultation with designers and based on preliminary calculations, an eccentricity ratio of 25% was selected.

Finally, most columns geometries were tested twice: once in long-term and once in short-term. This difference in loading allowed direct comparison of the behavior and stiffness of identical columns. The short-term columns were tested under constantly increasing load to failure, and the long-term columns were subject to a sustained load for up to approximately 100 days, after which they were tested under increasing load to failure. The sustained load was selected based on

preliminary calculations and ACI 318 provisions and designed to be analogous across column types, explained further in Section 8.2. It was intended that the sustained loads were realistic service loads. A duration of 100 days was chosen for the study based on the desire to produce sufficient creep effects while considering practical time considerations.

Table 3.2 provides a summary of the short column tests. They were designed to match the cross-section of the slender column tests, but these columns were much shorter ($kl_u/r \approx 13$) and assumed not to exhibit any second-order effects. Two different cross-sections were used: four #3 reinforcing bars ($A_{st}/A_g \approx 1.2\%$) and plain concrete. The eccentricity ratios of the columns were used (10% and 25%) as well as concentric loading (0%). Six columns were subject to sustained load for approximately 365 days, and four specimens were not loaded and used as control specimens to monitor shrinkage.

Table 3.2 –Short Column Testing Matrix

Column ID	Reinforcement	Slenderness Ratio, kl_u / r	Eccentricity Ratio, e / h
PL-13-0-LT	None (Plain Concrete)	13	0%
PL-13-10-LT			10%
PL-13-25-LT			25%
PL-13-25-S(1)			N/A
PL-13-25-S(2)			N/A
R3-13-0-LT	4 – #3s	13	0%
R3-13-10-LT			10%
R3-13-25-LT			25%
R3-13-25-S(1)			N/A
R3-13-25-S(2)			N/A

3.2.2 Column Design

The columns were designed in accordance with ACI 318 when possible. Due to the small scale, however, some provisions were not able to be followed. Because the loading conditions caused extreme localized forces at the columns ends, the end regions of the columns were specially designed.

3.2.2.1 Cross-Section

Figure 3.2 shows a typical cross-sectional view of the columns. To maintain consistency between reinforcement types, the cross-section was slightly modified to maintain consistent spacing. As noted in the figure, the distance between the steel was 4 in. regardless the steel size. This was done to maintain the same effective depth. As such, the tie dimensions and concrete cover changed accordingly. The ties with 135 degree standard hooks were designed in accordance with ACI 318.

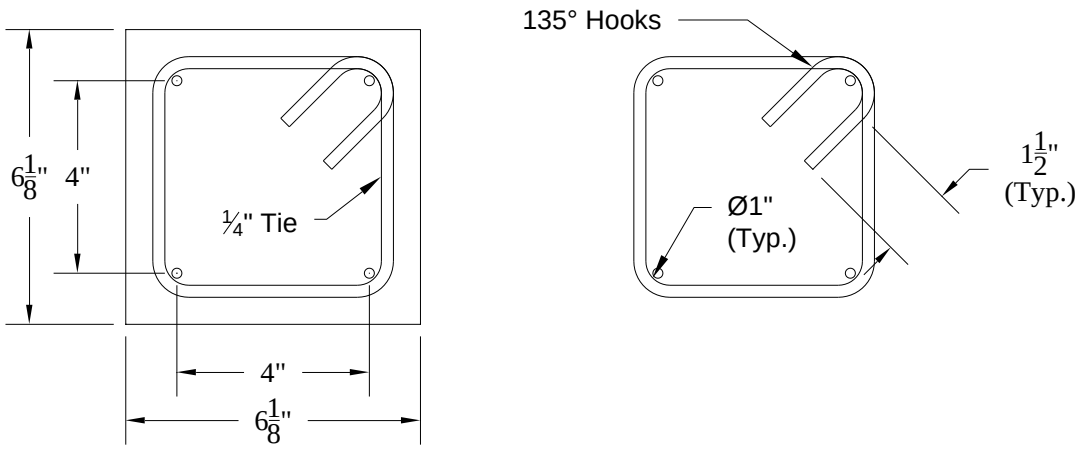

Figure 3.2 – Typical Column Cross-Section

3.2.2.2 End Regions

A steel end plate was fabricated and fastened to the column ends. The steel plate helped to resist the high localized forces caused by the loading and helped to direct the location of the loading to allow accurate eccentric loading. Figure 3.3 shows a view of two end plate assemblies used in this project. Section 3.4.3 explains the method of fastening as well as the reason different end plate assemblies were used.

As shown, a circular groove was milled into the steel to facilitate the pinned end conditions. The groove had a depth of 1/2 in. and a diameter slightly larger than the loading pin. The lowest point of the groove was aligned with the desired amount of eccentricity, measured from the center of the steel plate. A steel rod with a diameter of 1-1/2 in. was used for the pinned end. Based on this setup, the theoretical length of the columns was measured from pin to pin or an additional 1/4 in. from the end of the steel plate on either end of the column.

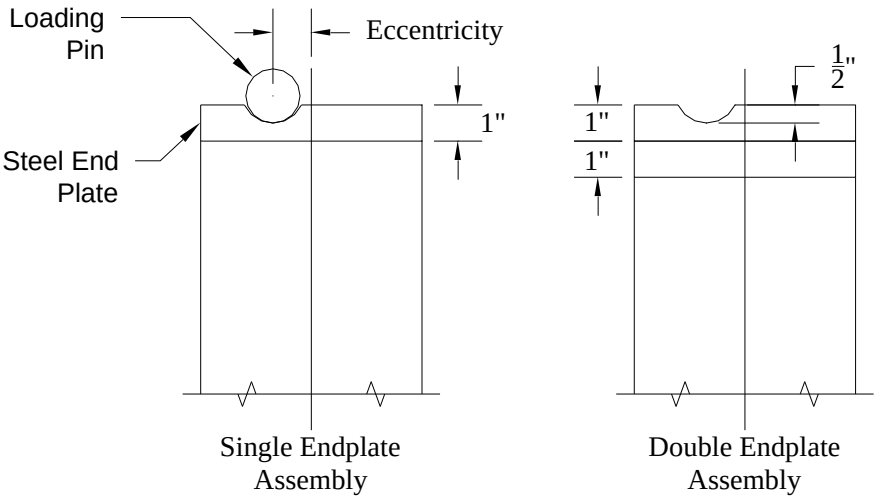

Figure 3.3 – Column End Regions

3.2.2.3 Column and Specimen Layout

Figure 3.4 shows the typical column layout for both lengths of slender columns, including tie locations. As noted previously, the theoretical lengths of 6 ft and 10 ft-6 in. are measured between the centers of the pins. To maintain consistency, all columns, regardless of reinforcement, were constructed with the same tie layout, which was designed in accordance with ACI 318. Based on the maximum permitted spacing, the ties over the majority of the length of the columns were spaced at 6 in. on-center. Because of the high localized stressed in the end regions, however, the tie spacing was decreased to 2 in. for approximately 1 ft at both ends.

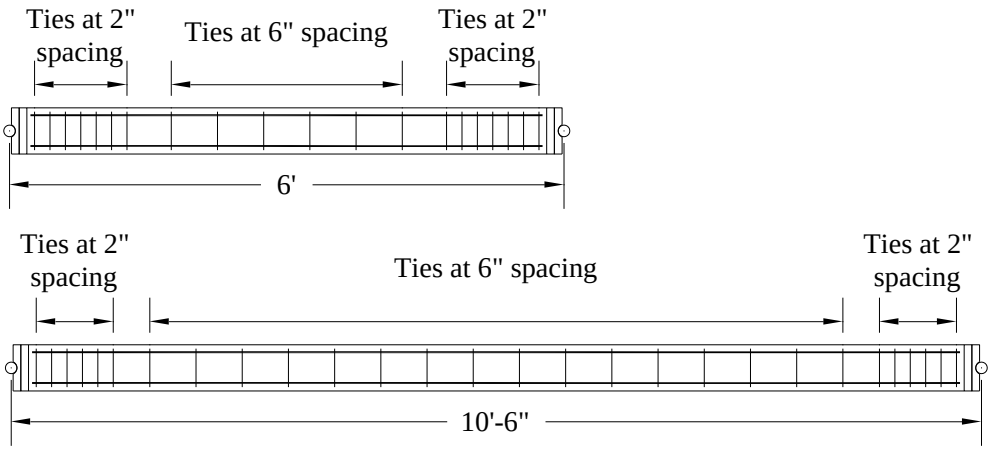

Figure 3.4 – Slender Column Tie Layout

Figure 3.5 shows the typical layout for the short specimens. Three ties were used on each specimen end, spaced at 2 in. For the plain specimens, the same tie layout was used to maintain consistency. The layout exceeds the maximum permitted spacing for ties, but it was deemed more important to remove ties from the measured area of interest, detailed in Section 3.5.2.

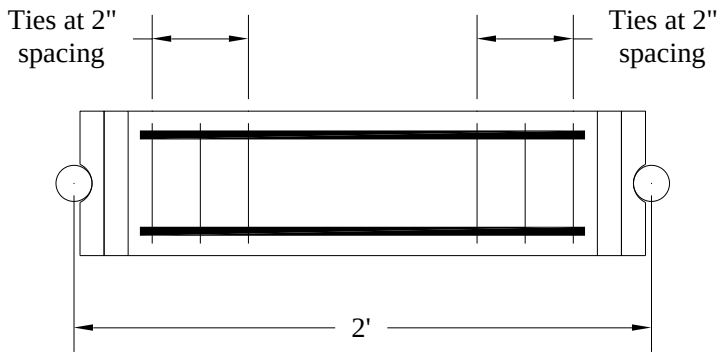

Figure 3.5 – Short Column Tie Layout

3.3 Material Properties and Testing

The materials were chosen to correspond with currently and typically used building materials and were tested in accordance with ASTM and ACI standards.

3.3.1 Concrete

The concrete mix was designed to represent typical structural concrete and have a target compressive strength ($f_c^{'}$) of 6000 psi. Due to the small scale of the tests, a nominal maximum aggregate size of 3/8 in. was used as well as a high-range water-reducing admixture (HRWRA) to increase flowability while maintaining a low water-cement ratio. The concrete was a five-and-a-half bag mix (517 lb per cubic yd) of Type I cement from Buzzi Unicem with a designed water-cement ratio was 0.467. The coarse aggregate was a gradated mix with a maximum aggregate size of 3/8 in. river gravel, and the fine aggregate was a gradated sand mix with 96.6% passing a #4 sieve. Table 3.4 presents the gradations in detail. MasterGlenium 3030 from BASF, a full-range water-reducing admixture, was added in varying amounts to attain the desired slump of 6 in. to 8 in. Water was only added on-site if the batch weights indicated the water content was low and only in amounts to attain the design quantities. Table 3.3 shows the design concrete mix proportions.

Table 3.3 – Concrete Mix Proportions

Material	Design Quantity per cubic yd
Coarse aggregate (3/8" max)	1650 lb
Fine aggregate	1504 kip
Type I Portland Cement	517 lb
Water	241.6 lb
HRWRA	20.7 fl oz

Table 3.4 – Aggregate Gradation

Coarse Aggregate	
Sieve Size	**Percent Passing**
3/8"	99.8-100
#4	42
#8	1-1.5
#30	0.3
#200	0.1-0.2

Fine Aggregate	
Sieve Size	**Percent Passing**
3/8"	100
#4	96.5
#8	84.5
#16	72.3
#30	56.8
#50	22.2
#100	1.7
#200	0.4

To measure the compressive strength and static modulus of elasticity of the concrete, 6 in. diameter cylinders were cast in accordance with ASTM C31 (2012). Curing conditions of the test cylinders were modified to correspond to the curing methods of the main concrete columns as described in Section 3.4.4.

The compressive strength ($f_c^{'}$) was tested in accordance with ASTM C39 (2012) using unbonded caps. In general, the concrete compressive strength was tested at 3, 7, 14, and 28 days as well as any day the columns were tested. Throughout the project, four separate concrete casts were performed. Table 3.5 shows a summary of the concrete compressive strengths, and Figure 3.6 shows the compressive strengths in detail as a function of concrete age. All presented concrete strengths are the average of three test cylinders.

The static modulus of elasticity (E_c) was tested using a modified version of ASTM C469 (2010). Instead of only including strain readings at near zero stress and 40% of ultimate load for calculations, 5 to 6 readings were recorded from 1 kip to 50% of ultimate load and then all

readings were included in a linear regression analysis to determine an average static modulus of elasticity. Figure 3.7 shows a representative modulus test and linear regression result from Cast 2 at a concrete age of 49 days, and the complete results are provided in Table 3.5.

Table 3.5 – Concrete Tests Results

Cast	Date of Test	Age of Concrete, days	f_c' , psi	E_c , ksi
1	7/8/2013	28	6170	--
	8/2/2013	53	6630	4120
	8/14/2013	65	6450	3940
	11/14/2013	157	7020	4260
2	1/8/2014	30	5610	--
	1/14/2014	36	5710	3500
	1/27/2014	49	5980	3440
	3/28/2014	109	5780	--
	4/29/2014	141	5570	3330
3	4/25/2014	3	3360	3070
	5/20/2014	28	5710	--
	5/29/2014	37	5800	3840
	9/10/2014	141	6370	4010
4	7/21/2014	3	4070	3300
	8/14/2014	28	5860	--
	8/19/2014	32	5930	3930
	12/9/2014	144	6570	3820

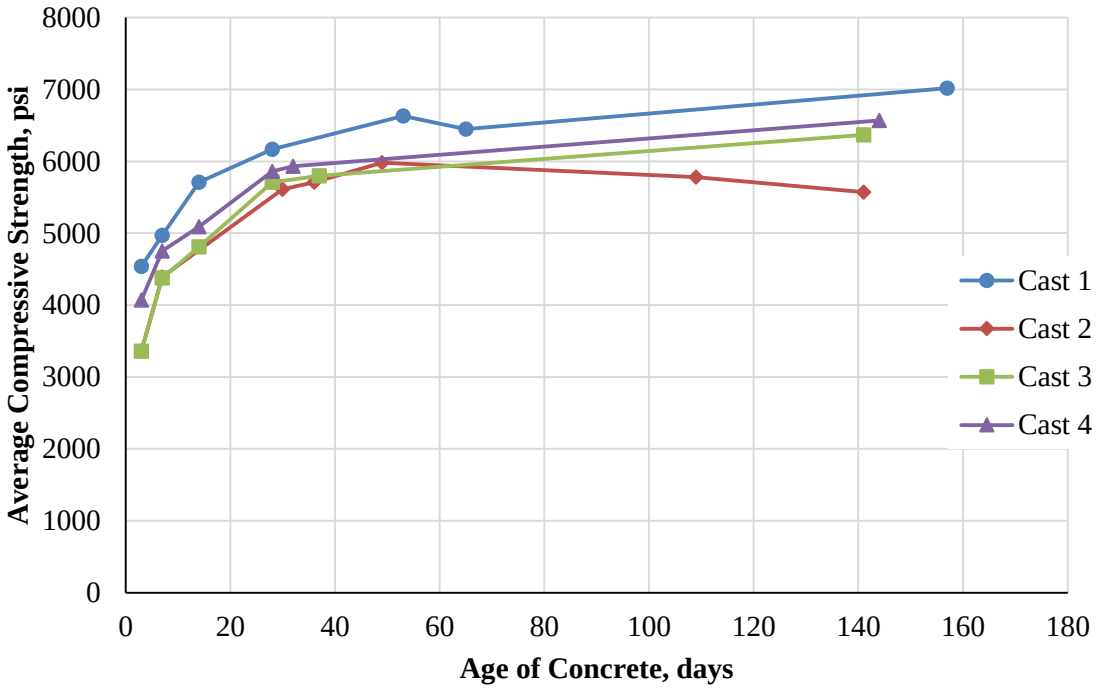

Figure 3.6 – Concrete Compressive Strength versus Time

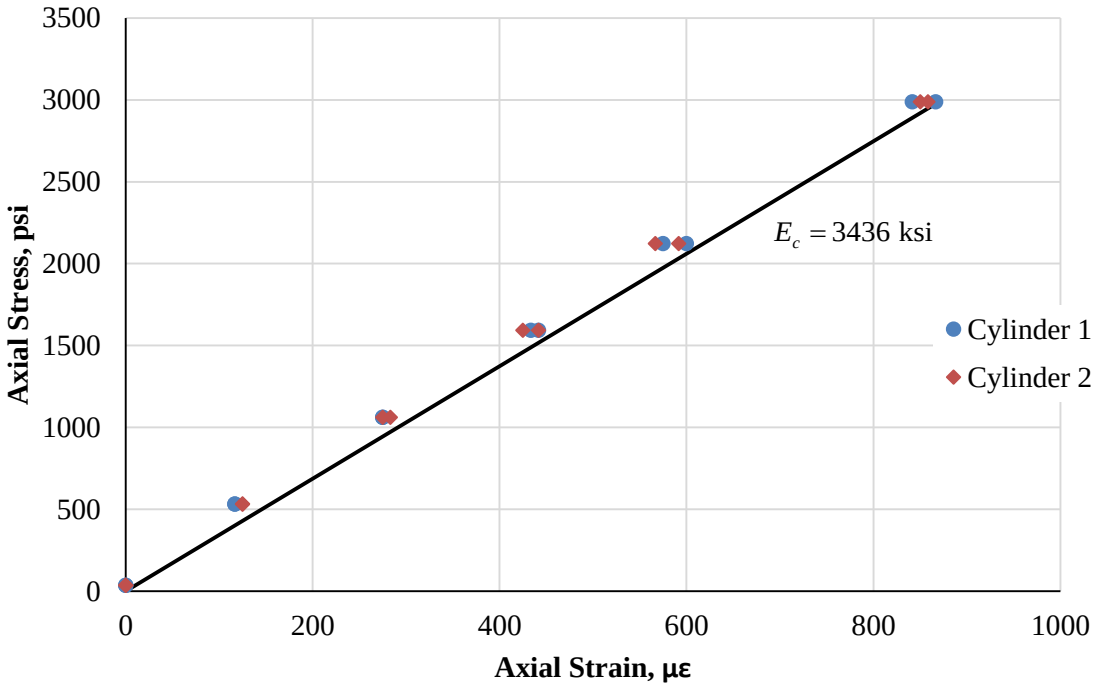

Figure 3.7 – Representative Static Modulus of Elasticity Test

3.3.2 Reinforcing Bar

For the nonprestressed columns, Grade 60, deformed, carbon-steel, reinforcing bars conforming to ASTM A615 (2012) were used for the primary, longitudinal steel. The reinforcing bars were donated and manufactured by Gerdau from their Muncie, Indiana plant with coordination by the Concrete Reinforcing Steel Institute (CRSI). All #3 and #5 reinforcing bars used in this project were obtained from the same heat of steel.

The tensile properties of the reinforcing bars were tested in accordance with ASTM A370 (2012). Using a linear regression analysis, the modulus of elasticity (E_s) was determined using test results from 6000 psi to 60,000 psi. The test force was measured with the testing machine's pressure transducer, and the strain was measured with an extensometer until 5% strain and thereafter measured with the machine's built-in string potentiometer.

Two methods were used to determine the yield points of the reinforcing bars. The offset method, using a 0.2% offset, was used to compute the yield point in accordance with ASTM A370. Additionally, the stress at 0.35% strain was used to compute the yield point in accordance with ACI 318 (2014). Table 3.6 provides a summary of the tensile properties for the steel reinforcing bar, and all presented values are the average of three test coupons. Figure 3.8 shows the stress-strain results from the tensile tests in detail.

Table 3.6 – Summary of Reinforcing Bar Tests Results

Material	f_y , ksi at 0.2% Offset	f_y, ksi at 0.35% Strain	E_s, ksi	f_u, ksi	Ultimate Elongation, %
#3 reinforcing bar	72.9	71.2	28400	115.7	9.5
#5 reinforcing bar	83.7	83.6	28300	100.9	10.6

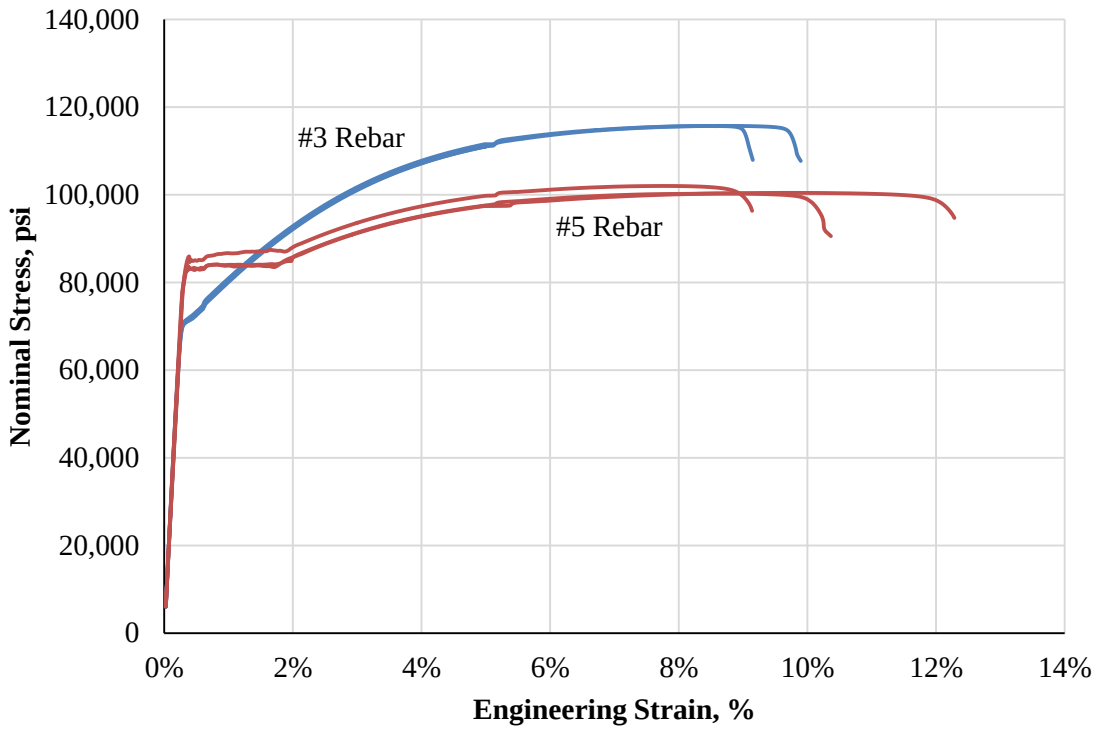

Figure 3.8 – Steel Reinforcing Bar Tests Results

3.3.3 Prestressing Steel

For the prestressed columns, the design of the prestressing was intended to represent typical prestressed columns in service. Because the columns in this project were small-scale, however, standard 0.5 in. or 0.6 in. prestressing strands were not appropriate. Instead, 5.32 mm diameter, steel wire conforming to ASTM A881 (2010) was used. Similar to typically used prestressing strand, ASTM A881wire is high-strength (≈ 262 ksi) and low-relaxation. Additionally, the wire is indented to improve transfer and development length. The wire was donated by the Spancrete in Wisconsin with coordination by the Precast/Prestressed Concrete Institute (PCI) and manufactured by Insteel Wire Products in Sanderson, FL. All prestressing wire for this project was obtained from a single coil.

The tensile properties of the steel wire were tested in accordance with ASTM A370. The steel wire was tested in the same machine and with the same methods as described in Section 3.3.2 except as follows. The modulus of elasticity (E_s) was determined using test results from 50,000 psi to 225,000 psi. The strain was measured with an extensometer until 2.5% strain and thereafter

measured with the machine's built-in string potentiometer. Table 3.7 shows a summary of the tensile properties for the steel wire, and all presented values are the average of three test specimens. Figure 3.9 shows the stress-strain results from the tensile tests in detail.

Table 3.7 – Summary of Prestressing Wire Tests Results

Material	f_y , ksi at 0.2% Offset	Stress, psi at 1% Strain	E_s , ksi	f_u , ksi	Ultimate Elongation, %
5.32 mm Steel Wire	265	259	29000	280	3.9

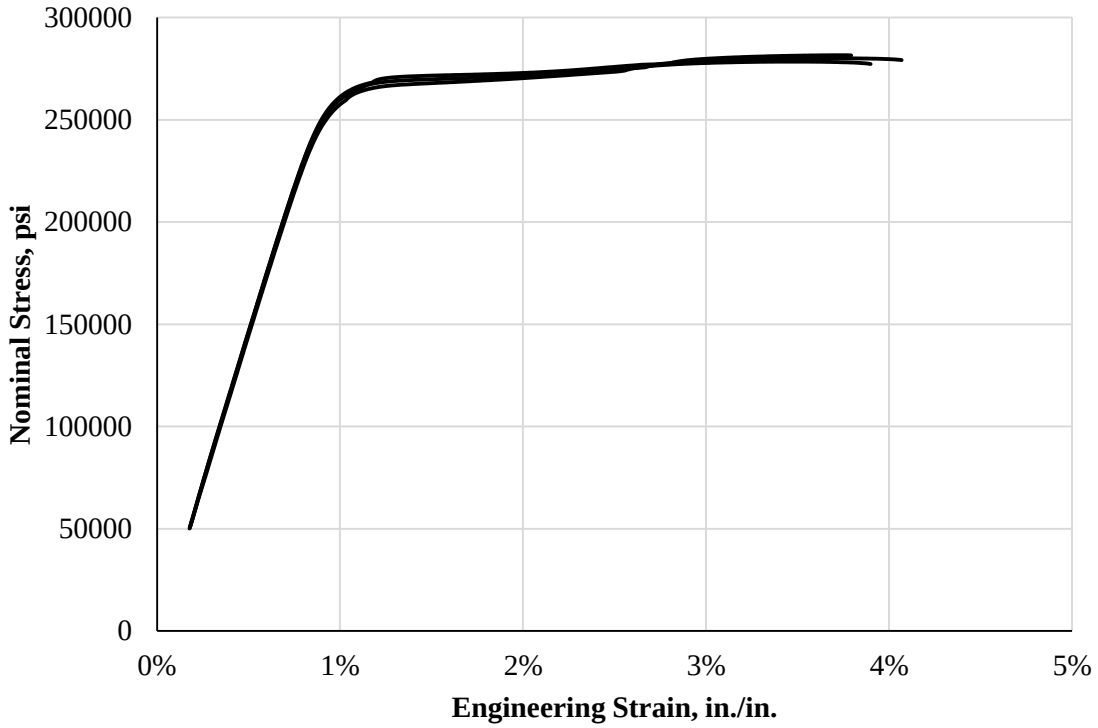

Figure 3.9 – Prestressing Wire Tests Results

3.3.4 Wire for Column Ties

For the column ties, a small diameter wire or bar was necessary because of the small bend radii required. The minimum size readily available in the United States for traditional reinforcing bar is #3. As an alternative, 1/4 in. diameter, plain, carbon-steel wire was used. The wire for this project was taken from two batches, and both batches were only referred to as pencil rod by the supplier. As such, the exact composition and conforming specification was unknown. Because

the ties were only necessary for confinement and not strength, however, the exact specification was not important.

The tensile properties of the steel wire were tested in accordance with ASTM A370. The steel wire was tested in the same machine and with the same methods as described in Section 3.3.2 except as follows. The modulus of elasticity (E_s) was determined using test results from 8000 psi to 80,000 psi. The strain was measured with an extensometer until 2% strain and thereafter measured with the machine's built-in string potentiometer. Table 3.8 presents a summary of the tensile properties for the steel wire, and all presented values are the average of three test specimens. Figure 3.10 shows the stress-strain results from the tensile tests in detail.

Table 3.8 – Summary of Wire for Ties Tests Results

Material	f_y, ksi at 0.2% Offset	E_s , ksi	f_u , ksi
1/4" wire (Batch 1)	91.3	28300	96.3
1/4" wire (Batch 2)	95.4	30200	99.3

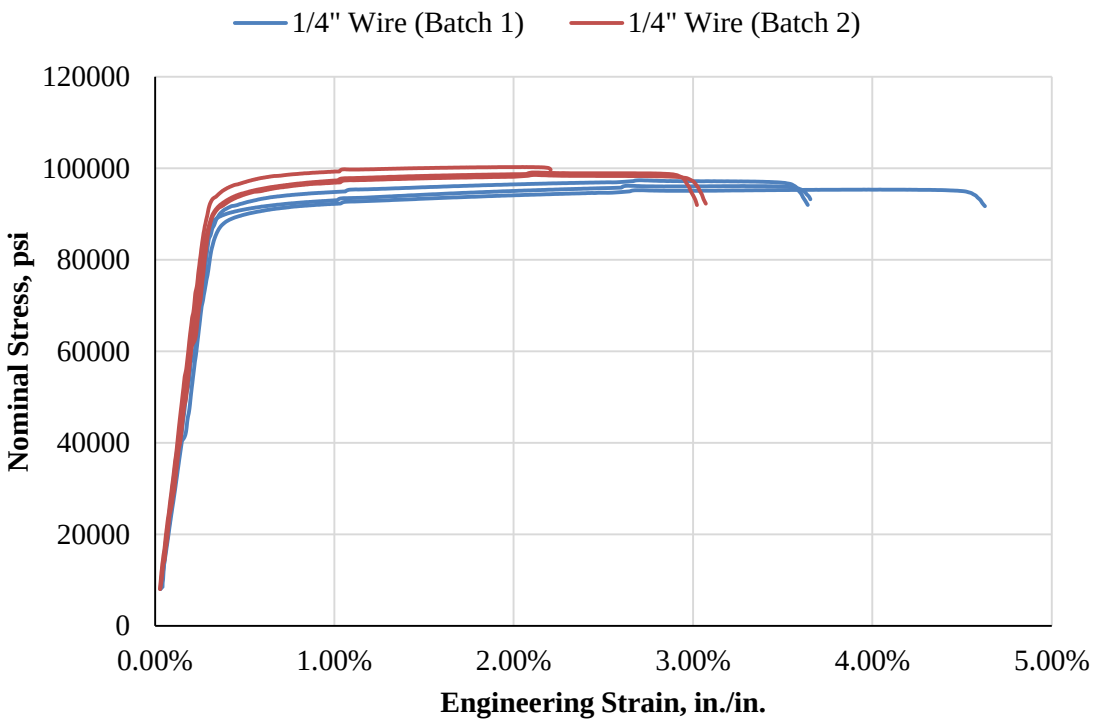

Figure 3.10 – Wire for Column Ties Tests Results

3.4 Construction

All specimens were constructed at the Bowen Laboratory of Purdue University in West Lafayette, Indiana. The columns were constructed in four phases. In general, the first two phases comprised the nonprestressed and short columns, while the last two phases comprised the prestressed columns.

For cast-in-place columns, the typical method of construction is vertically, but on the other hand, precast columns are constructed horizontally. All columns for this project were cast horizontally for practical construction reasons. Differences in behavior between horizontally and vertically cast columns was not considered significant in this testing program due to the small scale of the tests. Because the depth of the cast concrete was only 6 in., bleed water was not a significant concern. Additionally, the relatively long wet curing cycle helped further alleviate any bleeding concerns. The likelihood of shrinkage cracks, however, increase for horizontal casting, while cracks would be very unlikely for vertical casting. Columns from the first cast showed some evidence of shrinkage, and as a result, the method of wet curing was modified for subsequent casts to lessen the severity of cracks, as described in Section 3.4.4.

3.4.1 Formwork

The wooden formwork consisted of plywood braced with 2x4 dimensional lumber on a plywood base. The formwork was reused for subsequent casts until it was noticeably damaged or warped. Prior to each cast, the formwork was sprayed with an oil-based release agent until the wood surface was saturated. In addition to aiding with form removal after curing, the release agent was presumed to aid curing by limiting moisture from the concrete absorbed by the formwork.

3.4.2 Column Reinforcement

All reinforcement and prestressing wire were cut and assembled in Bowen Laboratory. The ties were cut to length from steel wire and bent to shape with a wire bender to a tolerance of 1/16 in. The ties were fastened to the reinforcement and prestressing wire with steel, loop ties and spaced with a tolerance of 1/4 in. For the nonprestressed columns, plastic form spacers were used to support the specimen in place and maintain spacing during casting. Figure 3.11 shows a representative reinforcing bar assembly, including the form spacers. The prestressed columns did not require form spacers because the prestressing wire maintained position and spacing after pretensioning.

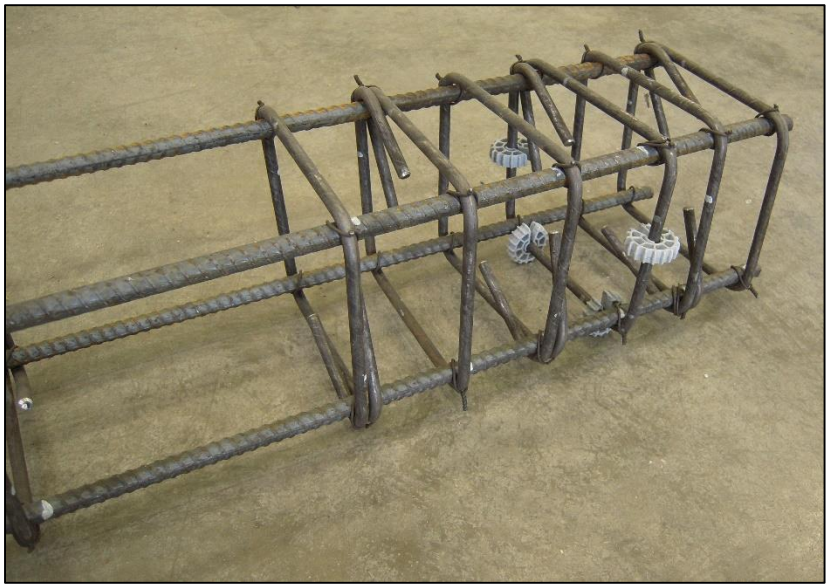

Figure 3.11 – Representative Reinforcing Bar Assembly

3.4.3 Column End Regions

To facilitate the attachment of the steel, end plates, 1/4 in. diameter, threaded, high-strength steel rods were cast into the column end regions, as shown in Figure 3.12. The rods extended 6 in. into the column, measured from the edge of the concrete, and the rods were held in place during casting with washers and nuts on the inside and outside of the formwork.

Figure 3.12 – Representative End Region Assembly

Throughout the project, several iterations of the end plate assemblies were used due to problems with end region failures during testing. For the first cast, a single, steel, end plate was used and cast integral with the concrete as noted in Section 3.2.2. A few columns, however, exhibited

significant cracks and ultimately failure in the end region during testing. As a solution, a steel plate assembly was fabricated and attached to the column end region with threaded steel rods as shown in Figure 3.13. The rods were tightened snugly, and the assembly was intended to increase confinement, reduce cracking, and prevent failure of the end region. In most cases, the assembly prevented subsequent end regions failures, but this was not always the case. When discussing test results in subsequent sections, all tests that experienced significant end region cracking or failure are noted clearly, as well as any tests that used the confinement plate assembly.

Figure 3.13 – Representative Confinement Plate Assembly

Because of the end region problems experienced for columns of the first cast, subsequent tests used an additional 1 in. steel plate as discussed in Section 3.2.2. It was observed that the reduced plate thickness at the location of the groove allowed the plate to bend under loading and produce a concentrated stress in the concrete at this location, causing splitting. The addition of a 1 in. plate was designed to increase the bending resistance and allow for a more uniform distribution of stresses under the plate.

For the second cast, both steel end plates were cast integral with the concrete. Due to the increased end region robustness, no columns from the second cast experienced end region

failures, and only a few tests showed any visible signs of cracking. For the third and fourth casts, the end plates were not able to be cast integrally because the prestressing wire was continuous through several columns. As a result, the end plates were attached with the threaded rods that were cast in the concrete. For the long-term columns of the third cast, a 1/8 in. sheet of neoprene was inserted in between the concrete and end plate to improve the interface. This method, however, did not adequately distribute the stresses, and a few columns experienced cracking in the end region during sustained loading. Therefore, the confinement plate assembly was attached before these columns were tested to failure in short-term loading.

A different end region assembly was used for subsequent columns of the third cast and all columns of the fourth cast. The end plates were placed into position using the installed threaded rods leaving an approximately 1/4 in. gap between the end plate and concrete. This void was filled with high-strength, gypsum cement (Hydro-Stone), as shown in Figure 3.14. This end region assembly improved the interface and distributed the stresses more effectively than the neoprene. Accordingly, the columns constructed with this assembly showed very few signs of visible cracking in the end region.

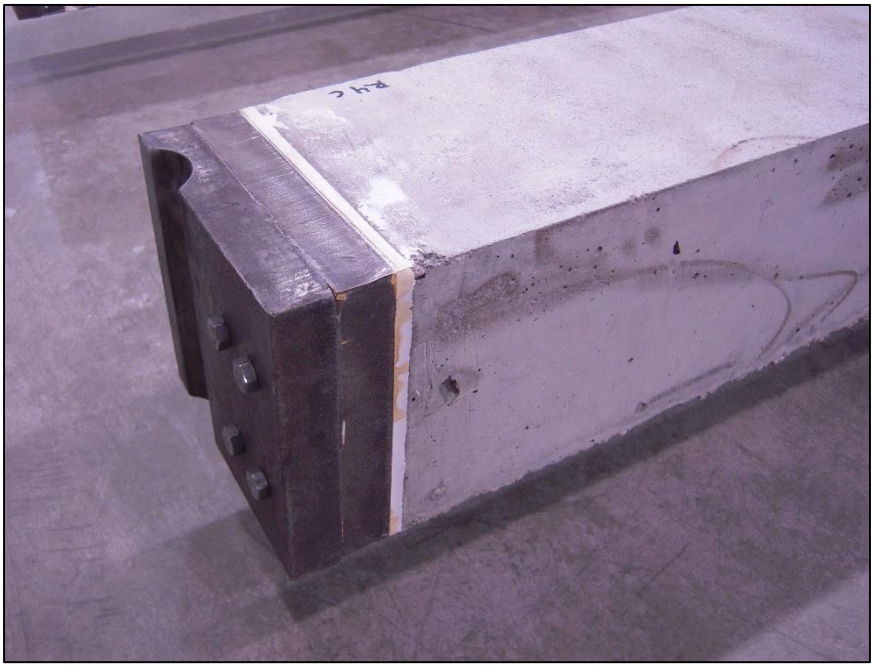

Figure 3.14 – Representative Prestressed Column End Region

All short-term columns, except for R3-40-10-ST, from Cast 1, used the end region, confinement assembly when loaded to failure. All prestressed columns used the end region, confinement

assembly when loaded to failure. All prestressed columns from Cast 3 used neoprene in the end regions, and all prestressed columns from Cast 4 used gypsum cement in the end regions.

3.4.4 Casting and Curing

The concrete was provided by a local, ready-mix concrete supplier and delivered by an in-transit, concrete mixer. Only one batch was required for each cast. The concrete was placed by various means: concrete truck chutes, concrete buckets, and shovels. The columns were cast in two lifts, with each being internally vibrated. After vibrating the second lift, the concrete was screeded to elevation with a magnesium, hand float and finished with a steel trowel after initial set.

Following final set of the concrete, burlap was placed over all exposed concrete and further extended in all directions at least 12 in. The burlap was saturated with water, and 6 mil plastic was placed on top to limit moisture evaporation. For the duration of wet-curing, the burlap was kept saturated by reapplying water as necessary. All columns were wet-cured for at least seven days, and the concrete test cylinders were cured in the same manner as each corresponding cast.

For the first cast, the columns were wet-cured for seven days, after which all burlap and plastic as well as the wooden formwork were immediately removed. Because several columns from the first cast exhibited significant shrinkage cracks, the wet curing for subsequent casts was modified. For the second and third casts, the wet-curing was extended to 10 days because of the lower projected concrete strength, as shown in Figure 3.6. After 10 days, the plastic was removed, and the burlap was allowed to air dry for two additional days. The burlap was then removed, and the columns were further allowed to air dry for one day, after which the columns were removed from the wooden formwork. The delayed removal of the coverings was intended to allow the columns to equilibrate to the laboratory atmospheric conditions more slowly, thereby reducing shrinkage cracking. Generally, this method reduced visible shrinkage cracking. The fourth cast employed the same equilibration methods as described but were only wet-cured for seven days due to the higher projected strength.

Due to the length of the project, the concrete was cast at different times throughout the year, resulting in different atmospheric temperature and humidity environments. Figure 3.15 and Figure 3.16 show the average daily temperature and relative humidity, respectively, for an outdoor weather center located within one mile of the laboratory for the duration of the experimental portion of this study. All concrete was cast and kept in the laboratory, but only the

temperature was controlled. The laboratory temperatures of were maintained between 50° F and 85° F.

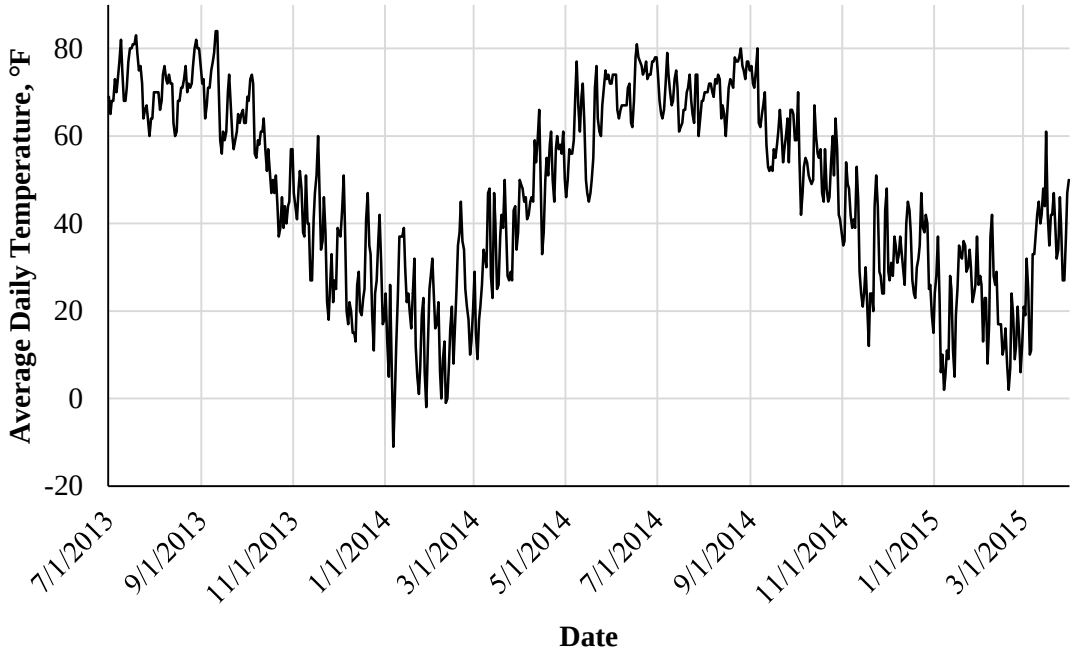

Figure 3.15 – Average Daily Temperature

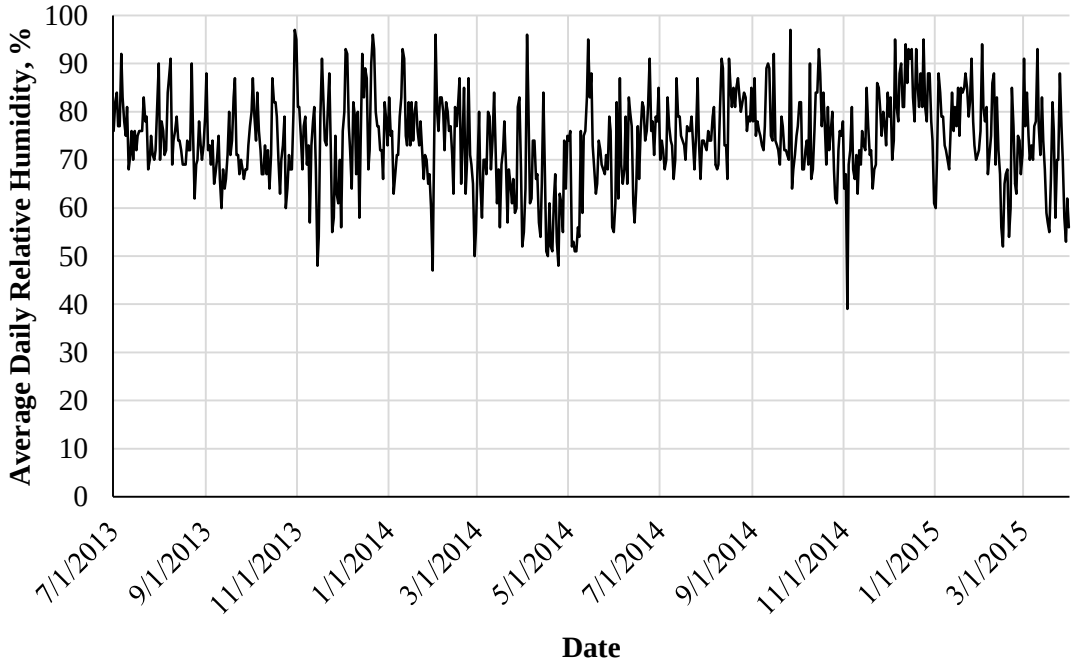

Figure 3.16 – Average Daily Relative Humidity

3.4.5 Prestressing

The prestressed columns were constructed on a 56 ft casting bed using custom-made abutments for wire anchoring that had holes spaced at 2 in. Up to six columns were cast in a row using continuous runs of wire, and two rows were used per cast, resulting in up to 12 columns per cast. The third cast included 10 prestressed columns, and the fourth cast included 12 columns. Figure 3.17 shows the prestressing column layout as well as the prestressing abutment and wires in place.

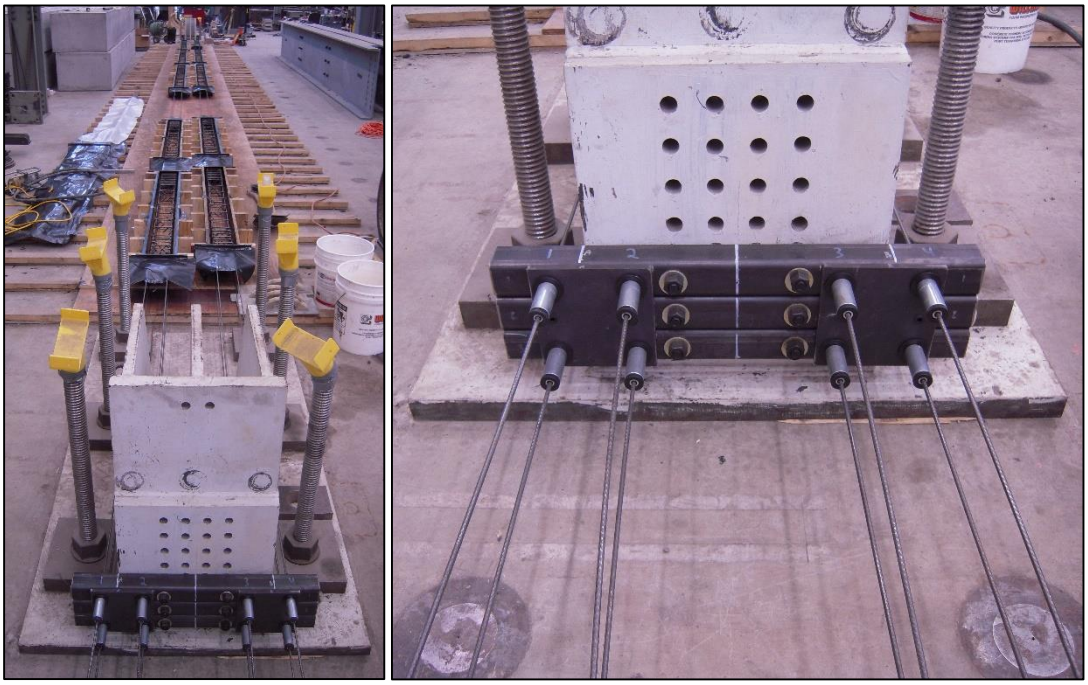

Figure 3.17 – Prestressing Column Layout and Abutment

To accurately stress the wires, strain gages were used, and the wires were initially stressed taut to 1000 lb (≈ 30 ksi) to simplify the installation of the gages. The strain gages were monitored during stressing as described below, and details of the strain gages are noted in Section 3.5.2. The target force for the wires, considered fully stressed, was 6750 lb or 75% of the nominal, ultimate capacity of the wires (≈ 196 ksi). After the gages were installed, the wires were fully pretensioned in two stages due to equipment limitations caused by the elongations required. First, the wires were pulled to 4000 lb. and then, after resetting the hydraulic cylinders, the wires were pulled to the target 6750 lb. To address seating losses of the prestressing anchors, the wires were slightly overstressed. First, the measured strain was noted at a force of 6750 lb, and the wire was further stressed to approximately 6900 lb. After releasing from the increased load, the strain

returned to the value at the target stress due to the seating losses. This increased value was found by trial and error during stressing of the first wire and, while repeatedly verified, was used for all remaining wires. All wires from all casts were fully stressed.

The concrete was allowed to cure for three days before releasing the strands. The strands were released by heating with an oxy-acetylene torch and one at a time in an order that minimized the effective eccentricity. Each row of columns were released independently of each other. Care was taken to slowly heat the wires to encourage gradual release, but because they were single wires, the release was rather sudden. The wires were torched at one end adjacent to the abutment. After all the wires were released, the wires in gaps between columns were cut with a cutting wheel to ensure there was no residual stress in any section of the wire due to friction between the columns and the plywood formwork base.

3.4.5.1 Transfer Length and Prestress Losses

To measure prestressing losses and transfer length, surface strains along the length of several columns were measured at different stages of prestressing. These measurements were made using a DEMEC mechanical strain gage, further detailed in Section 3.5.2.1. Because of the symmetrical layout of the prestressing wire, the strains due to the prestressing and losses should be constant throughout the column cross-section. Figure 3.18 shows the surface strain profile of one 6 ft column that had six prestressing wires, and each data point indicates the center of the strain measurement. The distance from column end is referenced from the theoretical end (center of pin). As shown, the transfer length strains increase roughly linearly, as expected, and the transfer length is approximately 20 in. for both concrete ages. Similar transfer lengths were noted at both the live (torched) and dead (free) ends. The concrete was from Cast 4.

The maximum strain at release corresponds to the elastic shortening losses. The average of the middle six measurements for the release strains was 390 με or an average of 11 ksi in the prestressing wire. Table 3.9 and Figure 3.18 show a summary of the losses for the same column as calculated with the procedures outlined in the PCI Design Handbook (2010) using the measured material properties. Details of the calculations can be found in Appendix A. For elastic shortening, the estimated loss of 9.1 ksi compares well to the measured loss of 11 ksi. Similarly the estimated total losses of 39.2 ksi compare well with the measured loss of 50 ksi.

Table 3.9 – Representative Estimated Prestress Losses

Type of Loss	Estimated Loss, ksi	Estimated Loss, με
Elastic Shortening	9.1	314
Creep of Concrete	15.7	542
Shrinkage of Concrete	10.8	372
Relaxation of Tendons	3.6	124
Total Losses	39.2	1352

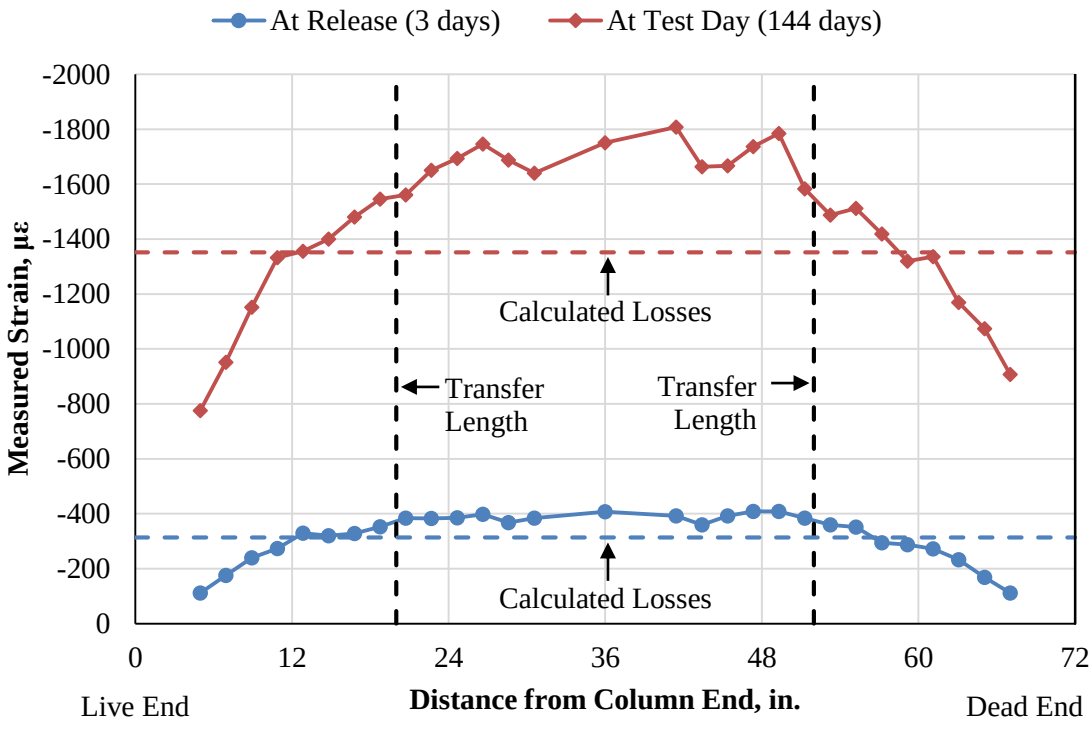

Figure 3.18 – Representative Prestressed Column Strain Profile

3.5 Testing Setup

The testing setup was designed to allow all loading types to be tested in each frame and to ensure the testing assumptions were satisfied: equal end eccentricities, columns braced against sidesway, and pinned-pinned loading conditions.

3.5.1 Loading Frames

The loading frames consisted of steel plates and high-strength post-tensioning bars and acted as a self-contained, external post-tensioning frame. Several frames were constructed, which allowed

several columns to be tested simultaneously. The frames also allowed the sustained load to be increased periodically, which was necessary because time-dependent losses resulted in decreasing frame loads. Figure 3.19 shows a plan view of an example loading frame for a 6 ft column.

As shown, the frame consists of four post-tensioning bars and three steel plates. The columns were positioned between two steel plates, and the loading rams were positioned between two steel plates. The column was located in the center of the four post-tensioning bars. Using hex nuts to resist the post-tensioning, the loading rams were extended to apply load to the column. To apply sustained load, the load frames were stressed to the desired load, and a set of interior hex nuts were snug tightened to the middle frame plate, which maintained load in the column when the loading rams were released. To hold the column in place before initial loading, wooden pedestals were used. The pedestals were topped with two separate sheets of Teflon to reduce the influence of friction in the direction of bending.

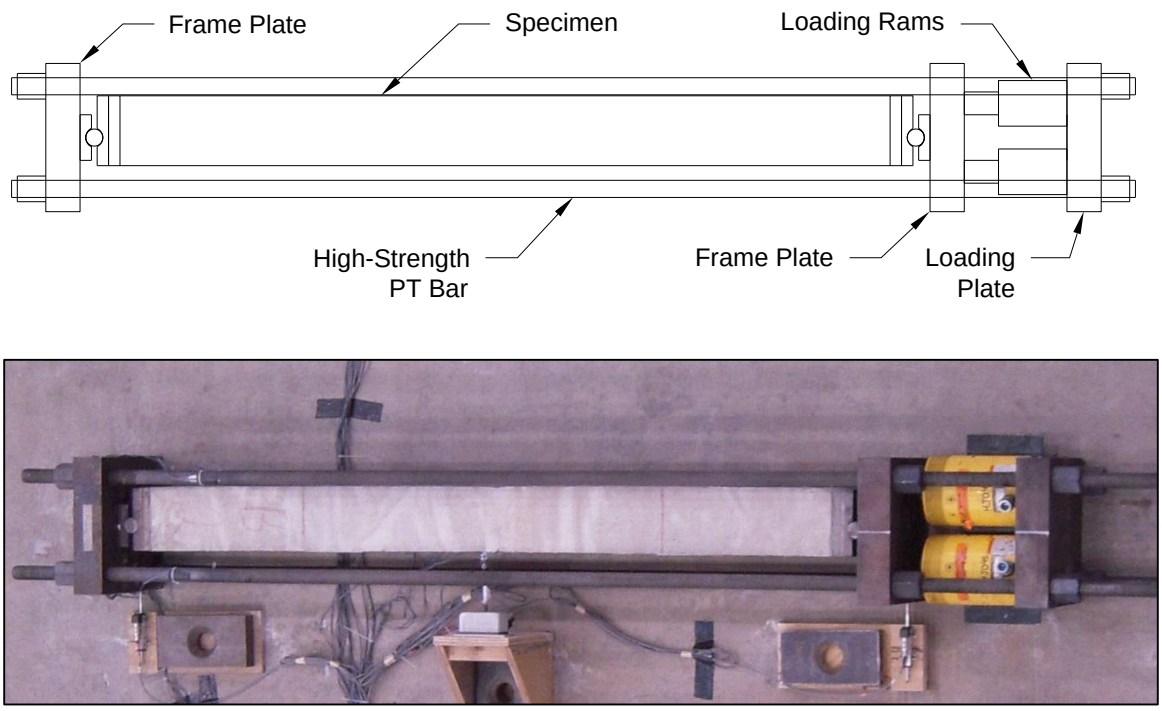

Figure 3.19 – Slender Column Loading Frame

Figure 3.20 shows a detail of the end region of a loading frame. A roller plate with an identical bevel as the end plate was attached to the frame plate. This allowed the load from the column to be transferred to the center of the frame plate while ensuring a pinned-pinned connection. This

method of loading also eliminated sidesway movement and provided significant stiffness in the out-of-plane direction, which allowed one-way bending to dominate the behavior. Before initial loading, the loading pins were greased to reduce friction.

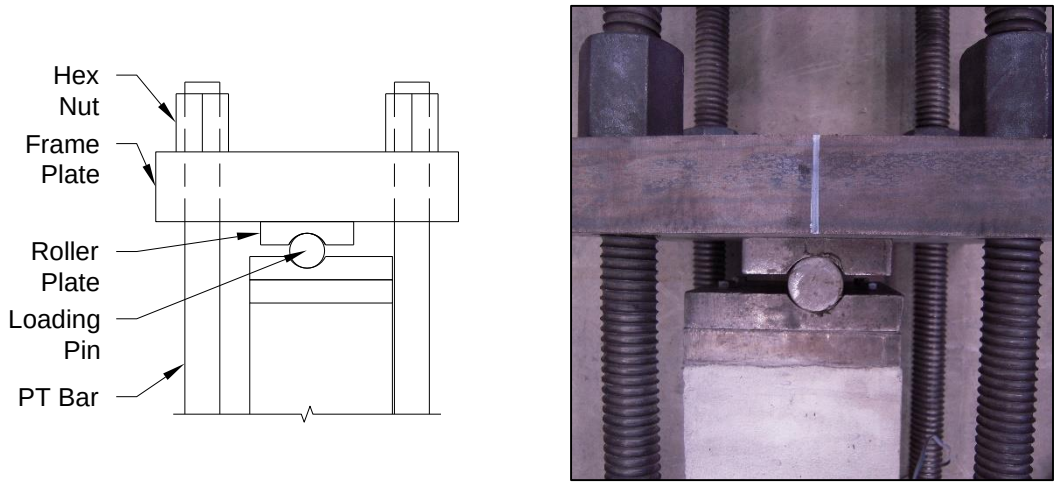

Figure 3.20 – Loading Frame Detail

3.5.1.1 Short Columns Loading Frames

The loading frames for the short columns were slightly modified. As shown in Figure 3.21, an additional frame plate was placed in between the two outside frame plates. This design allowed two columns to be tested simultaneously, which halved the number of frames required for testing. The columns placed in the same frames had the same eccentricity ratios but different a reinforcement configuration (four #3s versus plain). Hex nuts were only placed outside of the two outer frame plates, and therefore, the columns sharing a test frame were subject to identical axial loads.

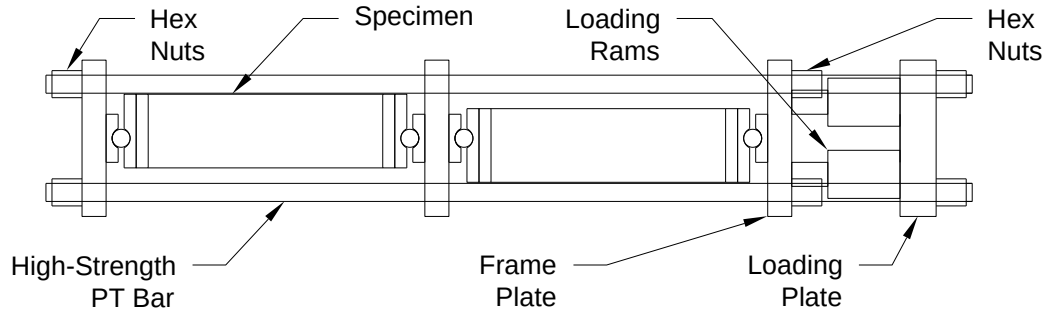

Figure 3.21 – Short Column Loading Frame

3.5.2 Measurement Sensors

The measurements of interest for the column tests were axial load, deflections, and cross-sectional strain. For the axial load, a pressure transducer was used to monitor the hydraulic pressure provided to the loading rams. Due to different load demands throughout the study, two different sets of loading rams were used: two 30-ton rams and two 60-ton rams. When using two 30-ton rams, the calibrated accuracy of the measurements was approximately 250 lb, and when using two 60-ton rams, the accuracy was approximately 500 lb. All axial load values are reported with increments of 100 lb.

Because of the use of equal end moments, all columns should theoretically deflect symmetrically, with the maximum deflection occurring at the column midspan. As a result, the deflections of the columns were only measured at the column midspans. Because the load frames were self-contained, however, the frame could move independently from the floor, which was used as a reference for displacement measurements. To take this into account, the displacements of the frame plates on either side of the column were monitored. With three known displacement measurements, the midspan column deflection was calculated. For all three measurements, potentiometers were used. Displacement sensors were not used for the short columns because deflection was not a consideration. The sensors used to measure the displacement of the frame plates were calibrated with an accuracy of 0.001 in., and the sensors used to measure the column deflection were calibrated with an accuracy of 0.01 in. All displacements values are reported with increments of 0.01 in.

Finally, cross-sectional strains were monitored using 120-ohm electrical resistance strain gages. All gages were placed at the column longitudinal midspans. For each specimen, 60 mm gages were placed on the concrete surface on the centerline of both the compressive and tensile faces. The longer length gages allowed the non-homogenous concrete to be measured more accurately. In addition, 6 mm gages were placed at the midspan of all reinforcing steel in the specimens. All of these gages were placed on the side nearest the concrete surface in the direction of bending, unless otherwise noted. All strain values are reported with increments of 10 με, which was the expected accuracy.

Due to the long-term nature of some of the tests, electrical drift of the sensors was a concern. Three control sensors were used and placed in ambient lab conditions. The two types of displacement sensors were attached to a wooden frame and held at fixed locations. The

displacements were monitored over the entire length of the project. The sensors calibrated to 0.01 in. drifted approximately 0.01 in. over time, and the sensors calibrated to 0.001 in. drifted approximately 0.005 in. over time. Since these drifts were within the calibrated accuracy of the system (0.01 in.), the drifts were ignored in calculations. Additionally, a 6 mm strain gage was placed on a piece of reinforcing bar that was free to thermally expand. The strain gage drifted approximately 30 με over time, and due to the relatively small drift, the strain gage measurements were not adjusted.

3.5.2.1 DEMEC Mechanical Strain Gages

Because more detailed strain measurements were required for the short columns and for monitoring prestressing losses, a mechanical based strain measurement was employed. Known as a DEMEC gage and shown in Figure 3.22, the apparatus consists of an electronic dial gage attached to a main metallic beam. At the ends of the beam lies conical locating points, one of which pivots. These conical points measure the distance between two points, which are precision drilled discs that are attached to the concrete surface and shown in Figure 3.22. Successive measurements, specifically changes in these measurements, were used to calculate strain. All measurements were made using a standard 100 mm gage length, thus the strain measurements were average strain over 100 mm. All strain values are reported with increments of 10 με, which was the expected accuracy. All strain values presented are located at the center of the respective strain measurement.

Four measurements were made on each loaded short column at different time steps. Shown in Figure 3.22, the measurements were made at the column midspans, on the compressive and tensile faces, and 1 in. above and below the centerline, to avoid interference with the electrical resistance strain gages placed along the centerline. For the short specimens not subject to load, two measurements, each located 1 in. from the centerline, were made on the top of each specimen.

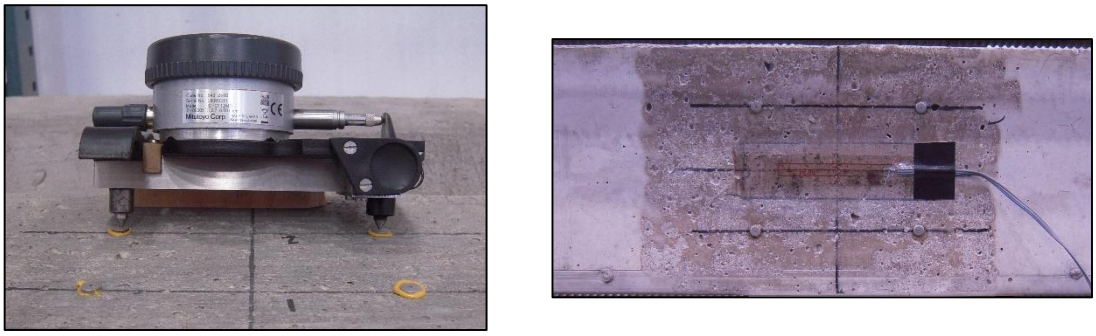

Figure 3.22 – DEMEC Gage and Measurement Discs

DEMEC gages were also used to measure transfer length and losses for a select number of prestressed columns. Discs were installed with a 50 mm spacing, which allowed a running average of strain measurements every 50 mm. The first disc was located 0.75 in. from the edge of the concrete, which resulted in the first average strain having a center approximately 5 in. from the theoretical column end (center of pin). Subsequent measurements were centered with increments of approximately 2 in. In all, 29 measurements were made on the 6 ft columns, and 31 measurements were made on the 10 ft-6 in. columns.

3.6 Testing Procedure

Each column test began by placing the column in the frame, supported by wooden pedestals. The loadings pins were inserted, and the frame plates were moved snug against the pins and columns. The displacement sensors were placed against the end frame plates and attached to the column midspan. The loading rams were placed between the middle frame plate and the loading plate. The loading rams were extended nearly to the frame plate, and all displacement sensors were zeroed. For the redundant strain gages in the long-term tests, explained in Section 3.6.1, the zeros were also recorded so the gages could be swapped in the event of primary gage failure.

Due to the mechanics of the loading frame, the column and loading pins shifted during initial loading. The shift was not corrected automatically by the three displacement sensors but was corrected on a test-by test basis. Figure 3.23 presents a representative example of the correction in deflection measurements for column R5-70-10-ST. When a slender column is under relatively low load, the load-deflection relationship is approximately linear due to minimal second-order effects, and as a result, the initial response should be linear. Using engineering judgement, a linear portion of the load-deflection relationship was selected so that the curve could be shifted to extend the linear region back to the origin. As shown, this produced a horizontal shift of the load-

deflection response. This type of correction was performed for all of the column deflection measurements. In subsequent results chapters, only the corrected data is shown. Appendix B provides the uncorrected load-deflection results for all column tests. For all columns, the maximum correction was 5.2% of the applied eccentricity. The shifting of the columns and pins, therefore, provided a minimal effect on the target applied eccentricity.

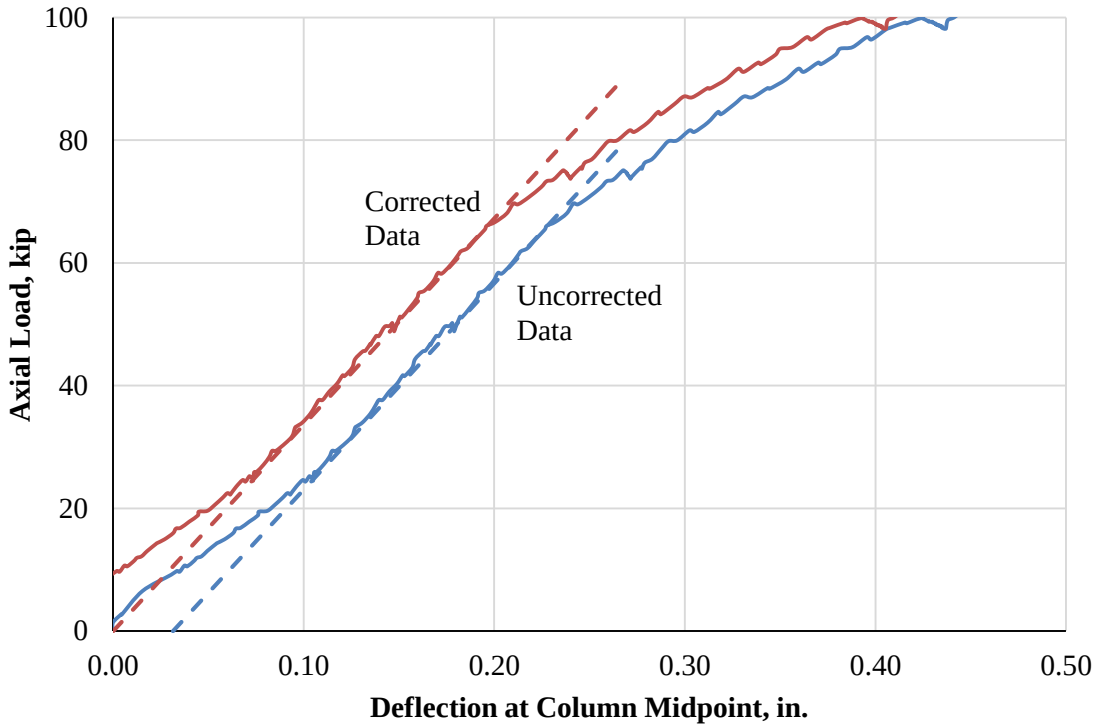

Figure 3.23 – Method to Correct Column Deflection Measurements

Once the data acquisition was started, the loading rams were gradually increased until approximately 1000 lb to allow full contact of the entire frame. After 1000 lb, the loading was increased at a constant rate of approximately 1000 lb per second. Loading was paused at predetermined steps to allow for photographs and manual data entry. For the short-term columns, the loading was repeatedly paused until approximately 70% to 80% of the expected ultimate strength, at which point the loading continued to increase without pause until failure.

For the long-term columns, the loading was stopped at the predetermined sustained load, and the load was sustained with the loading rams for approximately three hours. After that time, the hex nuts were snug tightened to the middle frame plate and the loading rams were released. Strain gages were attached to unthreaded sections of each of the post-tensioning bars and monitored

during the periods of sustained load. Once the target sustained load was reached, the average of the strain gages for that frame was recorded. The average strain was monitored over time to detect load reductions in the frame. The columns were maintained at an axial load within 5% of the target sustained load, though a smaller deviation of 1% was typically maintained after the first few days of sustained load when the losses were less. As the axial load decreased due to creep and other losses such as shrinkage, the loading rams were reinserted into the frame and increased to the appropriate load, and the hex nuts were retightened. This process was repeated for the duration of the sustained load, up to approximately 100 days. After this time, the loading rams were increased until failure in the same manner as the short-term columns.

3.6.1 Data Acquisition Scheme

Each slender column, with few exceptions, had nine sensors: three displacement sensors and six strain gages. Due to channel limitations with the data acquisition system, only four strain gages, located at each cross-section location, were monitored for the long-term tests, and two redundant steel gages were not monitored unless a primary gage failed during a test. For the short-term tests, all nine sensors were monitored. For the short columns, two gages were monitored for the plain columns, and four gages were monitored for the reinforced columns.

During initial loading of the long-term columns, data was recorded once per second, and during the sustained load portion of the tests, data was recorded once per hour. During final loading for the long-term columns and during loading of the short-term columns, data was recorded 10 times per second.

CHAPTER 4 SHORT-TERM BEHAVIOR OF NONPRESTRESSED COLUMNS

4.1 Introduction

Although short-term behavior of slender columns is better understood than long-term behavior, current design methods were developed primarily from the results of experimental tests using, in many case, obsolete materials. Recent research has proposed design modifications (Jenkins 2011), and eight nonprestressed column tests were conducted in this current study to evaluate the accuracy of the proposed design modifications. Furthermore, the accuracy of the computational model discussed in Chapter 3 as well as the current design equations are evaluated. The experimental tests are supplemented with the results of historical, slender column tests to further evaluate design and analysis methods and provide a better perspective on their accuracy.

4.2 Existing Design Methodology

As described in Section 1.3, the moment magnification procedure relies on a column stiffness (*EI*). Because the stiffness of a concrete column varies along the length, the column stiffness used in the procedure must be an effective stiffness that results in an accurate estimate when using the moment magnification procedure. ACI 318 (2014) currently permits the following equations to be used to calculate the effective stiffness when using the moment magnification procedure.

$$EI = 0.2E_cI_g + E_sI_{se} \quad \text{(Eq. 4.1)}$$

$$EI = 0.4E_cI_g \quad \text{(Eq. 4.2)}$$

$$EI = \left(0.80 + 25\frac{A_{st}}{A_g}\right)\left(1 - \frac{M}{Ph} - 0.5\frac{P}{P_0}\right)E_cI_g \le 0.875E_cI_g \quad \text{(Eq. 4.3)}$$

where:

A_g = gross area of concrete section, in.^{2}

A_{st} = total area of nonprestressed longitudinal reinforcement, in.^{2}

$E_c = 57,000\sqrt{f_c'}$ psi = modulus of elasticity of concrete, psi

E_s = modulus of elaticity of reinforcement, psi

EI = flexural stiffness of compression member, in.^{2}-lb

h = depth of compression member, in.

I_g = moment of inertia of gross concrete section, in.^{4}

I_{se} = moment of inertia of reinforcement, in.^{4}

M = end moment of compression member, in.-lb

P = axial force, lb

$P_0 = 0.85 f_c'\left(A_g - A_{st}\right) + f_y A_{st}$ = nominal axial strength, lb

Partly due to its simplicity, it is believed that Equation 4.2 is primarily used for design. Equations 4.1 and 4.3 require additional section parameters that are typically not known at the onset of design. As such, these equations, particularly Equation 4.3, are more suited for analysis than design. Recently, Equations 4.4 and 4.5 have been proposed for analysis and design, respectively (Jenkins 2011). Note that the eccentricity ratio (M/Ph) shall not be taken less than 0.1 for these equations, or in other words, if the eccentricity ratio is less than 0.1, it shall be taken as 0.1 in the equation. Equations 4.4, when compared to Equation 4.3, and Equation 4.5, when compared to Equations 4.1 and 4.2, were shown to be more accurate while resulting in fewer unconservative estimates of effective stiffness. Under extreme geometric and loading circumstances, the stiffness can reach a lower bound of 0.30 E_cI_g, but for typical service columns, the lower bound is 0.40 E_cI_g. For this reason, the higher lower bound of 0.40 E_cI_g is used for the design equation.

$$EI = \left[1.05 - 0.6\frac{P}{P_0}\right]\left[1.0 + 3\left(\frac{A_{st}}{A_g} - 0.01\right)\right]\left[1.2 - 2\frac{M}{Ph}\right]E_c I_g \geq 0.30 E_c I_g \qquad \text{(Eq. 4.4)}$$

$$EI = \left[1.0 - 0.5\frac{P}{P_{0g}}\right]\left[1.2 - 2\frac{M}{Ph}\right]E_c I_g \geq 0.40 E_c I_g \qquad \text{(Eq. 4.5)}$$

where:

$P_{0g} = 0.85 f_c' A_g$ = axial strength of gross concrete section, lb

$\frac{M}{Ph}$ shall not be taken less than 0.1

4.3 Experimental Program

Eight short-term tests were conducted on nonprestressed columns. Due to differences in behavior and code approaches, the short-term tests of prestressed columns will be discussed separately in Chapter 5. Table 4.1 provides a summary of the short-term tests, including the concrete properties used in the subsequent analyses. The concrete for the columns with #3 bar was from Cast 1, and the concrete for the columns with #5 bars was from Cast 2.

Table 4.1 – Summary Short-Term Tests (Nonprestressed Columns)

Column ID	Reinforcement	Slenderness Ratio, kl_u / r	Eccentricity Ratio, e / h	f_c' on Test Day, psi	E_c on Test Day, ksi
R3-40-10-ST	4 – #3s	40	10%	7020	4260
R3-40-25-ST			25%	7020	4260
R3-70-10-ST		70	10%	7020	4260
R3-70-25-ST			25%	7020	4260
R5-40-10-ST	4 – #5s	40	10%	5570	3330
R5-40-25-ST			25%	5570	3330
R5-70-10-ST		70	10%	5570	3330
R5-70-25-ST			25%	5570	3330

4.4 Experimental Results

The results of the tests are summarized in two types of figures: axial load versus deflection and axial load versus moment (also known as an interaction diagram). The moment demands on the columns were computed by multiplying the axial load by the sum of the eccentricity and deflection ($M = P\ (e + \delta)$). The load-moment figures include the nominal strength, which was computed with the model outlined in Chapter 2. The nominal strength for the columns as well as the estimates by the computational model were computed using the as-measured, test-day material properties of the concrete and reinforcing steel. The load-moment figures also include the behavior of short columns, which represents the first-order moment (axial load times the eccentricity) and helps to illustrate the amount of second-order effects experienced by the tested columns. Finally, the figures include the ACI 318 total moment limit of 1.4 times the first-order moment ($1.4\ M_0$). Figure 4.1 (#3 bars) and Figure 4.2 (#5 bars) show the results of the short-term tests (solid lines) as well as the estimates of behavior from the computation model (dashed lines).

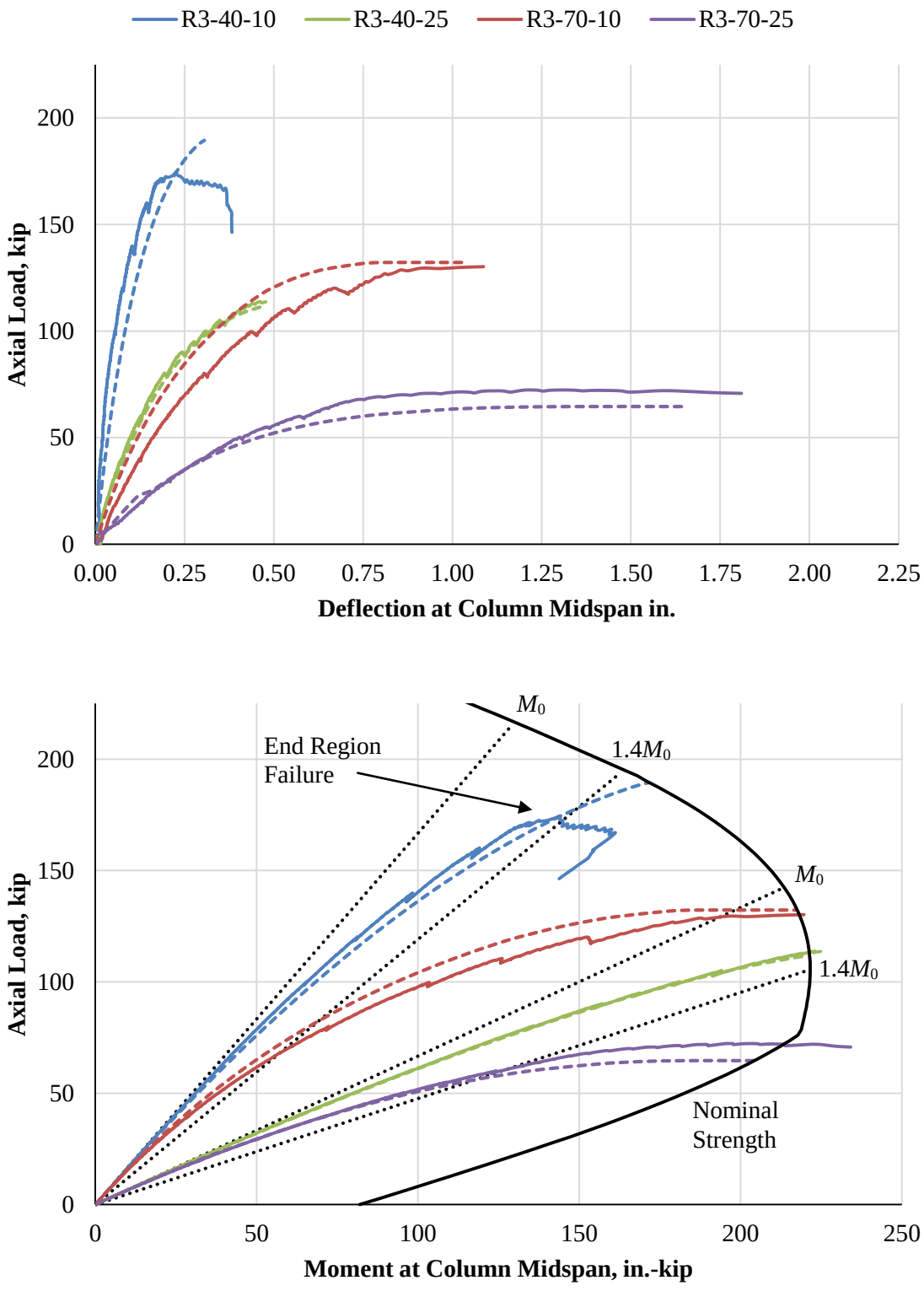

Figure 4.1 – Short-Term Tests Results (#3 bars)

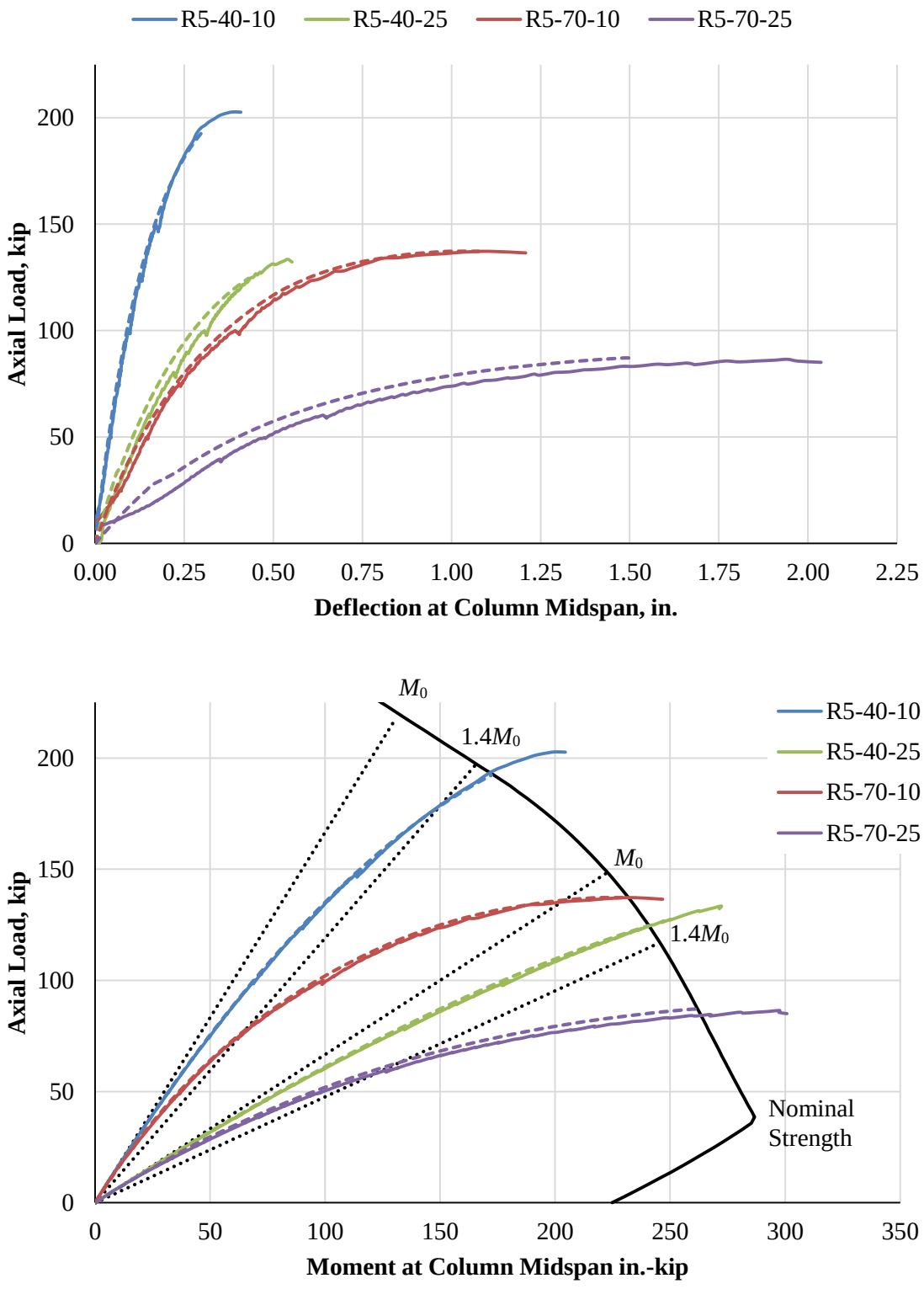

Figure 4.2 – Short-Term Tests Results (#5 bars)

In general, the computational model estimated the behavior of all of the columns with similar accuracy. For the columns with #3 reinforcing bars, the model estimations are less stiff than the tests results, except for the R3-70-10 column. Conversely, for the columns with #5 reinforcing bars, the model estimations are consistently stiffer than the test results. This difference can be partially explained by the assumption of the stress-strain relationship in the computation model. Assuming linear elastic-plastic behavior is consistent with code approaches, but it is not consistent with the measured properties of the reinforcing bar. The #3 reinforcing bar continues to increase in stress after yield, while the #5 reinforcing bar plateaus for approximately 1.5% strain then continue to increase in stress. This would only explain the difference, however, under very high stress loads after yielding of the reinforcing steel. The reason for the discrepancy under lower loads is unknown.

The end region of the R3-40-10 column failed completely, which explains the decrease in axial load capacity and the column not reaching the nominal strength. This failure precipitated the modified end region design noted in Section 3.4.3. Because the column reached over 90% of its estimated strength and the end region only began to fail at high loads, the column was not retested. Though subsequent columns showed cracks in the end region, it was assumed the additional measures to protect the region prevented the cracks from affecting the global behavior of the columns.

The estimates for the failure deflections of all of the columns was consistently less than the measured deflection. The computational model assumed a maximum concrete compressive strain of 0.003 and peak reinforcing bar stress equal to the yield stress. Both of these assumptions are conservative and result in underestimation of the failure deflection. The estimates of the peak axial load were more accurate than the peak deflection. This comparison is, arguably, more important since the design of columns is based on strength. The estimates for peak load were conservative for the R3-40-25 and R3-70-25 columns and, while unconservative, within 1% accurate for the R3-70-10 column. Obviously, the R3-40-10 column cannot be compared due to its premature failure. For the columns with #5 reinforcing bars and a higher slenderness, the estimates of peak load were higher than the test values, but the estimations were both within 3%. The estimates for the R5-40-25 and R5-40-10 were much lower than the test values, but the axial loads when the moments reached the nominal capacity were within 1%. The estimates of the nominal strength were conservative for every column, or in other words, every column (except

for R3-40-10) failed outside of the computed nominal strength curve as shown on the interaction diagram.

The estimations of the load-moment behavior appear more accurate than those for the load-deflection behavior. Though this is technically the case, note that the load-moment behavior was derived from the load-deflection behavior. Because the load-moment behavior includes the eccentricity, however, it is less sensitive to errors of column deflection. The design of columns is based on load-moment behavior, though, and the increased accuracy is advantageous.

Of the eight tests, five columns exceeded the ACI 318 total moment limit of 1.4 times the first-order moment. If the end region of Column R3-40-10 had not failed, it, too, would likely have exceeded the limit. For the 40-10 columns, the additional capacity beyond crossing the limit was less than 10%, assuming the R3-40-10 column behavior was extrapolated. For the 70-25 columns, the additional capacity ranged from 25-30%. The additional capacity for the 70-10 columns was much greater and approximately 80%. Only considering short-term behavior, the ACI 318 total moment limit greatly restricts the possible behavior of slender columns, particularly more slender columns. Of concern for the limit, a few columns exhibited near zero or negative stiffness before failure, which indicates a stability failure, but the computational model estimated the behavior and stability failure accurately.

Table 4.2 provides a summary of the peak axial load during the experimental tests as well as the corresponding failure loads computed with the model. The table also includes the ratio of the peak test load to the computed load, which illustrates both accuracy and conservatism. Besides the R3-40-10 columns, the computational model estimated the failure loads conservatively or within 1.5%. For the columns with #3 bars, only the 70-25 column failure load was computed relatively inaccurately, but it was estimated conservatively. For the columns with #5 bars, the shorter columns were estimated greater than 5% conservative while the longer columns were estimated within 1%.

Table 4.2 – Summary of Short-Term Tests Results (Nonprestressed Columns)

Column ID	Peak Test Load, kip	Computed Failure Load, kip	P_{test} / P_{model}
R3-40-10-ST	174.7*	189.5	--
R3-40-25-ST	113.7	111.7	1.02
R3-70-10-ST	130.5	132.2	0.99
R3-70-25-ST	72.4	64.6	1.12
R5-40-10-ST	203.8	192.6	1.06
R5-40-25-ST	133.7	124.5	1.07
R5-70-10-ST	137.5	137.2	1.00
R5-70-25-ST	86.5	87.1	0.99

*Column end region failed prematurely

4.4.1 Column Failure Types

The column failure types were assumed from a post-failure inspection of the columns as well as qualitative evidence during testing. Because of the mechanics of the test and loading frame, these failures may or may not coincide with columns in service and subject to normal gravity loads. In addition, the stiffness of the loading frames was relatively low, and the hydraulic system was sometimes not able to maintain the load and loading rate when the columns' stiffness neared or fell below zero. In any case, the failure types shed light on the different types of possible failures for these columns. Of all of the column failures, there were two primary types, which was primarily driven by the eccentricity ratio and not the slenderness ratio. The columns with the lower eccentricity ratio (10%) showed evidence of bar buckling, as shown in Figure 4.3. Columns with the higher eccentricity ratio (25%) exhibited a stiffness failure, as shown in Figure 4.4. The columns subject to a stiffness failure exhibited excessive spalling of the concrete on the compressive side and, in some cases, excessive cracking and reinforcement yielding on the tensile side of the columns. All concrete removed from the failed columns was loose and able to be removed easily by hand.

(a) R5-40-10-ST

(b) R5-40-10-ST

(c) R3-70-10-ST

Figure 4.3 – Bar Buckling Failure of Short-Term Tests (Nonprestressed)

(a) R3-70-25-ST

(b) R5-40-25-ST

Figure 4.4 – Stiffness Failure of Short-Term Tests (Nonprestressed)

The bar buckling failures were rapid and explosive and showed few physical signs of distress before failure. A post-failure inspection noted extreme bar buckling as shown in Figure 4.3. While there was also cracking on the tensile face, this was thought to be primarily caused by a post-failure collapse of the load frame on the failed column. The failures were violent enough to not only cause the exterior concrete to spall, but dislodge interior concrete within the ties. Though the concrete within the two ties was damaged, the concrete outside of each adjacent tie remained intact. This indicates that the ties maintained the integrity of the core, but the explosive buckling of the bars locally damaged the concrete. A few columns failed within ties adjacent to the center group, but no columns failed farther from the center.

ACI 318 specifies the spacing of the vertical ties shall not exceed 16 longitudinal bar diameters. This provision is intended to limit or help to prevent bar buckling, which is a dangerous, non-ductile failure. In certain seismic resisting frames, which can be subject to more extreme loadings, this limit is reduced to 6 or 8 bar diameters. For the columns with #3 reinforcing bars, the spacing was 16 bar diameters, and for the columns with #5 reinforcing bars, the spacing was 9.6 bar diameters. Considering these limits, it is not surprising the columns with #3 bars failed in this manner. Even though the ties for the columns with the #5 bars were spaced at a smaller bar diameter ratio, it was not sufficient to completely eliminate bar buckling. In spite of bar buckling occurring in several columns, all of the columns reached the computed nominal strength.

Interestingly, the 70-10 columns demonstrated a global stability failure, as evidenced by the essentially zero-slope at failure on the interaction diagram (Figure 4.1 and Figure 4.2). Based on this, one would infer a stiffness failure. These columns, however, ultimately failed rapidly and showed evidence of bar buckling. This behavior indicates the global behavior of the columns weren't necessarily linked to the ultimate localized behavior or failure.

Figure 4.4 illustrates the more ductile stiffness-related failure, which occurred without major bar buckling. This failure occurred in columns with a steeper cross-sectional curvature, which was most prevalent in the columns with higher eccentricity (25%). Columns with a high curvature resist a very high percentage of their compressive force near the edge of the column, particularly outside of the core. As the axial load and curvature increase, the compressive force moves farther to the compressive side of the column. For the columns tested, eventually the concrete began to spall. Once this occurred, the effective cross-section decreased, and this process continued until the spalling reached the core. By this point, the reduced cross-section and ever higher curvature

cause yielding of the tensile reinforcement in some columns, as shown in Figure 4.4(a). In other cases, the reduction in cross-section reduced the net stiffness of the column, and it could no longer resist the applied axial load. As shown in Figure 4.4(b), the ultimate failure was typically minor buckling of the reinforcing bars, extreme deflections, and a reduction in the capacity of the column, after which the test was eventually stopped.

4.5 Evaluation of Design Methodology

The results of the experimental tests were used to evaluate the accuracy of current and proposed design methodology. The load-moment results of the tested columns were compared against the behavior computed using the moment magnification procedure outlined in Section 1.3, using all current and proposed flexural stiffness values, Equations 4.1 through 4.5. The flexural stiffness values were computed using nominal design values for steel strength (60 ksi) and concrete modulus ($57\sqrt{f_c'}$). To provide better comparison between casts, however, the test day, as-measured concrete strengths (f_c'), noted in Table 4.1, were used in the computation due to significant time-dependent strength variations of the different concrete casts. To provide a baseline for the comparison of the results and calculations, the nominal strength was computed with the computation model using the aforementioned material properties.

Figure 4.5 shows a sample comparison of the R5-40-10 column test results as well as the calculations using the moment magnification procedure. The values of interest were considered when the experimental results or calculations passed through the nominal strength curve. In this case, the test results had a capacity of 186.2 kips, and Equations 4.4 and 4.5 had capacities of 178.5 kips and 169.4 kips, respectively.

In addition to the nominal strength, the design strength was also computed using strength reduction factors (ϕ) computed in accordance with ACI 318. The strength reduction factors were applied to the nominal axial and moment strengths. Comparing the results and procedure to design level loads provides a perspective of the accuracy of the equations under lower loads that would be the maximum strength considered in design. Actual service loads, due to load factors, would be even lower.

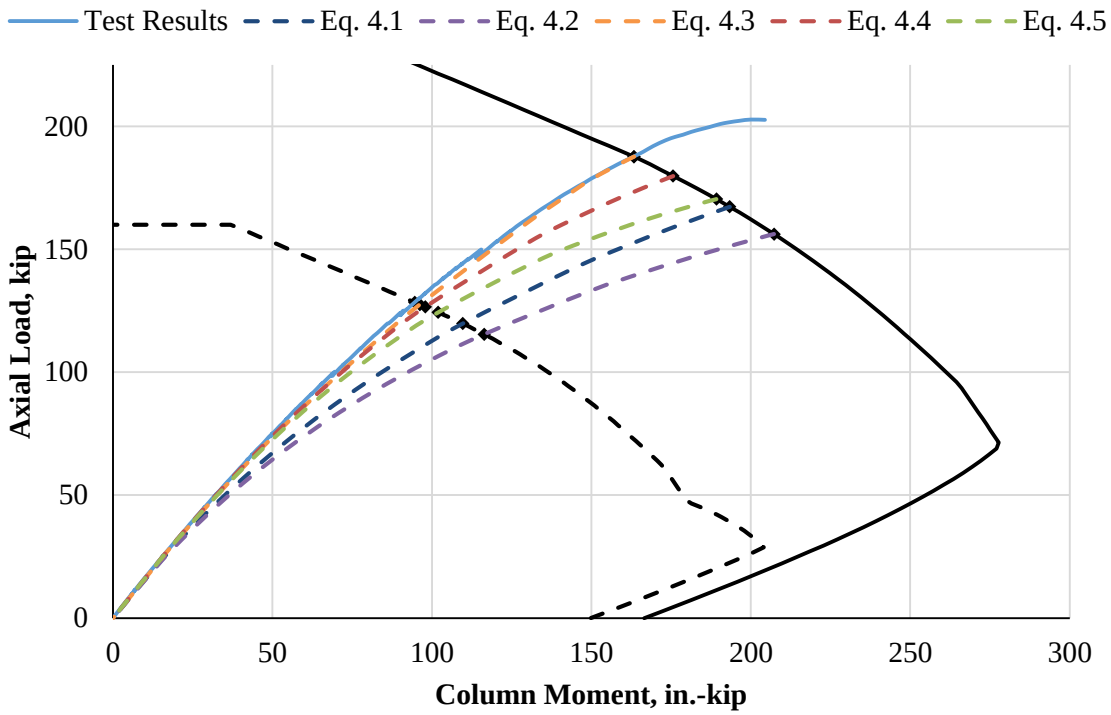

Figure 4.5 – Evaluation of Short-Term Design Equations (R5-40-10)

As shown, the accuracy of the calculations varies significantly. Equation 4.3 was very accurate, though still conservative, and the other equations were less accurate but always conservative. For this particular column, all of the equations computed conservative capacities when compared against the test results, though this was not the case for every column evaluated. As expected, Equations 4.3 and 4.4, which were the most complex and included the most variables, were the most accurate. Equation 4.5 was the next most accurate, while Equations 4.1 and 4.2 were the least accurate. Because this column had a high reinforcement ratio, Equation 4.1 was more accurate than 4.2, but for columns with less reinforcement, the opposite was typically true.

Figure 4.6 shows a summary of the results of the short-term columns with #3 reinforcing bars compared with corresponding calculations based on the aforementioned methods, while Figure 4.7 shows the same comparison for the columns with #5 reinforcing bars. Because Equation 4.1 is only accurate for columns with certain reinforcement ratios and Equation 4.3 was found to be overly complex and possibly unconservative (Jenkins 2011), the results of those equations were omitted from the figures to improve clarity.

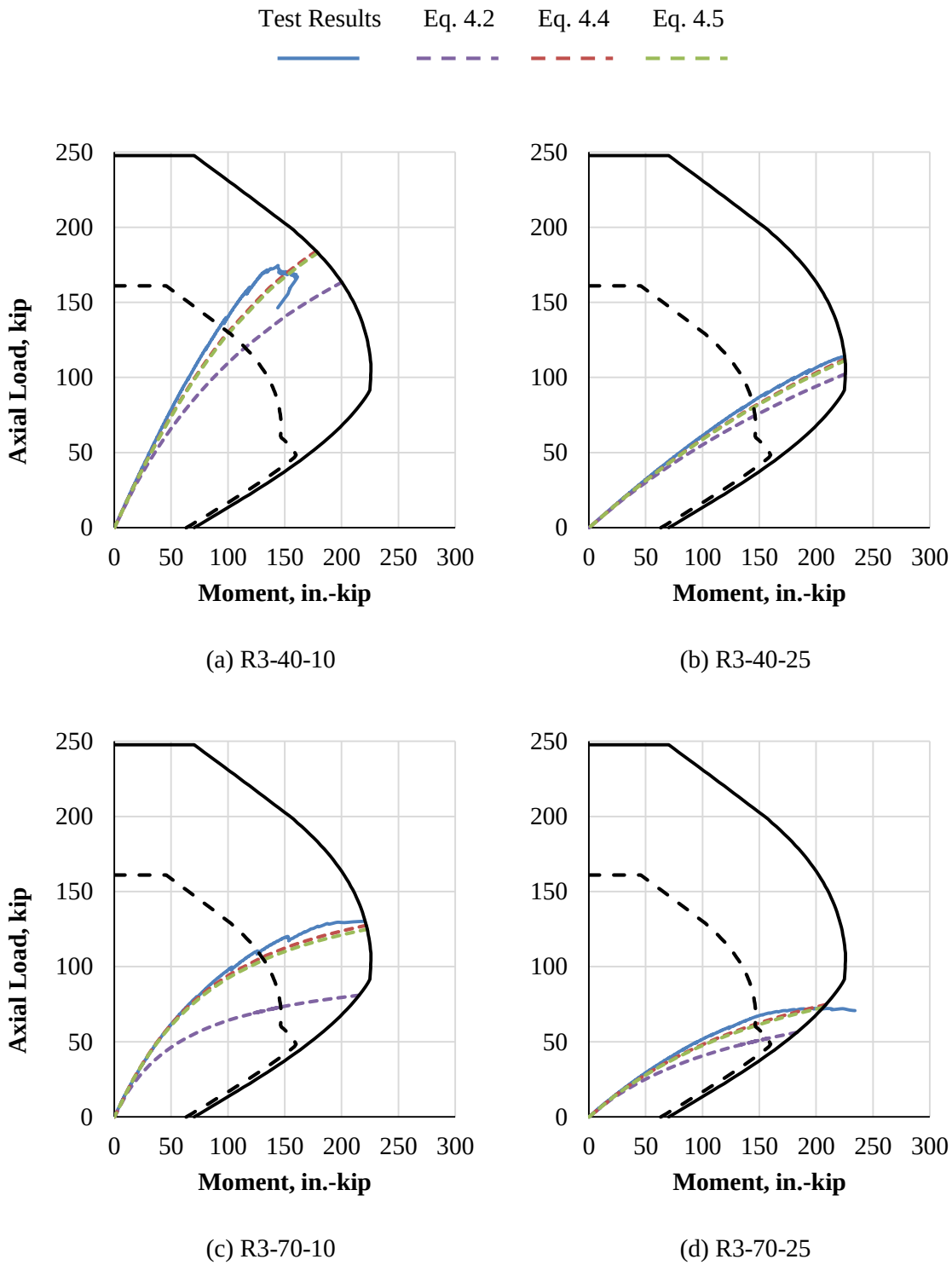

Figure 4.6 – Evaluation of Short-Term Design Equations (#3 bars)

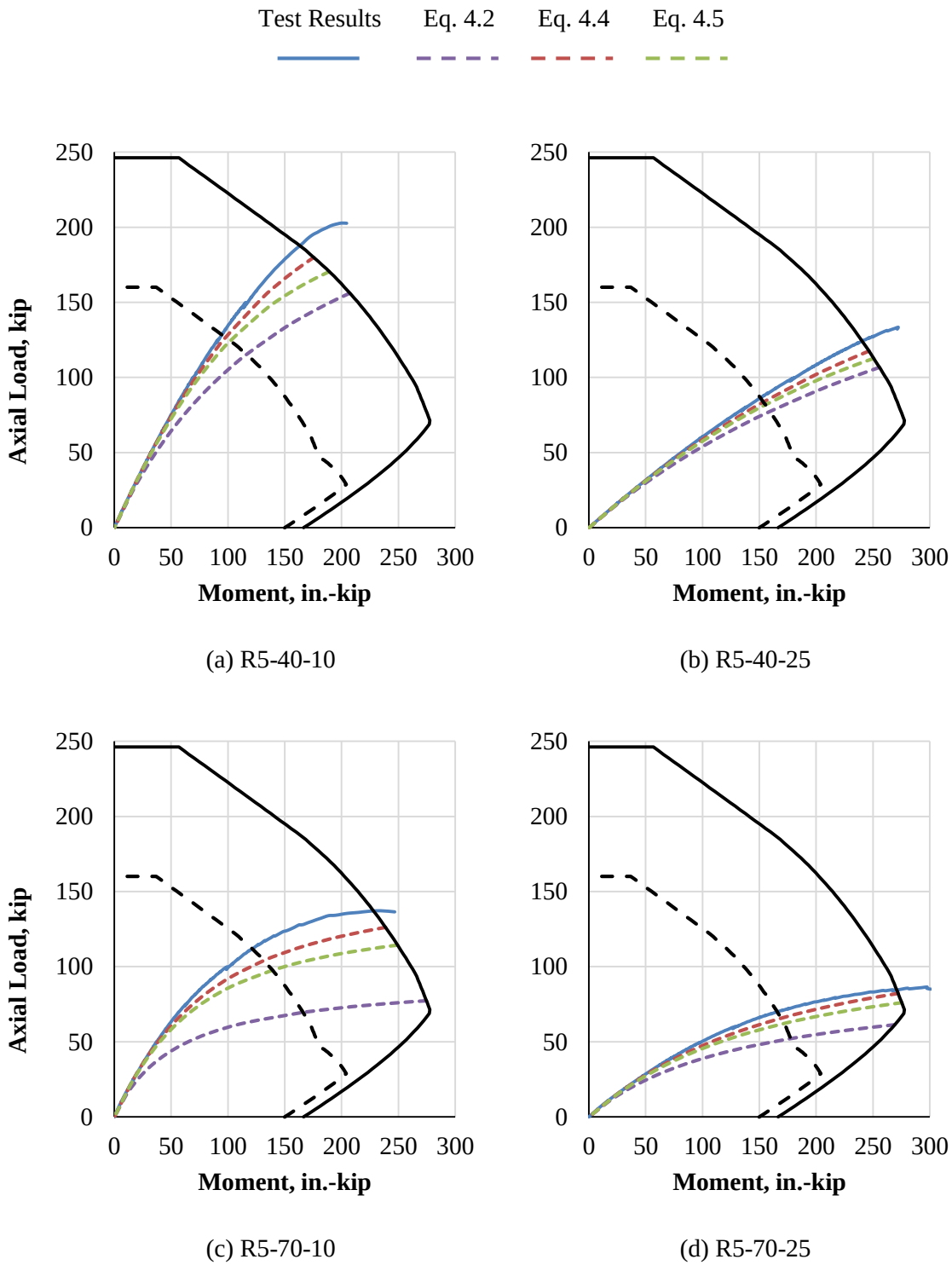

(a) R5-40-10

(b) R5-40-25

(c) R5-70-10

(d) R5-70-25

Figure 4.7 – Evaluation of Short-Term Design Equations (#5 bars)

These figures provide a qualitative examination of the accuracy of the equations for various column types and axial loads. For all columns, Equations 4.4 and 4.5 were more accurate than Equation 4.2, which was anticipated because Equation 4.2 provides a lower bound stiffness that does not vary with axial load. Equation 4.2 is intended to be accurate only near the nominal strength, which is the value of concern for design. Also, Equation 4.4 was consistently more accurate than 4.5, and the difference in accuracy was greater for the columns with #5 reinforcing bars. These comparisons were anticipated based on the respective development of the equations (Jenkins 2011).

Generally, Equations 4.4 and 4.5 showed similar accuracy independent of the axial load, slenderness ratio, and eccentricity ratio. The equations did, however, tend more conservative near ultimate failure. The only comparison of concern for Equation 4.4 and 4.5 were for the 70-25 columns. For these, the test results showed a lower stiffness than the equations under high axial load. For the R3-70-25 column, the difference was enough to provide slightly unconservative calculations. The calculations for Equation 4.4 were 3% unconservative, while the calculations for Equation 4.5 were less than 1% unconservative.

Conversely, the accuracy of the Equation 4.2 varied significantly depending on the slenderness ratio and eccentricity ratio. The equation was more accurate for columns with a higher eccentricity ratio. This was also expected, since a higher eccentricity ratio leads more quickly to a cracked minimum stiffness, which the equation emulates. The equation was the least accurate for the 70-10 columns. Due to the low eccentricity ratio, these columns exhibit few second-order effects until the axial load rises, at which point the behavior quickly changes and the second-order effects greatly increase. Equation 4.2 very poorly estimates this extreme difference in behavior as a function of axial load.

In general, the equations estimated the general behavior accurately. As the axial load increased, the amount of second-order effects correspondingly increased. Equations 4.4 and 4.5 remained more accurate throughout the axial load range, with the exception of R3-70-25. Other than the 70-10 columns, all of the equations showed reasonable accuracy near failure. The calculations were generally conservative, and when not the case, were within 3%. The calculations were more accurate at lowers load, and none were unconservative at design strengths.

4.5.1 Statistical Analyses

While the figures provide a qualitative evaluation of the equations, the results were also compiled statistically to provide a quantitative evaluation. The same calculations and methods of analysis for the figures were used for the statistical analyses, and the values of the capacities were compiled for both nominal and design strengths. Table 4.3 and Table 4.4 present the computed capacities of the nonprestressed, short-term tests at nominal and design strengths, respectively.

Table 4.3 – Short-Term Design Equations at Nominal Strengths (Nonprestressed)

Column ID	Computed Axial Capacity, kip					
	Test	Eq. 4.1	Eq. 4.2	Eq. 4.3	Eq. 4.4	Eq. 4.5
R3-40-10-ST	*	141.3	163.3	182.4	184.0	183.0
R3-40-25-ST	113.7	91.1	102.3	113.2	112.2	111.2
R3-70-10-ST	130.2	61.4	80.9	124.0	127.5	124.9
R3-70-25-ST	72.3	44.8	56.3	77.3	74.8	73.0
R5-40-10-ST	187.7	167.3	156.2	187.6	179.8	170.4
R5-40-25-ST	124.2	112.8	106.7	125.2	117.5	112.7
R5-70-10-ST	137.0	90.5	77.3	133.3	126.1	114.3
R5-70-25-ST	84.9	70.4	61.3	94.7	82.1	76.0

*Test did not reach computed axial strength

Table 4.4 – Short-Term Design Equations at Design Strengths (Nonprestressed)

Column ID	Computed Axial Capacity, kip					
	Test	Eq. 4.1	Eq. 4.2	Eq. 4.3	Eq. 4.4	Eq. 4.5
R3-40-10-ST	134.2	110.4	119.9	129.6	130.2	129.8
R3-40-25-ST	83.8	68.9	74.7	81.3	80.6	80.1
R3-70-10-ST	110.5	58.3	73.1	104.1	106.2	104.6
R3-70-25-ST	66.7	43.6	52.2	63.2	61.7	60.7
R5-40-10-ST	128.4	119.8	115.4	127.5	126.6	124.3
R5-40-25-ST	86.4	80.3	77.4	86.6	83.7	81.8
R5-70-10-ST	112.0	79.3	69.6	105.1	104.1	97.7
R5-70-25-ST	70.1	57.5	52.1	71.3	65.7	62.3

Table 4.5 presents a statistical summary of the capacities for the tested columns at nominal and design strengths. The axial load capacity of the each test result was divided by the axial load capacities computed from the equations for the corresponding strength. As such, a value of 1.0 indicates perfect accuracy, while values greater than 1.0 are conservative and values less than 1.0 are unconservative. The averages and standard deviations of the ratios are listed, which provide a perspective on the accuracy and conservatism of the equations when compared to the tested

columns. For the nominal strength comparison, Column R3-40-10 was omitted because it did not reach nominal strength.

Table 4.5 – Statistical Analysis of Short-Term Design Equations (Nonprestressed)

Analysis		Eq. 4.1	Eq. 4.2	Eq. 4.3	Eq. 4.4	Eq. 4.5
Nominal Strength, S_n	Average	1.42	1.36	0.99	1.03	1.08
	Std. Dev.	0.34	0.23	0.05	0.03	0.06
Design Strength, ϕS_n	Average	1.33	1.28	1.03	1.05	1.07
	Std. Dev.	0.26	0.18	0.03	0.02	0.04

Both the averages and standard deviations vary widely for the different equations. Equations 4.1 and 4.2 are the most conservative with an average of approximately 40% conservative for nominal strengths and 30% conservative for design strengths. These equations were also the least accurate with standard deviations greater than 0.15. As expected, these equations are more accurate and less conservative at design strengths than at nominal strengths.

The results for Equations 4.3, 4.4, and 4.5 were more similar to each other than when compared to the results of Equations 4.1 and 4.2. Equation 4.3 was the least conservative and, the average was unconservative for the nominal strength comparison. For this equation, three of the seven columns considered provided unconservative calculations at nominal strengths, and two of the seven columns were unconservative at design strengths. In fact, the equation calculations for Column R5-70-25 were over 10% unconservative for nominal strength; at design strength, however, the equations calculations were less than 2% unconservative for this column. Note that the 0.75 stiffness reduction factor was used in these computations. Because the measured modulus of elasticity of the concrete was low as a function of concrete strength (approximately $45\sqrt{f_c'}$ to $50\sqrt{f_c'}$), the use of $57\sqrt{f_c'}$ for the modulus in the equations was high, but the stiffness reduction factor brought the equations estimations close to the behavior. This effect illustrates the necessity to account for possible variations in material and geometric properties when computing the column stiffness for estimations of second-order effects.

Equations 4.4 and 4.5 resulted in more conservative results than Equation 4.3 while showing similar accuracy. Each of the equations calculated one column unconservative at nominal strengths, though the calculations were less than 3% unconservative. More importantly, the equations did not calculate any unconservative capacities at design strengths. Equation 4.4 had similar averages when compared to Equation 4.3, but the standard deviations for Equation 4.4

were much lower, showing that the equation has greater accuracy while computing more conservative results. Equation 4.5 had similar standard deviations when compared to Equation 4.3, but the averages for Equation 4.5 were on the order of 5% more conservative. Because this equation is simpler, however, and intended for design, the more conservative results are considered appropriate, especially with similar accuracy maintained.

For Equations 4.4 and 4.5, the averages for nominal strengths and design strengths were similar and varied by less than 2%, showing the equations are more accurate as a function of axial load than Equations 4.1, 4.2, and 4.3, which varied by greater than 3.5%. All five equations showed similar decreases in standard deviations from nominal to design strengths.

4.5.1.1 Slender Column Database

While the previous summary does evaluate the accuracy of the equations, the use of eight columns for the comparison does not provide a confident analysis. Consequently, test results from previous, similar tests were compiled and also evaluated. Only testing programs with very similar methods were used, particularly the use of roller pins or knife edges to load the columns and single-curvature bending with equal end eccentricities. This limitation ensured that the results being compared were not influenced by other variables.

Test results from one additional experimental program on nonprestressed columns was included in the analysis: Lloyd and Rangan (1995). The testing program included 35 columns, all of which were slender as defined by ACI 318. When combined with the current study, this led to 43 columns of varying concrete strengths, slenderness ratios, eccentricity ratios, and reinforcement ratios. Again, all of the columns were tested by very similar methods. Table 4.6 presents a statistical summary of the capacities for the column database at nominal and design strengths. When evaluating the computed axial capacity, the column was ignored if the test did not reach the computed axial nominal or design strength. Several columns did not reach the computed nominal strength, and one column did not reach the computed design strength. Appendix C provides a summary of the columns tests as well as the test results and computed capacities at nominal and design strengths.

Table 4.6 – Statistical Analysis of Short-Term Design Equations (Column Database)

Analysis		Eq. 4.1	Eq. 4.2	Eq. 4.3	Eq. 4.4	Eq. 4.5
Nominal Strength, S_n	Average	1.41	1.18	0.91	0.98	1.00
	Std. Dev.	0.45	0.29	0.14	0.11	0.12
Design Strength, ϕS_n	Average	1.28	1.14	0.97	1.01	1.02
	Std. Dev.	0.30	0.18	0.08	0.05	0.06

The results of this analysis are similar to those based solely on the tests from this study. Equations 4.1 and 4.2 were excessively conservative with standard deviations twice that of the other equations. Equation 4.2 was less conservative than the previous comparison because the average reinforcement ratio of the total dataset was less than the average reinforcement ratio of the tests from this study. Because Equation 4.2 is a lower bound estimation that is accurate for low reinforcement ratios, it is reasonable it would be more accurate for columns with a lower reinforcement ratio. Equation 4.1 had similar conservatism as the previous evaluation but larger standard deviations. Because Equation 4.1 accounts for the effect of reinforcement, the conservatism should be similar, but with wider ranges of applied load eccentricity and column slenderness, the standard deviations increased compared with the previous analysis.

The conservatism for Equations 4.3, 4.4, and 4.5 decreased when all of the tests were evaluated. For nominal strengths, Equation 4.3 was nearly 10% unconservative, but the equations was only 3% unconservative at design strengths. Additionally, the standard deviations for Equation 4.3 nearly tripled compared to the previous evaluations. Equations 4.4 and 4.5 had similar increases in standard deviations; Equations 4.4 and 4.5, however, were more conservative than Equation 4.3. At nominal strengths, Equation 4.4 was 2% unconservative, and Equation 4.5 was near unity. At design strengths, Equations 4.4 and 4.5 were 1% and 2% conservative, respectively. In addition to being safer, the standard deviations of Equations 4.4 and 4.5 were less than those of Equation 4.3. Surprisingly, Equation 4.5 produced a lower standard deviation than Equation 4.3 even though the equation is simpler. This result is the opposite from the previous evaluation, which only included results from the tests from this study.

4.5.2 Effects of High-Strength Reinforcing Bar

When compiling the results of these comparisons, an important discrepancy was noted for Equations 4.3 and 4.4. Both equations are a function of the nominal axial strength (P_0) but these equations were calibrated as a function of cross-sectional stiffness and not axial strength. When using the nominal strength of the reinforcing steel, the equations showed accurate and relatively

conservative results. If the actual strength of the reinforcing steel was used, though, the equations showed results that were less conservative. A practical view of these equations would infer that using actual material properties would increase their accuracy, which was found not to be true. This discrepancy is also important for the use of higher strength reinforcing steel, towards which the industry is moving. The effects is illustrated as follows.

First, Figure 4.8 shows the results from the computational model, which used the as-measured, test-day material properties. The results include the R5-40-10 and R5-70-25 columns, which bounded the behavior of the other columns. The columns with #5 bars were chosen because a higher reinforcement ratio exacerbates the effect. Behavior was computed for the columns assuming reinforcement yield strengths of 60 ksi, 80 ksi, and 100 ksi, which are typical and proposed grades of reinforcing bar. As shown, the difference in behavior is very minimal, beyond the nominal strength. For the 40-10 column with 60 ksi reinforcing steel, the behavior deviates from the other columns immediately before failure, which is when the bar begins to yield. Other than that difference, the behaviors are qualitatively identical for all columns.

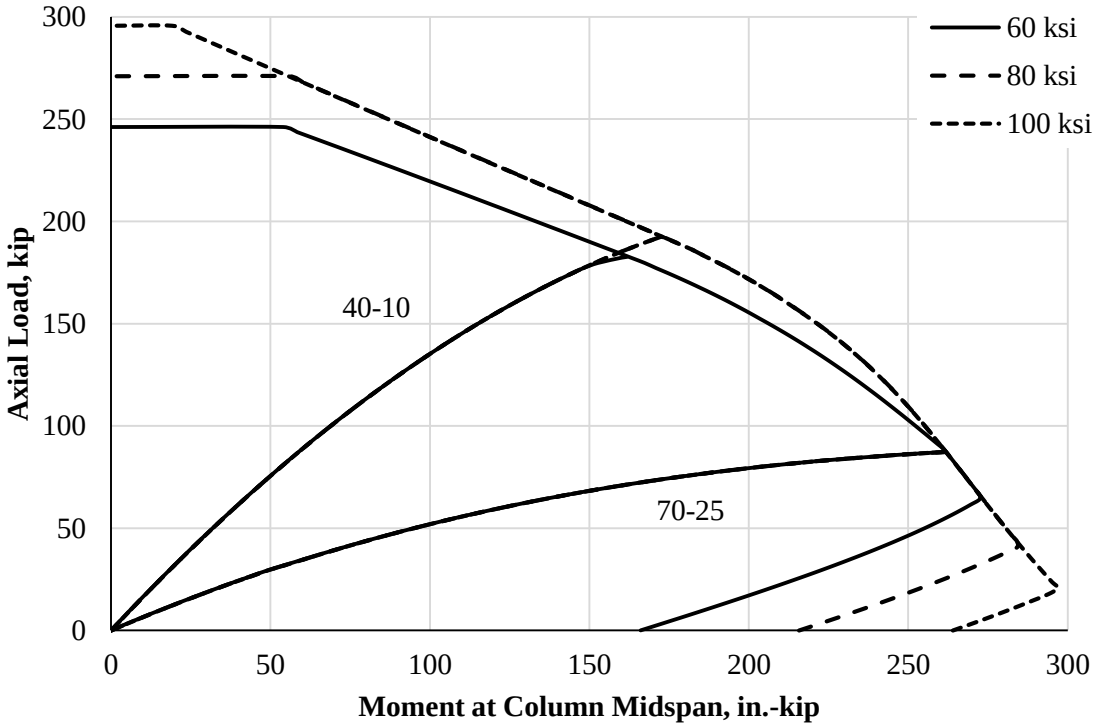

Figure 4.8 – Effect of High-Strength Reinforcing Bar (Computational Model)

The strengths for the columns with 80 ksi and 100 ksi reinforcing steel are identical for a large portion of the compression-controlled region of the interaction diagram. Identical strengths result based on the definition of the nominal strength. In the computational model, the concrete is assumed to fail at a strain of 0.003. Reinforcement with a yield strength of 80 ksi yields at a strain of approximately 0.0027. Because of the curvature of the cross-section under moment, the steel is at a lower strain than the concrete at the maximum compressive stress face of the section, which is assumed as 0.003. As a result, the 80 ksi reinforcing steel does not yield except for sections with very little applied moment. For 100 ksi reinforcement, the strain is similarly limited to 0.003 at the maximum compressive face, resulting in the same strain in the reinforcement and corresponding stress, which again is in the elastic range. As a result, the same column strengths are computed, in this range, for columns with these different reinforcement strengths.

From the results of the computational model, it is clear that reinforcement strength does not affect the behavior of the columns. Figure 4.9 shows the same comparisons when using Equation 4.4. For the computations, the 0.75 stiffness reduction factor was omitted from the moment magnification procedure, and the as-measured-test-day modulus of elasticity was used.

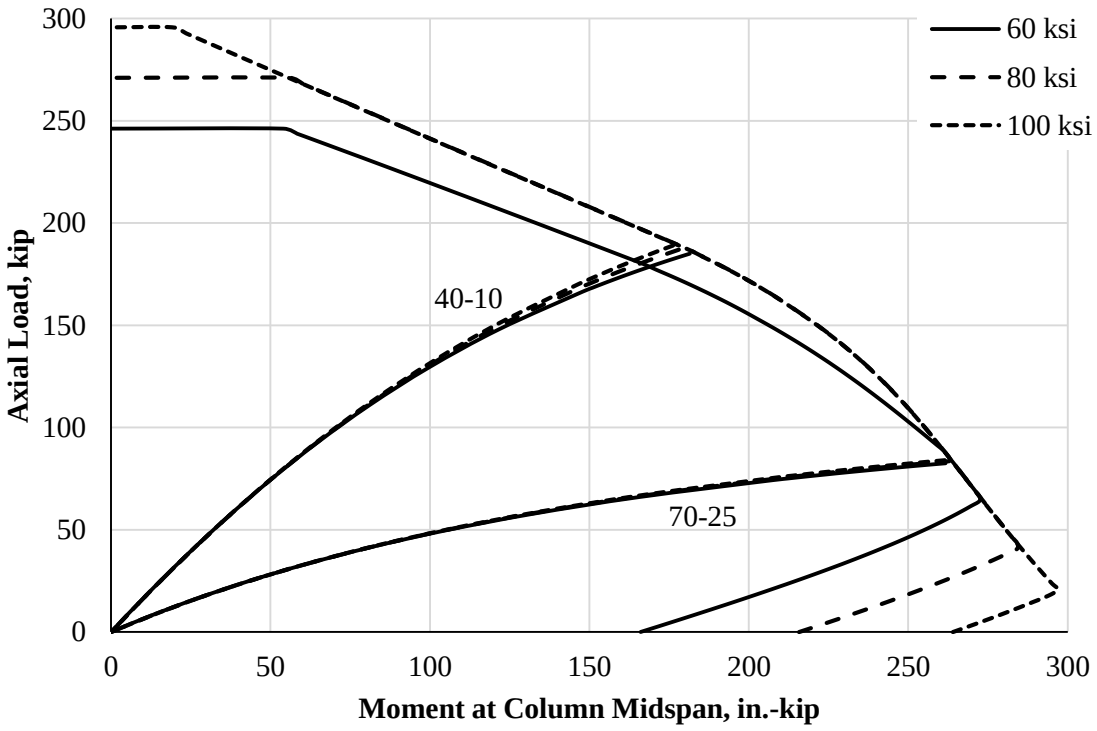

Figure 4.9 – Effect of High-Strength Reinforcing Bar (Equation 4.4)

When using Equation 4.4, the differences in behavior are noticeable, particularly for the 40-10 columns. With an increase in reinforcement strength, the stiffness of the column increases, resulting in lower moments for a given axial load. As shown by the computational model, this change in stiffness due to the use of a higher strength steel should not occur. For reinforcement with a yield strength greater than 60 ksi, the flexural stiffness is overestimated because of the use of the nominal axial strength (P_0) in the calculations. It should be noted that these equations were developed specifically considering reinforcement with a yield strength of 60 ksi.

As a result, the application of these equations should be modified to require the computation of the nominal axial strength (P_0) to use a reinforcing steel strength of 60 ksi, independent of the actual or nominal strength of the reinforcing bars. This difference need only be applied when computing the flexural stiffness (EI) of the columns and not when computing the nominal or design strength of the columns. Alternatively, the computation of the nominal axial strength can be modified for use in the equation to have a reduction factor for high-strength steel.

4.6 Findings

Eight slender columns were tested under shot-term loading to failure. The results were compared against a computational model as well as current and proposed design equations. The columns varied in concrete strength, slenderness ratio, eccentricity ratio, and reinforcement ratio. In addition, similar, historical tests were included and compared against the design equations. Based on the results of the tests and their comparison to analysis and design methods, the following conclusions were made.

1. The computational model estimated the behavior and capacity of all columns similarly. The accuracy of the computed behavior was very similar for varying slenderness ratios and eccentricity ratios. The model was consistently stiffer than the test results for the #5 columns, while the stiffness relation varied for the #3 columns. The computed failures loads were more accurate than the computed failure deflections. The computation model estimated the behavior of a few columns unconservatively, but the computed strength was conservative for every column when viewed in the context of an interaction diagram.
2. The tested columns exhibited two different failure types: bar buckling and local stiffness failure. In general, the columns with the lower eccentricity ratio were subject to bar buckling, while the columns with higher eccentricity ratio were subject to a stiffness failure. The type of failure was independent of the global behavior and failure. Except

for one column with end damage, all of the columns failed within one tie group of the column midspan.

3. Five of the eight tested columns exceeded the ACI 318 second-order limit of 1.4 times the first-order effects. Even after exceeding this limit, all of the columns had at least 10% additional residual strength while some of the columns had up to 80% additional residual strength. Though several columns approached or surpassed zero stiffness, the computational model and the equations estimated the overall behavior accurately.
4. The current and proposed design methods varied widely in accuracy and conservatism when compared to current and previous test results. Equations 4.1 and 4.2 were less accurate but more conservative than the other equations. Equation 4.3 computed a higher percentage of unconservative results when compared to Equations 4.4 and 4.5. Equations 4.3 and 4.4 were more accurate than Equation 4.5 for the tests in this study, but Equations 4.4 and 4.5 were more accurate than Equation 4.3 was all of the tests results were considered. Equation 4.5 was consistently more conservative than Equations 4.3 and 4.4. Equations 4.4 and 4.5 maintained more accuracy as a function of nominal or design strength when compared to Equations 4.1, 4.2, and 4.3. Equation 4.4 was the most accurate equation, while the standard deviations for Equations 4.1 and 4.2 were at least twice that of the other equations.
5. Equations 4.3 and 4.4 were found to be inaccurate for columns with reinforcement strengths different than 60 ksi. Specifically, the equations became less conservative for increasing reinforcement strengths. This effect is caused by the use of the nominal axial strength (P_0) in the equations for the flexural stiffness. Because the reinforcing bar strength does not affect column stiffness, it should be removed from the computations. As such, only when used to calculate the column flexural stiffness (EI), the nominal axial strength (P_0) should be computed with a reinforcing bar strength of 60 ksi, regardless of the strength of the bar used in the column.

CHAPTER 5 SHORT-TERM BEHAVIOR OF PRESTRESSED COLUMNS

5.1 Introduction

The ACI 318 Building Code (2014) provides significant guidance for the design of nonprestressed concrete columns; but few provisions exist for prestressed columns, and no provisions exist for slender, prestressed columns. Furthermore, few experimental results exist for prestressed concrete columns, especially those that are slender. Twelve short-term tests of slender, prestressed columns were conducted. The loading and geometric parameters were similar to the nonprestressed columns, but the columns were prestressed with three different arrangements of steel. The results of the short-term tests were compared against design equations recommended by the PCI Design Handbook (2010) as well as other equations intended for nonprestressed columns. The results of these tests are also used to evaluate the accuracy of a computational model in estimating prestressing effects on the short-term behavior of slender columns. Increased confidence in the computational model allows for the development of improved design procedures for slender, prestressed columns as outlined in Chapter 6.

5.2 Existing Design Methodology

As mentioned, ACI 318 (2014) includes little guidance on the design of prestressed columns. Most of the provisions provide for the definition of a prestressed column and specify its detailing requirements. In general, columns with an average compressive stress greater than 225 psi, due to effective prestressing force only, do not require the typical, minimum, longitudinal reinforcement. Transverse reinforcement requirements are also modified by eliminating the 16 bar diameters spacing requirements. This limit generally defines a prestressed column, and all columns constructed for this experimental program would be classified as prestressed columns according to this definition.

Designers typically refer to the PCI Design Handbook for the design of prestressed construction. The Handbook is not a code but provides guidance on design that is in accordance with ACI 318. Because most prestressed columns do not satisfy the minimum longitudinal steel requirements of

ACI 318, the Handbook states the use of the moment magnification procedure, particularly Equations 4.1 through 4.5, is generally not recommended. The Handbook suggests designers use elastic, second-order elastic analysis, but as discussed in Chapter 1, this analysis is typically only satisfactory for the sway effects of frames, not second-order effects due to moment magnification between the column ends. Consequently, the PCI Committee on Prestressed Concrete Columns (1988) provided an alternative method of design. This method, summarized by the following equations, computes a flexural stiffness for use in the moment magnification procedure outlined in ACI 318. It should be noted that Equation 7.4 corresponds to a cross-section without a compression flange.

$$EI = E_c I_g / \lambda \qquad \text{(Eq. 7.1)}$$

$$\lambda = \eta\theta \geq 3.0 \qquad \text{(Eq. 7.2)}$$

$$\eta = 2.5 + \frac{1.6}{P / P_0} \qquad \text{(Eq. 7.3)}$$

$$\theta = \frac{27}{kl_u / r} - 0.05 \qquad \text{(Eq. 7.4)}$$

where:

$6 \leq \eta \leq 70$

A_{pt} = total area of prestressing reinforcement, in.^{2}

$E_c = 57,000\sqrt{f_c'}$ psi = modulus of elasticity of concrete, psi

E_p = modulus of elasticity of prestressing reinforcement, psi

f_{se} = effective stress in prestressing reinforcement, psi

I_g = moment of inertia of gross concrete section, in.^{4}

l_u = unsupported length of compression member, in.

P = axial force, lb

$P_0 = 0.85 f_c'\left(A_g - A_{pt}\right) - \left(f_{se} - 0.003E_p\right)A_{pt}$ = nominal axial strength, lb

r = radius of gyration of gross cross-section, in.

The Committee explains that these equations, developed by and based on an analytical study, are recommended if using the moment magnification procedure in ACI 318. It should be noted that the calculation of the nominal axial strength (P_0) is different from that for the nonprestressed columns. Also, the calculation assumes only prestressed reinforcement is included, or in other words, the use of nonprestressed reinforcement and ducts are not included.

5.3 Experimental Program

Twelve short-term tests were conducted on columns with prestressed reinforcement. Table 5.1 shows a detailed summary of the tests. Three different prestressing arrangements were tested and the cross-sectional geometries and loading details were identical to the nonprestressed columns. The concrete for the columns with four wires was from Cast 3, and the concrete for the columns with two and six wires was from Cast 4.

Table 5.1 – Summary of Short-Term Tests (Prestressed Columns)

Column ID	Reinforcement	Slenderness Ratio, kl_u / r	Eccentricity Ratio, e / h	f_c' on Test Day, psi	E_c, on Test Day, ksi
P2-40-10-ST	2 – PS Wires	40	10%	6570	3820
P2-40-25-ST			25%	6570	3820
P2-70-10-ST		70	10%	6570	3820
P2-70-25-ST			25%	6570	3820
P4-40-10-ST	4 – PS Wires	40	10%	6370	4010
P4-40-25-ST			25%	6370	4010
P4-70-10-ST		70	10%	6370	4010
P4-70-25-ST			25%	6370	4010
P6-40-10-ST	6 – PS Wires	40	10%	6570	3820
P6-40-25-ST			25%	6570	3820
P6-70-10-ST		70	10%	6570	3820
P6-70-25-ST			25%	6570	3820

As described in Section 2.5, an offset strain (ε_{si}) was required to calibrate the computational model to include the effect of prestressing. Table 5.2 shows the results of two methods to obtain the offset. Both methods were referenced at a concrete age of 140 days, which was the average age of concrete for the tests.

Table 5.2 – Effective Prestressing Losses

Column and Method		Total Losses, ksi	f_{se}, ksi	f_c, psi	E_c, ksi	ε_{si}, με
2 – PS wires	Calculations	23.6	172.6	317	3820	6030
	Strain Gages	24.4	171.9	316	3820	6010
4 – PS wires	Calculations	31.4	164.8	607	4010	5830
	Strain Gages	38.7	157.5	580	4010	5580
6 – PS wires	Calculations	39.2	157.0	869	3820	5640
	Strain Gages	43.1	153.1	847	3820	5500

First, the total losses were computed using calculations outlined in Appendix A. From those results, the offset strain was calculated as summarized in Section 2.5. In addition, the total losses were recorded using the strain gages attached to the prestressing wire and the offset strain was recalculated. Due to the violent nature of releasing prestressed wires, several of the strain gages failed and others showed apparently erroneous results. Because of this, the strain gage values were selected with engineering judgment, and the selected values were averaged. As shown in the table, the two methods had similar results, particularly for the two and six prestressing wire columns. Because of the judgment required to select the strain gage measurements and the simplicity and repeatability of the calculations, the results from the calculations were used for the offset strain in the computational model.

5.4 Experimental Results

The results of the short-term tests were summarized in load-deflection and interaction diagram figures. The interaction diagram figures include the computed nominal strength, which used the as-measured, test-day material properties of the concrete and prestressing steel. The load-moment figures also include the behavior of short columns, which represents the first-order moment as well as ACI 318 total moment limit (1.4 M_0). The figures show the results of the short-term tests (solid lines) as well as the estimates of behavior from the computation model (dashed lines).

Figure 5.1 shows the results of the tests on the columns with two prestressing wires. Compared to the results of the nonprestressed short-term tests, the estimations by the computational model were less accurate. Except for moderate loads on the P2-40-10 columns, the model estimated less stiff column behavior, which can be considered a conservative estimation. The model also estimated conservative failure loads, with the model estimating the columns up to 20% conservatively. The estimated failure deflections, however, were more accurate. While the deflection estimate for the P2-70-25 column was unconservative, all of the estimated failure deflections were consistent.

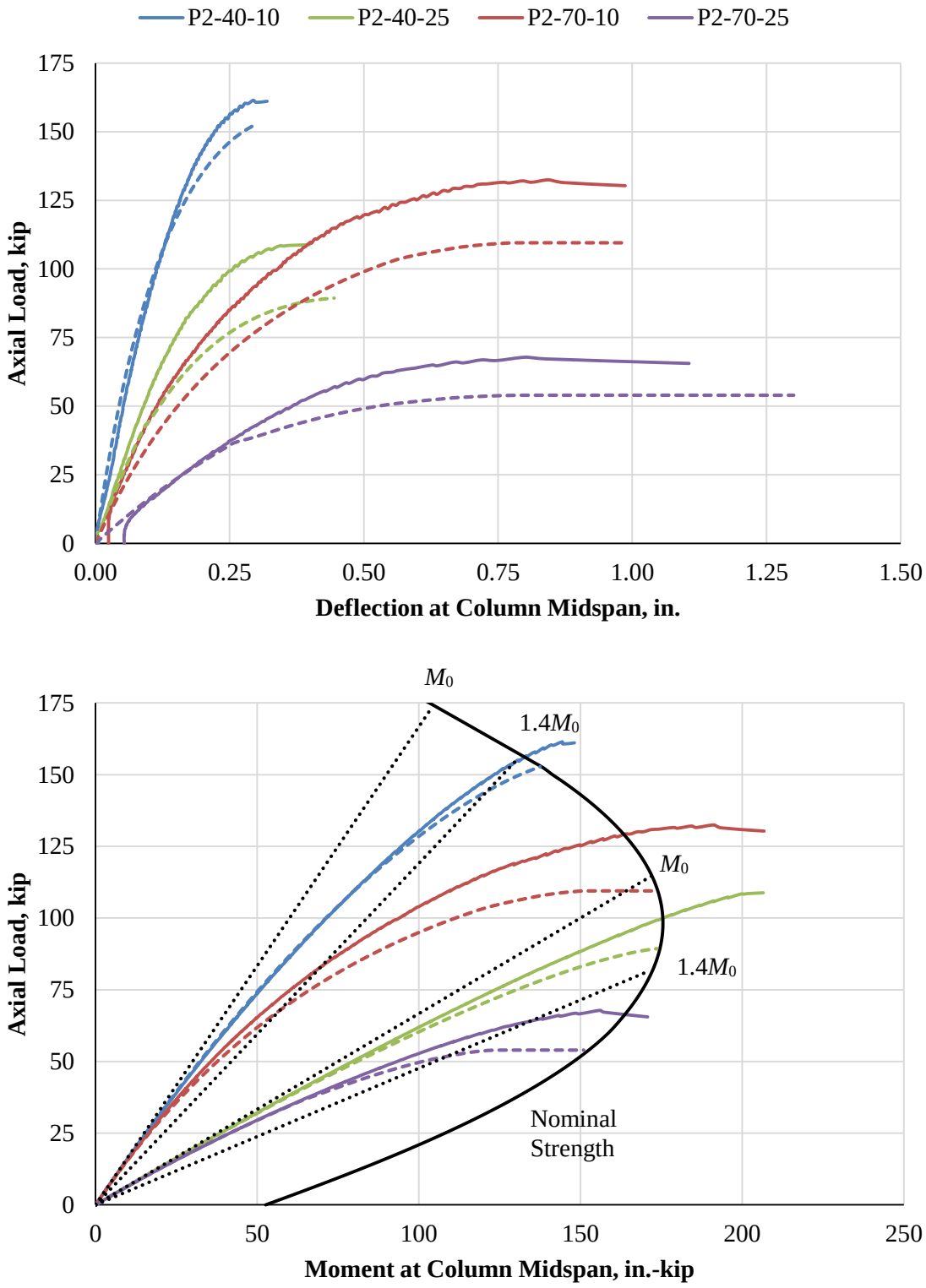

Figure 5.1 – Short-Term Tests Results (2 – PS Wires)

The model estimated the nominal strength conservatively for all four columns. For the P2-40-25 and P2-70-10 columns, the failure moment was much higher than the computed nominal strength, but the P2-70-10 columns approach global instability once it exceeded the nominal strength. Only two of the columns, the P2-70 columns, exceed the ACI 318 total moment limit, while the P2-40-10 column met the limit at the nominal strength level. Compared to the nonprestressed short-term tests, the P2 columns showed less second-order effects at failure.

Figure 5.2 shows the results of the short-term tests on the columns with four prestressing wires. The computation model estimations were more accurate for these columns compared to the P2 columns. The estimations of peak load were within 12%, and the failure deflections were similarly accurate. The capacity of the columns at nominal strengths, however, were estimated more closely than for the P2 columns. The error in peak failure load estimates were a result of the conservatism of the nominal strength estimations, not differences in behavior of the columns. The P4-40 columns were estimated less stiff than the experimental tests, and the P4-70 columns were estimated less stiff under high loads, similar to the comparisons for the P2 columns.

The nominal strength was estimated conservatively for all four columns and was more accurate than for the P2 columns. Also similar to the P2 columns, the P4-70 columns experienced global instability near failure. As before, only two columns exceeded the ACI 318 total moment limit, while the P4-40-10 column met the limit near failure. With the exception of the P4-70-10 columns, the load-moment estimates were accurate, even at near-failure load levels.

Figure 5.3 shows the results of the short-term tests on the columns with six prestressing wires. The comparison to the computational model was more similar to the P2 columns than the P4 columns. Note that the P2 and P6 columns were cast at the same time with the same concrete, while the P4 columns were part of a different cast. While this should not affect the model since the material properties were measured for each cast, there are some errors and differences that are possible that could have affected the comparisons. The model estimated less stiff column behavior for all six wire columns under all axial loads. Three of the four failure deflections were estimated unconservatively. The failure loads were estimated conservatively with less than 21% error.

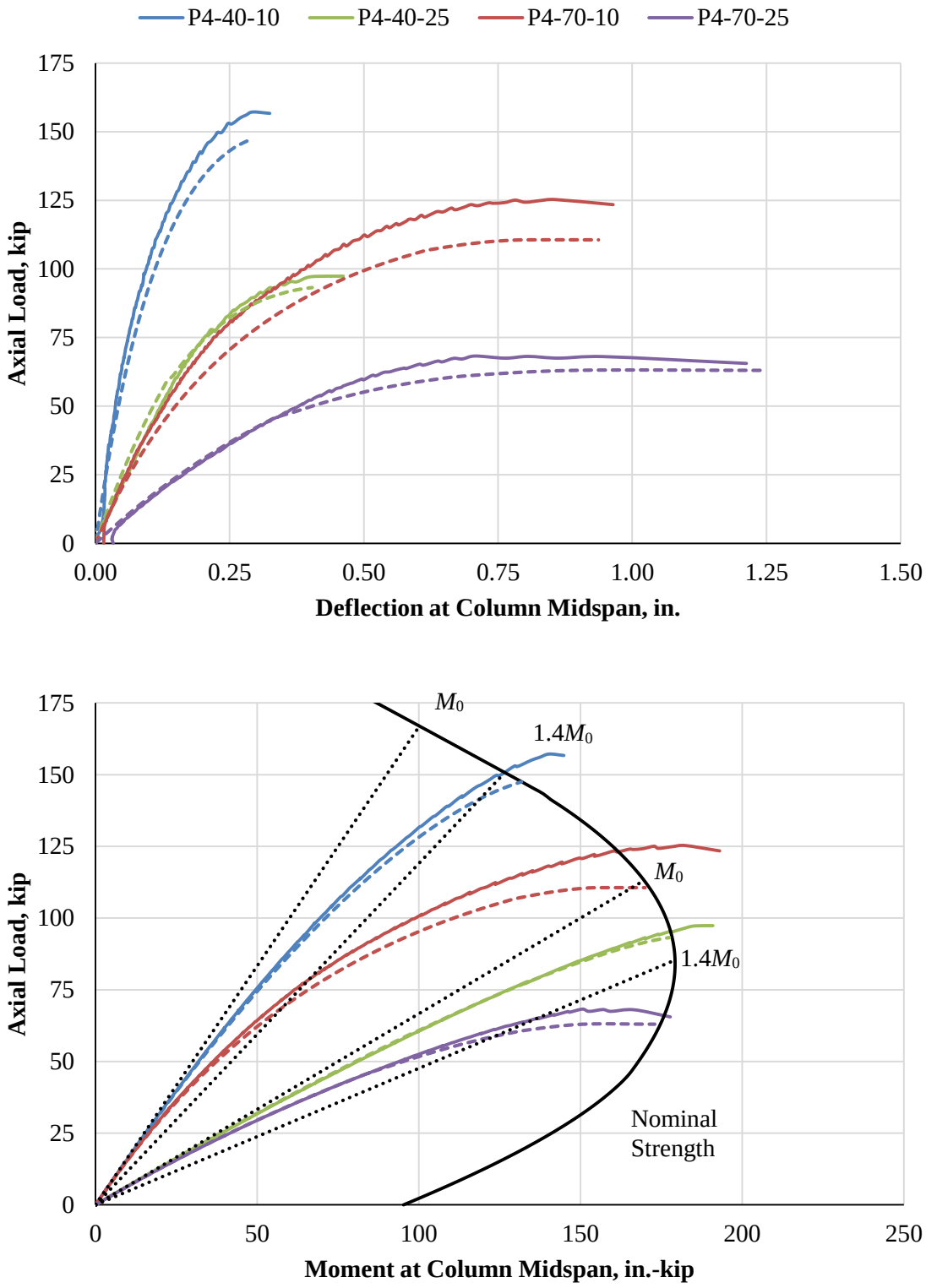

Figure 5.2 – Short-Term Tests Results (4 – PS Wires)

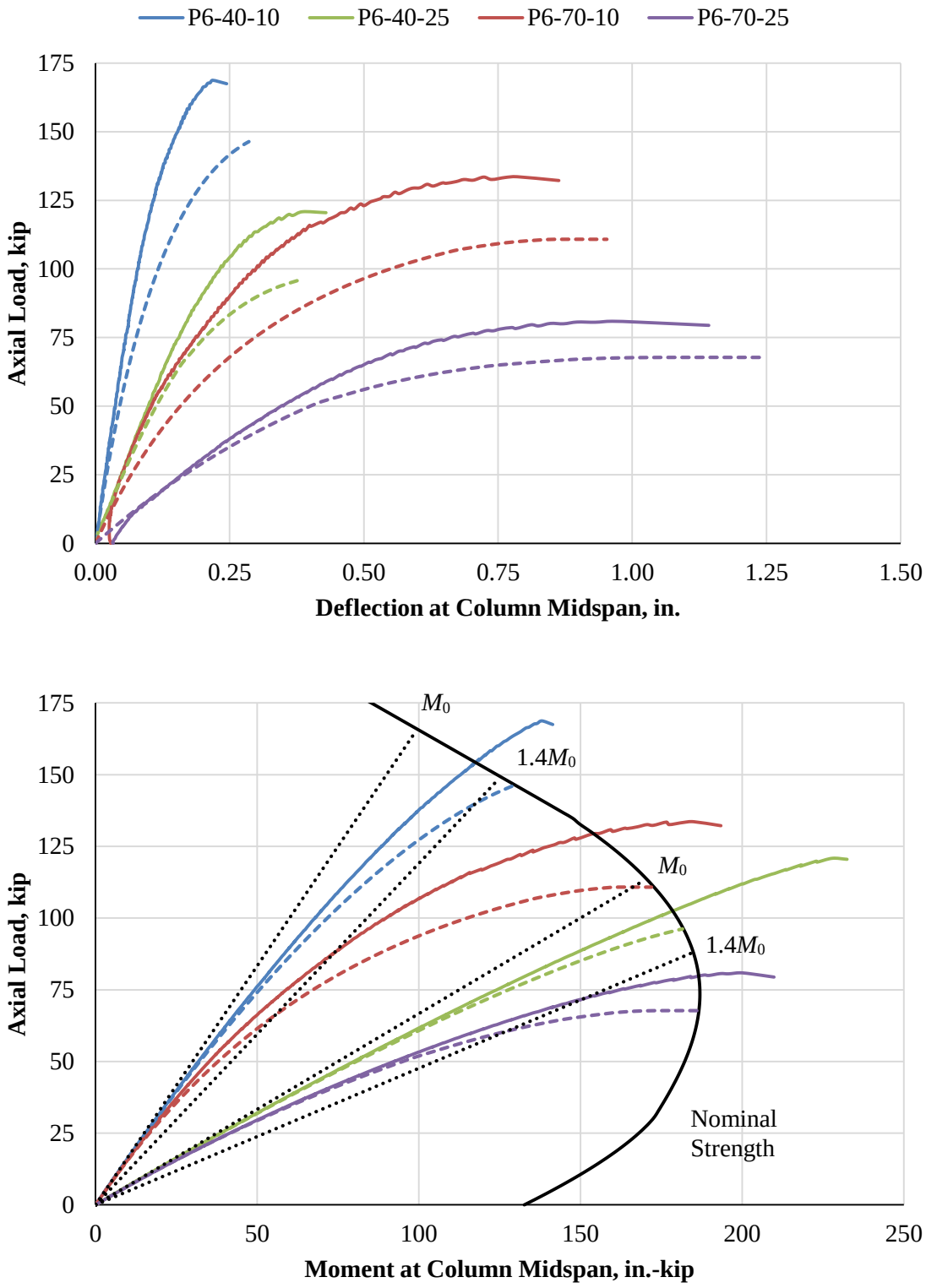

Figure 5.3 – Short-Term Tests Results (6 – PS Wires)

The nominal strength was estimated conservatively for all four columns but was less accurate than when compared to the P2 and P4 column strengths. The P6-40 columns showed greater axial load and moment strength at failure relative to the computations, while the P6-70 columns showed greater moment strength but experienced global instability near failure. Two columns exceeded the ACI 318 total moment limit, as before, but the P6-40-10 column did not reach the limit at failure. In general, the load-moment estimations were accurate but diverged near failure, particularly for the P6-70 columns.

Figure 5.4 (a) shows a load-moment comparison of the experimental results for the P2 (dashed lines) and P6 (solid lines) columns, while Figure 5.4 (b) shows the comparison of estimates from the computation model. These are the same results and model estimates shown in Figure 5.1 and Figure 5.3. Because the P4 columns were part of a different concrete cast, they were excluded from this comparison to provide a more consistent evaluation and illustrate the range of the tested prestressing ratios.

The amount of prestressing steel had a minor effect on the stiffness of the columns, particularly at moderate loads. When looking at the experimental results, the P6-40-10 column was stiffer than the P2-40-10 column and failed at a higher load. When looking at the computational model, however, the opposite is true, though the difference is minimal. This indicates that the difference in behavior is likely inconsequential for columns with low slenderness and eccentricity, and possible errors and tolerance in the experimental tests accounted for the difference in the experimental tests results.

For the 40-25 and 70-10 columns, the differences in behavior were even less for both the experimental and computational model results. The only difference between these column behaviors' was the computed nominal and experimental strength of the columns. For the 70-25 columns, the P6 columns compared with the P2 columns were both stiffer, particularly at higher loads, and had higher failure moments and axial loads.

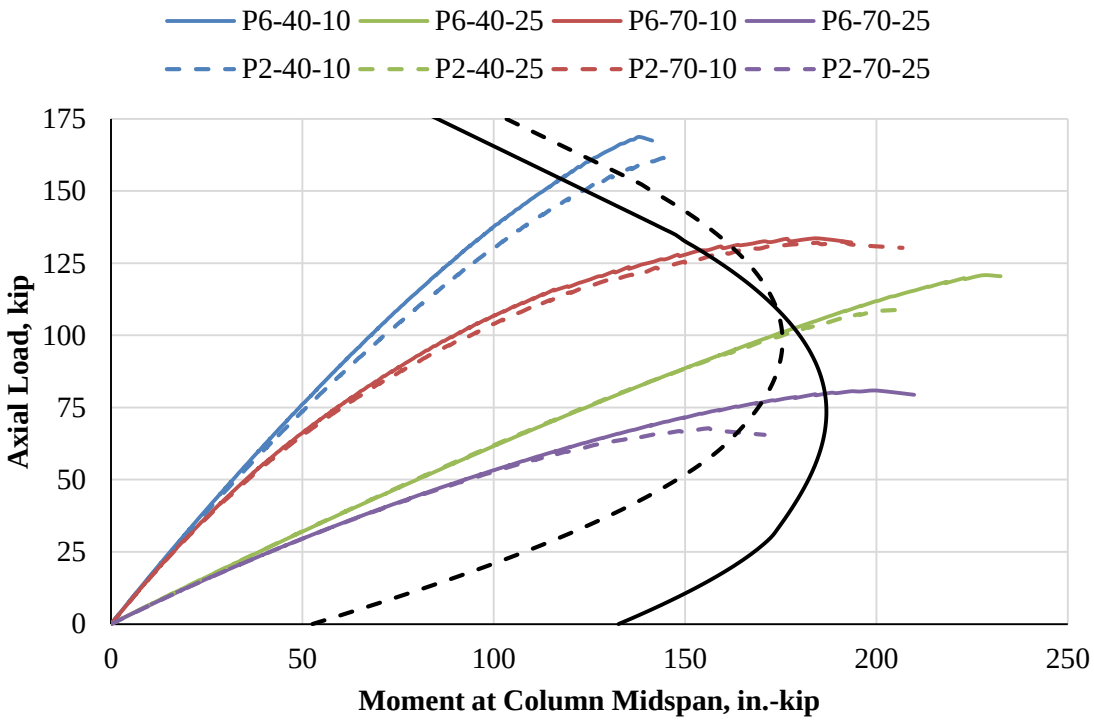

(a) Experimental Tests Results

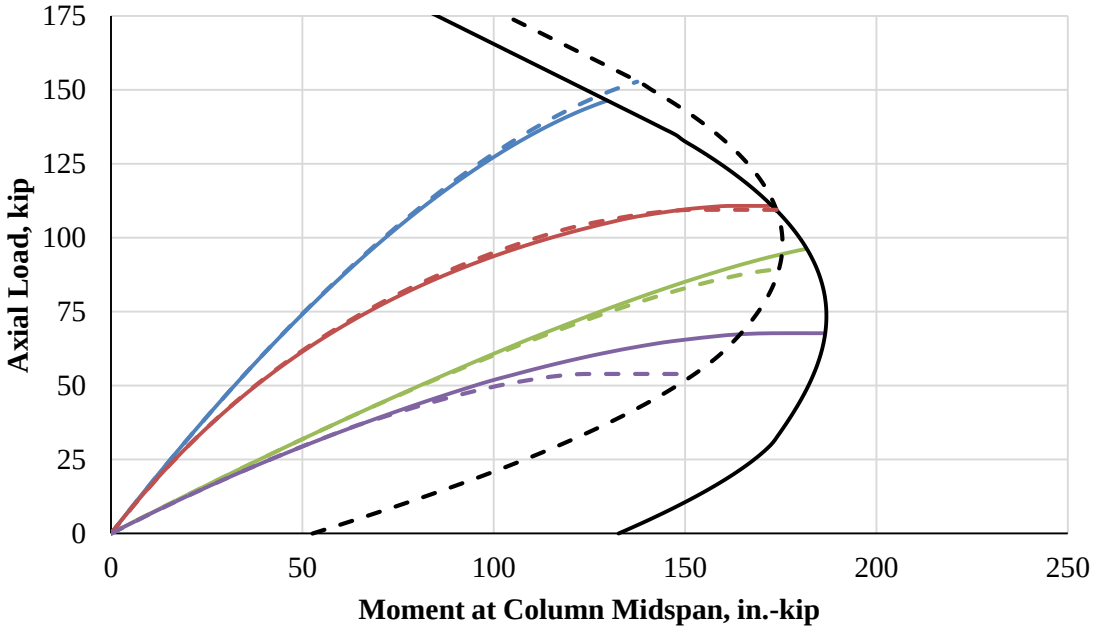

(b) Computational Model Results

Figure 5.4 – Effect of Prestressing Ratio on Column Behavior and Strength

These differences in behavior can be explained by the effect of prestressing force on the column cross-section. With more prestressing force, the axial load capacity of the columns with higher axial failure loads decreases due to the applied forces of the prestressing, evidenced by the difference in the strength curves. Due to the small amount of steel stiffness, however, the prestressing barely affects the behavior of the column. For columns with lower axial failure loads, the effect of prestressing is opposite. This change in effect occurs near the maximum moment region of the nominal strength, which is the location that the column changes from compression controlled to tension controlled. Here, the P6 columns have a much higher moment strength, and tend to have a slightly higher stiffness, particularly for the 70-25 columns. At zero axial load, the moment strength is nearly three times as high, which is to be expected because there was three times as much steel.

Table 5.3 provides a summary of the peak axial load during the experimental tests as well as the corresponding failure loads estimated by the model. The ratio of the peak test load to the computed load is also included, which illustrates both accuracy and conservatism. All of the columns were estimated at least 5% conservative. The estimations for the P4 columns were, on average, less conservative than the other columns. Because these columns were part of a different cast, the discrepancy may be due to material variability. In general, the behavior of the columns was estimated reasonably well, and the nominal strength estimations were conservative.

Table 5.3 – Summary of Short-Term Tests Results (Prestressed)

Column ID	Peak Test Load, kip	Computed Failure Load, kip	P_{test} / P_{model}
P2-40-10-ST	162.0	152.8	1.06
P2-40-25-ST	109.3	89.3	1.22
P2-70-10-ST	132.6	109.5	1.21
P2-70-25-ST	67.9	53.9	1.26
P4-40-10-ST	157.3	147.5	1.07
P4-40-25-ST	97.9	93.2	1.05
P4-70-10-ST	125.6	110.6	1.14
P4-70-25-ST	68.2	63.0	1.08
P6-40-10-ST	169.5	146.4	1.16
P6-40-25-ST	121.1	96.2	1.26
P6-70-10-ST	134.1	110.8	1.21
P6-70-25-ST	81.2	67.7	1.20

As mentioned previously, the computational model was less accurate for the prestressed columns compared to the nonprestressed columns. One possible reason for this discrepancy is illustrated by Figure 5.5. The results from the experimental tests as well as the computational model are shown for two representative columns: P4-40-10-ST and P4-70-10-ST. The computational model was used to estimate the behavior of these columns using two different concrete moduli of elasticity. First, the measured modulus of elasticity was used, identical to the previous computations. Next, the modulus of elasticity was calculated with the ACI 318 suggested value of $57\sqrt{f_c'}$. The results of both analyses are shown.

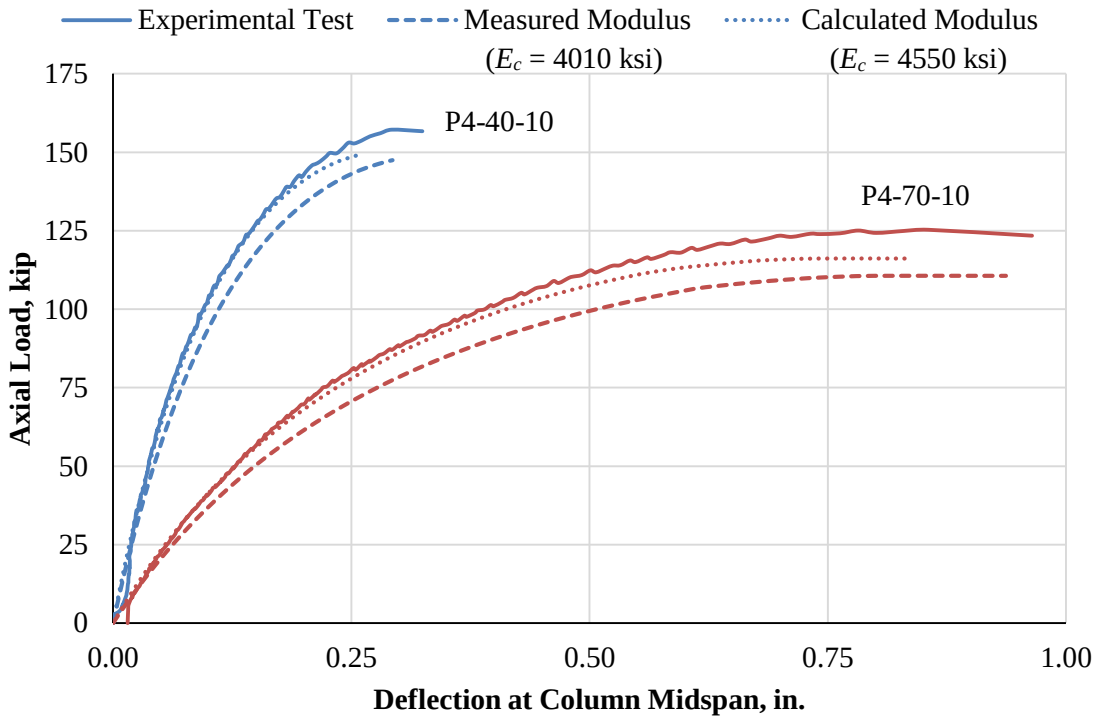

Figure 5.5 – Effect of Modulus of Concrete on Computed Behavior (Prestressed)

As shown, the accuracy of the model was improved when the computed modulus of elasticity according to ACI 318 was used. The comparison between this result and those of the experimental tests was more similar to the accuracy of the model for the nonprestressed columns. This difference can be partially explained by the following. The modulus of elasticity was measured as detailed in Section 3.3.1, and the columns were loaded to failure at a similar rate as the modulus of elasticity test. With similar strain rates, the modulus of elasticity during the tests should be similar to the measured modulus of elasticity. This was the case for the nonprestressed

columns. The prestressed columns, however, experienced creep prior to testing due to the prestressing. Already having experienced creep, the rate of creep during the tests was decreased. While the loading was relatively quick, the concrete does experience some degree of short-term creep effects. Because of this, the prestressed columns may have a higher effective modulus of elasticity. While other experimental errors may have contributed to this difference in accuracy, the modulus of elasticity can explain some of the difference in accuracy of the computational model for the nonprestressed and prestressed columns. It should also be noted that the modulus of elasticity as measured by the test cylinders can differ from that experienced by the columns.

5.4.1 Column Failure Types

All of the failures for the short-term prestressed columns were qualitatively similar, regardless of the prestressing amount, slenderness ratio, or eccentricity ratio. Figure 5.6 shows the failures for three of the prestressed columns. All failures demonstrated more post-failure damage compared to the nonprestressed columns. In addition, the damage was typically wider than one column tie and not necessarily centered on the column ties. Though this was the case, the concrete within the core was only damaged within about one tie spacing length, and the damage outside of that region was concentrated near the surface, particularly as shown in Figure 5.6 (b). Because the prestressing wires were tensioned, compression buckling of the wires was not a concern, explaining why the failure was not necessarily centered between ties. As shown in Figure 5.6 (b), some of the wires showed buckling post-failure, but this was undoubtedly a post-failure response of the column.

(a) 4P-40-25-ST

(b) 4P-40-10-ST

(c) 2P-40-25-ST

Figure 5.6 – Typical Failures of Short-Term Tests (Prestressed)

While the nonprestressed columns consistently failed within one tie spacing of the midspan of the columns, the prestressed columns failed at other locations. Because these failures were not caused by bar buckling, the failure location was less sensitive to the area of maximum moment and curvature. The different locations of the failures was evidence that the failure was more predicated on a weak point in the concrete, compared to the weak point of the reinforcement. Though the locations of failures varied, all of the failures occurred within the middle third of the column length, which indicated the failure was influenced at least somewhat by the increased moment and curvature of the concrete section. Due to the shape of the deflection profile of the columns, similar moments are expected across this region, even though the highest moment is located at the column midspan.

During the post-failure examination of the columns, it was discovered that several of the wires on the tensile side of the columns had fractured, an example of which is shown in Figure 5.6 (c). This occurred for all of the 2P columns, most of the 4P columns, and some of the 6P columns. Though the prestressing wire for this project had a smaller specified fracture elongation than typical prestressing strand (3.0% versus 3.5%), strand fracture was not an expected failure mode for these columns. After the fractures were first discovered, several of the subsequent columns

tests were recorded with a high-speed camera at 3000 frames per second to visually investigate the failure mode. Figure 5.7 shows several frames of one representative high-speed video.

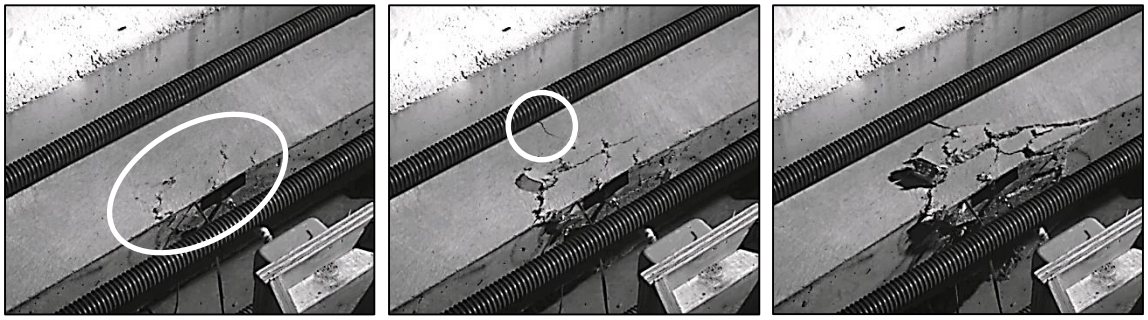

(a) Initiation of concrete failure (b) Initiation of tensile failure (c) Final failure

Figure 5.7 – Progression of Failure for Prestressed Columns (2P-40-25-ST)

As shown in Figure 5.7 (a), the concrete began to fail before any noticeable tensile cracks formed. Figure 5.7 (b) shows significant tensile cracks well after the concrete had failed. All of the recorded videos showed similar results. Based on this evidence, it was concluded that concrete failure always initiated column failure, and the strands fractured during the post-failure collapse of the load frame on the column.

5.5 Evaluation of Design Methodology

Similar to the nonprestressed columns, the results of the experimental tests were used to evaluate the accuracy of the current design methodology. The load-moment results of the tested columns were compared against the behavior computed using the moment magnification procedure outlined in Section 1.3, using the suggested flexural stiffness equations presented by Equations 5.1 through 5.4. Additionally, the behavior was computed using Equations 4.2, 4.4, and 4.5.

The stiffness equations in ACI 318 were not based on prestressed column behavior, but the code is not clear if they can't be used for this purpose. In fact, the code indicates their use for non-composite columns. As a result, Equation 4.2 could be used by design engineers for prestressed columns due to the ambiguity of the code. Because Equation 4.2 provided a reliable minimum stiffness for nonprestressed columns, its accuracy for prestressed columns is of particular interest. For similar reasons, Equations 4.4 and 4.5 were used in the comparisons. These equations were developed after evidence showed the most important factors that determine stiffness are axial

load and eccentricity ratio (Jenkins 2011). Because these factors do not change with prestressed columns, the equations may result in accurate estimations of flexural stiffness.

The flexural stiffness values were computed using nominal design values for steel strength, steel modulus, and concrete modulus. To maintain simplicity, the steel stress was assumed to be 65% (≈ 170 ksi) of the nominal ultimate strength, which was the average of the three types of columns constructed. This simplification was used for two reasons. First, the steel stress was shown to have little effect on column behavior. Second, in a typical design scenario, values such as stresses after losses are assumed at the start of an iterative method and may or may not be updated if the final design is within 10% of the initial iteration. To provide better comparison between casts, however, the test day, as-measured concrete strength was used in the computation due to significant time-dependent strength variations of the different concrete casts.

To provide a baseline for the comparison of the results and calculations, the nominal strength was computed with the computation model using the aforementioned material properties. In addition to the nominal strength, the design strength was also computed using strength reduction factors (ϕ) computed in accordance with ACI 318. The strength reduction factors were applied to the nominal axial and moment strengths. Comparing the results and procedure to design level loads provides a perspective of the accuracy of the equations under lower loads that would be the maximum strength considered in design. Actual service loads, due to load factors, would be even lower.

Figure 5.8 shows a summary of the results of the short-term columns with two prestressing wires compared with corresponding calculations based on the various methods previously discussed. To improve clarity, only the comparisons for Equations 4.2, 4.5, and 5.1 are shown. For all columns, Equations 4.5 was more accurate than equations 4.2 and 5.1. For column P2-70-25, however, the stiffness of the equations was greater than the stiffness of the test results at failure. Even with this discrepancy, the equation estimated a conservative failure load. In addition, Equation 4.2 was more accurate than Equation 5.1 for all of the columns. Equation 5.1 results in a maximum stiffness that is less than that of Equation 4.2, but Equation 4.2 always remained conservative, which led to excessively conservative results from Equation 5.1.

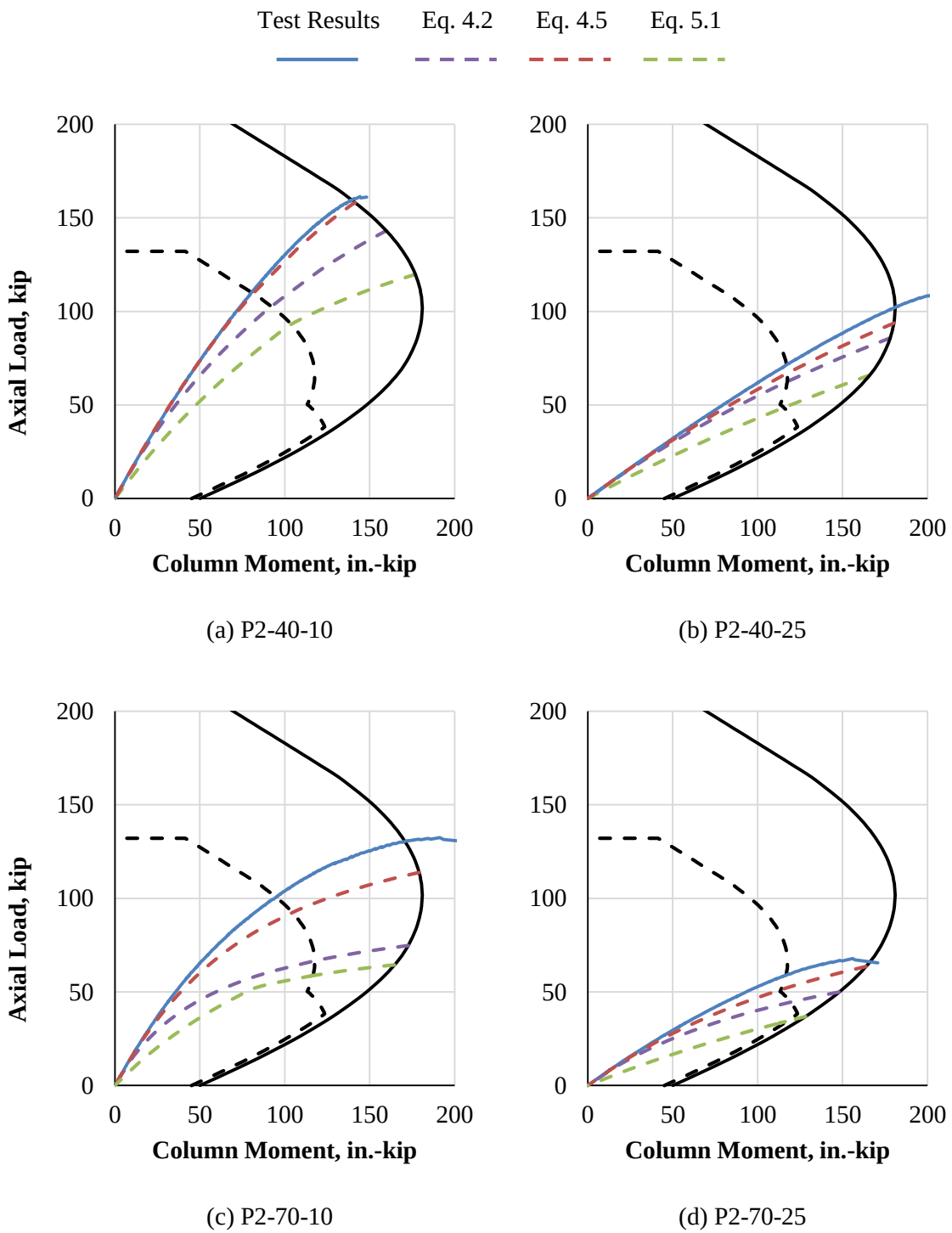

(a) P2-40-10

(b) P2-40-25

(c) P2-70-10

(d) P2-70-25

Figure 5.8 – Evaluation of Short-Term Design Equations (2 – PS Wires)

The equations were qualitatively more similar for the columns with a higher eccentricity ratio, which as before, was expected because these columns approach the minimum stiffness faster as a function of axial load. Similar to the comparisons with the computational model, the 70-10 column was estimated the least accurately. A column with a high slenderness ratio but a lower eccentricity ratio most closely fits the definition of a column that is susceptible to theoretical buckling. Because of this, the stability of these columns is very sensitive to any and all parameters of the experimental tests. From a design perspective, it is advantageous that the computational model and equations estimate this type of column conservatively.

Figure 5.9 shows a summary of the results of the short-term columns with four prestressing wires compared with corresponding calculations based on the aforementioned methods, and Figure 5.10 shows the same comparison for the columns with six prestressing wires. The comparisons for these sets of columns were similar to those for the P2 columns. The 70-10 columns were estimated least accurately, but all columns were estimated conservatively. The P4-70-25 column was estimated with a stiffer response near failure, but the failure load was estimated conservatively. Conversely, the slope of the behavior of P6-70-25 was estimated more accurately by Equation 4.5 than the 70-25 columns for the other prestressing arrangements, for which the experimental results showed zero stiffness while the equations estimated a positive stiffness. This was likely due to the increased steel. Even under higher moments, the P6-70-25 column was able to maintain stability, and its stiffness was positive when it crossed the nominal strength. This was evidence that while Equation 4.5 resulted in conservative and accurate failure loads, it might not truly capture the behavior of these columns near failure, particularly under states near stability failure. Due to the lower percentage of steel, the columns are more susceptible to stability problems, and different equations may be necessary for prestressed columns.

For all columns, Equation 4.2 was more accurate than Equation 5.1. None of the columns showed a stiffness lower than Equation 4.2, and thus, the increased complexity of Equation 5.1 was unnecessary. Even if Equation 5.1 were modified to permit a higher maximum stiffness, there was no evidence that this equation was more accurate than Equation 4.2 at any axial load level.

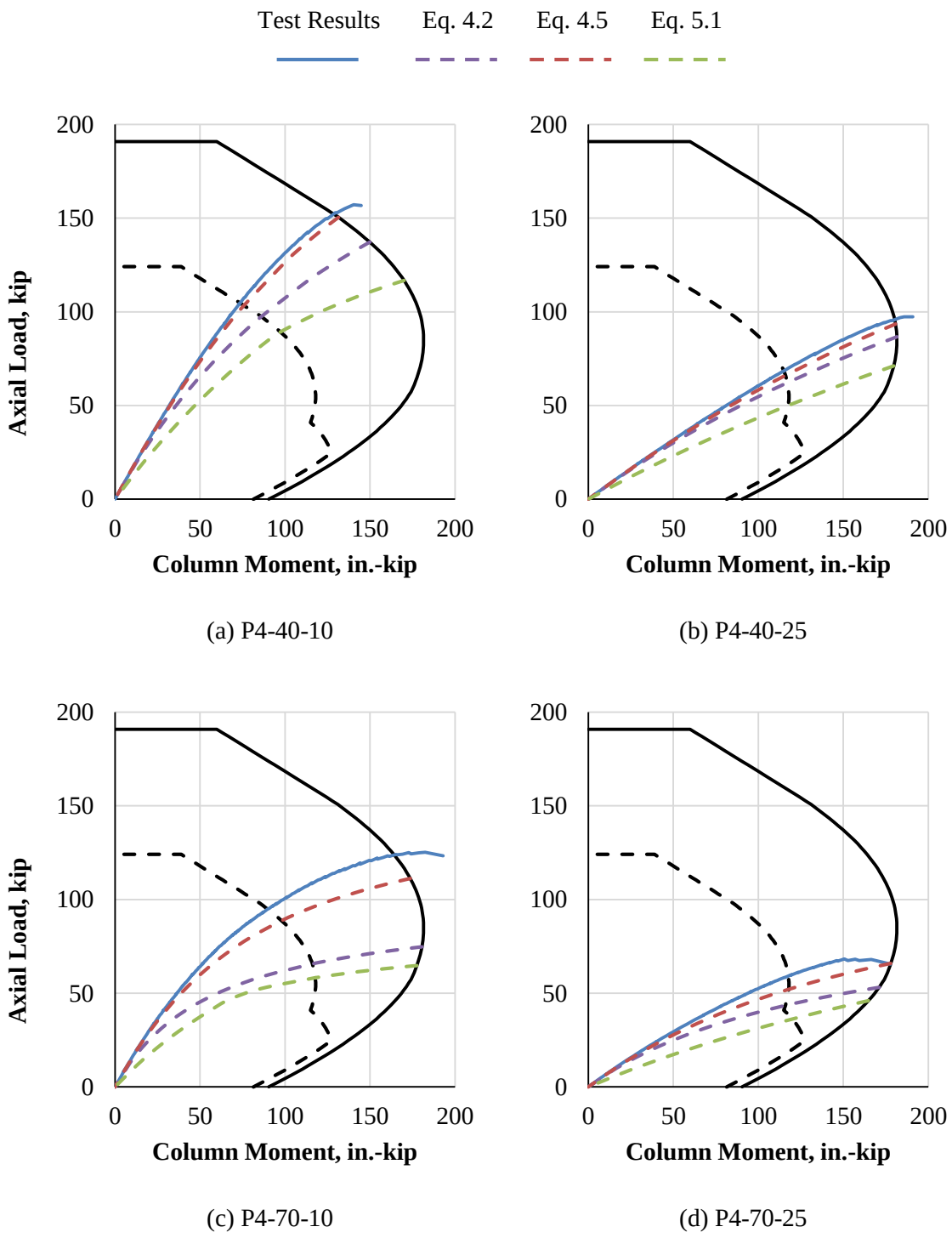

(a) P4-40-10

(b) P4-40-25

(c) P4-70-10

(d) P4-70-25

Figure 5.9 – Evaluation of Short-Term Design Equations (4 – PS Wires)

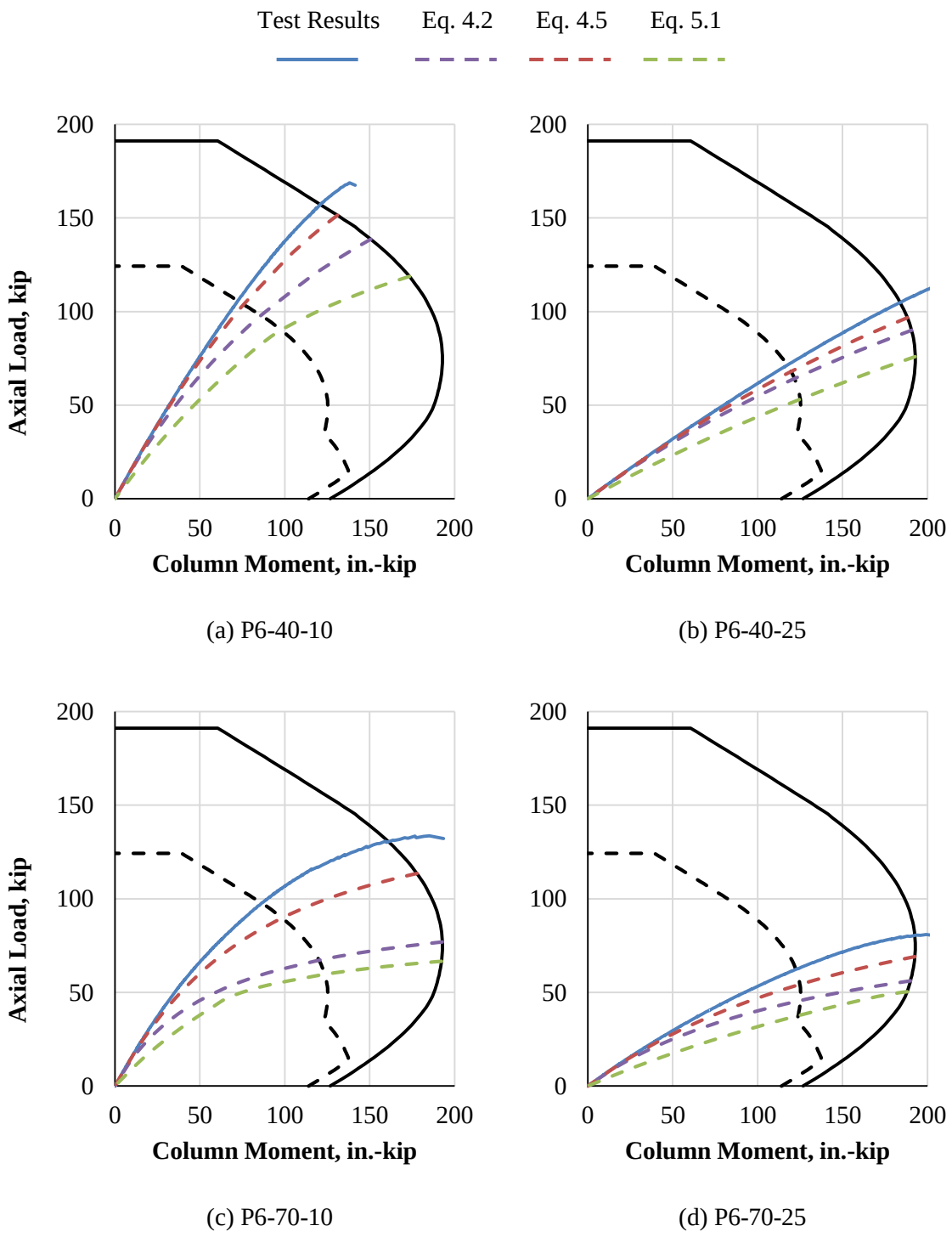

(a) P6-40-10

(b) P6-40-25

(c) P6-70-10

(d) P6-70-25

Figure 5.10 – Evaluation of Short-Term Design Equations (6 – PS Wires)

5.5.1 Statistical Analyses

Similar to the nonprestressed columns, the same calculations and methods of analysis were used for the statistical analyses, and the values of the capacities were compiled for both nominal and design strengths. Table 5.4 and Table 5.5 present the computed capacities of the prestressed, short-term tests at nominal and design strengths, respectively.

Table 5.4 – Short-Term Design Equations at Nominal Strengths (Prestressed)

Column ID	Computed Axial Capacity, kip				
	Test	Eq. 4.2	Eq. 4.4	Eq. 4.5	Eq. 5.1
P2-40-10-ST	159.7	143.1	156.1	158.2	119.8
P2-40-25-ST	102.2	85.8	93.1	93.7	65.8
P2-70-10-ST	130.6	74.8	111.5	113.8	64.4
P2-70-25-ST	67.1	49.9	63.3	63.6	36.9
P4-40-10-ST	152.2	137.3	148.3	150.5	116.8
P4-40-25-ST	96.0	86.6	92.8	93.5	71.2
P4-70-10-ST	123.9	74.8	108.6	111.2	64.8
P4-70-25-ST	65.5	53.1	65.5	65.9	46.0
P6-40-10-ST	157.2	138.6	149.2	151.4	118.8
P6-40-25-ST	104.9	90.1	96.0	96.7	75.9
P6-70-10-ST	130.9	76.9	110.6	113.6	66.7
P6-70-25-ST	80.5	56.2	68.7	69.1	50.4

Table 5.5 – Short-Term Design Equations at Design Strengths (Prestressed)

Column ID	Computed Axial Capacity, kip				
	Test	Eq. 4.2	Eq. 4.4	Eq. 4.5	Eq. 5.1
P2-40-10-ST	110.2	102.6	109.3	109.6	93.1
P2-40-25-ST	71.4	62.5	66.9	67.0	48.6
P2-70-10-ST	100.7	66.7	91.7	92.4	58.8
P2-70-25-ST	59.0	44.5	51.2	51.2	34.5
P4-40-10-ST	104.7	97.5	103.1	103.4	89.3
P4-40-25-ST	68.5	62.2	65.9	66.0	50.1
P4-70-10-ST	94.8	65.7	88.0	88.7	58.3
P4-70-25-ST	59.2	43.5	52.0	52.0	36.2
P6-40-10-ST	105.8	97.9	103.5	103.8	90.2
P6-40-25-ST	71.4	64.3	67.9	68.0	53.2
P6-70-10-ST	97.7	67.2	89.0	89.8	59.8
P6-70-25-ST	62.4	45.7	54.2	54.3	37.6

Table 5.6 presents a statistical summary of the capacities for the tested columns at nominal and design strengths. The axial load capacity of the each test result was divided by the axial load capacities computed from the equations for the corresponding strength. As such, a value of 1.0 indicates perfect accuracy, while values greater than 1.0 are conservative and values less than 1.0 are unconservative. The averages and standard deviations of the ratios are listed, which provide a perspective on the accuracy and conservatism of the equations when compared to the tested columns.

Table 5.6 – Statistical Analysis of Short-Term Design Equations (Prestressed)

Analysis		Eq. 4.2	Eq. 4.4	Eq. 4.5	Eq. 5.1
Nominal Strength, S_n	Average	1.33	1.09	1.07	1.58
	Std. Dev.	0.24	0.06	0.06	0.26
Design Strength, ϕS_n	Average	1.25	1.08	1.07	1.47
	Std. Dev.	0.16	0.05	0.05	0.21

Equations 4.2 and 5.1 computed excessively conservative column capacities at nominal and design strengths. For all of the equations and comparisons, only one computed capacity was unconservative. This occurred using Equation 4.5 for column P4-70-25 and was less than 1% unconservative. Equation 4.2 showed similar conservatism and accuracy as the comparisons for the nonprestressed columns shown in Table 4.5. This similarity indicates that prestressed columns have a similar minimum stiffness to that of nonprestressed columns. While Equation 4.2 was approximately 25% conservative for nominal and design strengths, Equation 5.1 was even more conservative. This is expected, however, because Equation 5.1 permits a maximum stiffness that is lower than the stiffness of Equation 4.2. Equation 5.1 is more complicated than Equation 4.2 but did not provide additional accuracy and was excessively conservative.

Equations 4.4 and 4.5 resulted in very similar averages and standard deviations. This was expected because the primary difference between the equations is the consideration of the area of the longitudinal steel. Because the steel ratios for the prestressed columns were small, the difference in the equations were minimal. The other primary difference is the use of the nominal axial strength (P_0) versus the gross axial strength ($0.85 f_c' A_g$). The use of prestressing decreases the nominal axial strength of a column; thus, the gross axial strength resulted in a higher value than the nominal axial strength. This difference was the primary reason that Equation 4.5 was less conservative than Equation 4.4, opposite of the results from the evaluation of design equations for the nonprestressed columns.

Compared to the results from the nonprestressed columns, Equation 4.4 was more conservative while Equation 4.5 was similarly conservative, but both equations were less accurate considering the standard deviations. Because twelve experimental tests do not result in a statistically significant analysis, a parametric study, shown in Chapter 6, was conducted to further evaluate the design equations for prestressed columns.

5.6 Findings

Twelve slender columns were tested under short-term loading to failure. The results were compared against a computational model as well as current design equations. The columns varied in slenderness ratio, eccentricity ratio, and prestressing arrangement. Based on the results of the tests and their comparison to analysis and design methods, the following conclusions were made.

1. The computational model estimated the behavior and capacity of all columns conservatively. The accuracy of the computed behavior was very similar for varying prestressing arrangements. The model was similarly accurate for all slenderness and eccentricity ratios except for the 70-10 columns, for which the model was more conservative than for the other column types. The computed failures loads and failure deflections were similarly accurate, except for the 70-10 columns, which were more conservative. The reduced accuracy of the computational model compared to the results of the nonprestressed columns can be partially explain by an increased effective modulus of elasticity because they had previously experienced concrete creep due to the prestressing.
2. The tested columns exhibited one failure type: explosive failure of the concrete core within one tie. The columns did not fail within one tie group of the column midspan, but all columns failed in the middle third of the column. Several columns showed strand fracture during a post-failure inspection, but this was determined to have been caused by the post-failure response of the column and loading frame.
3. Several of the columns exceeded the ACI 318 second-order limit of 1.4 times the first-order effects. Compared with the nonprestressed columns, however, the prestressed columns had less residual capacity after exceeding the limit. This indicates that prestressed columns are more susceptive to global stability failure. Several columns

approached or surpassed zero stiffness, but the computational model and the equations estimated the overall behavior accurately.

4. The current design methods were excessively conservative when compared to the test results. Equations 4.2 and 5.1 showed similar standard deviations, but Equation 4.2 was less conservative. In addition, these equations showed similar results at nominal and design strengths. Equations 4.4 and 4.5, intended for nonprestressed columns, were more accurate while remaining conservative for the prestressed columns. The level of conservatism and accuracy, however, differed from the results of the nonprestressed columns, which may indicate that these equations can be modified to better account for the effect of prestressing.

CHAPTER 6 DESIGN STFFNESS OF SLENDER, PRESTRESSED COLUMNS

6.1 Introduction

While the equations intended for nonprestressed columns were found in Chapter 5 to be moderately accurate for prestressed columns, further investigation of the stiffness of prestressed columns was desired. Using the analytical model, a study was conducted to determine the influence of column and loading parameters on the stiffness of prestressed columns. Improved stiffness equations were developed and compared to results from the analytical model for accuracy and conservatism. In addition, current and proposed equations intended for nonprestressed columns are compared to the results from the analytical model.

6.2 Parametric Study

Based on the results of a previous parametric study for nonprestressed columns (Jenkins 2011), the primary parameters of interest for prestressed columns are as follows:

1. Axial Load
2. Prestressing Ratio
3. Degree of Eccentricity
4. Column Slenderness

While other parameters affect the stiffness of columns, it was shown that the moment magnification procedure properly accounted for these by means of the gross section stiffness. In the previous study, columns slenderness was also shown to be properly accounted by the moment magnificent procedure. Prestressed columns have very low steel ratios, however, and are more susceptible to instability failure. As a result, column slenderness was reevaluated.

6.2.1 Methodology

The methodology and framework for the parametric study were similar to the previous study conducted for nonprestressed columns (Jenkins 2011). The computational model was used to

estimate the behavior of theoretical columns, and several assumptions were maintained: equal end eccentricities, non-sway columns bent in single curvature, and pinned-pinned ends.

Using assumed material and geometric properties as well as assumed loading details, an analysis was conducted that yielded the total moments due to second-order effects. Rearranging Equations 1.1 through 1.3, Equation 6.1 computes the flexural stiffness of that particular column scenario that results in the correct amplified moment. Note that the 0.75 factor was removed from the equations. This factor is a stiffness reduction factor based on allowable tolerances for material and geometric properties of an as-built column. Because the computational model is theoretical, this factor was unnecessary and assumed to be 1.0.

$$EI = \left(\frac{P l_u^2}{\pi^2} \right) \frac{1}{1 - \frac{M}{M_c}} \qquad \text{(Eq. 6.1)}$$

where:

EI = flexural stiffness of compression member, in.^{2}-lb
l_u = unsupported length of compression member, in.
M = end moment of compression member, in.-lb
M_c = moment amplified for the effects of member curvature, in.-lb
P = axial force, lb

For the parametric study, a control column was assumed. Detailed in Table 6.1, the control column was designed to provide a minimum stiffness given realistic service conditions and code provisions. For the parameters that were deemed to be properly accounted for by the moment magnificent procedure, common design values were assumed. Each parameter of interest was analyzed over a range to determine its influence on column stiffness.

The prestressing ratio was defined by the ratio of prestressing steel to the gross area of the column (A_{pt}/A_g). A value of 0.125% was chosen because it roughly results in a compressive stress in the concrete of 225 psi due to effective prestressing force only, which minimally defines a prestressed column. Because the parametric study was based on theoretical columns, the steel area was computed disregarding available steel sizes and assumed as four wires placed in the four corners. The concrete cover was chosen considering ACI 318 (2014) provisions for concrete cover of columns manufactured under plant control condition (3/4 in. clear cover) and was defined as the distance to the center of steel. Lastly, the steel was assumed to be low-relaxation,

have a tensile strength of 270 ksi, and have an effective stress after losses of 0.65 f_{pu}. The tensile stress in the steel was found to have a minor impact on column behavior, and this assumption was made for simplification.

Table 6.1 – Control Column Parameters

Parameter	Value
Cross-section, *h x b*	12 in. x 12 in.
Length, kl_u	144 in.
Eccentricity, *e*	0.6 in. (e / h = 0.05)
f_c' at 28 days	7000 psi
E_c	$57\sqrt{f_c'}$ ksi
A_{pt} / A_g	0.125%
Concrete cover (to center of steel)	1.5 in.
f_{pu}	270 ksi
f_{se}	0.65 f_{pu}
E_{ps}	28,500 ksi

6.2.2 Axial Load

Based on previous research (Jenkins 2011), the primary parameter affecting column stiffness is axial load. The influence of axial load was determined first, and used to further normalize subsequent results. The axial load was varied from 0.05 P_0 to 0.85 P_0 in 0.05 P_0 increments or until the column theoretically failed. The upper bound was chosen based on ACI 318 provisions for the maximum permitted axial load on a column with spiral reinforcement ($P_{n,\max}$ = 0.85 P_0). Table 6.2 shows tabulated results for the control column subject to varying axial load. Equation 6.1 was used to determine an effective column stiffness that resulted in the correct amplified moment. To provide a consistent approach, the axial load was normalized by the nominal axial strength (P_0), and the computed stiffness was normalized by the gross section stiffness (E_cI_g).

Table 6.2 – Procedure to Compute Effective Stiffness

Analytical Model Output					Effective Stiffness	
P / P_0	P, kip	M, in.-kip	M_c, in.-kip		EI, in.^{2}-kip	EI / E_cI_g
0.05	42.0	25.2	25.5		7,801,000	0.95
0.10	84.0	50.4	51.6		7,649,000	0.93
0.15	125.9	75.6	78.3		7,484,000	0.91
0.20	167.9	100.7	105.9		7,308,000	0.89
0.25	209.9	125.9	134.2	→	7,147,000	0.87
0.30	251.9	151.1	163.5		6,968,000	0.85
0.35	293.8	176.3	194.0		6,780,000	0.82
0.40	335.8	201.5	225.7	**Equation 6.1**	6,590,000	0.80
0.45	377.8	226.7	258.8		6,388,000	0.78
0.50	419.8	251.9	293.8		6,182,000	0.75
0.55	461.7	277.0	330.9	→	5,963,000	0.72
0.60	503.7	302.2	370.6		5,734,000	0.70
0.65	545.7	327.4	413.8		5,490,000	0.67
0.70	587.7	352.6	461.7		5,227,000	0.63
0.75	629.7	377.8	516.0		4,939,000	0.60
0.80	671.6	403.0	580.7		4,611,000	0.56
0.85	713.6	428.2	665.2		4,208,000	0.51

Figure 6.1 shows the results in graphical form. The results are nearly linear and were approximated by Equation 6.2. This equation, as well as subsequent equations, were not developed by a statistical analysis but, rather, were developed to be accurate, simple, and conservative. As shown, the equation was unconservative for very high axial load ratios, but very accurate for moderate axial load ratios, where the typical behavior of service columns occurs.

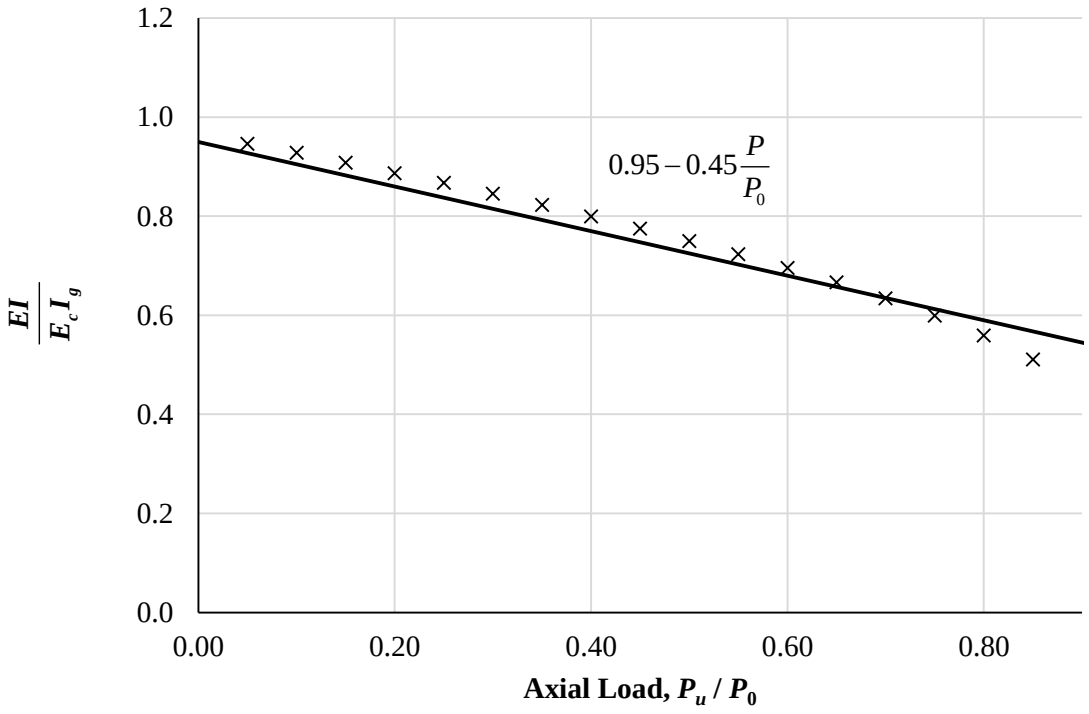

Figure 6.1 – Influence of Varying Axial Load

$$\frac{EI}{E_c I_g} = 0.95 - 0.45\frac{P}{P_0} \qquad \text{(Eq. 6.2)}$$

6.2.3 Prestressing Ratio

As shown by the experimental results, the prestressing ratio does not have a significant effect on the stiffness of columns. The influence, however, depends on other parameters, which is why it must be investigated further. For columns with a low eccentricity ratio, a high prestressing ratio decreases the stiffness of a column, but for column with a high eccentricity ratio, the opposite is true. In addition, the amount of prestressing affects the nominal axial strength negatively, with a higher prestressing ratio leading to a lower nominal axial strength.

Figure 6.2 shows the flexural stiffness versus axial load of the control column for two different prestressing ratios. A prestressing ratio of 0.55%, which equates to a concrete stress after losses to approximately 925 psi, was chosen as a practical maximum. As shown, when normalized by the nominal axial strength (P/P_0), the effect of the prestressing ratio is minimal.

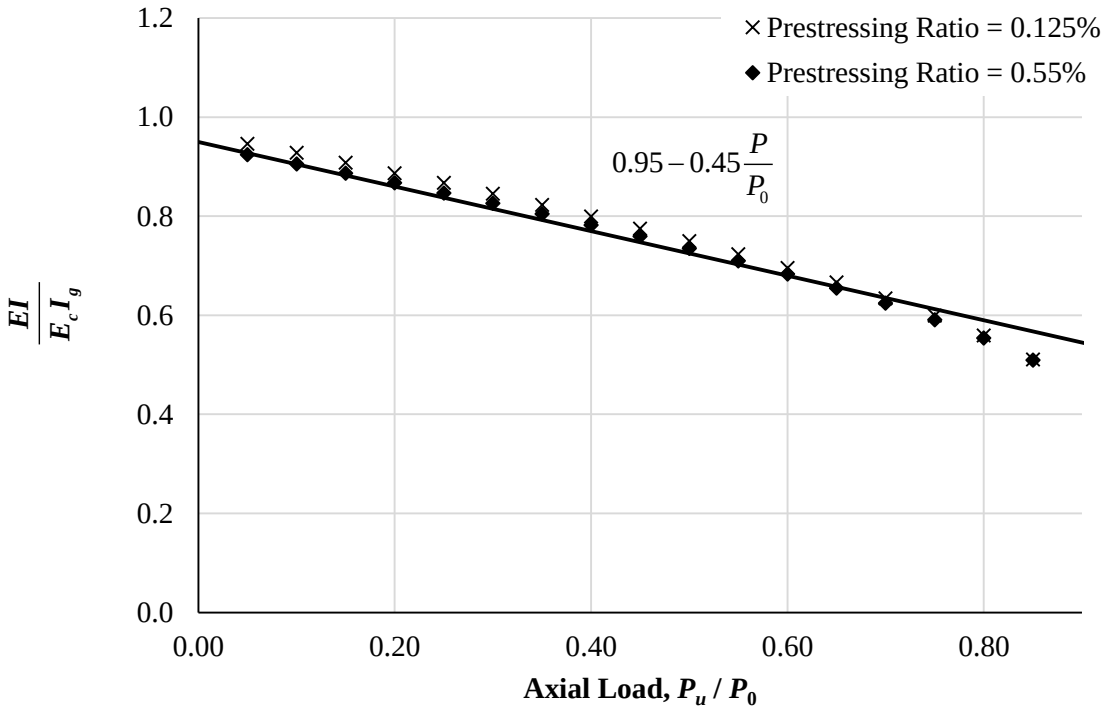

Figure 6.2 – Influence of Varying Axial Load and Prestressing Ratio

Figure 6.3 shows the results of the control column for various prestressing ratios. The results were normalized by Equation 6.2 and plotted as a function of prestressing ratio. The prestressing ratio is shown to have little effect on the stiffness when normalized by the nominal axial strength. While the results trend slightly negatively, the minimum values did not change, and the effect can be ignored while maintaining sufficient accuracy.

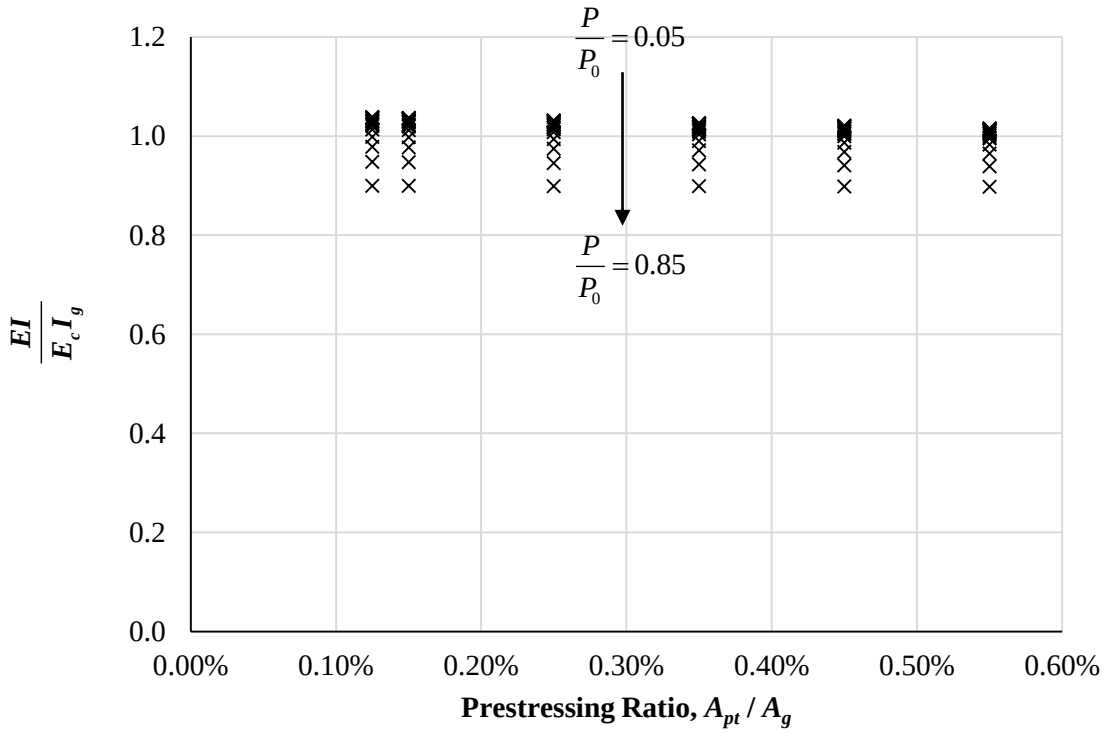

Figure 6.3 – Influence of Prestressing Ratio

6.2.4 Degree of Eccentricity

Figure 6.4 shows the effect of the eccentricity ratio on the control column. The results were normalized by Equation 6.2 and plotted as a function of the eccentricity ratio. Compared to the other parameters, the effect of eccentricity ratio is much less consistent. For eccentricity ratios below 10%, columns do not typically have tensile stresses. As a result, the degree of eccentricity did not affect the behavior of the column. For larger eccentricities, applied loads causes tensile stresses in columns. Due to pre-compression caused by the prestressing steel, however, tensile stresses are not created under very low axial loads. As a result, the stiffness of prestressed columns with eccentricities greater than 10% was found to vary significantly as a function axial load. Equation 6.3, included in the figure, provides a fairly reliable lower bound value and is consistent with the eccentricity factor for nonprestressed columns in Equations 4.4 and 4.5. While some results lie below the line, these columns were very close to failure and not likely to be seen in service columns. The ultimate lower bound of the stiffness, regardless of eccentricity ratio, was found to be 0.30 E_cI_g, consistent with the results for the evaluation of nonprestressed columns (Jenkins 2011).

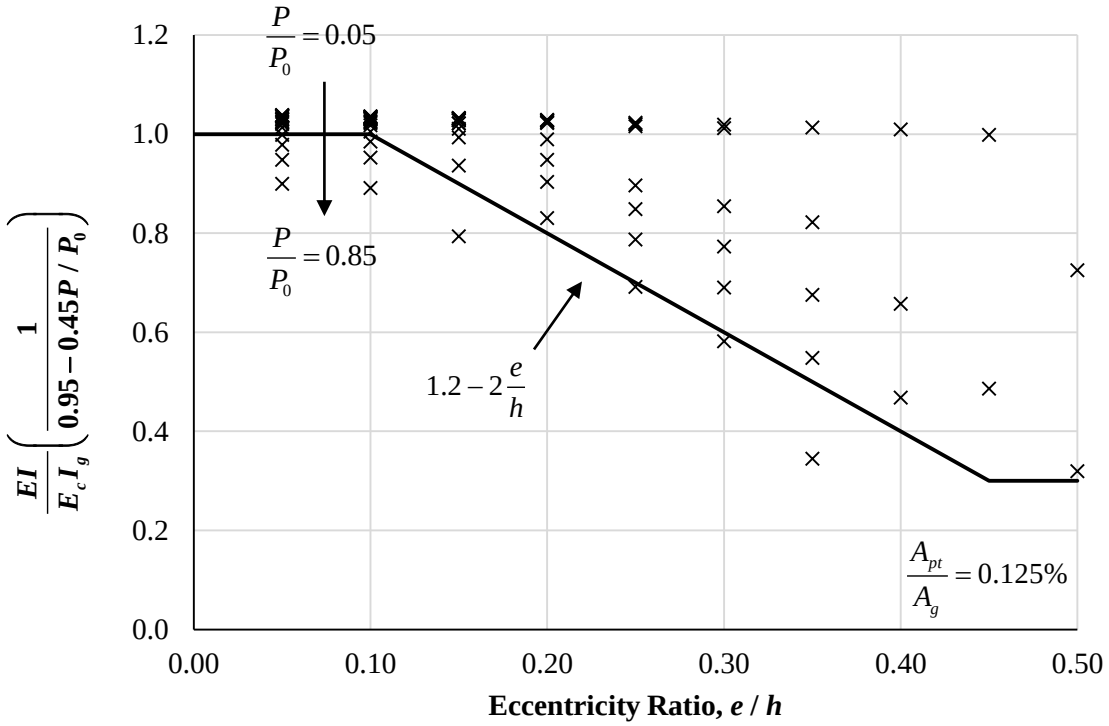

Figure 6.4 – Influence of Eccentricity Ratio

$$\frac{EI}{E_c I_g}\left(\frac{1}{095 - 0.45\frac{P}{P_0}}\right) = 1.2 - 2\frac{e}{h} = 1.2 - 2\frac{M}{Ph} \qquad \text{(Eq. 6.3)}$$

The effect of the eccentricity ratio was also evaluated for the maximum practical prestressing ratio of 0.55%, as shown in Figure 6.5. Because of the increased pre-compression due to the higher steel ratio, the influence of the eccentricity ratio was lessened. These results were consistent with the experimental tests, which showed a higher prestressing ratio was only advantageous for columns subject to a higher eccentricity. To maintain simplicity, the improved behavior due to the higher prestressing ratio can be conservatively ignored.

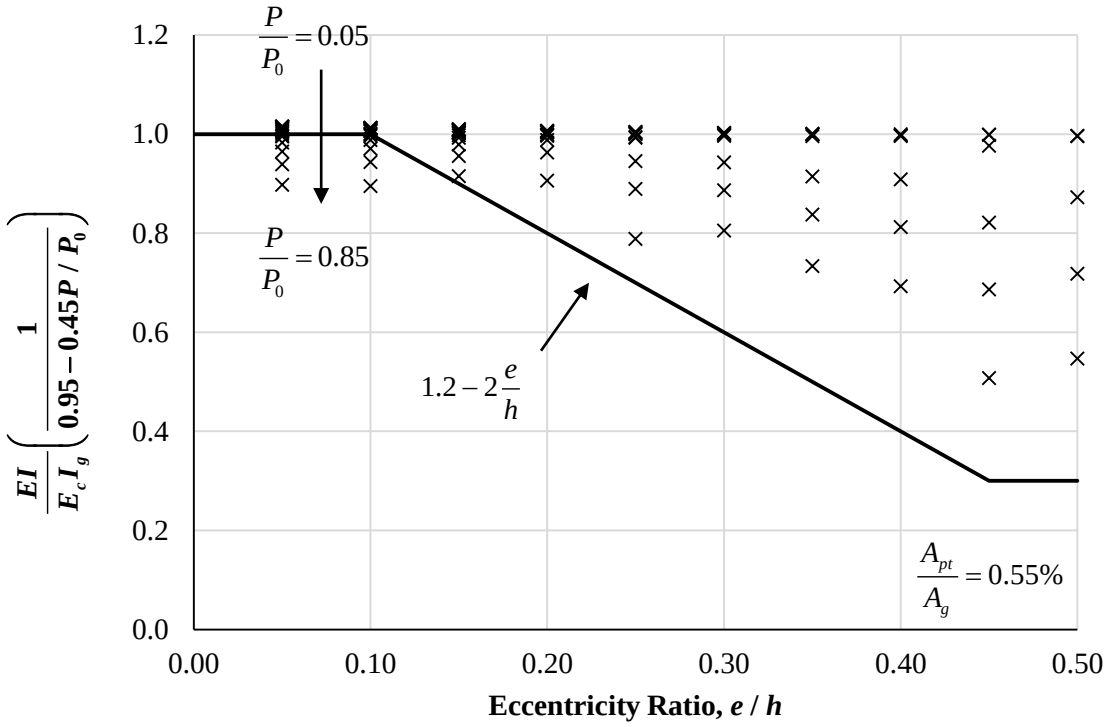

Figure 6.5 – Influence of Eccentricity Ratio (A_{pt} / A_g = 0.5%)

6.2.5 Column Slenderness

As previously mentioned and as shown in Equation 6.1, the slenderness ratio is indirectly considered by the moment magnification procedure, even if it is not explicitly included in the flexural stiffness equation. Nevertheless, the slenderness ratio was reevaluated because previous research indicated these columns were extremely susceptible to buckling (Nathan 1985). Figure 6.6 shows the effect of slenderness ratio on the control column normalized by Equation 6.2. The effects of two eccentricity ratios are included to further evaluate the effect of slenderness ratio. From the minimum slenderness, the results trend positively. Because the results only show increases in column stiffness, the effect of slenderness ratio was conservatively ignored and assumed to be completely addressed by the methodology of the moment magnification procedure.

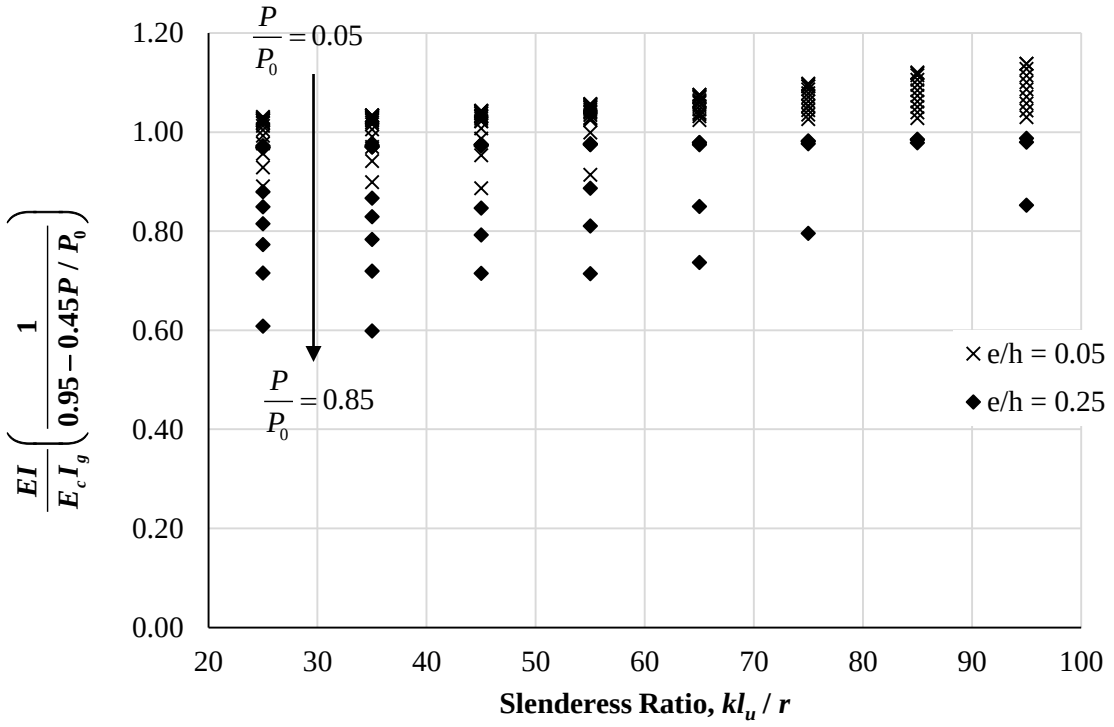

Figure 6.6 – Influence of Slenderness Ratio

6.3 Design Stiffness

Using the results of the parametric study, two equations were developed to estimate the behavior of prestressed columns. First, an equation was developed that provided the most accurate estimation of column behavior. This equation could be used for more detailed design or analysis. Next, a simplified equation was developed. This equation, developed as a modification of Equation 4.5, could be used in a typical design approach. Using the computational model, a database of theoretical columns was created and used to evaluate the accuracy of the proposed and existing stiffness equations for prestressed columns.

6.3.1 Proposed Stiffness Equations

The two primary parameters found to affect prestressed columns were the axial load ratio and eccentricity ratio. The effect of the axial load ratio was found to be approximately linear, and the effect of the eccentricity ratio was found to be approximately piecewise linear. To maintain simplicity, the two parameters were linearly combined, as shown by Equation 6.4.

Equation 6.4

$\frac{M}{Ph} = \frac{e}{h}$	**Column Flexural Stiffness, *EI***
≤ 0.1	$\left[0.95 - 0.45\frac{P}{P_0}\right] E_c I_g \geq 0.30 E_c I_g$
> 0.1	$\left[0.95 - 0.45\frac{P}{P_0}\right]\left[1.2 - 2\frac{M}{Ph}\right] E_c I_g \geq 0.30 E_c I_g$

From a design perspective, Equation 6.4 requires simplification. While most of the necessary information is available from structural analysis and first iteration guesses, the nominal axial capacity (P_0) requires additional information typically not known during design. As a result, this variable should be modified. Consistent with previous research (Jenkins 2011), the nominal axial strength was replaced with the gross section strength (P_{0g}). Figure 6.7 shows the flexural stiffness versus gross axial load ratio of the control column for the minimum and maximum prestressing ratio.

When normalized by the gross section strength, the prestressing ratio affected the column behavior more than when normalized by the nominal axial strength. The behavior was conservatively estimated, however, by Equation 6.5.

$$\frac{EI}{E_c I_g} = 0.9\left(1.0 - 0.5\frac{P}{P_{0g}}\right) \qquad \text{(Eq. 6.5)}$$

where:

$$P_{0g} = 0.85 f_c^{'} A_g$$

While a more accurate equation was possible, Equation 6.5 was used because it is simply a fractional reduction of the load factor for nonprestressed columns. As a result, the effective stiffness of prestressed columns can be approximated by a fractional reduction of the equation for nonprestressed columns, simplifying design approach. Equation 6.6 shows the simplified equation for the effective column stiffness of prestressed columns.

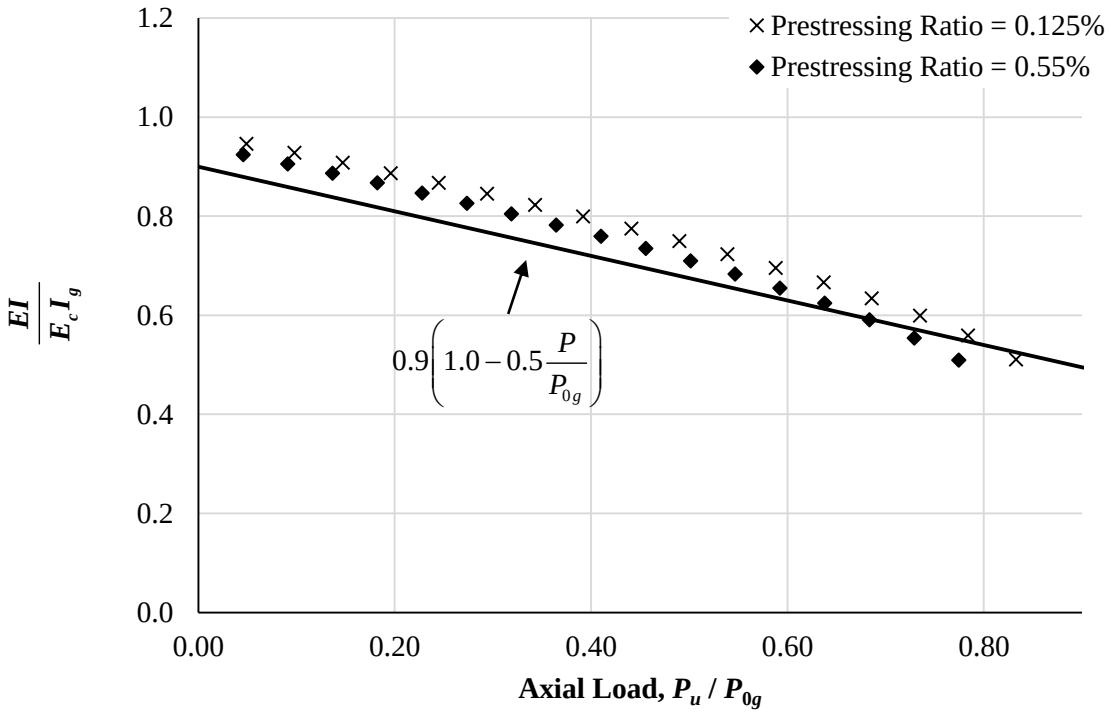

Figure 6.7 – Simplification of Axial Load Factor

Equation 6.6

$\frac{M}{Ph}=\frac{e}{h}$	**Column Flexural Stiffness, *EI***
≤ 0.1	$0.9\left[1.0-0.5\frac{P}{P_{0g}}\right]E_c I_g \geq 0.30E_c I_g$
> 0.1	$0.9\left[1.0-0.5\frac{P}{P_{0g}}\right]\left[1.2-2\frac{M}{Ph}\right]E_c I_g \geq 0.30E_c I_g$

6.3.2 Evaluation of Stiffness Equations

To evaluate the accuracy of the proposed equations, theoretical columns were analyzed with the computational model. The columns were chosen as a realistic range of service columns using common geometric sizes and material properties. Table 6.3 shows a summary of the column evaluation array. The properties of the columns were consistent with the control column from the parametric study unless otherwise specified. The strands were 0.5 in., low-relaxation, seven-wire strand conforming to ASTM A416 (2012), which is the most common strand used by the

industry. All strands were uniformly distributed about the column and the number of strands was chosen based on prestressing ratio bounds of 0.125% and 0.6%. The slenderness ratios were reduced as the cross-section increased; the maximum unsupported lengths considered were 30 ft to 40 ft, a practical maximum. Additionally, the cross-section sizes were chosen based on industry practice of columns constructed in 2 in. increments. The analysis resulted in approximately 9500 data points.

Table 6.3 – Prestressed Column Array for Analytical Evaluation of Design Equations

Column Parameters			**Loading Parameters**	
Cross-Section, *b x h*	**Prestressing, A_{pt}/A_g**	**Slenderness, kl_u/r**	**Axial Load, P/P_0**	**Eccentricity, *e/h***
12 in. x 12 in. 14 in. x 14 in.	4 – strands	25 35 45 55	0.05 0.10 0.15 0.20 0.25 0.30 0.35 0.40 0.45 0.50 0.55 0.60 0.65 0.70 0.75 0.80 0.85	5% 10% 15% 20% 25% 30% 35% 40% 45% 50%
16 in. x 16 in.	4 – strands 8 – strands	65 75 85 95		
18 in. x 18 in. 20 in. x 20 in. 22 in. x 22 in.	4 – strands 8 – strands 12 – strands	25 35 45 55 65 75		
24 in. x 24 in. 26 in. x 26 in. 28 in. x 28 in. 30 in. x 30 in.	8 – strands 12 – strands	25 35 45 55		

The estimations of the effective columns stiffness were computed using Equations 4.2, 5.1, 6.4, and 6.6. The column stiffness estimations were used to compute the amplified moment according to Equations 1.1 to 1.3. As before, the 0.75 stiffness reduction factor was omitted from the calculations. The computed amplified moments were compared to the amplified moments from the computational model to determine the relative accuracy and conservatism of each equation. Because the equations typically result in conservative assumptions of column behavior, the number of data points for each equation is different because the equations can predict column failure before the theoretical model. To limit the extent of second-order effects, the column was assumed to fail if the applied load was greater than 75% of the critical buckling load calculated

for the respective equation. This value, which coincides with the stiffness reduction factor, results in an amplified moment of four times and was considered a practical maximum.

The results of the comparisons are presented qualitatively in the form of histograms. For each data point, the amplified moment as calculated by the equation was divided by the amplified moment as calculated by the computational model. As such, a value of 1.0 is perfect accuracy, while values less than 1.0 are unconservative and values greater than 1.0 are conservative. The computed ratios were compiled as a histogram in 0.05 bin sizes. The histograms are presented as percentages because, as previously mentioned, each equation resulted in a different number of data points. Figure 6.8 shows the evaluation of Equation 6.4.

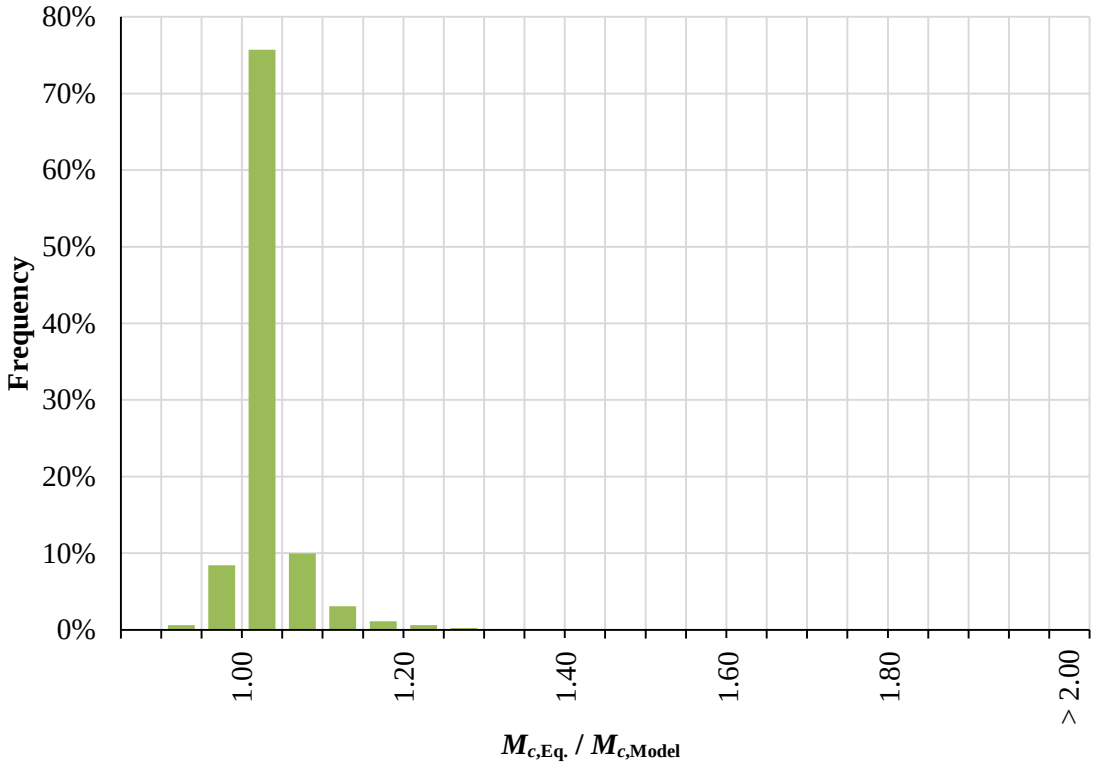

Figure 6.8 – Evaluation of Equation 6.4 (Computational Model)

Nearly 76% of the values were between 1.0 and 1.05, and the distribution was roughly symmetric, with approximately 9% of values between both 0.95 and 1.0 and 1.05 and 1.1. While 9.1% values were below 1.0, only 0.6% of the value were below 0.95. The equation was very accurate with very few results greater than 5% unconservative.

Figure 6.9 shows the evaluation of Equation 6.6. While this equation is simpler because it only requires the gross section strength, the results were similar to the evaluation for Equation 6.4. Specifically, nearly 75% of the results were between 1.0 and 1.05. The results had a positive skew which resulted in fewer unconservative values. Only 3.4% of the values were less than 1.0, and 0.3% were less than 0.95. Compared to Equation 6.4, Equation 6.6 was more conservative but no excessively so.

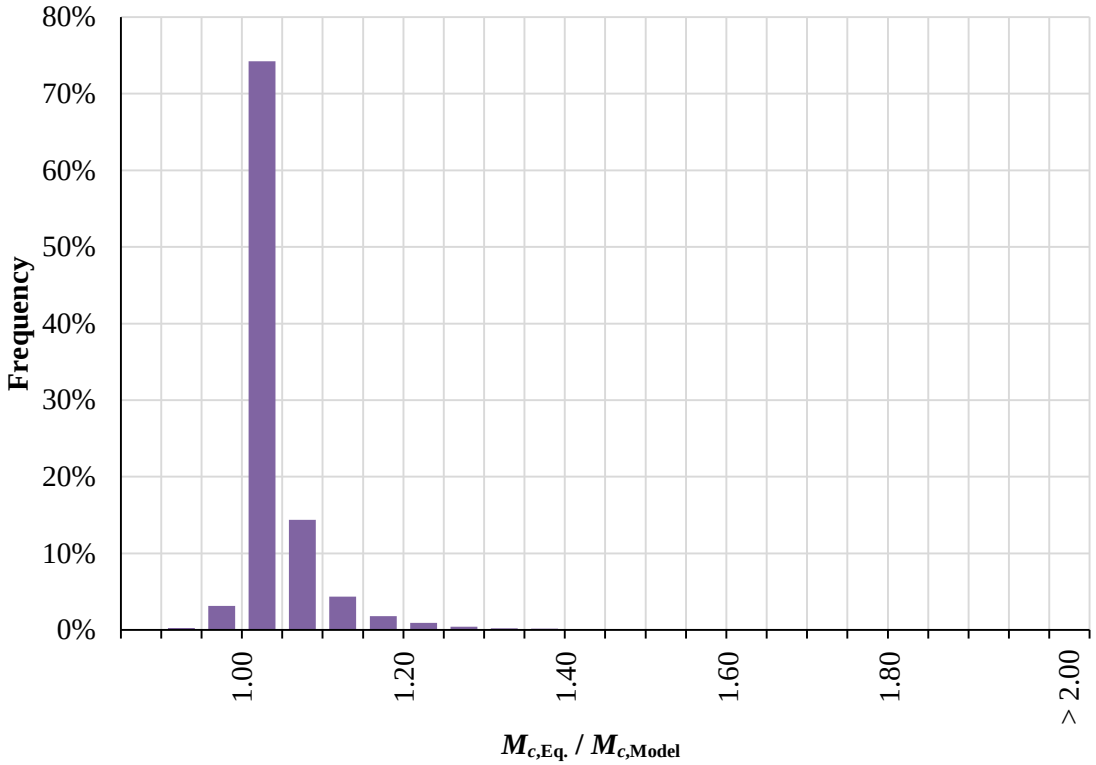

Figure 6.9 – Evaluation of Equation 6.6 (Computational Model)

Figure 6.10 shows the evaluation of Equations 4.2, 5.1, 6.4, and 6.6. Equations 4.2 and 5.1, while conservative, were significantly less accurate than Equations 6.4 and 6.6. Equation 5.1 was the least accurate, with only 12% of the values between 1.0 and 1.2. Equation 5.1 did not have a single unconservative value, however. Equation 4.2, considering its simplicity, is reasonably accurate. Nearly 77% of the values were between 1.0 and 1.2, and only 1.7% of the values were less than 1.0. Equation 4.2, however, was much less accurate than Equations 6.4 and 6.6. Additionally, Equation 4.2 still resulted in estimations that were excessively conservative, with over 20% of the results greater than 20% conservative.

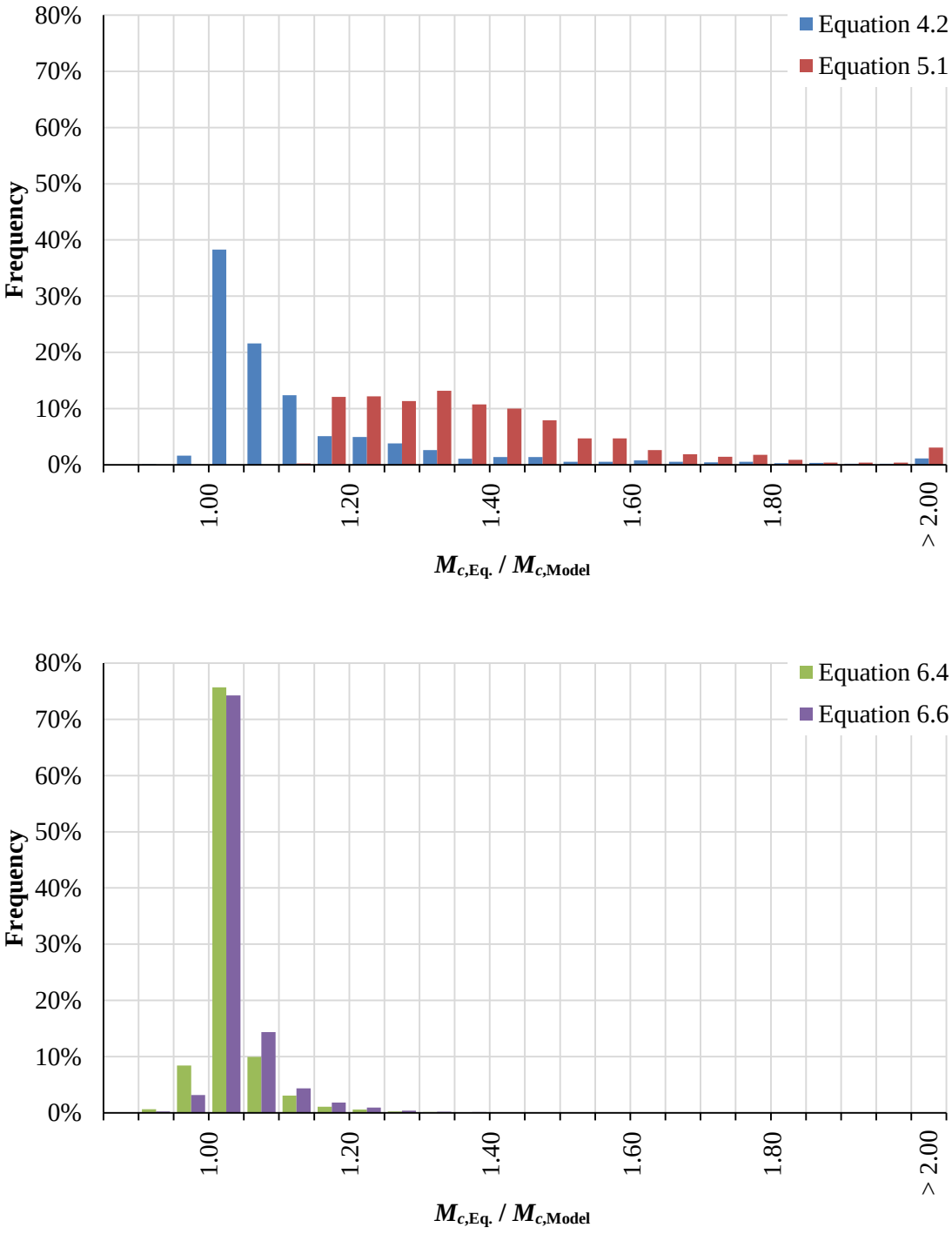

Figure 6.10 – Evaluation of Short-Term Design Equations (Computational Model)

Table 6.4 presents a statistical summary of the evaluations. Consistent with the figures, Equations 4.2 and 5.1 were more conservative and less accurate than Equations 6.4 and 6.6. The standard deviations for Equations 4.2 and 5.1 were comparable to each other and over four times the standard deviations for Equations 6.4 and 6.6. Based on the results of the evaluations and parametric study, a lower bound of 0.30 E_cI_g for prestressed columns is recommended. While the lower bound for nonprestressed columns is proposed to be equal 0.40 E_cI_g (Jenkins 2011), prestressed columns have a lower bound than nonprestressed columns due to the lower steel ratio.

Table 6.4 – Statistical Summary of Short-Term Design Equations for Prestressed Columns

Statistical Analysis	Eq. 4.2	Eq. 5.1	Eq. 6.4	Eq. 6.6
Median	1.06	1.36	1.01	1.02
Average	1.14	1.41	1.03	1.04
Standard Deviation	0.20	0.23	0.04	0.05
Coefficient of Variation	18%	16%	4.2%	4.8%
Below 1.0	1.7%	0.0%	9.1%	3.4%
Below 0.95	0.1%	0.0%	0.6%	0.3%
Between 1.0 and 1.2	77.4%	12.3%	89.8%	94.8%

6.4 Evaluation of Design Methodology

The experimental results from Chapter 5 were used to evaluate the accuracy of Equations 6.4 and 6.6, similar to Section 5.5. The same calculations and methods of analysis were used for the statistical analyses, including the inclusion of 0.75 stiffness reduction factor. The values of the capacities were compiled for both nominal and design strengths. Table 6.5 and Table 6.6 present the computed capacities of the prestressed, short-term tests at nominal and design strengths, respectively.

Table 6.5 – Proposed Short-Term Design Equations at Nominal Strengths (Prestressed)

Column	Computed Axial Capacity, kip			P_{test} / $P_{Eq.}$	
	Test Results	Eq. 6.4	Eq. 6.6	Eq. 6.4	Eq. 6.6
P2-40-10-ST	159.7	157.3	155.6	1.01	1.03
P2-40-25-ST	102.2	92.8	91.5	1.10	1.12
P2-70-10-ST	130.6	111.5	108.1	1.17	1.21
P2-70-25-ST	67.1	62.1	60.3	1.08	1.11
P4-40-10-ST	152.2	149.3	148.2	1.02	1.03
P4-40-25-ST	96.0	92.5	91.5	1.04	1.05
P4-70-10-ST	123.9	108.5	105.9	1.14	1.17
P4-70-25-ST	65.5	64.3	62.8	1.02	1.04
P6-40-10-ST	157.2	150.0	149.4	1.05	1.05
P6-40-25-ST	104.9	95.6	94.8	1.10	1.11
P6-70-10-ST	130.9	110.3	108.3	1.19	1.21
P6-70-25-ST	80.5	67.4	66.0	1.19	1.22

Table 6.6 – Proposed Short-Term Design Equations at Design Strength (Prestressed)

Column	Computed Axial Capacity, kip			P_{test} / $P_{Eq.}$	
	Test Results	Eq. 6.4	Eq. 6.6	Eq. 6.4	Eq. 6.6
P2-40-10-ST	110.2	109.3	108.8	1.01	1.01
P2-40-25-ST	71.4	66.6	66.0	1.07	1.08
P2-70-10-ST	100.7	91.2	89.4	1.10	1.13
P2-70-25-ST	59.0	50.3	49.6	1.17	1.19
P4-40-10-ST	104.7	103.0	102.7	1.02	1.02
P4-40-25-ST	68.5	65.6	65.2	1.04	1.05
P4-70-10-ST	94.8	87.5	86.1	1.08	1.10
P4-70-25-ST	59.2	51.1	50.2	1.16	1.18
P6-40-10-ST	105.8	103.4	103.1	1.02	1.03
P6-40-25-ST	71.4	67.5	67.2	1.06	1.06
P6-70-10-ST	97.7	88.4	87.3	1.11	1.12
P6-70-25-ST	62.4	53.3	52.4	1.17	1.19

Table 6.7 presents a statistical summary of the capacities for the tested columns at nominal and design strengths. The axial load capacity of the each test result was divided by the axial load capacities computed from the equations for the corresponding strength. As such, a value of 1.0 indicates perfect accuracy, while values greater than 1.0 are conservative and values less than 1.0 are unconservative. The averages and standard deviations of the ratios are listed, which provide a perspective on the accuracy and conservatism of the equations when compared to the tested

columns. To provide further comparison, the results from Equations 4.2 and 5.1, presented in Section 5.5, were included in the table.

Table 6.7 – Statistical Analysis of Proposed Short-Term Design Equations (Prestressed)

Analysis		Eq. 4.2	Eq. 5.1	Eq. 6.4	Eq. 6.6
Nominal Strength, S_n	Average	1.33	1.58	1.09	1.11
	Std. Dev.	0.24	0.26	0.06	0.07
Design Strength, ϕS_n	Average	1.25	1.47	1.08	1.10
	Std. Dev.	0.16	0.21	0.06	0.06

Consistent with the comparisons in Section 6.3.2, Equations 6.4 and 6.6 were more accurate than Equation 4.2, and 5.1, while maintaining sufficient conservatism. The proposed equations were approximately 10% conservative for both nominal and design strengths, while the current equations were greater than 25% conservative. With other design safety factors such as load factors, the current equations would be excessively conservative. The results for Equations 6.4 and 6.6 are nearly identical to each other. While Equation 6.6 is slightly more conservative than Equation 6.4, and the standard deviations are within 0.01 for both strength levels. Equation 6.4 would be more accurate for a broader range of prestressed columns, but for the range of columns tested, the equations were nearly identical.

6.5 Findings

An analytical study was conducted to determine the influence of column and loading parameters on the stiffness of prestressed columns. From those results, improved stiffness equations were developed. Using the computational model, a range of typical service prestressed columns were analyzed, and the results were used to evaluate proposed and current design equations for accuracy and conservatism. The experimental results presented in Chapter 5 were also used to evaluate the accuracy of the proposed equations. The following conclusions were made.

1. The level of axial load and eccentricity ratio were found to have the greatest influence on the stiffness of slender, prestressed columns, but the effects can be accurately and reliably estimated by Equations 6.2 and 6.3. The lower bound stiffness of prestressed columns was determined to be 0.30 E_cI_g. Other parameters such as the prestressing ratio, column slenderness, and section geometry were found to be sufficiently accounted for by normalization by the nominal axial strength or the gross section strength as well as the methodology of the moment magnification procedure.

2. Equation 6.4, developed from the results of the parametric study, was found to reliably estimate the stiffness of prestressed columns for a wide range of typical service parameters. Equation 6.6, a simplification of Equation 6.4 and a modification of Equation 4.5, was also found to reliably estimate the stiffness of prestressed columns, albeit with less accuracy than Equation 6.4.
3. When compared to the computational model, Equations 6.4 and 6.6 were shown to be significantly more accurate than current design methods while maintaining sufficient conservatism. These conclusions were substantiated by the evaluation of the equations using experimental data.

CHAPTER 7 CREEP AND SHRINKAGE BEHAVIOR OF SHORT COLUMNS

7.1 Introduction

Long-term behavior of concrete columns subject to sustained loads is complex. Time-dependent factors such as creep, shrinkage, and relaxation interact with short-term factors such as material strength and stability. Moreover, the loading conditions of columns in service can change over time, particularly during early ages due to construction loadings. As such, it is important to first understand long-term behavior of concrete columns without the added complexity of second-order effects. An experimental program was devised to test long-term effects of short concrete columns, principally creep and shrinkage behavior. The results of the program were used to calibrate existing models for predicting these effects, which guided analytical modeling of the long-term behavior of slender columns.

7.2 Existing Design Methodology

Previous researchers have developed several models to estimate creep and shrinkage of concrete, and these models vary in complexity as well as accuracy. ACI 209.2R (2008) provides a summary of four material models with comparisons against a creep and shrinkage databank. To maintain simplicity, the ACI 209R-92 Model, which is the most basic model, is presented hereafter. This model shows moderate accuracy when compared to the other models but is empirically based and does not model material phenomena. The model, however, is recommended for use in structural design due to its simplicity and insensitivity to unknown design variables. The shrinkage model is given as Equation 7.1, and the creep model is given as Equation 7.2. Both equations are modified to consider the shape and size effect in accordance with ACI 209.2R. Typically, the ultimate values are determined based on design parameters, but it is suggested to use experimental data from actual materials for increased accuracy.

$$\varepsilon_{sh}\left(t,t_c\right)=\frac{\left(t-t_c\right)}{f+\left(t-t_c\right)}\varepsilon_{shu} \quad \text{(Eq. 7.1)}$$

where:

t = age of concrete, days

t_c = age of concrete at end of curing, days

$f = 26.0e^{(0.36V/S)}$ = member shape and size factor

V/S = volume-suface ratio, in.

ε_{sh} = shrinkage strain at concrete age

ε_{shu} = notional ultimate shrinkage strain

$$\phi\left(t,t_0\right)=\frac{\left(t-t_0\right)}{f+\left(t-t_0\right)}\phi_u \quad \text{(Eq. 7.2)}$$

where:

t_0 = age of concrete at loading, days

ϕ = creep coefficient (ratio of creep strain to intial strain)

ϕ_u = ultimate creep coefficient

The equations rely on several parameters which must be within a standard range, but most service material, geometric, and atmospheric conditions satisfy the ranges. The loading parameters, however, assume concentric compression and a stress-strength ratio less than 50%. The model also assumes plain concrete. These assumptions do not correspond with service conditions of columns, especially slender columns. As a result, an experimental program was devised to test the applicability of these models to typical concrete sections in columns, and if necessary, use the results to modify the models accordingly.

7.3 Experimental Program

As noted previously, the tests consisted of six, short columns subjected to sustained load and four specimens not subjected to load and monitored for shrinkage. The columns and loading mimicked the conditions of the columns from this project. As such, eccentricity ratios of 10% and 25% were tested. Additionally, two columns were tested with concentric loading to better correlate with the existing creep models. Table 7.1 shows a detailed summary of the short column tests. The concrete for the creep tests was from Cast 2, and the concrete for the shrinkage tests was from Cast 3.

Table 7.1 – Summary of Short Column Tests

Column ID	Reinf.	Eccentricity Ratio, *e/h*	Sustained Load, kip	f_c' at Initial Loading, psi	E_c at Initial Loading, ksi
PL-13-0-LT	Plain	0%	105.2	5980	3440
PL-13-10-LT		10%	66.2	5980	3440
PL-13-25-LT		25%	40.2	5980	3440
PL-13-25-S(1)		*	*	*	*
PL-13-25-S(2)		*	*	*	*
R3-13-0-LT	4 – #3s	0%	105.2	5980	3440
R3-13-10-LT		10%	66.2	5980	3440
R3-13-25-LT		25%	40.2	5980	3440
R3-13-25-S(1)		*	*	*	*
R3-13-25-S(2)		*	*	*	*

*Shrinkage specimens

The axial load in each set of columns was varied to achieve a target stress on the compressive face of the columns of 50% of the 28-day compressive strength of the concrete ($0.5 f_c'$). This value was chosen because 50% is generally assumed to be the upper limit of the linear behavior of concrete as well as falling within the creep and shrinkage model limits. Calculations were based on the gross section properties of plain concrete, and because two columns were tested in one frame, the reinforced columns were subject to slightly less stress in the concrete due to the transformed section, which increases both the axial and bending resistance of the cross-section. The axial load for the 25% eccentric column was designed assuming cracked section properties for the plain column. Figure 7.1 shows the computed stress profiles for the three plain columns as a function of cross-section location. All three columns had a maximum compressive stress in the concrete within 5% of the target compressive stress (2990 psi).

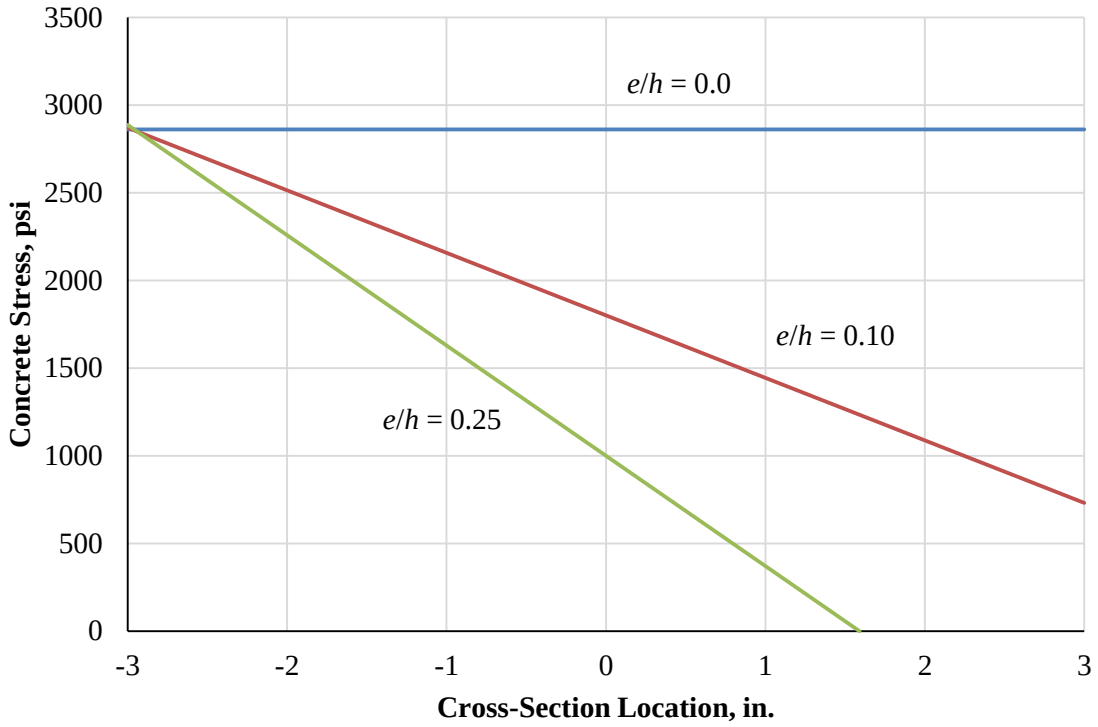

Figure 7.1 – Stress Profiles for Plain Columns

7.4 Experimental Results

The results of the tests were summarized as a function of strain versus time. For the shrinkage specimens, the time was the age of concrete, and for the sustained loaded columns, the time was the duration of loading. The strain values were recorded from electrical resistance strain gages approximately once a day, and the DEMEC measurements were recorded approximately every seven days. The results for the shrinkage and sustained loaded specimen tests were compared against the existing design methodology described in Section 7.2 to determine the applicability of Equations 7.1 and 7.2 for the specimens tested.

7.4.1 Shrinkage Tests

Figure 7.2 shows the results of the shrinkage specimens: two plain and two reinforced. Each data point is the average of two DEMEC measurements at the midspan of the specimen, which is the case for all of the shrinkage and sustained loaded specimens. Because of scheduling and curing techniques, the strain was measured beginning at a concrete age of approximately 25 days, which was 15 days after the end of wet curing. The early age shrinkage data was unimportant, however,

since all long-term specimens in the project were not loaded until at least a concrete age of 28 days. The results are not smooth and appear heavily influenced by atmospheric conditions. The specimens were kept indoors, but the temperature and humidity of the laboratory fluctuated depending on the outdoor weather.

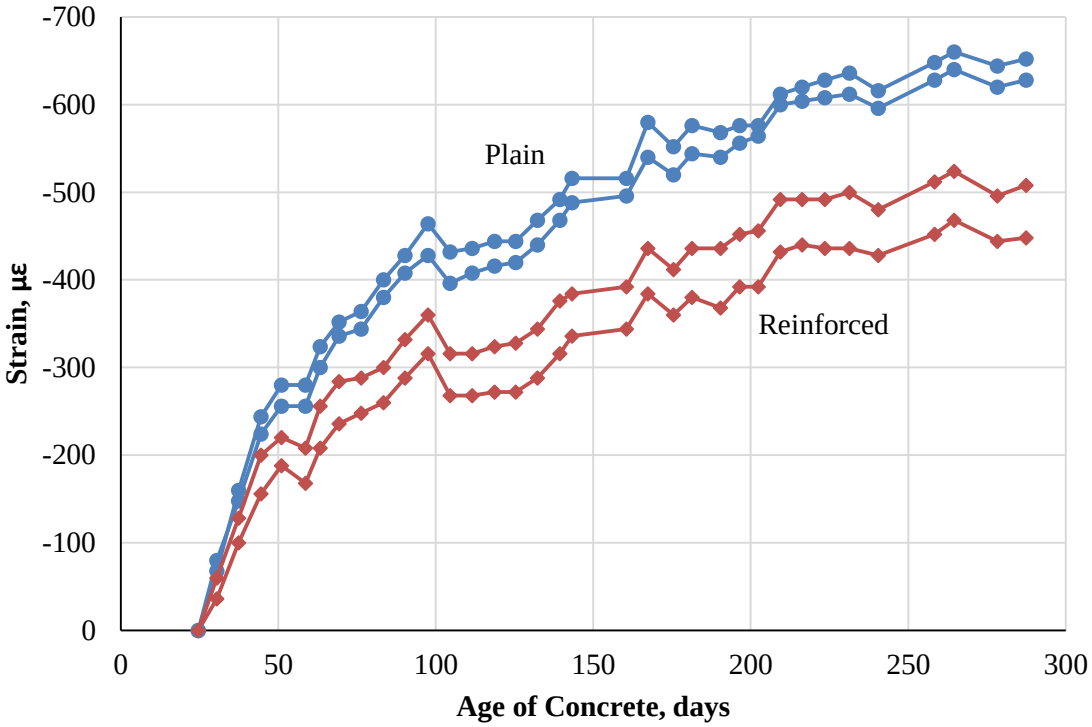

Figure 7.2 – Shrinkage Specimen Tests Results

As expected, the shrinkage rate was higher for younger concrete, and the plain specimens were subject to more shrinkage than the reinforced specimens. The duplicate specimens behaved very similarly, and differences in shrinkage values can be attributed to scatter. Because shrinkage measurements did not begin until a concrete age of 25 days, the measured shrinkage strain was zero at that age. Shrinkage begins at the end of wet curing, however, and that discrepancy is addressed below.

A regression by linear least squares was used to correlate Equation 7.1 to the shrinkage test data. The only unknown of the equation was the notional ultimate shrinkage strain (ε_{shu}). The measured data was shifted using Equation 7.1 to account for the measurements beginning at a concrete age of 25 days, and this shift was updated during the regression analysis so as not to greatly affect the results. The plain and reinforced specimens were considered separately, and for

all specimens, the age of concrete at the end of wet curing was 10 days. Figure 7.3 shows the results of the analyses.

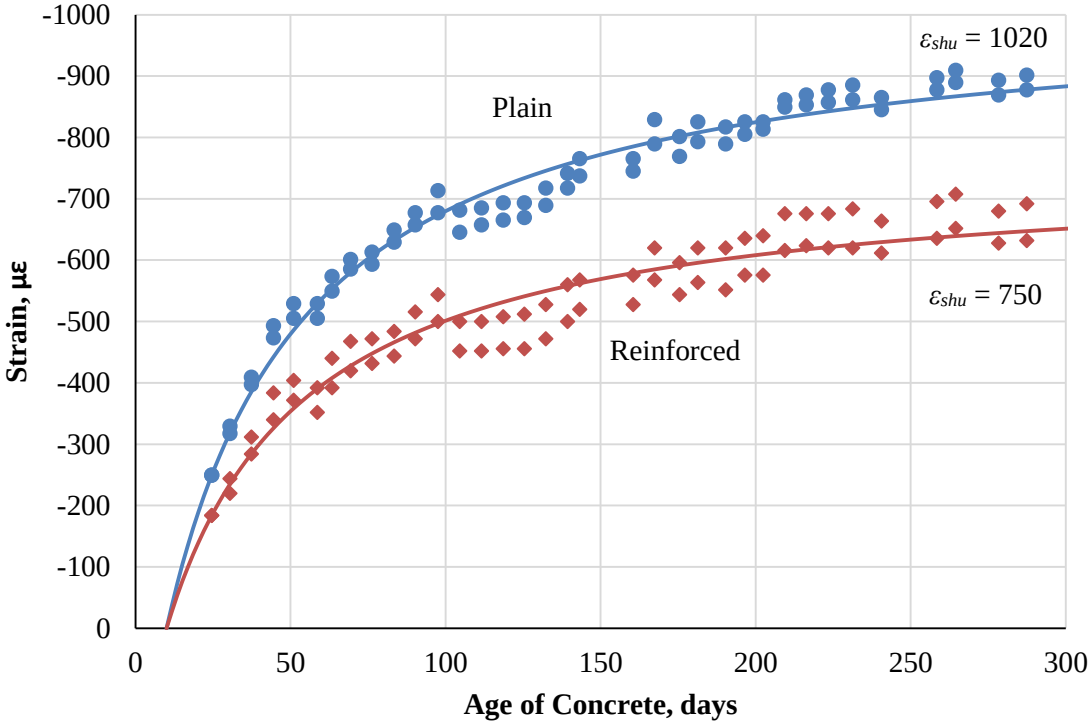

Figure 7.3 – Regression Analysis for Shrinkage Specimen Tests

The estimated ultimate notional shrinkage strain for the plain and reinforced specimens is 1020 με and 750 με, respectively, and the analysis shows good correlation with a Pearson correlation coefficient for the plain and reinforced specimens of 0.97 and 0.92, respectively. ACI 209.2R suggests an ultimate strain of 780 με for design, which can be modified by factors that include curing, relative humidity, and member size, among others. The calculated ultimate strain for the plain specimens is higher than the recommended value, and the ultimate strain for the reinforced specimens is lower, though this was anticipated.

7.4.2 Sustained Load Tests

Figure 7.4 shows the results of the sustained loaded columns with 0% eccentricity. Results are shown for both strain gages and DEMEC measurements at opposite faces of the concrete as a function of the duration of loading. In general, the strain gages and DMEC measurements yielded similar results. As shown, he results of the different measurement types are more

consistent for the reinforced columns. For the plain columns, one set of measurements are more similar than the other.

Theoretically, the strains of both faces of these columns with zero eccentricity should have been the same for each column type, but the magnitudes were slightly different. This is not unexpected, however, because of unintended eccentricity from the column end plates. It is impossible to produce truly zero eccentricity. For subsequent analyses, the strain values for each of the columns of zero eccentricity were averaged to yield one measurement.

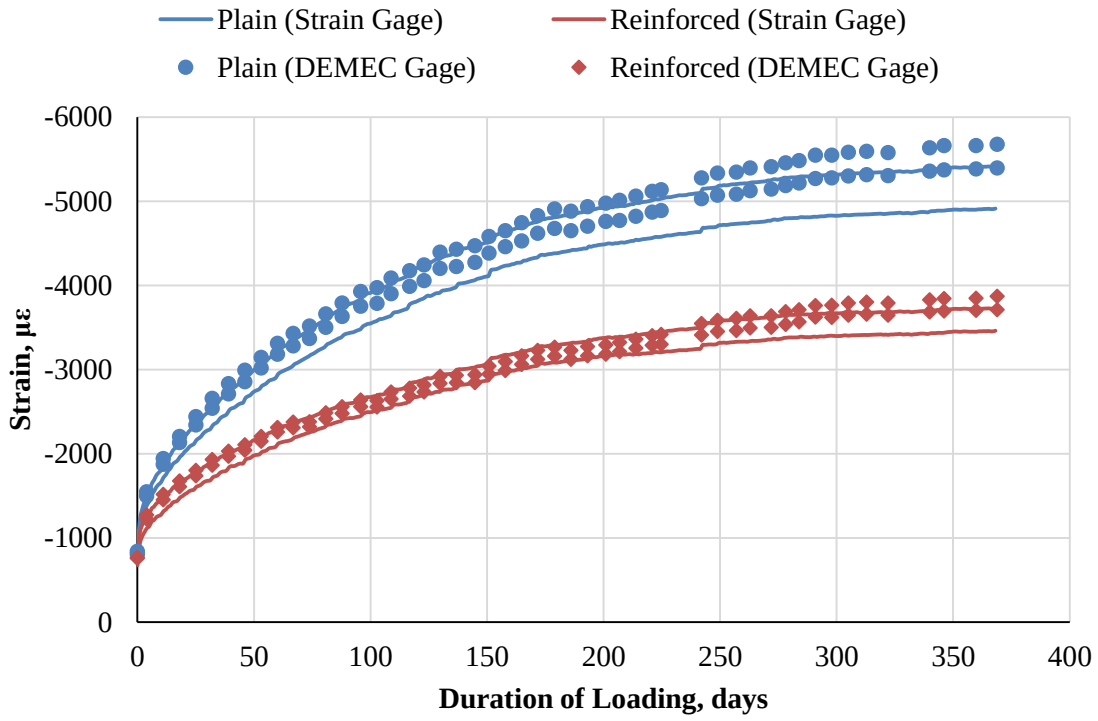

Figure 7.4 – Short Column Tests Results (0% Eccentricity)

While the strains for the plain and reinforced columns were similar immediately after loading, the plain columns experienced greater long term strain increases. Plain sections experience more shrinkage than reinforced sections, but that does not account for the entire discrepancy. Because the reinforcing bar did not yield under initial loading, the reinforcing steel accumulated stress as the strains increased over time due to creep. The effective stress on the concrete decreased thereby decreasing the creep rate of the concrete.

Figure 7.5 shows the results of the sustained loaded columns with 10% eccentricity. Because of the eccentricity, the strains of the opposite concrete faces were different, but the entire sections remained in compression. The comparison of the measurement types are similar to the previous tests, but the measurements on the concrete faces with higher strains were more consistent than those with lower strains. As noted in the figure, the strain gage and DEMEC measurements for the plain column diverged at approximately 130 days. Because of the abrupt divergence, it is assumed the bonding of the strain gage failed, and all subsequent strain measurements for that gage were unreliable. Because one column face was subject to more stress, the creep increases were much greater than those on the other face, which for both column types were very similar.

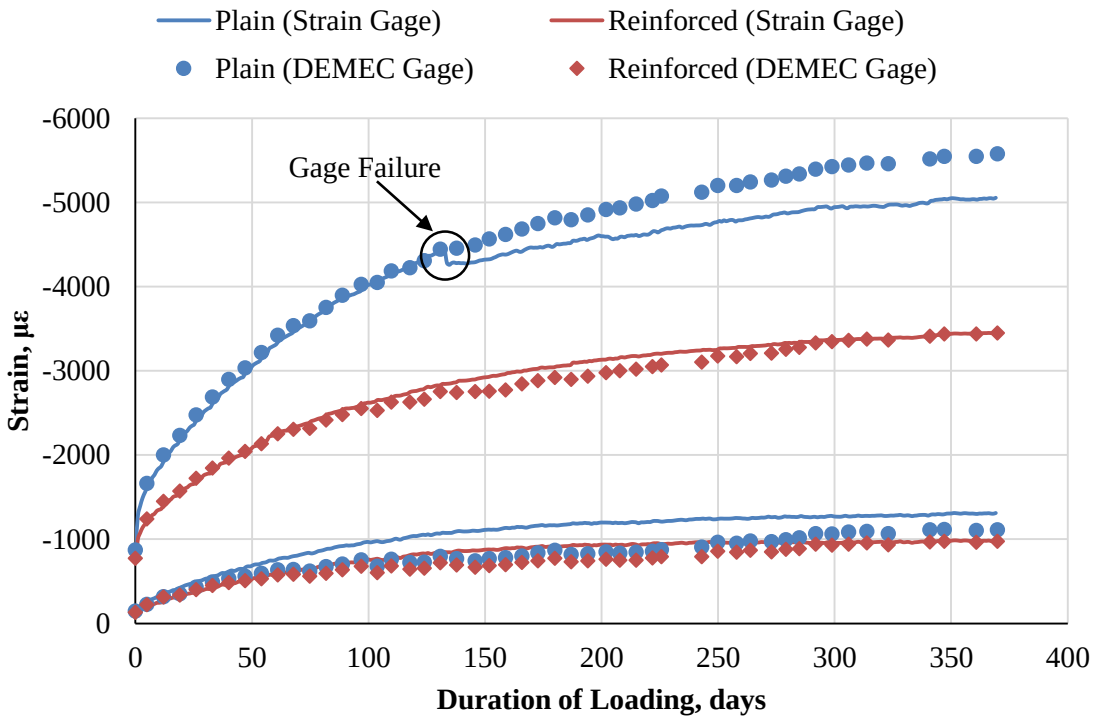

Figure 7.5 – Short Column Tests Results (10% Eccentricity)

Figure 7.6 shows the results of the sustained loaded columns with 25% eccentricity. Because of the high eccentricity, the opposite face of the column experienced tensile stresses. While the measurement types on the compressive face compare favorably, the measurements on the tensile faces do not correspond. This discrepancy can be explained a few ways. First, the DEMEC measurements were average strains over 100 mm, while the strain gages were 60 mm in length. Depending on the location of cracks, the measurements could have been incompatible. Also, if a

strain gage spans a crack, the measurement is affected more greatly than if the DEMEC measurements spans a crack. Extreme stretching of a strain gage over a crack does not result in proper strain averaging along the length of the gage. In any case, concrete strain gages are not expected to be accurate for tensile stresses, and the DEMEC measurements are assumed to be more accurate.

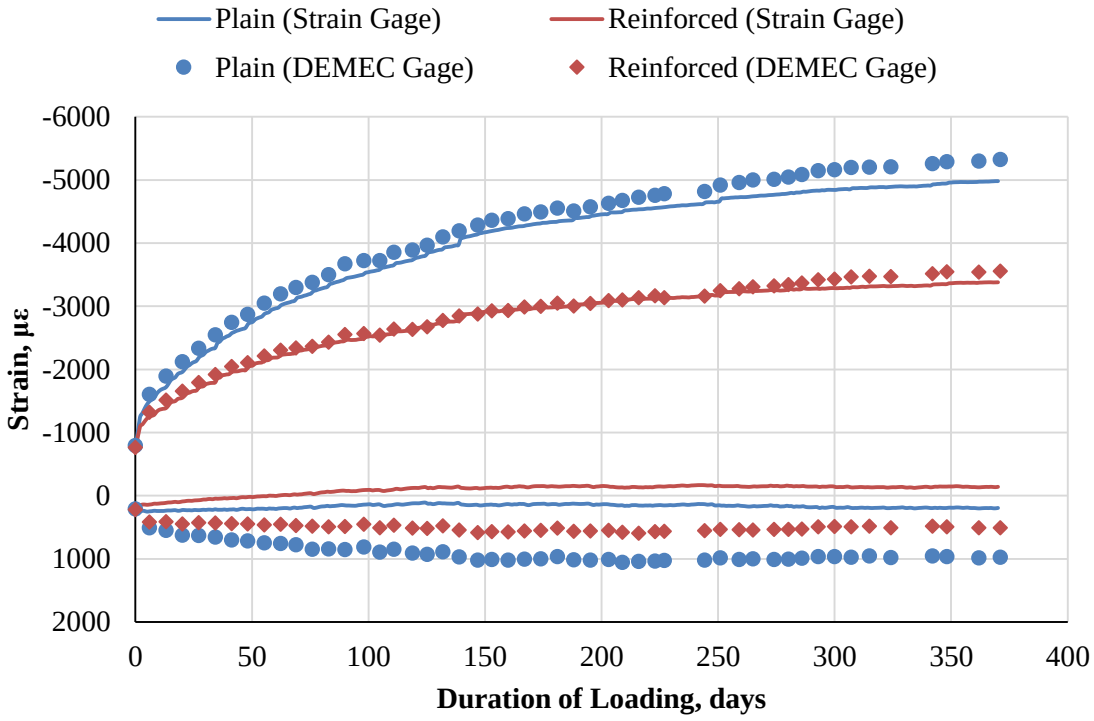

Figure 7.6 – Short Column Tests Results (25% Eccentricity)

Figure 7.7 shows a summary of the results for the sustained loaded columns. Only the DEMEC measurements on the more compressive faces are shown, and the strains of both concrete faces on the zero eccentric columns were averaged. There was no trend indicating that eccentricity and stress gradient affected the strain increases over time. In fact, the magnitudes of the strains for the plain and reinforced columns were in a different order, and the magnitudes were also not in order of increasing or decreasing eccentricity value. The strains for both column types began to diverge at a longer duration of loading, but the difference was minimal. Based on these conclusions, it can be assumed that the creep behavior of cross-sections is predominantly a function of the stress at the extreme compressive fiber.

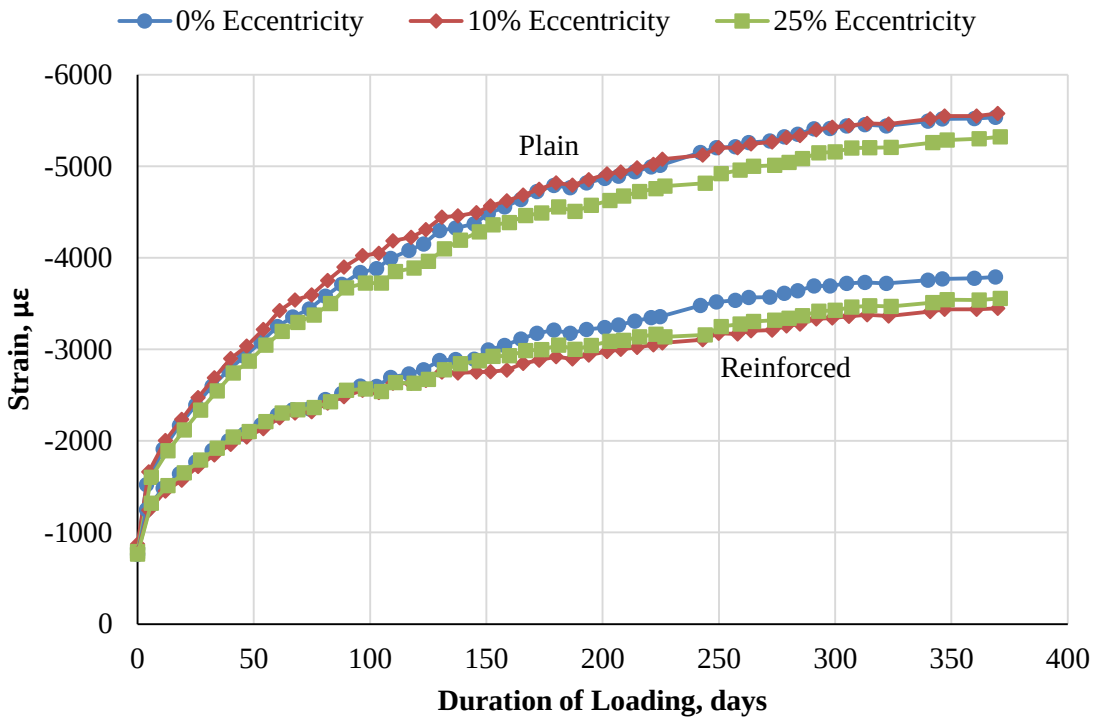

Figure 7.7 – Summary of Short Column Tests Results

Similarly, a regression analysis was used to correlate Equation 7.2 to the sustained loaded column test data using the same methods as the shrinkage analyses. Equation 7.2, however, only considers creep strains, and the sustained loaded column data included both creep and shrinkage effects. To account for the difference, the results were modified by subtracting the estimated shrinkage strains as calculated by Equation 7.1. The respective results from the analysis of the shrinkage tests were used with a concreate age at loading of 50 days. Although the shrinkage and sustained loaded specimens were cast at different times and experienced different atmospheric conditions, the results of the analyses was thought to be more accurate than using general recommended design values for Equation 7.1. Figure 7.8 shows the results of the analyses.

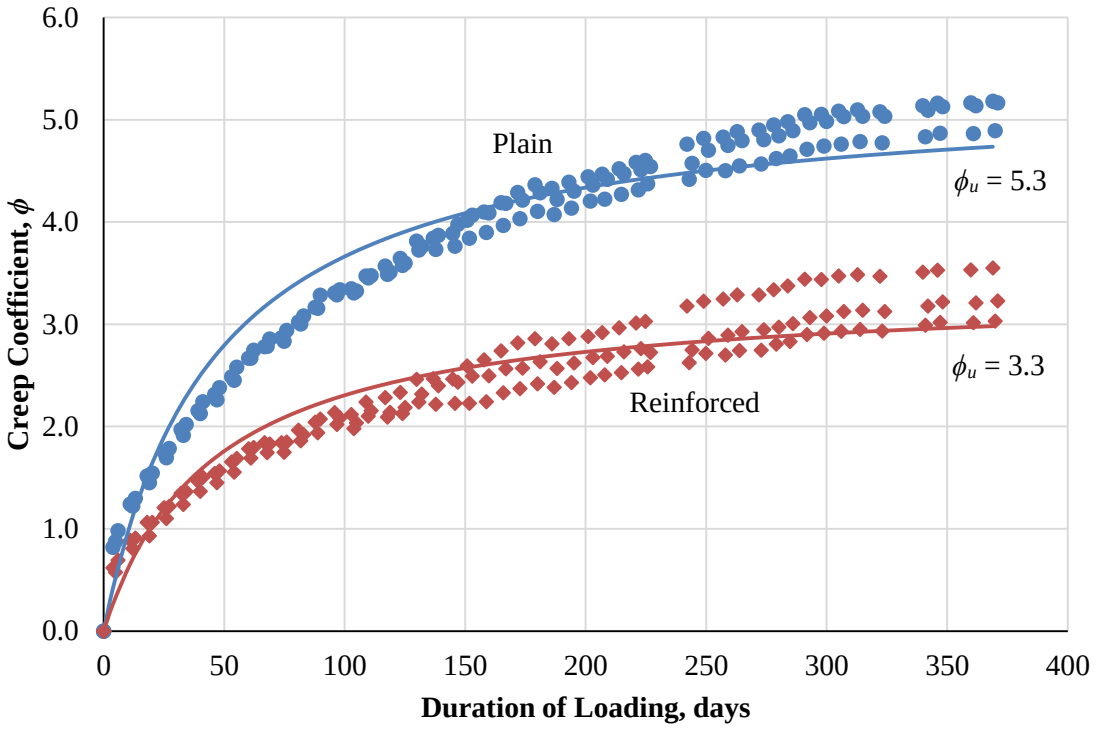

Figure 7.8 – Regression Analysis for Short Column Tests

The results are plotted as the creep coefficient or the ratio of creep strain to initial strain minus shrinkage strains. The estimated ultimate creep coefficient for the plain and reinforced tests is 5.3 and 3.3, respectively, and the Pearson correlation coefficient for the plain and reinforced tests is 0.97 and 0.91, respectively. ACI 209.2R suggests an ultimate creep coefficient of 2.35, which can be modified with similar factors as the ultimate shrinkage strain. The computed creep coefficient would be reduced due to the relatively late age (50 days) at which the columns were loaded. The computed coefficient, therefore, would be unconservative by a factor greater than 2.0. While creep data presents with significant scatter, the discrepancy between the computed and measured value is very high. ACI 209.2R, however, recommends using measured data when available.

The correlated equation is less accurate for columns at recent loading compared to longer loading. After approximately 25 days, the equations begin to produce accurate estimations of creep. In addition, the creep coefficient results for each column type are more consistent for the first 100 days of loading, after which the columns with different eccentricities begin to diverge. The divergence, however, is small and not considered to be caused by the eccentricity ratio.

7.5 Findings

Six short columns were tested under sustained load to measure the time-dependent effects of shrinkage and creep, and four specimens were monitored solely for shrinkage. In addition, the results were compared to the computational model. Based on the analyses of the results of these tests, the following conclusions were made.

1. The presence of reinforcement decreased the shrinkage rates of the concrete specimens. Equation 7.1, when correlated with experimental data, provides accurate shrinkage estimates for both the plain and reinforced specimens.
2. The presence of reinforcement decreased the creep rates of the sustained loaded columns. The eccentricity ratio, however, did not influence creep rates of the columns, and it was concluded that only the stress magnitude at the extreme compressive fiber affected the creep rates. It was further assumed that, consistent with ACI 209.2R, the creep coefficient is linear as a function of stress, at least for compressive stresses equal to or less than 50% of the concrete strength. Equation 7.2, when correlated with experimental data, provides accurate creep estimates for both the plain and reinforced columns, but Equation 7.2 is less accurate for the columns when the duration of loading was less than 25 days.
3. The ultimate creep coefficient (ϕ_u) based on the experimental results was found to be more than twice the value computed based on ACI 209.2R. While creep data presents with significant scatter, the discrepancy between the computed and measured value is very high. ACI 209.2R, however, recommends using measured data when available.

CHAPTER 8 LONG-TERM BEHAVIOR OF REINFORCED COLUMNS

8.1 Introduction

Though short-term behavior is the primary mode of behavior of most columns, long-term behavior is important and cannot be neglected. For columns subject to high dead loads and high load eccentricities, long-term effects can be significant and alone lead to column failure. These effects, though, are much more complex than short-term effects. As well as all of the parameters that influence short-term effects, long-term effects are influenced by concrete creep, age of loading, stress levels, and order of applied loads, particularly during construction. Twelve nonprestressed and four prestressed column tests similar to those tested under short-term loads were conducted. The columns, however, were subject to lower axial loads, which did not cause initial failure, for extended periods of time. In Chapter 9, the results of the tests are used to develop methods to estimate the long-term behavior of columns under sustained load as well as evaluating current design methods for estimating long-term effects.

8.2 Experimental Program

Twelve long-term tests on nonprestressed columns and four long-term tests on prestressed columns were conducted. Table 8.1 provides a summary of the long-term tests and includes the normalized sustained load ratio of the columns. To further evaluate the long-term behavior of certain column loading combinations, four of the column tests were repeated at a slightly different axial load ratio. The repeated columns are denoted with a (1) and (2) following the Column ID as shown in Table 8.1.

As noted previously, the sustained load was chosen based on preliminary calculations and the ACI 318 (2014) provisions. Due to differences in concrete strength and reinforcement ratios, the sustained loads were assigned based on the load ratio and not absolute loads. The load ratio was defined as the applied load to the nominal strength (P_0) at 28 days using the nominal steel strengths. By using normalized applied loads, the comparison between columns of different concrete strengths and reinforcement ratios is more consistent.

Table 8.1 also includes the sustained load ratio of the prestressed columns, which matched the ratios applied to the nonprestressed columns (accounting for the different calculations of the nominal axial strengths). To reduce the number of columns tested under sustained load, only one reinforcement arrangement was tested. The four-wire arrangement was chosen because it was considered the most typical arrangement.

Table 8.1 – Summary of Long-Term Tests

Column ID	Reinf.	Slenderness Ratio, kl_u / r	Eccentricity Ratio, e / h	Sustained Load, P / P_0	Cast
R3-40-10-LT	4 – #3s	40	10%	40.0%	1
R3-40-25-LT(1)			25%	35.0%	1
R3-40-25-LT(2)				32.5%	2
R3-70-10-LT(1)		70	10%	30.0%	1
R3-70-10-LT(2)				32.5%	2
R3-70-25-LT			25%	15.0%	1
R5-40-10-LT	4 – #5s	40	10%	40.0%	2
R5-40-25-LT(1)			25%	35.0%	2
R5-40-25-LT(2)				37.5%	4
R5-70-10-LT(1)		70	10%	30.0%	2
R5-70-10-LT(2)				32.5%	3
R5-70-25-LT			25%	15.0%	2
P4-40-10-LT	4 – PS Wires	40	10%	40.0%	3
P4-40-25-LT			25%	35.0%	3
P4-70-10-LT		70	10%	30.0%	3
P4-70-25-LT			25%	15.0%	3

A maximum sustained load ratio of 40% was used based on ACI 318 provisions. Assuming a column with tie reinforcement, the maximum permitted axial load with reduction factors is $\phi P_{n,\max} = 0.80\ \phi P_0 = 0.52\ P_0$. Further applying a load factor of 1.4 for a column controlled by dead load, the maximum permitted service load is approximately 0.37 P_0, and based on this, a maximum sustained load of 0.40 P_0 was used. As the slenderness ratio and eccentricity ratio increased the demand on the column, the chosen sustained load ratio was correspondingly decreased.

Based on the results of some of the tests, four column tests were repeated at different loads. The repeated columns, which are denoted with a (2), included the parameters of greater interest. As

noted previously, the 40-10 columns do not exhibit much second-order effects while the 70-25 columns pushed the boundaries of realistic, service columns. Three of the repeated columns were subjected to a higher axial load ratio to induce greater long-term effects, while one column was subjected to a lower axial load ratio because the first test nearly caused failure under only sustained load.

Table 8.2 provides a detailed summary of the long-term tests. The table includes the applied sustained load on the columns and the material properties measured within one day of the initial loading as well as within one week of final loading to failure. For the few columns that failed under sustained load, only available material properties are listed.

Table 8.2 – Details of Long-Term Tests

Column ID	Sustained Load, kip	f_c' at Initial Loading, psi	E_c at Initial Loading, ksi	f_c' at Failure, psi	E_c at Failure, ksi
R3-40-10-LT	88.0	6630	4120	7020	4264
R3-40-25-LT(1)	77.0	6630	4120	7020	4264
R3-40-25-LT(2)*	66.0	5710	3500	5780	--
R3-70-10-LT(1)	66.0	6630	4120	7020	4264
R3-70-10-LT(2)*	66.0	5710	3500	--	--
R3-70-25-LT	33.0	6630	4120	7020	4264
R5-40-10-LT	98.5	5710	3500	5570	3330
R5-40-25-LT(1)	86.0	5710	3500	5570	3330
R5-40-25-LT(2)	95.6	5930	3930	6570	3820
R5-70-10-LT(1)	74.0	5710	3500	5570	3330
R5-70-10-LT(2)	81.4	5800	3840	6370	4010
R5-70-25-LT	37.0	5710	3500	5570	3330
P4-40-10-LT	68.6	5800	3840	6370	4010
P4-40-25-LT*	60.0	5800	3840	--	--
P4-70-10-LT	51.4	5800	3840	6370	4010
P4-70-25-LT	25.7	5800	3840	6370	4010

*Column failed under sustained load

8.3 Experimental Results

Due to the complexity of long-term loading, the results for the tests are summarized using several different types of figures to fully explore the columns' behavior. In addition to the figures shown

for the short-term tests results, figures that are time dependent are presented. Some of the figures in this section include nominal strengths, which were computed with the computational model using the as-measured, final test-day material properties of the concrete and reinforcing steel. To decrease clutter, only the nominal strengths for the primary columns are shown. In other words, the nominal strengths for the repeated columns, denoted by (2), are not included. Appendix D provides a comparison between the long-term tests and their companion short-term tests.

8.3.1 Nonprestressed Columns (#3 Bars)

Figure 8.1 shows the results of the long-term tests of the columns with #3 reinforcing bars. As before, both the load-deflection relationships and the interaction diagrams are shown. The interaction diagrams also include the behavior of short columns, which represents the first-order moment (M_0) and helps to illustrate the amount of second-order effects experienced by the tested columns. The diagram also includes the ACI 318 total moment limit of 1.4 times the first-order moment (1.4 M_0). It should be noted that absolute loads, not normalized loads, are plotted. Because Casts 1 and 2 had different concrete strengths, the applied loads for R3-70-10(1) and R3-70-10(2) were different normalized but the same absolute. The curves, therefore, are shown plotted on top of each other.

The general behavior of the columns was similar to that of the short-term columns, as expected. The difference lies in the region of sustained load. With no increase in axial load, the deflections, and thus moments, increased. While most columns were subjected to approximately 100 days of sustained load, the differences in behavior were affected by the amount of sustained load, the slenderness ratio, the eccentricity ratio, and the reinforcement ratio. Similar to the short-term columns, the end region of Column R3-40-10 failed under final short-term loading, which caused the column to fail at less than the computed nominal strength. The computed nominal strength was conservative for all other columns, even considering the different concrete strengths.

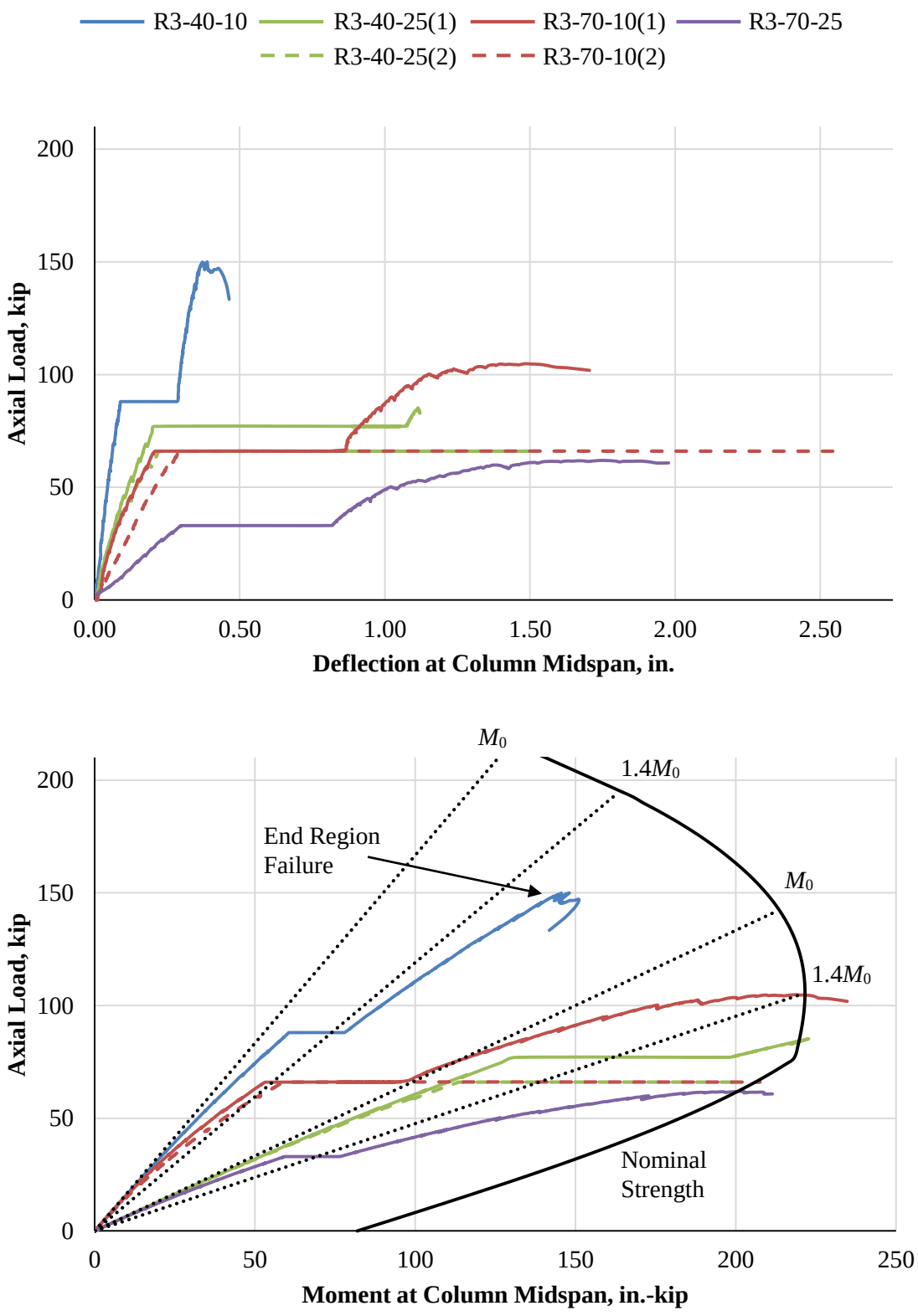

Figure 8.1 – Long-Term Tests Results (#3 bars)

Columns R3-40-25(2) and R3-70-10(2) failed solely under sustained load at 69 days and 42 days, respectively. Because R3-70-10(1) showed signs of reaching long-term equilibrium, the repeated column was subjected to a higher sustained load ratio. It was anticipated that this could cause failure under sustained load, which was the ultimate result. The failure of Column R3-40-25(2) was unexpected, however. Column R3-40-25(1) experienced significant long-term effects and almost failed after 100 days, and as a result, the sustained load ratio for the repeated test was reduced to evaluate the effect. At 28 days, the concrete strengths of Cast 1 and 2 were moderately similar at 6170 psi and 5710 psi, respectively. The concrete from Cast 1, however reached a compressive strength of 7020 psi while the concrete from Cast 2 decreased to a strength of 5570 psi based on cylinder results, which indicates lack of strength gain beyond 28 days. Due to a combination of these effects, Column R3-40-25(2) failed under sustained load even when subjected to a lower load ratio than Column R3-40-25(1).

Depending on the loading parameters, the columns experienced very different long-term effects. For the R3-40-10 column, the absolute deflection increase was the smallest at approximately 0.20 in. On a relative basis, however, the deflection at the end of sustained load was over three times the initial deflection. This increase was enough to extend the column behavior past the 40% second-order limit. Conversely, R3-70-25 had a larger absolute deflection increase at approximately 0.48 in., but the final deflection after sustained load was two-and-a-half times the initial deflection.

The R3-40-25 and R3-70-10 columns exhibited the largest second-order effects due to sustained loads with deflections after sustained load that were four and five times the initial deflections, respectively. These columns were subject to high sustained loads as well as either high eccentricity or high slenderness, both of which contributed to greater second-order effects. The columns greatly exceeded the 40% limit after the sustained load but had not even crossed the threshold under initial loading. The R3-40-25(1) column also showed instability and would likely have failed if the loading were continued.

While Figure 8.1 illustrates the behavior of columns subject to sustained loads, the variable of time was removed. Figure 8.2 shows the time-dependent behavior of the columns with #3 bars. The failure points of Columns R3-40-25(2) and R3-70-10(2), which failed under sustained load, are marked. These columns experienced very fast deflection increases as a function of time before ultimate failure. Column R3-40-25(2) appeared to have typical behavior during the first

20 days of loading, after which an inflection point is observed, indicating that long-term instability began to dominate. Once this inflection occurs, the increases in second-order effects due to increases in creep would likely always lead to ultimate failure after enough time. Column R3-70-10(2), on the other hand, never showed signs of long-term stability. After about 5 days, the deflections increased rapidly and led to an ultimate failure in less than 42 days.

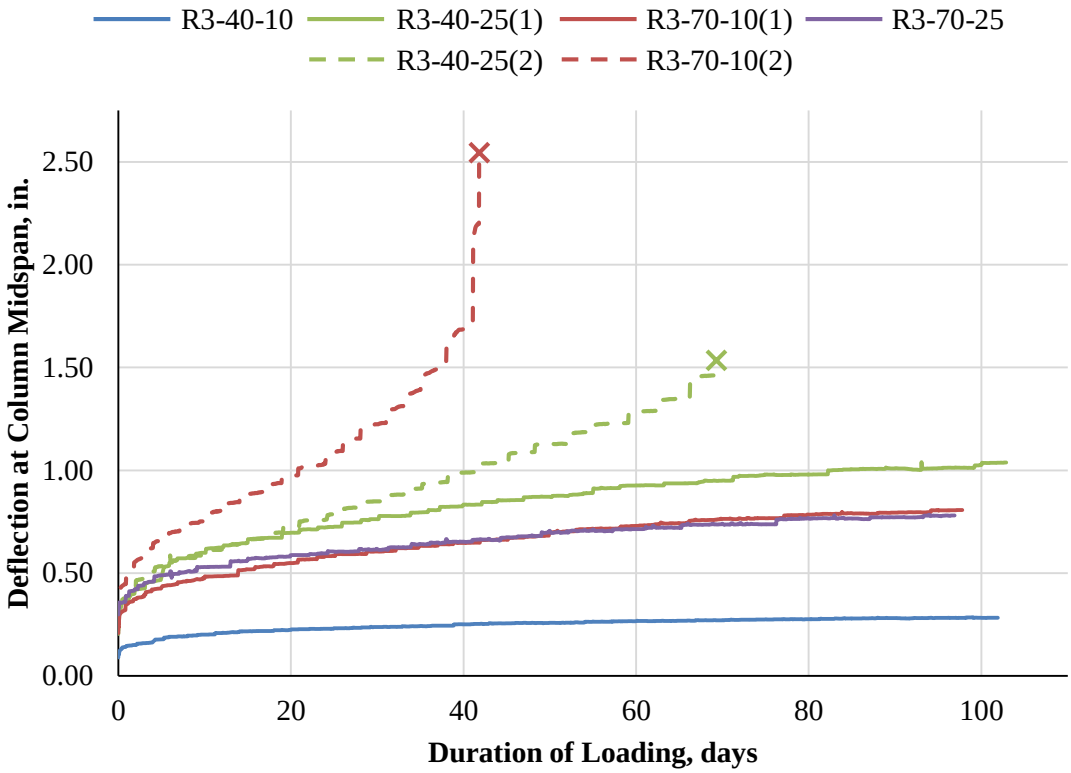

Figure 8.2 – Long-Term Deflection versus Time (#3 bars)

8.3.2 Nonprestressed Columns (#5 Bars)

Figure 8.3 shows the results of the long-term tests of the columns with #5 bars. As before, both the load-deflection relationships and the interaction diagrams are shown. The interaction diagrams also include the behavior of short columns, which represents the first-order moment (M_0) and helps to illustrate the amount of second-order effects experienced by the tested columns. The diagram also includes the ACI 318 total moment limit of 1.4 times the first-order moment (1.4 M_0). It should be noted that absolute loads, not normalized loads, are plotted.

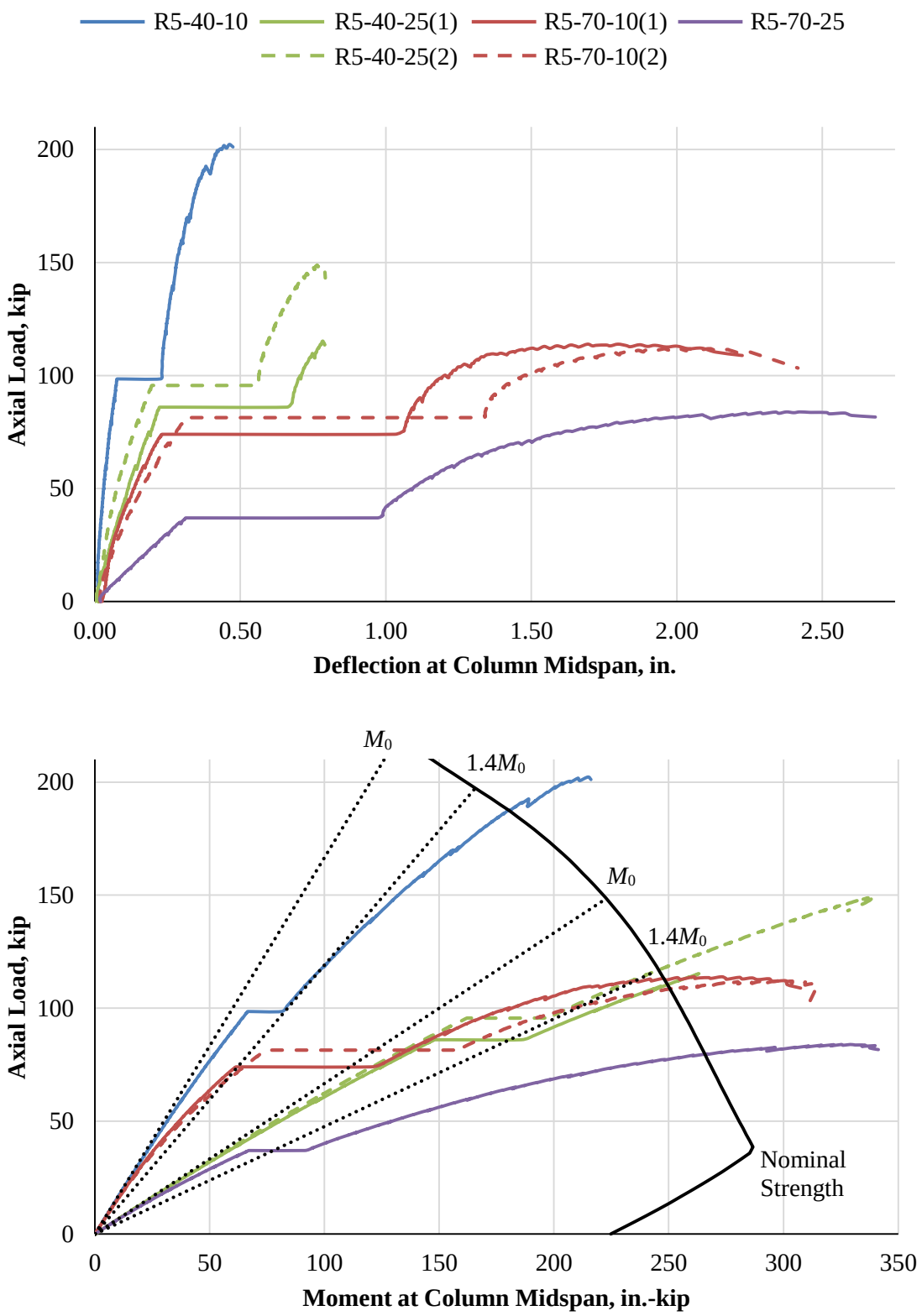

Figure 8.3 – Long-Term Tests Results (#5 bars)

As with the columns with #3 bars, the R5-40-25 and R5-70-10 columns showed the largest time-dependent increases. While the increases in deflections were approximately a factor of three for the 40-25 columns and a factor of four-and-a-half for the 70-10 columns, the columns did not show signs of long-term instability. Also, the R5-40-25 columns barely exceeded the 40% limit under sustained load, albeit they were only loaded for 100 days.

Both repeated columns were subject to higher sustained loads to increase the time-dependent effects. For the 70-10 columns, the time-dependent effects were noticeably larger for the repeated column. The higher sustained load caused both a higher initial deflection as well as a higher time-dependent deflection increase. The ratio of deflection after sustained load to initial deflection was very similar at approximately four-and-a-half. The difference between the 40-25 columns was less pronounced. Despite the repeated column being subject to a higher sustained load, the initial deflection was less than that of the primary column. The concrete for the repeated column, however, was approximately 15% stiffer than the concrete for the primary column, which contributed to this difference. The deflection increase under sustained load was slightly lower for the repeated column, but the ratios of deflection after sustained load to initial deflection were similar at approximately three.

While Figure 8.3 illustrates the behavior of columns subject to sustained loads, the variable of time was removed. Figure 8.4 shows the time-dependent behavior of the columns with #5 bars. As shown, the behavior of these columns demonstrated more stability than the columns with #3 bars. The 40-10 and 40-25 columns seemed to have nearly peaked by 100 days, with a slope of nearly zero. The other columns, specifically R5-70-10(2), did appear to be continuing to deflect after 100 days, but the slope appears less than that of the corresponding columns with #3 bars. None of the columns appeared to have an inflection point, which can indicate a long-term stability concern.

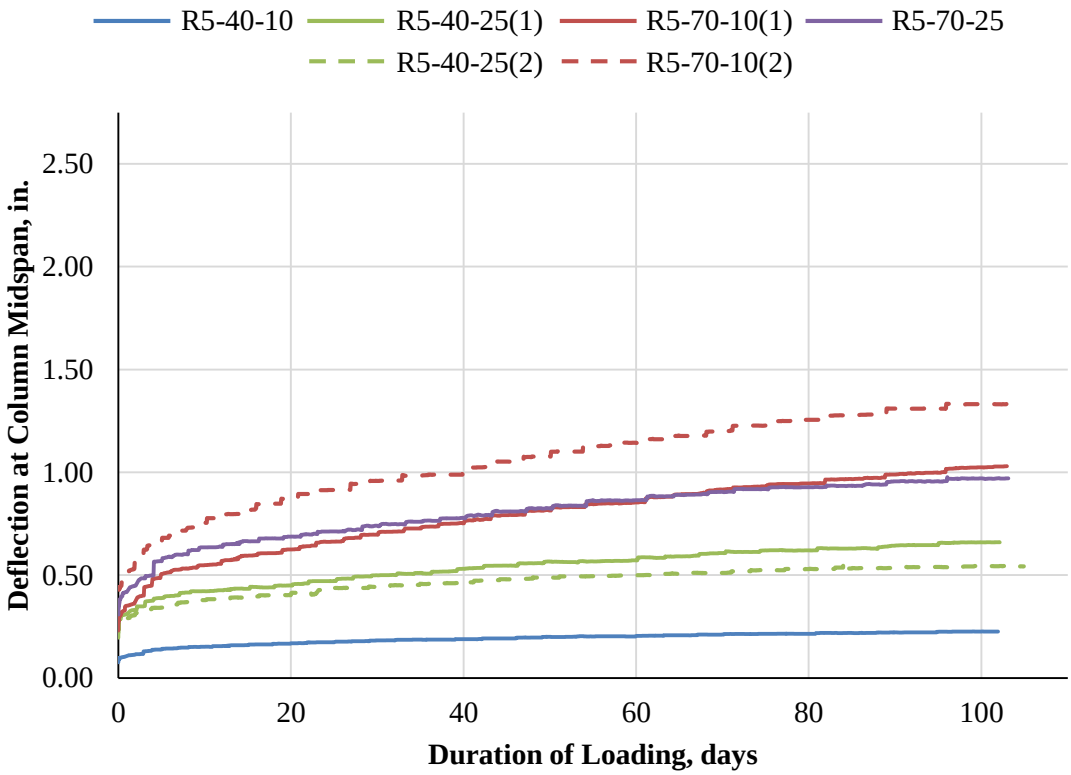

Figure 8.4 – Long-Term Deflection versus Time (#5 bars)

8.3.3 Summary of Nonprestressed Columns

Because the columns with #3 and #5 bars are both nonprestressed, the similarities and differences of the results are discussed. For both reinforcement types, the 40-10 columns exhibited the smallest increases in second-order effects due to sustained load. Interestingly, the 70-25 columns showed the next smallest increases, when viewed on the interaction diagrams. While these columns were very slender and had a high eccentricity, the sustained load ratio was very low because it was thought these columns would be very sensitive to sustained loads. Despite the low sustained loads, these columns had deflection increases similar to the 40-25 and 70-10 columns, showing they were, in fact, very sensitive to sustained loads. Minor increases in the sustained loads would likely have caused failure under sustained load.

In general, the columns with #3 bars showed greater second-order effects due to sustained loads. Both columns that failed were columns with #3 bars (R3-40-25(2) and R3-70-10(2)). The columns with #5 bars showed less effects for a few reasons. The nominal strength was used to

determine the applied sustained load, and as a result, the concrete stresses on the columns with #5 bars were slightly lower than the stress on the other columns even though the applied load ratio was the same. Additionally, as the creep strains increased, the columns with #5 bars were able to shed more of the forces to the extra reinforcing steel area. This force transfer allowed faster decreases in concrete stresses over time, which improved the long-term behavior of the columns.

Ten of the 12 columns tested exceeded the ACI 318 total moment limit (1.4 M_0) solely under sustained load, while the two columns with #5 bars that did not were within 3% of the limit. Because the sustained load was only applied for approximately 100 days, it can be assumed that all of the columns would have exceeded this limit if the sustained load was maintained long enough to allow for equilibrium. The residual strength after crossing the 40% limit was significantly different for the different columns. The difference was mostly driven by the increase of second-order effects due to the sustained load. As mentioned previously, two columns failed under sustained load, which means these columns had zero residual capacity. At the other end of the spectrum, the 40-10 columns had almost 100% additional strength after passing the limit, assuming the end region of the R3-40-10 column would not have been damaged.

Table 8.3 provides a summary of the long-term experimental tests for the nonprestressed columns. The durations of loading and deflections at the beginning and end of the sustained load are shown. Also, the peak test loads are shown.

Table 8.3 – Summary of Long-Term Tests Results (Nonprestressed)

Column ID	Duration of Load, days	Deflection During Sustained Load, in.		Peak Test Load, kip
		Beginning	End	
R3-40-10-LT	101.9	0.09	0.28	150.0**
R3-40-25-LT(1)	102.9	0.20	1.04	88.9
R3-40-25-LT(2)	69.3*	0.22	1.54	66.0*
R3-70-10-LT(1)	97.8	0.21	0.81	104.8
R3-70-10-LT(2)	41.8*	0.29	2.55	66.0*
R3-70-25-LT	96.9	0.30	0.78	62.0
R5-40-10-LT	101.9	0.08	0.23	202.3
R5-40-25-LT(1)	102.1	0.22	0.66	127.9
R5-40-25-LT(2)	104.9	0.20	0.54	149.2
R5-70-10-LT(1)	103.0	0.23	1.03	113.9
R5-70-10-LT(2)	103.0	0.32	1.33	112.0
R5-70-25-LT	103.1	0.31	0.97	83.9

*Column failed under sustained load
**Column end region failed prematurely

8.3.3.1 Column Failure Types

The column failure types were similar to those observed during the short-term tests. For all but Columns R3-40-10-LT and R5-40-10-LT, the failure types were the stiffness type failures with very minor to no bar buckling. Column R3-40-10 had an end region failure, while Column R5-40-10 experienced bar buckling similar to that seen previously. This column failed this way because it was subject to very little long-term effects and essentially behaved as a short-term column.

The reason for the higher prevalence of stiffness failures was undoubtedly caused by the sustained load. The high creep strains imparted on the concrete tended to soften the concrete. During final loading, the rate of spalling prior to the stiffness failure was much higher than that observed during the short-term tests, which would infer damage accumulated in the concrete over time.

Figure 8.5 shows the stiffness failures for two representative long-term columns. Figure 8.5 (a) shows the failure of a column type that demonstrated bar buckling under short-term testing. After being subject to sustained load, the failure was governed by a stiffness failure, where the concrete

slowly spalls reducing the cross-section. The capacity of the column continued to decrease until the test was stopped. For this column, there was minor bar buckling and only some concrete from within the core was damaged. Besides the columns that did not have stiffness failures, this level of damage was the most severe observed for the long-term columns. Conversely, Figure 8.5 (b) shows the failure pattern of a column that failed under sustained load. Because no additional load was applied to cause failure, there was very little visible damage to the column. As shown, the spalling was so little that the reinforcing bars were barely exposed. Consistent with the short-term tests, all of the columns failures were within one tie group of the center, with the exception of the column that failed in the end region.

(a) R3-40-25-LT(1)

(b) R3-70-10-LT(2)

Figure 8.5 – Typical Failures of Long-Term Tests (Nonprestressed)

8.3.4 Prestressed Columns

Figure 8.6 shows the results of the long-term tests of the columns with four prestressing wires. As before, both the load-deflection relationships and the interaction diagram are provided. The

nominal strength was computed with the computational model using the as-measured, final test-day material properties of the concrete and reinforcing steel. The interaction diagram also includes the behavior of short columns, which represents the first-order moment (M_0) and helps to illustrate the amount of second-order effects experienced by the tested columns. Finally, Figure 8.6 includes the ACI 318 total moment limit of 1.4 times the first-order moment (1.4 M_0).

The prestressed columns behaved similarly to the columns with #3 bars, but the deflections increases under sustained load were even higher. All four columns experienced final deflections of at least five times the initial deflection. P4-70-10-LT experienced a final deflection ten times the initial. Over that time, the final moment at the end of sustained loading was three times the moment at the beginning of sustained loading. The moment at the end of the sustained loading was four times the first-order moment of the column, which greatly exceeds the ACI 318 total moment limit. All four columns exceeded the ACI 318 total moment limit by the end of the sustained load. When the columns were brought to final failure, the columns exceeded the limit even further.

While the columns experienced significant second-order effects, several of the columns had a large amount of residual capacity. P4-40-10 had 100% additional residual capacity beyond the sustained load, even after it had already surpassed the ACI 318 total moment limit. P4-70-25 also had a residual capacity of 100% of the sustained load.

On the other hand, the other two columns did not have the same type of residual capacity. P4-70-10, as previously mentioned, had the greatest deflection and moment increase of the four columns. The column only had an additional 30% capacity above the sustained load. The last column, P4-40-25, failed under sustained load after only 20 days. As noted in the load-moment figure, the column failed slightly less than the nominal strength, but the strength on the figure was computed using the final concrete strength, which was approximately 10% higher than the concrete strength at initial loading. Using the concrete strength at initial loading results in a conservative nominal strength estimation. Besides P4-40-25, all of the other columns failed beyond the computed nominal strength.

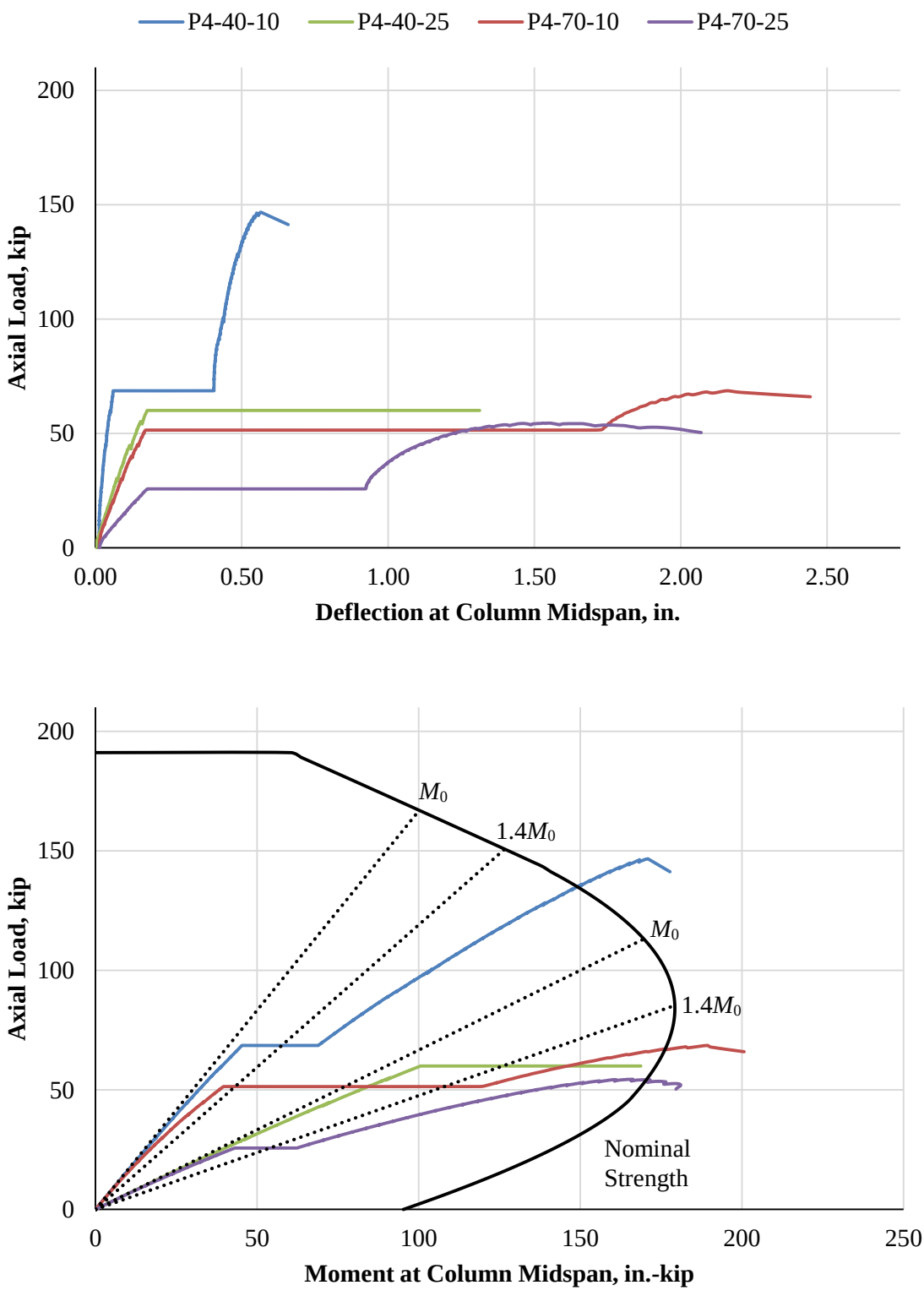

Figure 8.6 – Long-Term Tests Results (4 – PS Wires)

Figure 8.7 shows the time-dependent behavior of the columns with four prestressing wires. All columns experienced very high deflection increases. P4-40-25, which failed under sustained load, had a very rapid deflection increase beyond approximately 18 days. Because the stiffness decreased so quickly, the loading rams were not readjusted frequently enough to maintain adequate loading during the final days before failure. If the sustained loading was maintained more accurately, this column likely would have failed a few days earlier. P4-40-10 had a final deflection of over six-and-a-half times the initial deflection, but the behavior seemed to have stabilized. On the other hand, the P4-70 columns did not appear to stabilize. In particular, the deflections of P4-70-10 were increasing very rapidly, and it can be assumed this column would have failed under sustained load if it was given more time.

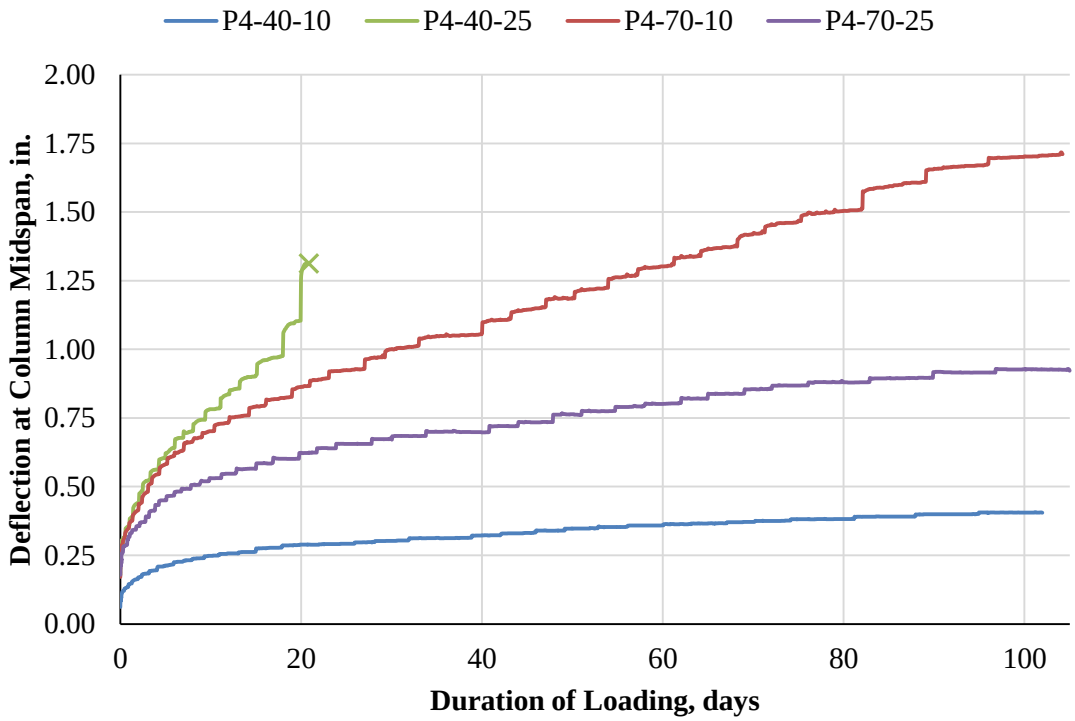

Figure 8.7 – Long-Term Deflection versus Time (4 – PS Wires)

Table 8.4 provides a summary of the long-term experimental tests for the prestressed columns. The durations of loading and deflections at the beginning and end of the sustained load are shown. Also, the peak test loads are shown.

Table 8.4 – Summary of Long-Term Tests Results (Prestressed)

Column ID	Duration of Load, days	Deflection During Sustained Load, in.		Peak Test Load, kip
		Beginning	End	
P4-40-10-LT	102.0	0.06	0.41	146.6
P4-40-25-LT	20.9*	0.18	1.10	60.0*
P4-70-10-LT	104.2	0.17	1.71	68.7
P4-70-25-LT	105.0	0.18	0.92	54.4

*Column failed under sustained load

8.3.4.1 Column Failure Types

The nonprestressed columns under sustained load showed lesser damage than their corresponding short-term tests, but the prestressed columns showed the same type of damage for both the short-term and long-term tests, which, as mentioned previously, were much more explosive than the failures for nonprestressed columns. The typical failure types for the prestressed, long-term columns were similar to those of the prestressed, short-term columns. Figure 8.8 shows two representative failures for the prestressed, long-term columns. For the less slender column shown in Figure 8.8 (a), the damage went beyond one column tie. In addition, there was minor wire buckling that was assumed to occur during the post-failure collapse of the load frames. For the more slender column shown in Figure 8.8 (b), the damage occurred over a smaller area and did not damage concrete as deep into the core of the column. Similar to several of the short-term tests, the wires on the tensile face fractured after failure of the column. The wires on the compressive face did not fracture during or after the test but were cut to facilitate removal of the column from the loading frame. All of the columns failed within the middle third of the column, consistent with the failures of the short-term tests.

(a) P4-40-10-LT

(b) P4-70-25-LT

Figure 8.8 – Typical Failures of Long-Term Tests (Prestressed)

8.4 Findings

Twelve nonprestressed and four prestressed, slender column were tested under long-term loading and were subject to a constant sustained load for 100 days. After that time, the columns were subject to constantly increasing load until failure. Three columns failed under sustained load prior to reaching 100 days. The following conclusions were made.

1. The increase of reinforcement from #3 bars to #5 bars aided the long-term stability of the columns. While the deflection increases between the columns were similar, the columns with #5 bars seemed to stabilize by 100 days while most of the columns with #3 bars did not. This difference was evident in spite of the fact that the columns with #5 bars had higher applied loads.

2. The prestressed columns exhibited higher long-term effects than the nonprestressed columns. One column had a final post-sustained load deflection of ten times the initial deflection.
3. Nearly all columns exceeded the ACI 318 total moment limit after 100 days of sustained load, but several columns retained significant post-sustained load residual capacity.
4. Most nonprestressed columns had a more ductile stiffness failure, even for the columns with a lower eccentricity. The prestressed columns, on the other hand, failed explosively, similar to the short-term tests.
5. All but two columns failed beyond the computed nominal strength. One of those columns had an end region failure, while the other column failed under sustained load at a young age.

CHAPTER 9 DESIGN STIFFNESS FOR LONG-TERM BEHAVIOR

9.1 Introduction

The results from the long-term tests were used to develop an improved design method for estimating the long-term behavior of slender columns. The proposed method was developed to be consistent with the current ACI 318 (2014) methodology and to be simple and reliable for use as a design approach. The results of the experimental tests were compared with the proposed method to determine its accuracy and conservatism. Additionally, current design methods for long-term effects were evaluated using the experimental results.

9.2 Behavior under Sustained Load

ACI 209 provides simplified analysis methods for creep affecting structural response (ACI Committee 209 1992). The first method is to reduce the modulus of elasticity of the concrete as a function of time (Equation 9.1). The creep coefficient (ϕ) is a function of several parameters, most importantly duration of loading, and the specifics and calibration of this variable were presented in Chapter 7. The coefficient based on the experimental results was used for the evaluations, instead of the coefficient computed from ACI 209.2R (2008). As mentioned, the computed value would provide unconservative results.

Equation 9.1 is suggested for "cases in which the gradual time change of stress due to creep and shrinkage is small and has little effect." For "cases in which the gradual time change of stress due to creep and shrinkage is significant," ACI 209 suggests a modified version of Equation 9.1 known as the age-adjusted effective modulus method. For slender columns subject to second-order effects, the time change of stress can be significant. Using the age-adjusted effective modulus method, however, results in smaller computed creep effects. As a result, Equation 9.1 is more conservative and, partly due to its simplicity, is used hereafter.

$$E_{eff} = \frac{E_c}{1+\phi(t)} \quad \text{(Eq. 9.1)}$$

where:

E_c = modulus of elasticity of concrete, psi

E_{eff} = effective modulus of elasticity of concrete, psi

t = duration of sustained load, days

ϕ = creep coefficient (ratio of creep strain to intial strain)

While the creep of plain concrete is relatively simple and fairly well understood, its effect on column cross-sections and member behavior, particularly for slender columns subject to second-order effects, is much more complex. Parameters such as reinforcement and time-dependent stress changes can greatly affect creep of the concrete. As a result, while the modulus of elasticity of concrete is a contributing factor, the section property of most interest for concrete column behavior is the flexural stiffness (*EI*). The flexural stiffness, however, is affected by several parameters beyond the modulus of elasticity of the concrete. To simplify analysis while maintaining a similar approach as Equation 9.1, the effective flexural stiffness (EI_{eff}) due to concrete creep can be approximated by Equation 9.2. The effective creep coefficient (ϕ_{eff}) is a modification of the creep coefficient accounting for relevant parameters contributing to the creep behavior of concrete cross-sections. To maintain simplicity, the proposed methodology is limited to a concrete column subject to a constant sustained load. It should also be noted that this equation does not account for the time-dependent increase of the concrete strength or the modulus of elasticity. These increases can be accounted for by suggested ACI 209 equations, but the omission of the corrections provides conservative results and improves simplicity.

$$EI_{eff}(t) = \frac{EI}{1+\phi_{eff}(t)} \quad \text{(Eq. 9.2)}$$

where:

EI = flexural stiffness of compression member, in.^{2}-lb

EI_{eff} = effective flexural stiffness of compression member, in.^{2}-lb

ϕ_{eff} = effective creep coefficient

9.2.1 Effective Stiffness of Columns under Sustained Load

The results of the experimental tests were used to calibrate and evaluate Equation 9.2. First, only the short column tests were compared with the equation to eliminate the added complexity of

second-order effects, which can significantly change the forces on the cross-section. In addition, only the short columns with applied eccentricity were compared, which results in a comparison with four columns. Once the method was shown to be accurate for simple cross-sections, the methodology was compared with all of the columns that were subject to sustained loads.

To determine the flexural stiffness of the short columns, the DEMEC measurements were used. At each time step, the difference in the strains of the DEMEC discs on either side of each specimen was divided by the precise measured depth of the specimen (6.0625"). This calculation resulted in an average curvature (φ) of the cross-section at a given time (t). Assuming a linear moment-curvature relationship, the flexural stiffness was determined by dividing the moment by the curvature ($EI = M/\varphi$). Because the short columns were loaded to a maximum compressive stress of 50% of the concrete strength, the assumption of a linear moment-curvature relationship is reasonable. To normalize the results, each computed flexural stiffness at a time step (EI_{eff}) was divided by the initial computed flexural stiffness at the beginning of sustained loading (EI). This method of normalization equates to an effective decrease in the flexural stiffness at a particular time under a constant sustained load. In other words, an $EI_{eff}/EI = 0.50$ equates to a stiffness that is 50% of the initial stiffness.

Figure 9.1 presents the results of comparisons for the short columns. The estimation of behavior is provided by a rearranged version of Equation 9.2, using the creep coefficient computed by Equation 9.3. Equation 9.3 is a simplified version of Equation 7.2 with the ultimate creep coefficient (ϕ_u) determined from regression analysis outlined in Section 7.4.2. As shown, Equation 9.3 estimated the behavior of the plain, short columns accurately. For durations of loading of 20 days and less, the equation estimated lower decreases in flexural stiffness, but beyond 20 days, the equation was very accurate. Beyond approximately 125 days, the equations resulted in unconservative estimations, but the overall creep behavior was estimated accurately.

$$\phi_{\mathrm{ACI}}(t) = \frac{t}{44.87 + t} 5.31 \qquad \text{(Eq. 9.3)}$$

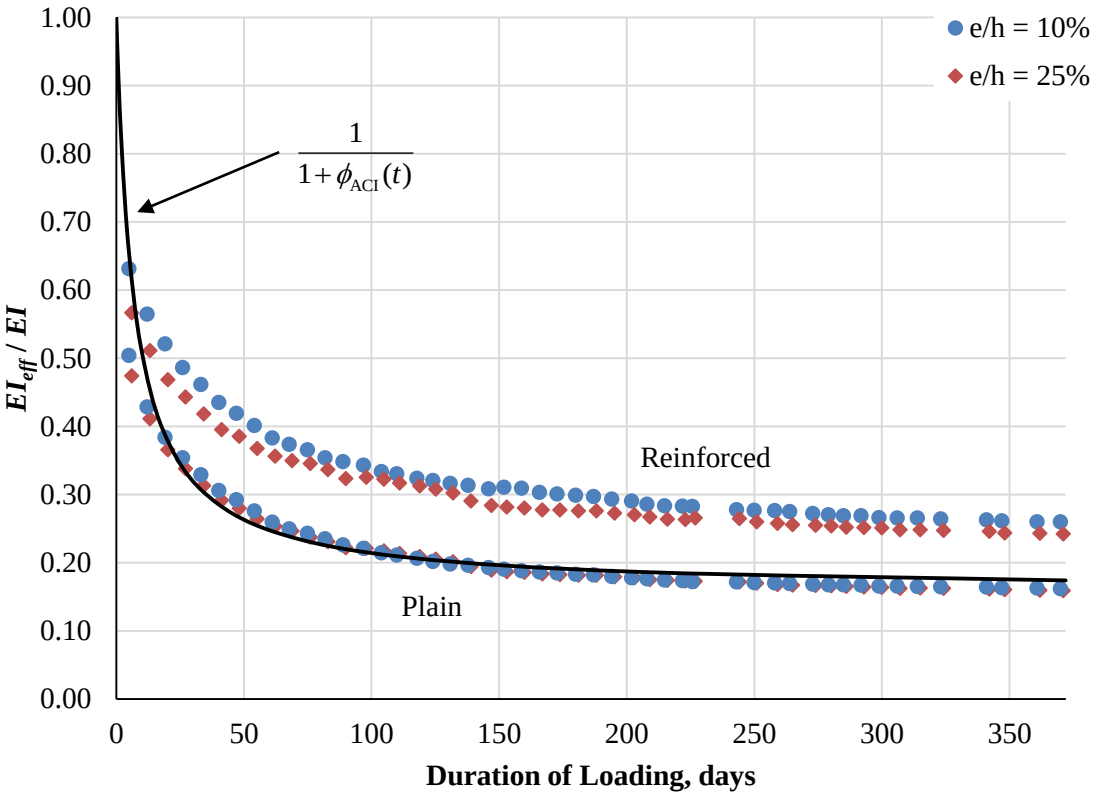

Figure 9.1 –Effective Flexural Stiffness (Short Columns)

For the reinforced columns, the behavior was markedly different. At 365 days, the effective stiffness was 0.16 for the plain columns and 0.25 for the reinforced columns. In addition, differences in behavior were observed in different time ranges. After 150 days, the difference between the reinforced and plain columns was approximately equal. Before that time, however, the reinforced columns had a more gradual reduction in effective stiffness while the plain columns had a very abrupt reduction in effective stiffness during early loading. While the reinforcement had an effect, the eccentricity did not appreciably affect the effective stiffness. The plain columns were almost identical. The reinforced columns were slightly different, but the differences seem to be within expected scatter.

To determine the flexural stiffness of the slender columns, Equation 6.1 was used. The first-order (Pe) and second-order (P (e + δ)) moments were computed from the experimental results. From the calculated moments and the geometric parameters for each column, an effective flexural stiffness (EI) was computed at various time increments. Similar to the short columns, the

effective flexural stiffness (EI_{eff}) at each time increment was divided by the initial flexural stiffness at the beginning of the sustained load (EI) to normalize the results.

Figure 9.2 shows the normalized effective flexural stiffness as a function of duration of loading for the columns with #3 bars. The estimations from Equation 9.3 are also shown. For the columns with #3 bars, the results are scattered, with the normalized flexural stiffness at 100 days ranging from 0.26 to 0.49. The 40-25 columns showed the greatest decrease in flexural stiffness, but as noted previously, these columns either failed or experienced significant long-term effects and were on the verge of failing under sustained load. Surprisingly, the two columns that failed (40-25(1) and 40-25(2)) showed very similar flexural stiffness decreases as their companion columns. Equation 9.3 resulted in a reliable lower bound for the results, but similar to the short columns, the equation was unconservative for durations of loadings less than approximately 20 days.

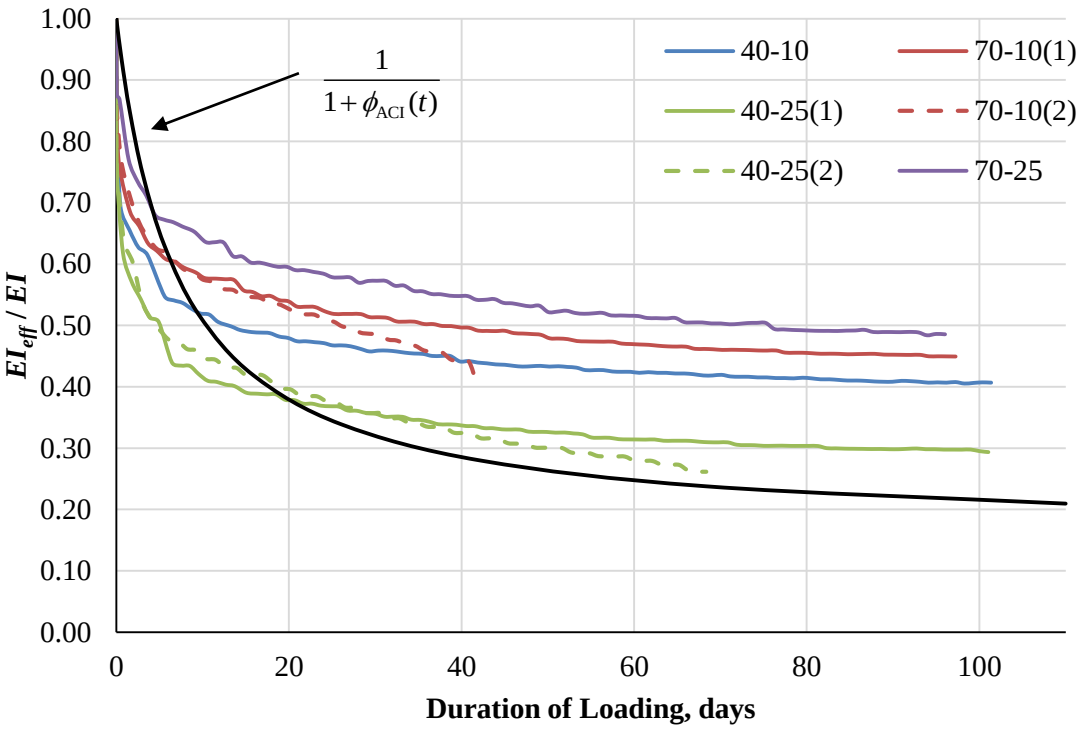

Figure 9.2 – Effective Flexural Stiffness (#3 bars)

Figure 9.3 shows the normalized effective flexural stiffness as a function of duration of loading for the columns with #5 bars. The estimations from Equation 9.3 are also shown. Compared to the previous comparison, the columns with #5 bars exhibited much less scatter, with the normalized effective stiffness at 100 days ranging from 0.41 to 0.50. Because the #5 bars are much stiffer than #3 bars, they tended to control and stabilize the long-term behavior of the columns. These columns were much less sensitive to other column parameters such as applied load eccentricity and slenderness ratio. Equation 9.3 is only unconservative for durations of loading less than 10 days but provides an excessively conservative lower bound.

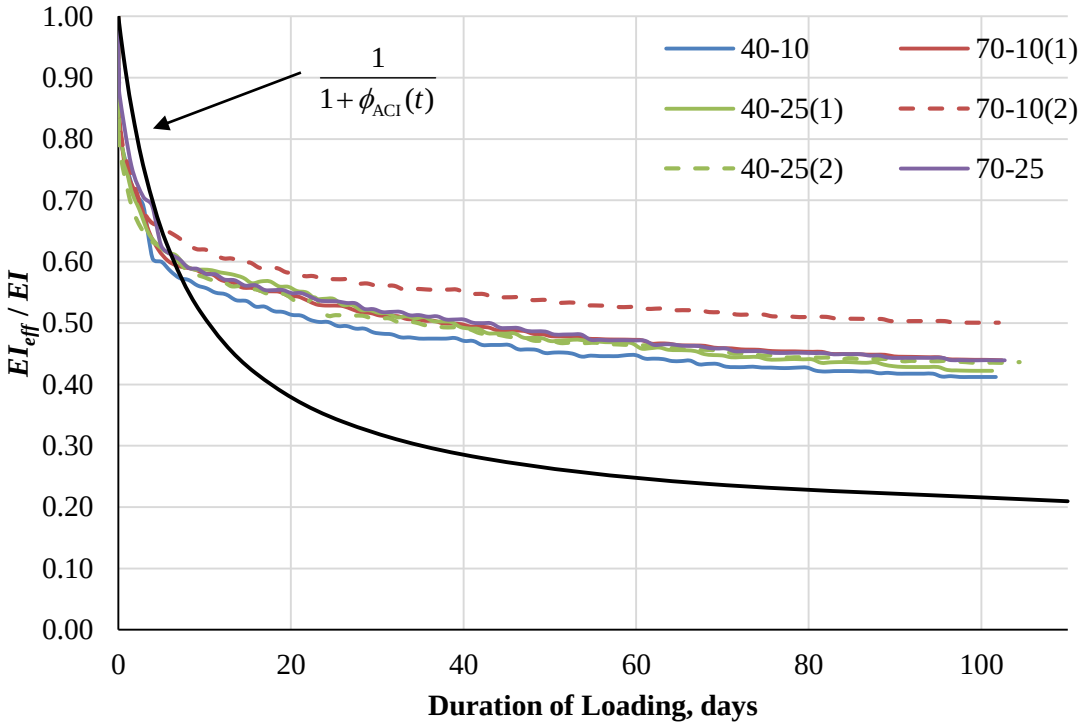

Figure 9.3 – Effective Flexural Stiffness (#5 bars)

Figure 9.4 shows the normalized effective flexural stiffness as a function of duration of loading for the columns with four prestressing wires. The estimations from Equation 9.3 are also shown. Compared to the results with mild reinforcement, the columns with prestressing steel exhibited a greater stiffness reduction, particularly as a function of time. After 20 days, all four columns were at less than 40% of the short-term stiffness, which was the lower bound for all of the other slender columns except for R3-40-25(1) and (2). Though these prestressed columns experienced a relatively quick stiffness reduction, the three that did not fail appeared to stabilize by the end of the loading duration. The equation provides a lower bound for the results beyond 50 days but was unconservative for one column before that time and was unconservative until 20 days for two of the other columns. The prestressed columns behaved very similarly to the plain, short columns with similar lower bounds but with a higher early age stiffness reduction.

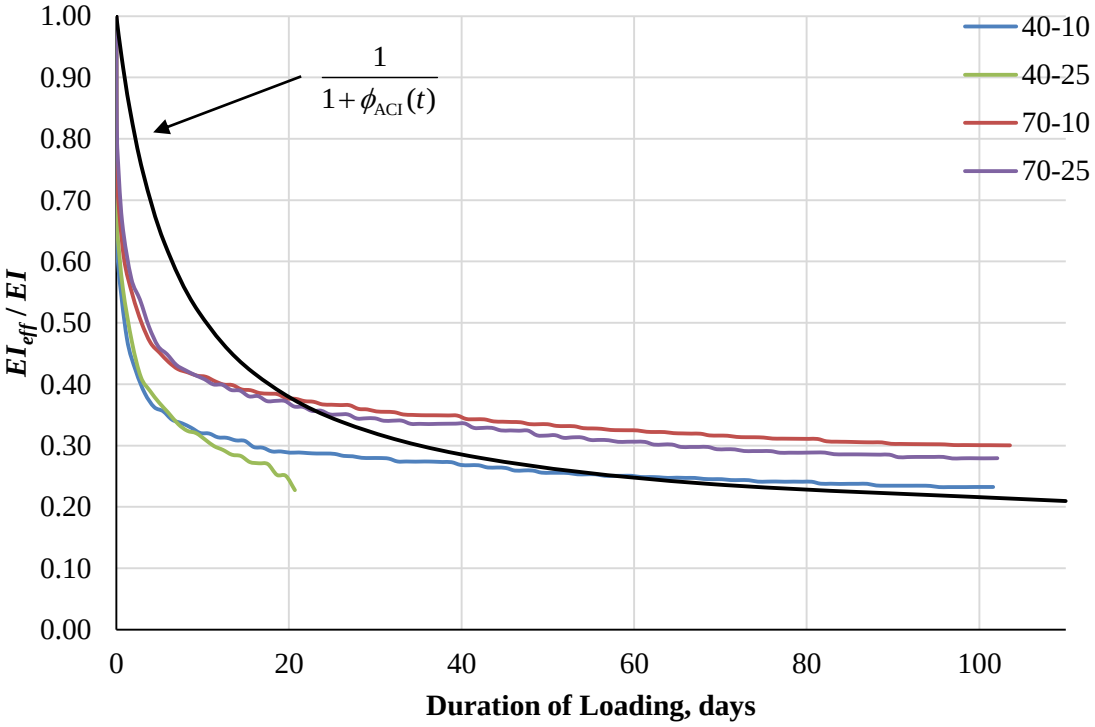

Figure 9.4 – Effective Flexural Stiffness (4 – PS Wires)

9.2.2 Effect of Column Parameters on Effective Stiffness

Based on the results of the previous comparisons, Equation 9.3 provides a reliable lower bound for the stiffness reduction of columns at longer load durations. It was clear, however, that the

different column types experienced different behaviors. To improve the accuracy of the design methodology, the effect of several parameters on the effective columns stiffness was investigated. To simplify the approach, it was assumed that the effect of the parameters was independent of time, or in other words, the parameters simply scale Equation 9.3. Based on this assumption, the effective column stiffness for each test was computed at a single time for relative comparison. Table 9.1 shows the computed effective stiffness reductions for several column tests at approximately 100 days, but the specific time depended on the column tests. For the short columns, the column stiffness was computed as the first recorded DEMEC measurements beyond 100 days. For the slender columns, the effective stiffness was computed at the end of the sustained loading, which was between 95 and 105 days. The three columns that failed under sustained load were excluded from this evaluation. Table 9.1 also includes the effective creep coefficient for each column at the given effective flexural stiffness, computed by rearranging Equation 9.2. Lastly, the computed creep coefficient given by Equation 9.3 using the respective duration of loading is provided.

Table 9.1 – Effective Column Stiffness at 100 days

Column ID	EI_{eff} / EI	ϕ_{eff} (Eq. 9.2)	Duration of Loading, days	ϕ_{ACI} (Eq. 9.3)
PL-13-10-LT	0.21	3.66	103.8	3.71
PL-13-25-LT	0.22	3.60	104.9	3.72
R3-13-10-LT	0.33	1.99	103.8	3.71
R3-13-25-LT	0.32	2.10	104.9	3.72
R3-40-10-LT	0.41	1.46	101.4	3.68
R3-40-25-LT(1)	0.29	2.41	101.0	3.68
R3-70-10-LT(1)	0.45	1.23	97.2	3.63
R3-70-25-LT	0.49	1.06	96.0	3.62
R5-40-10-LT	0.41	1.43	101.7	3.68
R5-40-25-LT(1)	0.42	1.37	101.3	3.68
R5-40-25-LT (2)	0.44	1.29	104.4	3.71
R5-70-10-LT (1)	0.44	1.28	102.4	3.69
R5-70-10-LT (2)	0.50	1.00	102.0	3.69
R5-70-25-LT	0.44	1.28	102.7	3.70
P4-40-10-LT	0.23	3.30	101.6	3.68
P4-70-10-LT	0.30	2.33	103.5	3.70
P4-70-25-LT	0.28	2.58	102.1	3.69

Figure 9.5 plots the normalized effective stiffness (EI_{eff} / EI) at approximately 100 days from Table 9.1 for each column versus the nominal maximum compressive stress at the beginning of sustained load. The maximum stress was determined based on the assumptions listed below. Because of the numerous assumptions, Figure 9.5 only provides a qualitative comparison of the column stresses to investigate their effect on the effective stiffness.

Assumptions:

1. Linear stress-strain behavior for both the concrete and steel.
2. Combined axial and bending forces that vary linearly across the cross-section, $P/A + Mc/I$.
3. Transformed section properties.
4. Moment based on the eccentricity plus the deflection at the beginning of sustained load, $M = P\,(e + \delta)$.

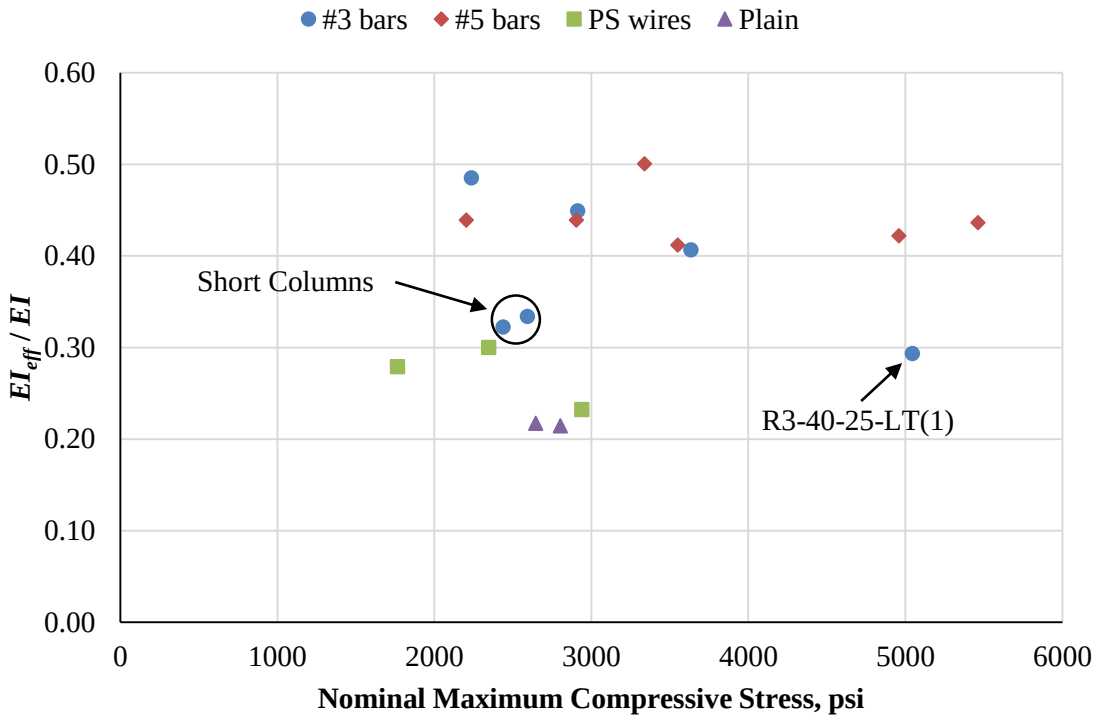

Figure 9.5 – Effective Column Stiffness versus Initial Maximum Compressive Stress

As shown, the maximum stresses varied by more than a factor of two. For comparison, the concrete strengths only varied by 1500 psi. For the columns with #5 bars, the maximum stresses varied from 2200 psi to 5500 psi. Even with this increase, no trend is observed, and the effective

stiffness remained essentially identical. Likewise, the columns with prestressing wires do not exhibit a trend with the compressive stresses ranging from 1800 psi to 2900 psi. The columns with #3 bars, however, show a downward trend of effective column stiffness as a function of the maximum compressive stress. The short columns show a decreased stiffness relative to the slender columns, but their behavior does not include the effects of slenderness. The slender column that predominantly supports that trend, R3-40-25-LT(1), nearly failed under sustained load and is not representative of normal service behavior of columns under sustained load. If that column as well as the short columns are omitted, the downward trend could be considered insignificant. For the nonprestressed columns, a normalized stiffness of 0.4 essentially provides a uniform lower bound. Based on this analysis, it is reasonable to assume that the applied maximum compressive stress, within practical ranges, does not influence the effective stiffness.

Figure 9.6 plots the normalized effective stiffness as a function of the slenderness ratio. While there is an upward trend, the scatter of the results is unpredictable, particularly for the columns with #3 bars. For columns in service, slender columns would typically be of greater concern for instability. Because of the scatter and uncertainty of more slender columns, it can be conservatively assumed that slenderness ratio does not affect the effective stiffness.

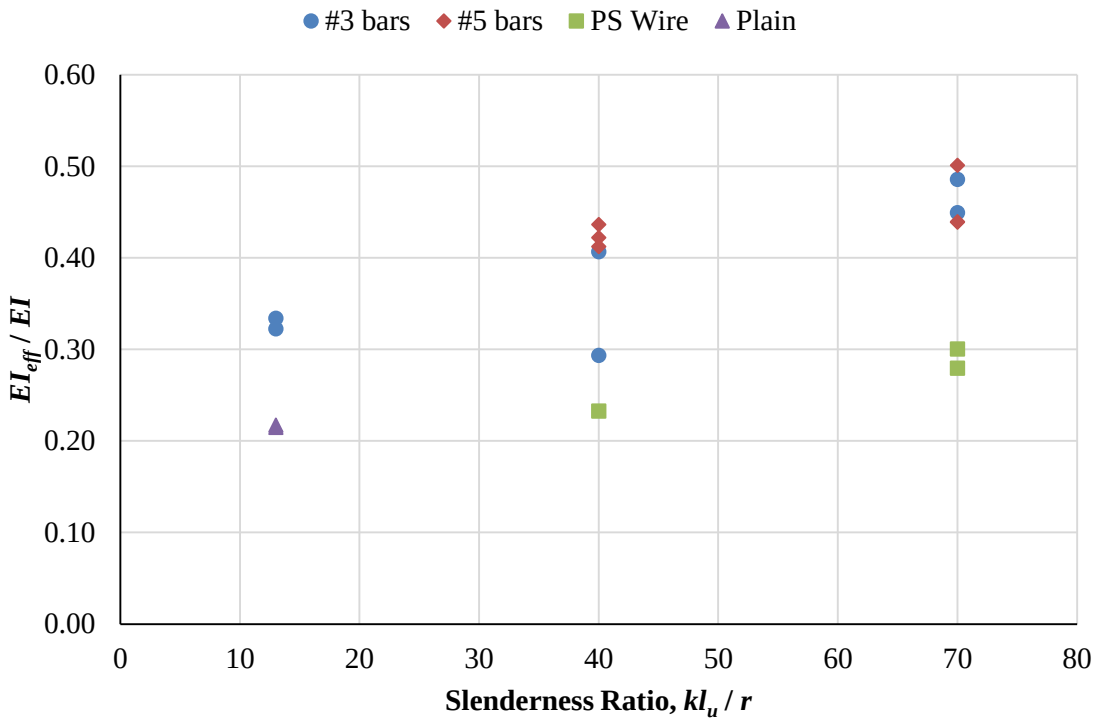

Figure 9.6 – Effective Column Stiffness versus Slenderness Ratio

Figure 9.7 plots the normalized effective stiffness as a function of the reinforcement ratio. The reinforcement ratio includes both mild and prestressing reinforcement. In this context, the effect of the reinforcement ratio is consistent with the previous evaluations. The columns with #5 bars showed less scatter than the columns with # 3 bars, and the prestressed columns behaved similar to the plain, short columns. It is evident that increased reinforcement ratio decreased the effects of other parameters such as compressive stress and slenderness ratio. While the results show considerable scatter, the lower bound of the results can be approximated as follows. For the nonprestressed columns, the lower bound can be approximated at 0.4 as mentioned before when omitting the short and nearly failed column. The prestressed columns behaved similarly to the plain columns and have a lower bound of approximately 0.2.

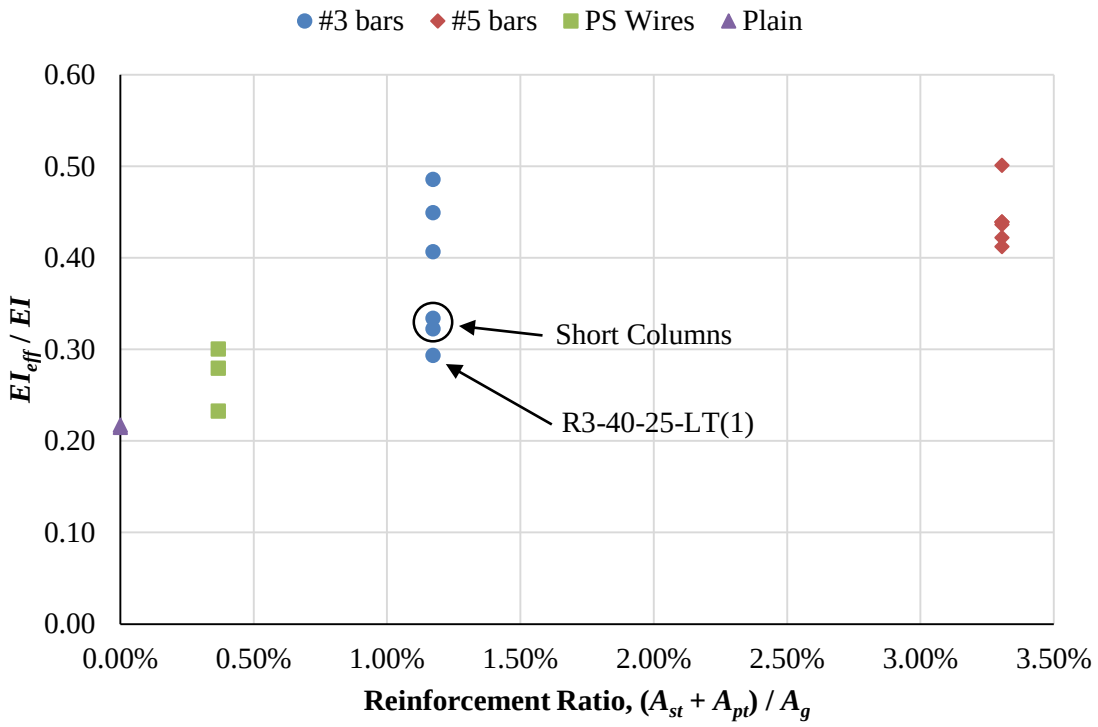

Figure 9.7 – Effective Column Stiffness versus Reinforcement Ratio

While the lower bounds for nonprestressed and prestressed columns are clear, viewing the results in the context of effective column stiffness does not lend itself to the development of a design equation. To allow for time-dependent calculations, it is more accurate to modify the creep coefficient. Figure 9.8 plots the normalized creep coefficient as a function of the reinforcement ratio. Based on this plot, the normalized creep coefficients for nonprestressed and prestressed (or plain) columns can be approximated as 2.5 and 1.0, respectively. As a result, an effective creep coefficient can be approximated by Equation 9.4, and in conjunction with Equation 9.2, an effective column flexural stiffness can be computed for use in the moment magnification procedure.

$$\phi_{eff}(t) = \frac{\phi_{ACI}(t)}{\alpha} \qquad \text{(Eq. 9.4)}$$

where:

$$\alpha = \begin{cases} 1.0 & \text{for prestressed or plain columns} \\ 2.5 & \text{for nonprestressed columns} \end{cases}$$

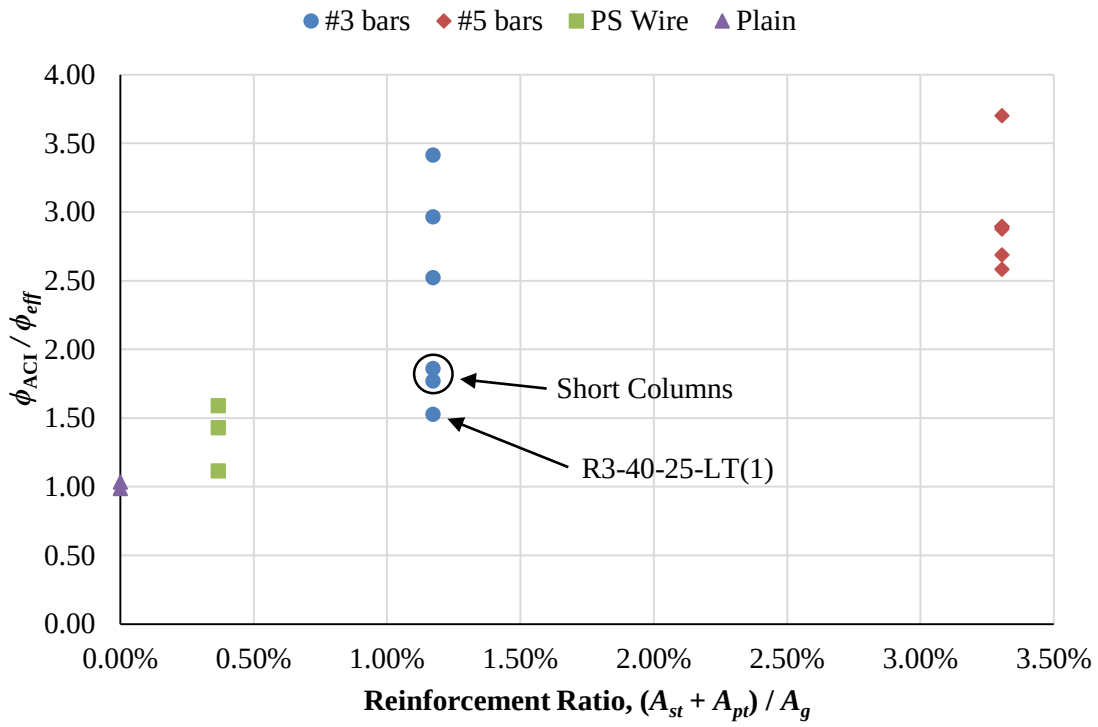

Figure 9.8 – Effective Creep Coefficient versus Reinforcement Ratio

Table 9.2 presents the computed effective flexural stiffness of the tested columns. The stiffness was computed based on the experimental results (Equation 6.1) and using the proposed design methodology (Equations 9.2 and 9.4). Only three columns were computed unconservatively. The short reinforced columns (R3-13) were computed approximately 25% unconservative and are considered of less importance because they do not include the effect of slenderness. The only unconservative point from a slender column, P4-40-10-LT, was computed at approximately 40% unconservative. This column is considered an unrealistic service column due to its high axial loading combined with large eccentricity, which caused an elastic stress in the column of over 5000 psi. Additionally, considering the use of load factors and strength reductions further reducing the demands on columns, the level of conservatism for the columns in general is considered reasonable. The columns tested were extreme cases with some approaching instability, which would not be the case for typical service columns. The columns that have the highest conservative estimates were the most slender, and as mentioned previously, increased safety for these columns that have a greater chance of instability failure is considered appropriate.

Table 9.2 – Evaluation of Sustained Load Design Equation (100 days)

Column ID	EI_{eff} / EI (Experimental)	ϕ_{eff} (Eq. 9.4)	EI_{eff} / EI (Eqs. 9.2 and 9.4)
PL-13-10-LT	0.21	3.71	0.21
PL-13-25-LT	0.22	3.72	0.21
R3-13-10-LT	0.33	1.48	0.40
R3-13-25-LT	0.32	1.49	0.40
R3-40-10-LT	0.41	1.47	0.40
R3-40-25-LT(1)	0.29	1.47	0.40
R3-70-10-LT(1)	0.45	1.45	0.41
R3-70-25-LT	0.49	1.45	0.41
R5-40-10-LT	0.41	1.47	0.40
R5-40-25-LT(1)	0.42	1.47	0.40
R5-40-25-LT (2)	0.44	1.49	0.40
R5-70-10-LT (1)	0.44	1.48	0.40
R5-70-10-LT (2)	0.50	1.48	0.40
R5-70-25-LT	0.44	1.48	0.40
P4-40-10-LT	0.23	3.68	0.21
P4-70-10-LT	0.30	3.70	0.21
P4-70-25-LT	0.28	3.69	0.21

Figure 9.9 shows the accuracy of the proposed design method compared to the experimental results where the line represents perfect accuracy. Points above the line are conservative while points below the line are unconservative. Consistent with the evaluation of the parameters, the results show significant scatter, but a consistent lower bound of the results is observed, beyond the three columns previously discussed.

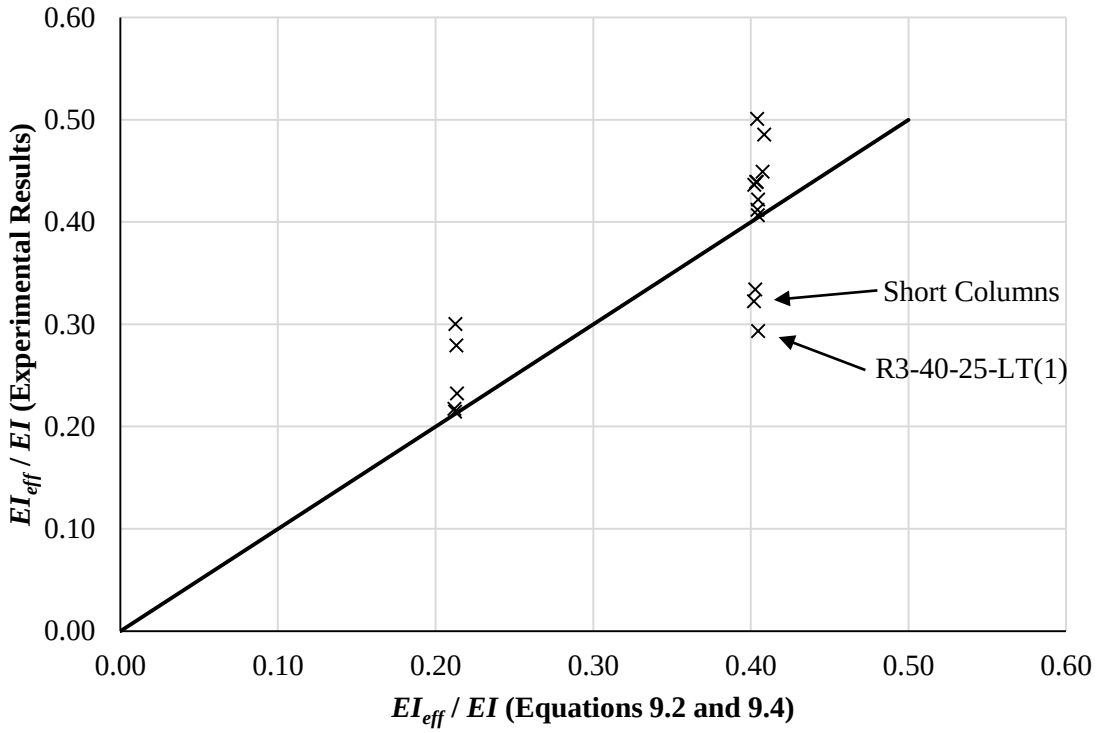

Figure 9.9 – Accuracy of Design Equations for Sustained Load Behavior

It should be noted that the number of columns tested in this study is small. While the maximum compressive stress and slenderness ratio were found to be insignificant to the reduction in stiffness, that conclusion is based only on the results from this study. Furthermore, the effect of the reinforcement ratio was concluded by disregarding a column that was tested, but nearly failed. Further research is necessary to provide increased confidence in the design recommendations. Specifically, additional slender column tests under varying sustained loads are recommended. The slenderness and eccentricity ranges tested are likely adequate based on typical design ranges, but exploring the behavior of those columns under varying loads using identical concrete would increase confidence in the provided recommendations as well as providing important data to calibrate computational modeling.

9.2.3 Comparison of Experimental Results to Proposed Equation

The previous evaluations were repeated with the updated effective stiffness equation accounting for the reinforcement ratio. Figure 9.10 shows the proposed, normalized effective flexural stiffness as a function of the duration of loading for the slender columns with #3 bars. Ignoring column 40-25(1) and the failed columns, the proposed equation provides a consistent lower bound of the results for sustained loads longer than 100 days. The slope of the equation at 100 days is steeper than those of the experimental results at 100 days, which suggests that the equation would become more conservative over time. The equation provides an asymptote of 0.32 under longer-term loading, which would appear to be conservative for all columns except for the 40-25 columns. Based on the asymptote, after 100 days, the columns have experienced 88% of their ultimate stiffness reduction.

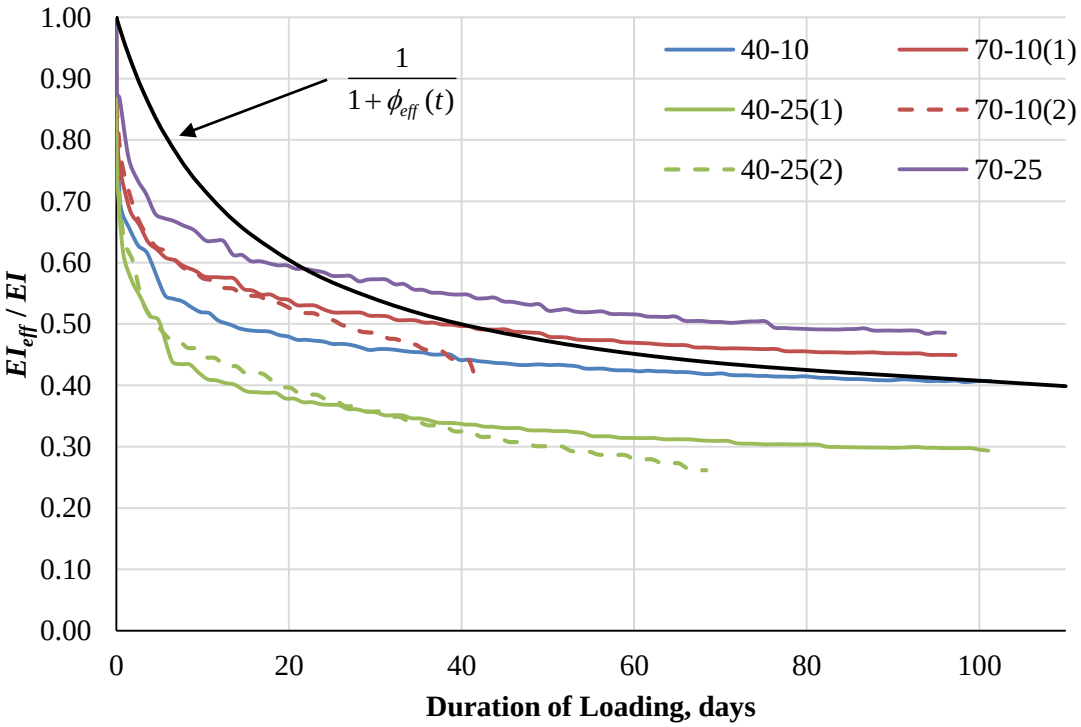

Figure 9.10 – Proposed Effective Flexural Stiffness (#3 bars)

Figure 9.11 shows the proposed, normalized effective flexural stiffness as a function of duration of loading for the columns with #5 bars. The equation is unconservative for all columns until a duration of approximately 60 days, after which the equation becomes increasingly conservative. Due to the reduced scatter of these columns, however, the proposed equation estimated the behavior very accurately. The slope of the equation at 100 days is steeper than those of the experimental results, which suggests the conservatism of the equation would continue to increase over time. The increase in conservatism appears greater than that for the columns with #3 bars. The equation provides an asymptote of 0.32 under longer-term loading, which would appear to be conservative for all columns. Based on the asymptote, after 100 days, the columns have experienced 88% of their ultimate stiffness reduction.

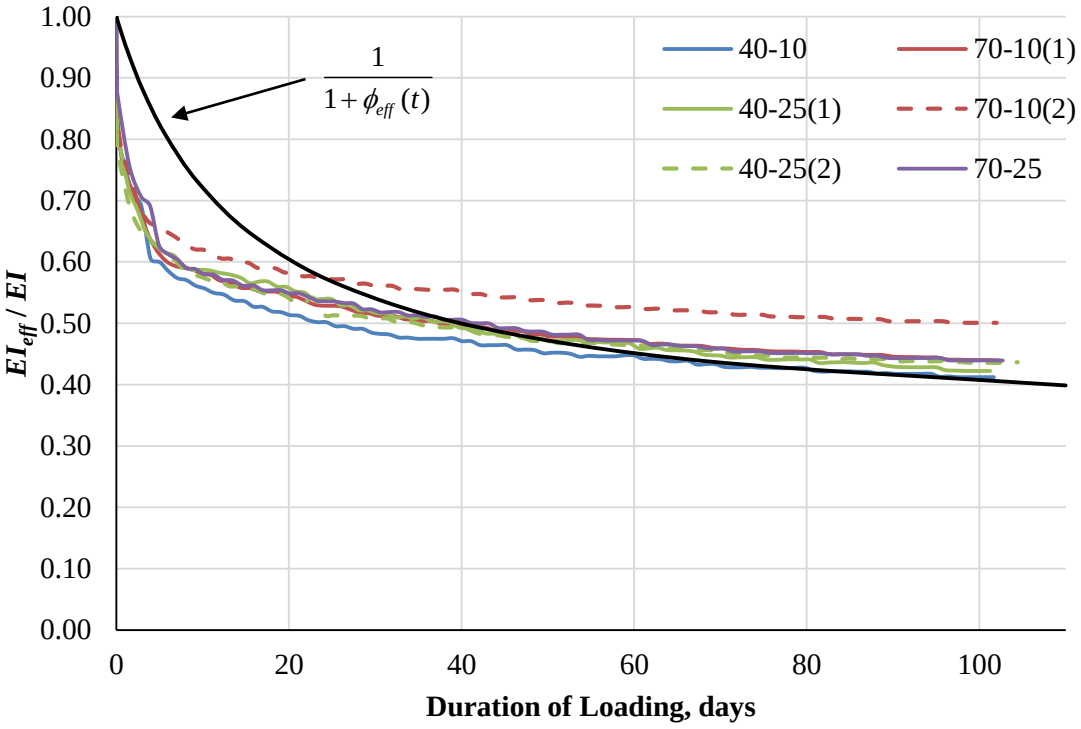

Figure 9.11 – Proposed Effective Flexural Stiffness (#5 bars)

Figure 9.12 shows the proposed, normalized effective flexural stiffness as a function of duration of loading for the columns with prestressing wires. Because the column is prestressed, the proposed equation is identical to Equation 9.3. The proposed equation is unconservative for the first 60 days of the 40-10 column. For the 70-10 and 70-25 columns, the equation was conservative beyond a duration of loading of approximately 25 days. Again, the slope of the equation at 100 days is steeper than those of the experimental results, indicating increased conservatism at later ages. It should be noted that the 40-25 column, however, is estimated very unconservatively. The column, which failed after 20 days, is estimated at nearly twice the effective stiffness measured at 20 days. This column, as with previous R3-40-25 columns, was loaded at very high stresses and can be considered out the range of typical service behavior. The equation provides an asymptote of 0.16 under longer-term loading, which would appear to be conservative for all columns. Based on the asymptote, after 100 days, the columns have experienced 93% of their ultimate stiffness reduction.

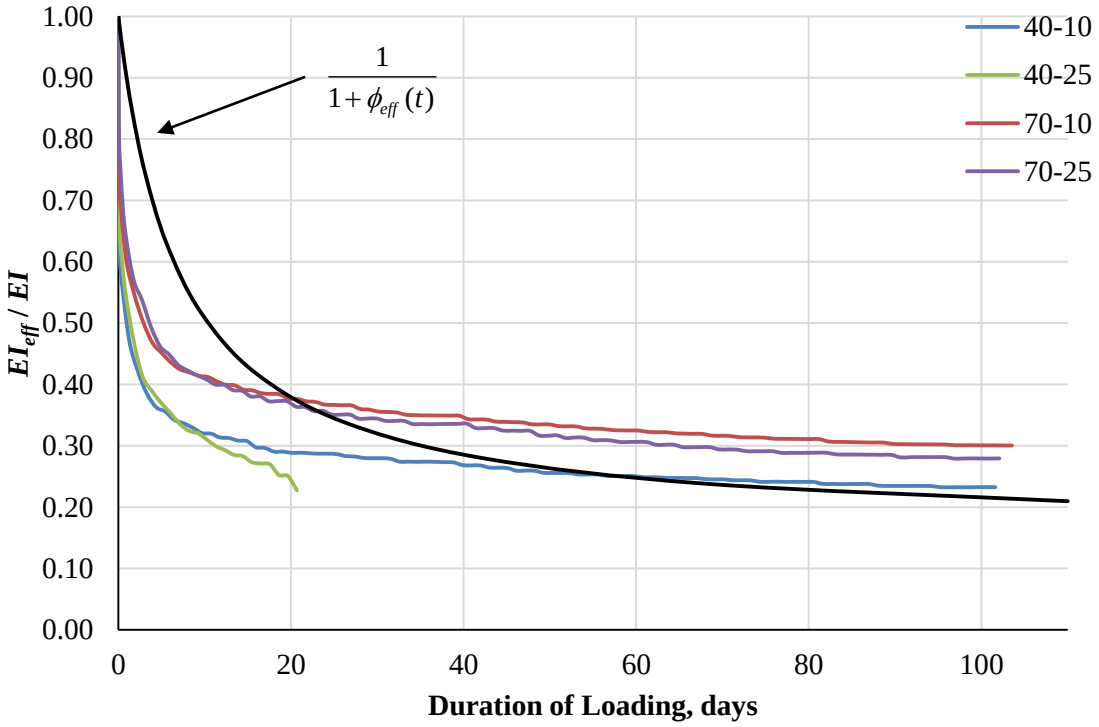

Figure 9.12 – Proposed Effective Flexural Stiffness (4 – PS Wires)

9.3 Long-Term Effects

While the behavior under sustained load can be approximated, most columns typically have additional residual capacity. In a service condition, this would be additional axial live load the column is able to resist. To account for sustained load effects as well as post-sustained load strength, ACI 318 employs a very simplistic approach to design for the total long-term effects of a slender column, shown by Equations 9.5 and 9.6. The building code applies a reduction factor to the short-term flexural stiffness of a column computed using Equations 4.1 through 4.5. The reduction factor is simply one plus the ratio of the sustained axial load to the total axial load for the load combination of interest. When used in a code context, both of the axial loads are factored. As such, a column subject to no sustained loads will have a stiffness equal to the short-term calculations, while a column with 100% of the load sustained will have a stiffness that is half of the short-term calculations.

$$EI_{eff} = \frac{EI}{1+\beta_{dns}} \qquad \text{(Eq. 9.5)}$$

$$\beta_{dns} = \frac{P_{sus}}{P} \qquad \text{(Eq. 9.6)}$$

where:

EI = flexural stiffness of compression member, in.^{2}-lb
EI_{eff} = effective flexural stiffness of compression member, in.^{2}-lb
P = factored axial force, lb
P_{sus} = maximum factored sustained axial force, lb
β_{dns} = ratio to account for effects of sustained axial loads

This method of analysis does not include any further details about the loading parameters of the column, however. Consider the case of a column with 100% dead load. When the equations are applied, the short-term stiffness of the column is reduced by a factor of two. If this load case is subjecting the column to a very low axial load (low stress), the real reduction in stiffness may not be near a factor of two. Though that particular load case may not ultimately affect the design of the column, this example illustrates a significant problem that may occur through the use of a simple reduction factor to account for long-term effects.

9.3.1 Evaluation of β_{dns} Method

Two different methods were used to evaluate the effectiveness of the ACI 318 approach to determine the long-term capacity of concrete columns. It should be noted that these evaluations are only for qualitative and comparative purposes. The columns were only under sustained load for up to approximately 100 days, which is much less than typical service columns would experience. If the columns would have been loaded for longer, the deflections would increase and the corresponding β_{dns} would increase. Conversely, typical service columns would not be subject to as high of sustained loads as the columns tested in this study. These evaluations are primarily intended to compare the effectiveness of the ACI 318 approach for different columns. The evaluations should provide a relative comparison because all columns were subject to sustained loads for approximately the same amount of time.

First, the experimental results were used to determine a β_{dns} factor that would lead to the same result. To determine this factor, the nominal and design strengths were computed. Similar to previous evaluations, the computations used nominal material properties but used the concrete strength on the final day of failure. Using the nominal and design strengths, a capacity was computed for the column tests, which was defined as when the load-moment behavior of the column exceeded the computed strength. Given loading parameters and a flexural stiffness, an effective β_{dns} was computed using Equation 9.7. The equation is a rearrangement of Equations 1.1 through 1.3 and Equation 9.5. The flexural stiffness, (EI) was computed using Equations 4.4 and 6.4 for nonprestressed and prestressed columns, respectively.

$$\beta_{dns} = \left(\frac{0.75\pi^2 EI}{Pl_u^2} \right) \left(1 - \frac{M}{M_c} \right) - 1 \qquad \text{(Eq. 9.7)}$$

where:

P = axial force, lb
l_u = unsupported length of column, in.
M = end moment of compression member, in.-lb
M_c = moment amplified for the effects of member curvature, in.-lb

Figure 9.13 shows a representative example of the evaluation for Column R5-70-10-LT(1). For illustrative purposes, the computed behavior for a column with a β_{dns} of 0.0 is included. This would correspond to the computed behavior under only short-term loading. As shown, the required β_{dns} for the nominal and design strength must be different to match the experimental results.

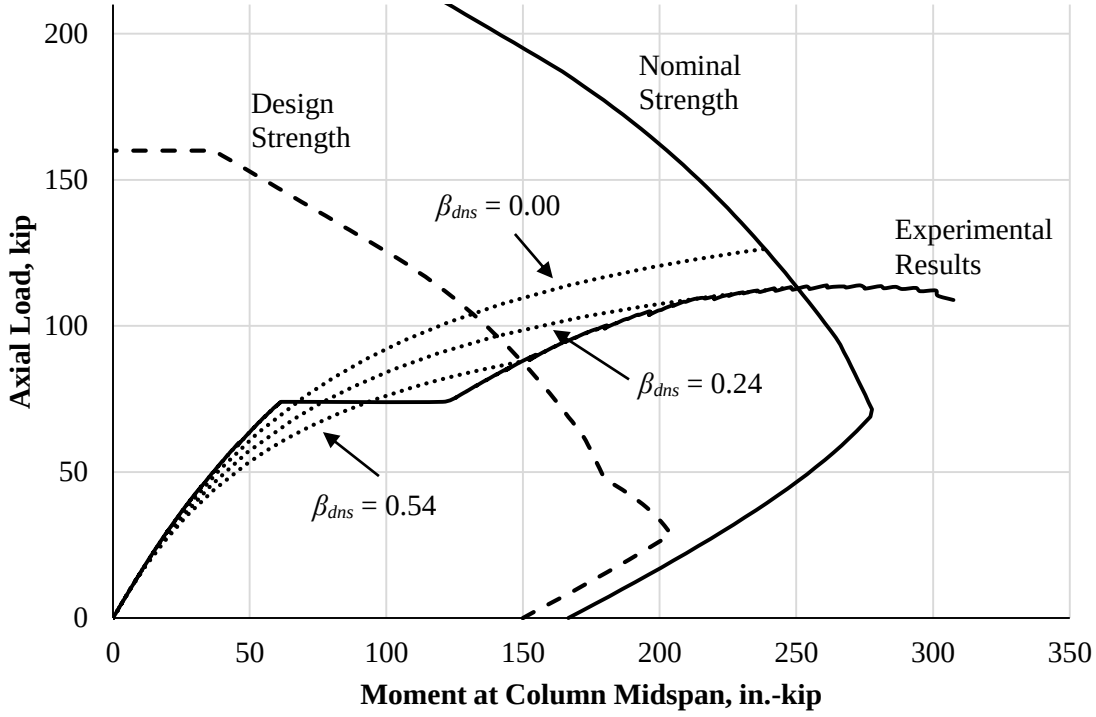

Figure 9.13 – Detailed Evaluation of β_{dns} Method (R5-70-10-LT(1))

In most cases, β_{dns} for nominal strength is lower than that for design strength. As noted in Figure 9.13, this is the expected outcome. The nominal strength results in a higher capacity, so the β_{dns} should be lower for the equation to accurately estimate this strength. For certain columns, however, this may not be the case. Figure 9.14 shows an representative example of one of these columns, R3-40-25-LT(1). The column was found to have a larger β_{dns} for nominal strength than for design strength. This occurred because the residual strength at the end of the sustained load was small. For other columns, this effect was caused as the column approached instability and zero stiffness. The stiffness at the moderately higher load was actually much lower, which resulted in a larger required β_{dns}.

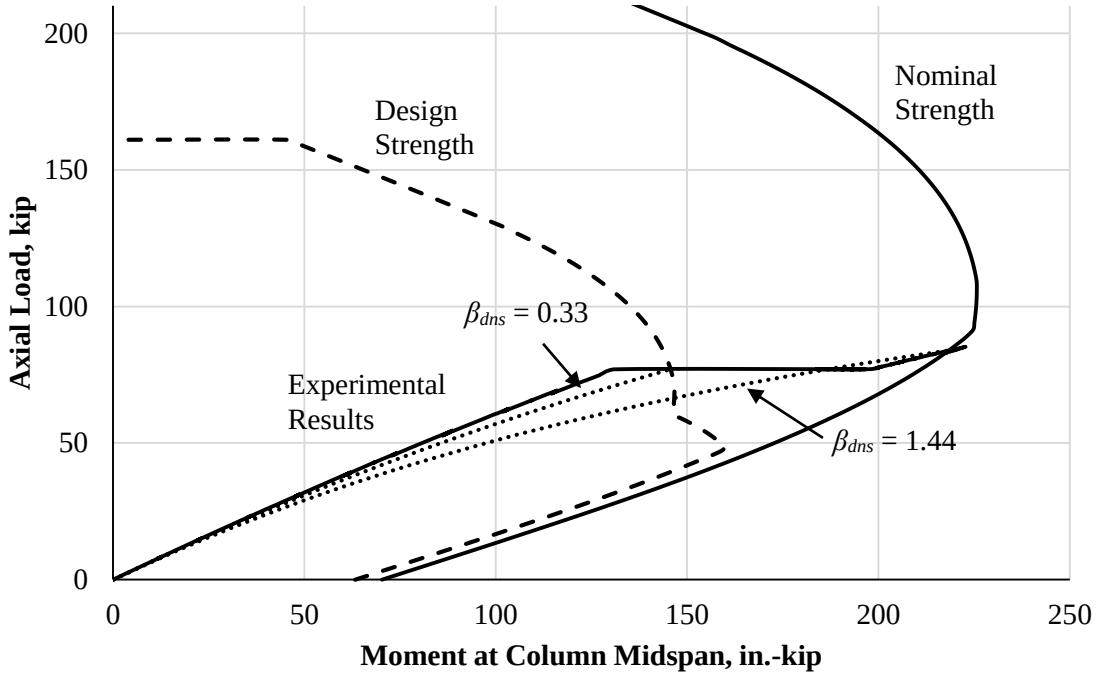

Figure 9.14 – Detailed Evaluation of β_{dns} Method (R3-40-25-LT(1))

Another interesting data point for this evaluation is Column R5-40-25-LT(1), shown by Figure 9.15. This column exceeded the design strength under sustained load. Additionally, the initial short-term behavior of the column was stiffer than the estimated behavior. Combining those effects, the required β_{dns} at design strength was found to be negative. Clearly, the column was not stiffer than its short-term counterpart. This effect, however, illustrates the inadequacy of the ACI 318 method to fully describe long-term effects, especially when coupled with stiffness equations that are only estimations of short-term behavior. This effect was also seen in columns that experienced very minimal moment increases under sustained load, such as R5-40-10-LT.

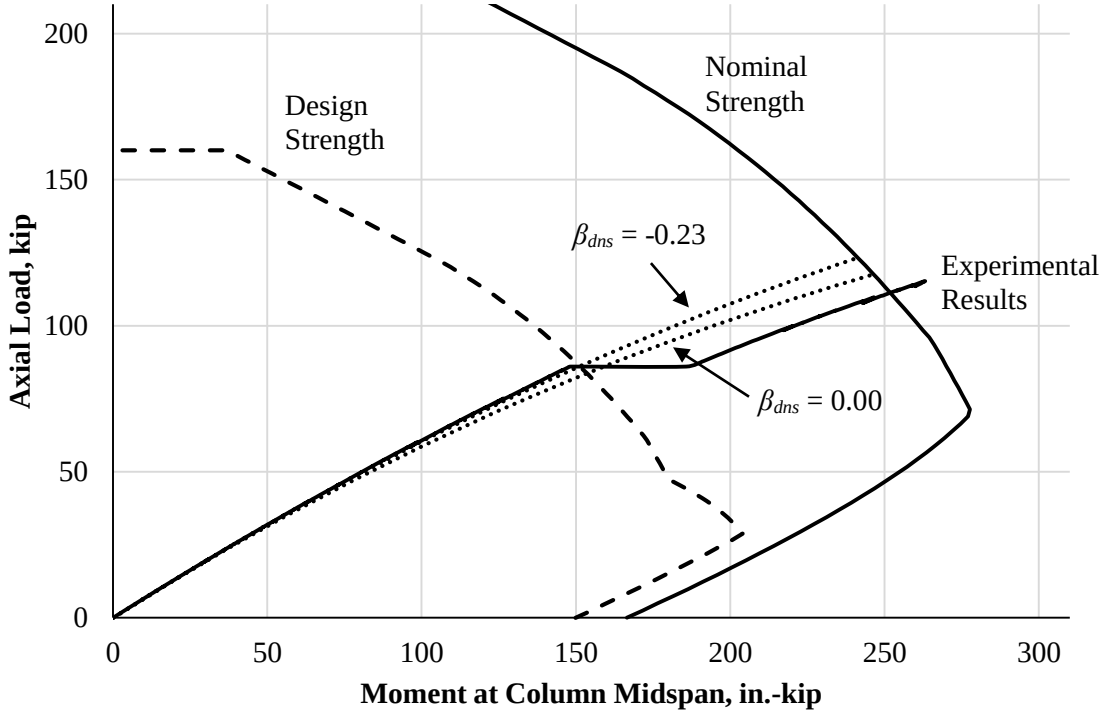

Figure 9.15 – Detailed Evaluation of β_{dns} Method (R5-40-25-LT(1))

Table 9.3 and Table 9.4 provide the results for the evaluation of the nonprestressed and prestressed columns, respectively. The columns that failed under sustained load are noted. The ACI 318 approach for long-term effects is primarily intended for columns that have all three phases of behavior: short-term, sustained load, and residual short-term strength. As such, the values for the columns that failed under sustained load are suspect, and definite conclusions cannot be made about the accuracy of these specific results.

Table 9.3 – Summary of Computed β_{dns} Factors (Nonprestressed)

Column ID	Design Strength		Nominal Strength	
	Capacity, kip	β_{dns}	Capacity, kip	β_{dns}
R3-40-10-LT	122.2	0.72	**	**
R3-40-25-LT(1)	77.0*	0.33	83.9	1.44
R3-40-25-LT(2)	66.0*	0.13	66.0*	2.00
R3-70-10-LT(1)	88.3	0.57	104.8	0.43
R3-70-10-LT(2)	66.0*	1.03	66.0*	1.37
R3-70-25-LT	56.0	0.37	61.6	0.41
R5-40-10-LT	123.2	0.35	182.1	-0.07
R5-40-25-LT(1)	86.0*	-0.23	111.3	0.27
R5-40-25-LT(2)	95.6*	-0.24	128.7	0.06
R5-70-10-LT(1)	87.8	0.54	113.3	0.24
R5-70-10-LT(2)	87.0	0.83	111.5	0.47
R5-70-25-LT	62.2	0.17	80.6	0.04

*Column failed under sustained load
**Column end region failed prematurely

Table 9.4 – Summary of Computed β_{dns} Factors (Prestressed)

Column ID	Design Strength		Nominal Strength	
	Capacity, kip	β_{dns}	Capacity, kip	β_{dns}
P4-40-10-LT	91.8	1.53	136.2	0.62
P4-40-25-LT	60.0*	0.69	60.0*	2.54
P4-70-10-LT	51.4*	1.97	67.5	1.26
P4-70-25-LT	44.7	0.41	53.9	0.38

*Column failed under sustained load

ACI 318 (2014) states, "for simplification, it can be assumed that $\beta_{dns} = 0.6$." In that case, the ACI 318 value seems accurate for nonprestressed columns at design strengths that did not fail under sustained load, as only three columns exceeded that value. These columns, though, were only loaded for approximately 100 days, and under longer-term loading, the corresponding β_{dns} would be higher. Furthermore, the computed β_{dns} values for all types of columns ranged from -0.24 to 1.97 for design strengths and -0.07 to 2.54 for nominal strengths. At design strengths, three computed values were greater than 1.0, which would be impossible given the existing ACI 318 design method. Based on these results, the current ACI 318 method could be modified to provide safe results but cannot lead to accurate results.

Specifically, at design strengths, a β_{dns} value of 1.0 can provide a reasonable lower bound flexural stiffness for nonprestressed columns. Appendix E provides a qualitative summary of all long-term tests computed with the method described earlier in this section. Results from both the analysis and design equations are provided. When assuming a β_{dns} value of 1.0, all columns were estimated conservatively at design strengths, even those that failed under sustained load. At nominal strengths, three nonprestressed columns have β_{dns} values greater than 1.0, including one column that did not fail under sustained load.

Due to the limited number of prestressed column tests, a recommendation cannot be provided for a β_{dns} value, but it would likely need to be higher than 1.0. Only one prestressed column did not require a β_{dns} value of greater than 1.0 at either nominal or design strength.

9.3.2 Design Effectiveness of β_{dns} Method

Comparing the computed β_{dns} factors based on the experimental results was illustrative, but the results did not provide any indication of effectiveness of the method for design purposes. Similar to the evaluations for short-term behavior, it was desired to evaluate the design method for long-term effects. Due to differences between the column tests from this study and in-service columns, it is difficult to provide a consistent approach to compare the columns further. Particularly, it was difficult to define the sustained load ratio (P_{sus}/P) for the tests, which is required to compute β_{dns} as shown in Equation 9.6.

To resolve this, ACI 318 (2014) states, "for simplification, it can be assumed that $\beta_{dns} = 0.6$." Making that assumption, the computed capacities for all the long-term tests were computed at nominal and design strengths. The behavior was computed using Equations 1.1 through 1.3. For these evaluations, the flexural stiffness was computed using Equations 4.2, 4.4 and 4.5 for the nonprestressed columns. For the prestressed columns, Equations 4.2, 6.4 and 6.6 were used. Based on the results from Chapters 4, 5, and 6, these equations were determined to be the most accurate or, in the case of Equation 4.2, most commonly used.

9.3.2.1 Nonprestressed Columns

Table 9.5 and Table 9.6 provide the computed capacities of the nonprestressed columns at nominal and design strengths, respectively. The capacity of the tests results was defined as the axial load at which the experimental results exceeded the strength. Additionally, the ratio of the test results to the equation estimations are provided. As such, a value of 1.0 is perfect accuracy,

while values less than 1.0 are unconservative and values greater than 1.0 are conservative. The columns that failed under sustained load were included in this evaluation. For those columns, the capacity of the experimental results was taken as the sustained load.

Table 9.5 – Computed Long-Term Capacities at Nominal Strengths (Nonprestressed)

Column ID	Computed Axial Capacity, kip				P_{test} / $P_{Eq.}$		
	Test	Eq. 4.2	Eq. 4.4	Eq. 4.5	Eq. 4.2	Eq. 4.4	Eq. 4.5
R3-40-10	**	129.6	164.7	162.9	**	**	**
R3-40-25(1)	83.9	84.4	98.9	97.5	0.99	0.85	0.86
R3-40-25(2)	66.0*	75.5	86.5	85.2	0.87	0.76	0.77
R3-70-10(1)	104.8	53.6	98.3	95.7	1.96	1.07	1.10
R3-70-10(2)	66.0*	48.6	87.1	84.5	1.36	0.76	0.78
R3-70-25	61.6	40.0	57.0	55.2	1.54	1.08	1.12
R5-40-10	182.1	123.4	161.5	149.8	1.48	1.13	1.22
R5-40-25(1)	111.3	97.6	115.5	109.6	1.14	0.96	1.02
R5-40-25(2)	128.7	135.4	179.9	168.2	0.95	0.72	0.76
R5-70-10(1)	113.3	51.2	97.9	87.9	2.21	1.16	1.29
R5-70-10(2)	111.5	54.6	105.6	95.5	2.04	1.06	1.17
R5-70-25	80.6	42.9	63.9	58.0	1.88	1.26	1.39

*Column failed under sustained load
**Column end region failed prematurely

Table 9.6 – Computed Long-Term Capacities at Design Strengths (Nonprestressed)

Column ID	Computed Axial Capacity, kip				P_{test} / $P_{Eq.}$		
	Test	Eq. 4.2	Eq. 4.4	Eq. 4.5	Eq. 4.2	Eq. 4.4	Eq. 4.5
R3-40-10-LT	122.2	104.6	123.5	122.7	1.17	0.99	1.00
R3-40-25-LT(1)	77.0*	65.7	74.2	73.4	1.17	1.04	1.05
R3-40-25-LT(2)	66.0*	57.6	64.3	63.6	1.15	1.03	1.04
R3-70-10-LT (1)	88.3	52.2	87.1	85.1	1.69	1.01	1.04
R3-70-10-LT (2)	66.0*	46.8	76.4	74.5	1.41	0.86	0.89
R3-70-25-LT	56.0	39.0	52.9	51.8	1.44	1.06	1.08
R5-40-10-LT	123.2	99.9	120.5	116.6	1.23	1.02	1.06
R5-40-25-LT (1)	86.0*	68.5	77.7	75.1	1.26	1.11	1.14
R5-40-25-LT (2)	95.6*	75.4	86.2	83.4	1.27	1.11	1.15
R5-70-10-LT (1)	87.8	48.7	86.0	79.1	1.80	1.02	1.11
R5-70-10-LT (2)	87.0	52.2	93.2	86.0	1.67	0.93	1.01
R5-70-25-LT	62.2	40.0	54.4	50.7	1.55	1.14	1.23

*Column failed under sustained load

The use of β_{dns} provides very inconsistent results for nonprestressed columns. At design strength, Equation 4.2 provided conservative results for every column and ranged from 15% to 80% conservative. For nominal strengths, Equation 4.2 provided a range of 13% unconservative to 121% conservative. Based on this, the use of β_{dns} coupled with Equation 4.2 as a design equation provided unreliable but conservative results at design strengths. When used with Equations 4.4 and 4.5, however, the method provided unconservative results at design strengths. For Equation 4.4, all of the results were less than 15% conservative, which indicates a small safety factor. For nominal strengths, Equations 4.4 and 4.5 were more unconservative. Equations 4.4 and 4.5 had less of a range of conservatism, however, which is expected because these equations are more accurate.

Table 9.7 provides a summary of the capacity ratios for the nonprestressed columns. Equation 4.2, on average, was 40% conservative at design strengths. Equations 4.4 and 4.5 were only 3% and 7% conservative, respectively. Equations 4.4 and 4.5 have standard deviations less than half of those for Equations 4.2 at both nominal and design strengths.

Table 9.7 – Statistical Summary of Long-Term Capacities (Nonprestressed)

Analysis		**Eq. 4.2**	**Eq. 4.4**	**Eq. 4.5**
Nominal Strength, S_n	Average	1.49	0.98	1.04
	Std. Dev.	0.45	0.18	0.21
Design Strength, ϕS_n	Average	1.40	1.03	1.07
	Std. Dev.	0.22	0.07	0.08

Based on these results, using β_{dns} as a design method provides inconsistent results for all stiffness equations. For Equation 4.2, however, all of the results at design strengths were conservative. This indicates that, while the method is inconsistent, it is conservative when coupled with a stiffness equation that provides a lower bound stiffness. If a more accurate stiffness equation is used (Equations 4.4 and 4.5), then the β_{dns} can result in unconservative results. Again, these results were only based on columns that were loaded up to approximately 100 days. For service columns that would be loaded for years, the results are expected to be more unconservative.

9.3.2.2 Prestressed Columns

Table 9.8 and Table 9.9 provide the computed capacities of the prestressed columns at nominal and design strengths, respectively. The capacity of the tests results was defined as the axial load at which the experimental results exceeded the strength. Additionally, the ratio of the test results

to the equation estimations are provided. As such, a value of 1.0 is perfect accuracy, while values less than 1.0 are unconservative and values greater than 1.0 are conservative. The columns that failed under sustained load were included in this evaluation. For those columns, the capacity of the experimental results was taken as the sustained load.

Table 9.8 – Computed Long-Term Capacities at Nominal Strengths (Prestressed)

Column ID	Computed Axial Capacity, kip				P_{test} / $P_{Eq.}$		
	Test	Eq. 4.2	Eq. 6.4	Eq. 6.6	Eq. 4.2	Eq. 6.4	Eq. 6.6
P4-40-10-LT	136.2	114.4	136.5	134.8	1.19	1.00	1.01
P4-40-25-LT	60.0*	73.7	82.1	80.8	0.81	0.73	0.74
P4-70-10-LT	67.5	51.0	84.3	81.6	1.32	0.80	0.83
P4-70-25-LT	53.9	39.0	50.6	49.0	1.38	1.07	1.10

*Column failed under sustained load

Table 9.9 – Computed Long-Term Capacities at Design Strengths (Prestressed)

Column ID	Computed Axial Capacity, kip				P_{test} / $P_{Eq.}$		
	Test	Eq. 4.2	Eq. 6.4	Eq. 6.6	Eq. 4.2	Eq. 6.4	Eq. 6.6
P4-40-10-LT	91.8	88.2	98.9	98.3	1.04	0.93	0.93
P4-40-25-LT	60.0*	55.7	60.8	60.2	1.08	0.99	1.00
P4-70-10-LT	51.4	47.2	73.4	71.6	1.09	0.70	0.72
P4-70-25-LT	44.7	35.1	42.3	41.3	1.27	1.06	1.08

*Column failed under sustained load

Due to the small number of prestressed columns tests, conclusions are difficult to make. The equations for prestressed columns, in general, are less conservative than those for the nonprestressed columns. This is to be expected because, as shown previously, prestressed columns have a lower short-term stiffness and exhibit greater stiffness reductions under sustained loads. For design strengths, Equation 4.2 provided conservative results for all columns, but for nominal strengths, it was 19% unconservative for a column that failed under sustained load. Equations 6.4 and 6.6 provided unconservative results for both nominal and design strengths and, in fact, did not estimate any column more than 10% conservative for both strength levels.

Table 9.10 provides a summary of the capacity ratios for the nonprestressed columns. Equation 4.2 is more than 10% conservative for both strengths, while Equations 6.4 and 6.6 were more than 7% unconservative for both strengths. Interestingly, the standard deviation for Equation 4.2 was less than those of Equations 6.4 and 6.6 for design strength. The standard deviations, however, are somewhat insignificant due to small number of tests.

Table 9.10 – Statistical Summary of Long-Term Capacities (Prestressed)

Analysis		Eq. 4.2	Eq. 6.4	Eq. 6.6
Nominal Strength, S_n	Average	1.18	0.90	0.92
	Std. Dev.	0.22	0.14	0.14
Design Strength, ϕS_n	Average	1.12	0.92	0.93
	Std. Dev.	0.09	0.13	0.14

Because prestressed columns exhibit greater stiffness reductions under sustained loads, the ACI 318 method of using β_{dns} provides more unconservative results for prestressed columns than for nonprestressed columns. This was even the case for Equation 4.2 (0.40 E_cI_g), which was previously found to be a relatively conservative lower bound for the short-term stiffness, though the actual lower bound was found to be closer to 0.30 E_cI_g. Thus, if Equations 6.4 and 6.6 are used to compute the flexural stiffness of prestressed columns, a greater β_{dns} should be used, likely greater than 1.0. Based on the few results, a definitive recommendation cannot be made.

9.4 Findings

9.4.1 Behavior under Sustained Load

In the framework of the current ACI 318 methodology, a method was developed to estimate the sustained load behavior of slender columns. The results of the experimental tests were used to evaluate and calibrate the proposed method. The following conclusions were made.

1. The effective flexural stiffness of a short column cross-section under sustained load can be approximated by Equation 9.2, which is a modification of the suggested ACI 209 creep equations. For plain sections, the equation is accurate for durations of loading beyond the first 10 days, and for reinforced sections, the equation is conservative beyond the first few days. Furthermore, Equation 9.2 can be used in conjunction with the moment magnification procedure to estimate the sustained load behavior of slender columns. The equation results in a conservative lower bound for reinforced and prestressed columns. For increased accuracy and reliability, the equations should be calibrated with results from short-column tests with concrete and cross-sections similar to the columns being analyzed.
2. The effective flexural stiffness was found to be, for the most part, independent of the initial maximum compressive stress of a column under sustained load. Under cases of extreme loading, such as those approaching the concrete compressive strength, this assumption is not valid. For the columns with #5 bars, the reduction in effective stiffness

was independent of the maximum compressive stress. For the columns with #3 bars, the reduction showed a minor trend, but overall, it is assumed that this effect can be neglected. For the prestressed columns, no trend was observed.

3. The slenderness ratio was found to increase the effective flexural stiffness. The scatter of the results, however, was unpredictable. Due to the unpredictability and concern of instability for increasingly slender columns, the increase in stiffness due to slenderness can be conservatively ignored.
4. The decrease in column effective flexural stiffness under sustained load was found to be significantly influenced by the reinforcement ratio. As the reinforcement ratio increased, the differences in effective stiffness (EI_{eff}/EI) over time was essentially eliminated. For the columns with #5 bars, the effective stiffness had essentially the same response over time. This indicates that columns with higher reinforcement ratio are influenced less by other parameters such as maximum compressive stress and slenderness ratio. The prestressed columns, due to the very low reinforcement ratio, behaved similarly to the plain columns. The effect of reinforcement on the effective stiffness was found to be approximated by Equation 9.4. For more reliable lower bound results, however, the reinforcement factor (α) can be taken as 1.0 for all columns.

It should be noted that the number of columns tested in this study is small. While the maximum compressive stress and slenderness ratio were found to be insignificant to the reduction in stiffness, that conclusion is based only on the results from this study. Furthermore, the effect of the reinforcement ratio was concluded by disregarding a column that was tested, but nearly failed. Further research is necessary to provide increased confidence in the design recommendations. Specifically, additional slender column tests under varying sustained loads are recommended. The slenderness and eccentricity ranges tested are likely adequate based on typical design ranges, but exploring the behavior of those columns under varying loads using identical concrete would increase confidence in the provided recommendations as well as providing important data to calibrate computational modeling.

9.4.2 Long-Term Effects

Current design methods for long-term effects were evaluated using the experimental results. The following conclusions were made.

1. For the nonprestressed columns, the use of β_{dns} = 0.6 when coupled with Equation 4.2 provided conservative results at design strengths and conservative results at nominal strengths for all but three columns. While the method was inaccurate, it provided a reliable lower bound. The use of β_{dns} = 0.6 when coupled with Equations 4.4 and 4.5, however, provided unconservative results at design strengths for three columns and unconservative results at nominal strengths for five columns. Equations 4.4 and 4.5, however, do lead to more accurate results than Equation 4.2.
2. For the prestressed columns, the use of β_{dns} = 0.6 when coupled with Equation 4.2 provided conservative results at design strengths and conservative results at nominal strengths except for one column. The level of conservatism for these columns was less than those for the nonprestressed columns. The use of β_{dns} = 0.6 when coupled with Equations 6.4 and 6.6 provided unconservative results at nominal strengths two columns and unconservative results at design strengths three columns. The level of conservatism for these columns was, again, less than those for the nonprestressed columns.
3. Based on the results, the ACI 318 method of using β_{dns} can provide a lower bound stiffness but cannot provide accurate results. When coupled with lower bound stiffness equations (Equation 4.2), the current assumption of β_{dns} = 0.6 is considered conservative for nonprestressed columns. For prestressed columns, the conservatism is significantly reduced. If more accurate stiffness equations are used (Equations 4.4, 4.5, 6.4 and 6.6), then the assumption of β_{dns} = 0.6 yields unconservative results. Due to the small number of experimental tests, recommendations are difficult to make, but a β_{dns} = 1.0 for nonprestressed columns seems reasonable, and a β_{dns} > 1.0 would likely be required for prestressed columns.

It should be noted that the number of columns tested in this study is small, particularly prestressed columns. Additionally, the columns were subject to very high sustained loads. Long-term stiffness reductions of typically loaded service columns may be less severe. In any case, the use of β_{dns} = 0.6 coupled with accurate short-term flexural stiffness equations is a potential safety concern.

CHAPTER 10 SUMMARY AND CONCLUSIONS

10.1 Summary

With the greater availability and affordability of high-strength concrete, designers have been able to reduce concrete column cross-sections, leading to in an increase in the prevalence of slender columns in building construction. In spite of this trend, provisions for the design of slender columns have not changed significantly since the provisions were first introduced 1971 (MacGregor, Breen, and Pfrang 1970). Improved understanding of as well as improved design provisions for slender, concrete columns can allow for further use while maintaining safety. The objective of this research was to better understand the behavior and limits of slender, concrete columns and, from the results, develop improved design procedures for incorporation into building codes.

10.2 Findings

The research program consisted of experimental testing coupled with computational modeling. The experimental testing was designed to expand the boundaries of practical column design while maintaining realistic service conditions. Additionally, the columns tests were designed to simulate theoretical conditions, which correspond better to code provisions and simplified computational analysis. The columns were tested with equal end eccentricities, braced against sidesway, and used pinned-pinned loading conditions.

A computational model was further developed from a previous study (Jenkins 2011). It incorporated commonly assumed material properties, simple mechanics, and structural analysis procedures. The results of the experimental tests were used to evaluate and calibrate the computational model. With increased confidence, the computational model was used to develop design methods through analysis and parametric evaluation.

10.2.1 Short-Term Behavior of Reinforced Columns

Eight short-term tests on nonprestressed columns and twelve short-term tests on prestressed columns were conducted. The parameters varied were reinforcement ratio, eccentricity ratio, and slenderness ratio.

10.2.1.1 Nonprestressed Columns

The results of the nonprestressed column tests were compared against both current and proposed design methods. To improve confidence in the comparisons, the results from a similar study were included (Lloyd and Rangan 1995). The database of columns resulted in 43 columns with varying loading, geometric, and material parameters. Existing and proposed design equations were used to estimate the nominal and design strengths of the columns. These calculations were then compared to the experimental results. The following conclusions were made:

1. Several columns surpassed the ACI 318 (2014) total moment limit of 1.4 times the first-order moment. In most cases, however, the equations estimated conservative behavior, particularly at design strengths. More importantly, while some of these columns experienced stability failure, the equations estimated the failure load accurately.
2. The proposed design equations (4.4 and 4.5) were found to be more accurate than the current design equations (4.1, 4.2, and 4.3) when the entire column database was evaluated. While Equation 4.3 was nearly as accurate as Equations 4.4 and 4.5, it was found to have more unconservative results. Equations 4.1 and 4.2 were found to be excessively conservative.
3. Higher reinforcing bar strength was found to decrease the accuracy and conservatism of Equations 4.3 and 4.4. It was determined that when computing the nominal axial strength (P_0) of the columns for use in the column flexural stiffness (EI), a reinforcing bar strength of 60 ksi should be used, regardless of the actual strength of the bar in the column. This is required because the effective stiffness equations were calibrated based on 60 ksi rebar.

10.2.1.2 Prestressed Columns

A computational model from a previous study (Jenkins 2011) was optimized and modified to also include the effects of prestressing steel. The results of the prestressed column tests were compared against the computation model. The results were also compared against current design methods, which clearly indicated improved design procedures should be developed. The computational model was used to conduct a parametric study on prestressed columns, and these results were used to develop improved design methods. The following conclusions were made:

1. Similar to the comparisons from the nonprestressed columns, several of the columns exceeded the ACI 318 total moment limit. These columns had less residual capacity as compared to corresponding nonprestressed columns. This difference in behavior indicates prestressed columns are more susceptible to global stability failure, which is expected due to their decreased flexural stiffness. Regardless, the computational model and equations estimated the failures conservatively.
2. Existing design equations were found to be excessively conservative. The proposed design equations for nonprestressed columns (Equations 4.4 and 4.5) were more accurate than the existing design equations for prestressed columns. The accuracy for the proposed equations, however, was different than when compared against the nonprestressed columns. This difference indicated improved design equations should be developed for prestressed columns.
3. From the results of the parametric study, it was found that the axial load ratio and the eccentricity ratio have the greatest influence on the behavior of slender, prestressed columns. Other parameters such as the prestressing ratio, column slenderness, and section geometry were found to be sufficiently accounted by normalization using the axial strength as well as the methodology of the moment magnification procedure.
4. Equations 6.4 and 6.6 were developed from the results of the parametric study as proposed design equations. Equation 6.4 is more accurate, while Equations 6.6 is simply a modification of Equation 4.5 for use as a simpler design equation. Both equations were found to be more accurate than existing equations for prestressed columns while maintaining conservatism.

10.2.2 Creep and Shrinkage Behavior of Short Columns

Six short columns were tested under sustained load to measure the time-dependent effects of shrinkage and creep, and four specimens were monitored solely for shrinkage. In addition, the results were compared to ACI 209.2R (2008) models. Based on the analyses of the results of these tests, the following conclusions were made:

1. The presence of reinforcement decreased the shrinkage rates of the concrete specimens. Equation 7.1, when correlated with experimental data, provides accurate shrinkage estimates for both plain and reinforced specimens.
2. The presence of reinforcement decreased the creep rates of the sustained loaded columns. The eccentricity ratio, however, did not influence creep rates of the columns, and it was concluded that only the stress magnitude at the extreme compressive fiber affected creep rates. It was further assumed that, consistent with ACI 209.2R, the creep coefficient is linear as a function of stress, at least for compressive stresses equal to or less than 50% of the concrete strength. Equation 7.2, when correlated with experimental data, provides accurate creep estimates for both the plain and reinforced columns, but Equation 7.2 is less accurate for the columns when the duration of loading is less than 25 days.
3. The ultimate creep coefficient (ϕ_u) based on the experimental results was found to be more than twice the value computed based on ACI 209.2R. While creep data presents with significant scatter, the discrepancy between the computed and measured value is very high. ACI 209.2R, however, recommends using measured data when available.

10.2.3 Long-Term Behavior of Reinforced Columns

Twelve nonprestressed and four prestressed, slender columns were tested under long-term loading and were subject to a constant sustained load for up to approximately 100 days. After that time, the columns were subject to constantly increasing load until failure. Three columns failed under sustained load prior to reaching 100 days. The following conclusions were made:

1. Increasing the reinforcement from #3 bars ($A_{st}/A_g \approx 1.2\%$) to #5 bars ($A_{st}/A_g \approx 3.3\%$) improved the long-term stability of the columns. While deflection increases between the columns were similar, the columns with #5 bars appeared to stabilize by 100 days while most of the columns with #3 bars did not. This difference was evident in spite of the fact that the columns with #5 bars had higher applied loads.
2. Prestressed columns exhibited greater long-term effects than nonprestressed columns.
3. Nearly all columns exceeded the ACI 318 total moment limit ($1.4M_0$) after 100 days of sustained load, but several columns retained significant post-sustained load residual capacity.

10.2.3.1 Behavior under Sustained Load

In the framework of the current ACI 318 and ACI 209 (1992) methodology, a method was developed to estimate the sustained load behavior of slender columns. The results of the experimental tests were used to evaluate and calibrate the proposed method. The following conclusions were made:

1. The effective flexural stiffness (EI/EI_{eff}) was found to be, for the most part, independent of the initial maximum compressive stress of a column under sustained load.
2. The slenderness ratio was found to increase the effective flexural stiffness, but to increase reliability of the equations, this effect can be conservatively ignored.
3. The reinforcement ratio, however, was found to significantly influence the effective flexural stiffness. As the reinforcement ratio increased, the amount of scatter decreased.
4. The effective stiffness over time of nonprestressed columns was similar to one another. At 100 days, the effective stiffness (EI/EI_{eff}) was approximately 0.40. Prestressed columns, however, behaved similarly to plain concrete columns, with a larger reduction in stiffness with time. At 100 days, the effective stiffness (EI/EI_{eff}) was approximately 0.20, or half of that for the nonprestressed columns.

5. The effective flexural stiffness of a short, concrete column under sustained load can be approximated by Equation 9.2, which is a modification of the suggested ACI 209 creep equation. Furthermore, Equation 9.2 can be used in conjunction with the moment magnification procedure to estimate the sustained load behavior of slender columns. The effect of reinforcement on the effective stiffness was found to be approximated by Equation 9.4. The reinforcement factor (α), however, can be taken as 1.0 for all columns, which ensures conservative results.

It should be noted that the number of columns tested in this study is small. While the maximum compressive stress and slenderness ratio were found to be insignificant to the reduction in stiffness, that conclusion is based only on the results from this study. Furthermore, the effect of the reinforcement ratio was concluded by disregarding a column that was tested, but nearly failed. Further research is necessary to provide increased confidence in the design recommendations.

10.2.3.2 Long-Term Effects

Current design methods for long-term effects were evaluated using the experimental results. The following conclusions were made:

1. For the nonprestressed columns, the use of β_{dns} = 0.6 when coupled with Equation 4.2 provided conservative results at design strengths and conservative results at nominal strengths for all but three columns. While the method was inaccurate, it provided a reliable lower bound. The use of β_{dns} = 0.6 when coupled with Equations 4.4 and 4.5, however, provided unconservative results at design strengths for three columns and unconservative results at nominal strengths for five columns. Equations 4.4 and 4.5, however, do lead to more accurate results than Equation 4.2.
2. For the prestressed columns, the use of β_{dns} = 0.6 when coupled with Equation 4.2 provided conservative results at design strengths and conservative results at nominal strengths except for one column. The level of conservatism for these columns was less than those for the nonprestressed columns. The use of β_{dns} = 0.6 when coupled with Equations 6.4 and 6.6 provided unconservative results at nominal strengths two columns and unconservative results at design strengths three columns. The level of conservatism for these columns was, again, less than those for the nonprestressed columns.
3. Based on the results, the ACI 318 method of using β_{dns} can provide a lower bound stiffness but cannot provide accurate results. When coupled with lower bound stiffness

equations (Equation 4.2), the current assumption of β_{dns} = 0.6 is considered conservative for nonprestressed columns. For prestressed columns, the conservatism is significantly reduced. If more accurate stiffness equations are used (Equations 4.4, 4.5, 6.4 and 6.6), then the assumption of β_{dns} = 0.6 yields unconservative results. Due to the small number of experimental tests, recommendations are difficult to make, but a β_{dns} = 1.0 for nonprestressed columns seems reasonable, and a β_{dns} > 1.0 would likely be required for prestressed columns.

It should be noted that the number of columns tested in this study is small, particularly prestressed columns. Additionally, the columns were subject to very high sustained loads. Long-term stiffness reductions of typically loaded service columns may be less severe. In any case, the use of β_{dns} = 0.6 coupled with accurate short-term flexural stiffness equations is a safety concern.

10.3 Design Recommendations

Based on the findings of this study, the following design recommendations are made. The recommendations are intended for use with non-sway columns in conjunction with the moment magnification procedure outlined in ACI 318 (2014).

10.3.1 Short-Term Stiffness of Nonprestressed Columns

Equations 10.1 and 10.2 are recommended for computing the flexural stiffness of nonprestressed columns. Equation 10.1 provides more accurate results than Equation 10.2 but requires the reinforcement ratio, which may not be known initially in design. Equation 10.1, therefore, is intended for either detailed analysis or design, while Equation 10.2 is intended for general design use.

Equation 10.1

$\frac{M}{Ph} = \frac{e}{h}$	**Flexural Stiffness of Compression Member, *EI***
≤ 0.1	$\left[1.05 - 0.6\frac{P}{P_0}\right]\left[1.0 + 3\left(\frac{A_{st}}{A_g} - 0.01\right)\right]E_c I_g \geq 0.30E_c I_g$
> 0.1	$\left[1.05 - 0.6\frac{P}{P_0}\right]\left[1.0 + 3\left(\frac{A_{st}}{A_g} - 0.01\right)\right]\left[1.2 - 2\frac{M}{Ph}\right]E_c I_g \geq 0.30E_c I_g$

Equation 10.2

$\frac{M}{Ph} = \frac{e}{h}$	**Flexural Stiffness of Compression Member, *EI***
≤ 0.1	$\left[1.0 - 0.5\frac{P}{P_{0g}}\right]E_c I_g \geq 0.40E_c I_g$
> 0.1	$\left[1.0 - 0.5\frac{P}{P_{0g}}\right]\left[1.2 - 2\frac{M}{Ph}\right]E_c I_g \geq 0.40E_c I_g$

where:

A_g = gross area of concrete section, in.^{2}

A_{st} = total area of nonprestressed longitudinal reinforcement, in.^{2}

$E_c = 57{,}000\sqrt{f_c'}$ psi = modulus of elasticity of concrete, psi

E_s = modulus of elaticity of reinforcement, psi

h = depth of compression member, in.

I_g = moment of inertia of gross concrete section, in.^{4}

M = end moment of compression member, in.-lb

P = axial force, lb

$P_0 = 0.85 f_c'\left(A_g - A_{st}\right) + f_y A_{st}$ = nominal axial strength, lb

$P_{0g} = 0.85 f_c' A_g$ = axial strength of gross concrete section, lb

10.3.2 Short-Term Stiffness of Prestressed Columns

Equations 10.3 and 10.4 are recommended for computing the flexural stiffness of prestressed columns. Equation 10.3 provides more accurate results than Equation 10.4 but requires the prestressing ratio to compute the nominal axial strength (P_0). Equation 10.3, therefore, is intended for more detailed design or column analysis, while Equation 10.4 is intended for general design use. Equation 10.4 is simply a fractional reduction of Equation 10.2.

Equation 10.3

$\frac{M}{Ph} = \frac{e}{h}$	**Flexural Stiffness of Compression Member, *EI***
≤ 0.1	$\left[0.95 - 0.45\frac{P}{P_0}\right] E_c I_g \geq 0.30 E_c I_g$
> 0.1	$\left[0.95 - 0.45\frac{P}{P_0}\right]\left[1.2 - 2\frac{M}{Ph}\right] E_c I_g \geq 0.30 E_c I_g$

Equation 10.4

$\frac{M}{Ph} = \frac{e}{h}$	**Flexural Stiffness of Compression Member, *EI***
≤ 0.1	$0.9\left[1.0 - 0.5\frac{P}{P_{0g}}\right] E_c I_g \geq 0.30 E_c I_g$
> 0.1	$0.9\left[1.0 - 0.5\frac{P}{P_{0g}}\right]\left[1.2 - 2\frac{M}{Ph}\right] E_c I_g \geq 0.30 E_c I_g$

where:

$A_g =$ gross area of concrete section, in.^{2}

$A_{pt} =$ total area of prestressed longitudinal reinforcement, in.^{2}

$E_c = 57{,}000\sqrt{f_c'}$ psi $=$ modulus of elasticity of concrete, psi

$E_p =$ modulus of elaticity of prestressing reinforcement, psi

$h =$ depth of compression member, in.

$I_g =$ moment of inertia of gross concrete section, in.^{4}

$M =$ end moment of compression member, in.-lb

$P =$ axial force, lb

$P_0 = 0.85 f_c'\left(A_g - A_{pt}\right) + \left(f_{se} - 0.003E_p\right) A_{pt} =$ nominal axial strength, lb

$P_{0g} = 0.85 f_c' A_g =$ axial strength of gross concrete section, lb

10.3.3 Long-Term Stiffness of Concrete Columns under Sustained Load

Equations 10.5 and 10.6 are recommended for computing the long-term behavior of slender columns under sustained load. The equations should be used in conjunction with the moment magnification procedure and provide an effective flexural stiffness for columns subject to a constant sustained load for a determined amount of time. The ultimate creep coefficient (ϕ_u) should be calibrated based on experimental results for cross-sections that are representative of those being analyzed. For this study, it was found that ϕ_u = 5.3, which is twice that computed in accordance with ACI 209.2R (2008). When using ACI 209.2R in absence of experimental data, the result can be grossly unconservative.

The equations are unreliable for durations of loading less than 20 days but become more accurate and reliable for longer-term loading. For reliable lower bound results, the reinforcement factor (α) can be taken as 1.0 for all columns, but for increased accuracy, the reinforcement factor (α) can be taken as 2.5 for nonprestressed columns with minimum reinforcement ($A_{st}/A_g \geq 1.0\%$). The reinforcement factor is based on limited experimental results and is intended for practical service level sustained loads. Under extreme loading scenarios, the factor may lead to unconservative results.

$$EI_{eff}(t) = \frac{EI}{1 + \phi_{eff}(t)} \qquad \text{(Eq. 10.5)}$$

$$\phi_{eff}(t) = \frac{t}{f + t} * \frac{\phi_u}{\alpha} \qquad \text{(Eq. 10.6)}$$

where:

EI_{eff} = effective flexural stiffness of compression member, in.^{2}-lb

EI = flexural stiffness of compression member, in.^{2}-lb

$f = 26.0e^{(0.36V/S)}$ = member shape and size factor

t = duration of sustained load, days

V / S = volume-surface ratio, in.

$$\alpha = \begin{cases} 1.0 & \text{for prestressed or plain columns} \\ 2.5 & \text{for nonprestressed columns} \end{cases}$$

ϕ_{eff} = effective creep coefficient

ϕ_u = ultimate creep coefficient

10.3.4 Long-Term Effects of Concrete Columns (β_{dns} Method)

The ACI 318 method of using β_{dns} can provide a lower bound stiffness but cannot provide accurate results. When coupled with lower bound stiffness equations (Equation 4.2), the current assumption of β_{dns} = 0.6 is considered conservative for nonprestressed columns. For prestressed columns, the conservatism is significantly reduced. If more accurate stiffness equations are used (Equations 4.4, 4.5, 6.4 and 6.6), then the assumption of β_{dns} = 0.6 yields unconservative results. Due to the small number of experimental tests, recommendations are difficult to make, but a β_{dns} = 1.0 for nonprestressed columns seems reasonable, and a β_{dns} > 1.0 would likely be required for prestressed columns.

10.3.5 ACI 318 Total Moment Limit (1.4 M_0)

When only considering short-term effects, the ACI 318 total moment limit of 1.4 times the first-order moment (1.4 M_0) is unnecessary. While stability was a failure mode for several columns, particularly prestressed columns, the recommended and lower bound equations provided conservative results, even at nominal strengths. For service columns with long-term effects, the total moment limit is considered necessary until the total behavior of columns subject to long-term effects is better understood. Limiting the second-order moments is considered even more important when more accurate flexural stiffness equations (Equations 10.1, 10.2, 10.3 and 10.4) are used. It was found that the more accurate equations provided unconservative results when coupled with the current ACI 318 β_{dns} method to account for long-term effects.

10.4 Proposed Future Research

The experimental and computational results of this research program provide a high level of confidence in the design recommendations for the short-term effects of nonprestressed and prestressed columns. A significant number of short-term tests results are available. In addition, computational modeling based on fundamental mechanics is capable of fully describing the behavior of these columns.

Tests results on long-term effects, however, is more limited. The overall conclusions are based, in general, on measured response, rather than theoretical behavior. While it was attempted to develop a more theoretical approach for the modeling of long-term behavior in this research, the modeling was limited by the test results available. Therefore, further research should be conducted to fully investigate the effect of sustained load on the behavior of slender columns.

With a focus on the behavior of short columns, tests should include different reinforcement ratios as well as different maximum compressive stresses and eccentricity ratios. Long-term tests results on short-columns are integral to improved computational modeling.

Furthermore, additional slender column tests under varying sustained loads are recommended. The slenderness and eccentricity ranges tested in this study are likely adequate based on typical design ranges, but exploring the behavior of those columns under varying sustained loads using identical concrete would increase confidence in the recommendations as well as providing important data to further calibrate computational modeling.

With increased confidence in the computational modeling of columns under sustained load, a parametric study can be conducted on the post-sustained load behavior of slender columns. From these results, more reliable and accurate design recommendations can be developed to describe the complete behavior of slender, concrete columns.

LIST OF REFERENCES

LIST OF REFERENCES

ACI Committee 209. 1992. “Prediction of Creep, Shrinkage, and Temperature (ACI 209R-92).” Farmington Hills, MI: American Concrete Institute.

ACI Committee 209. 2008. “Guide for Modeling and Calculating Shrinkage and Creep In Hardened Concrete (ACI 209.2R-08).” Farmington Hills, MI: American Concrete Institute.

ACI Committee 318. 2014. “Building Code Requirements for Structural Concrete (ACI 318-14) and Commentary.” Farmington Hills, MI: American Concrete Institute.

ASTM Standard A370. 2012. “Standard Test Methods and Definitions for Mechanical Testing of Steel Products.” West Conshohocken, PA: ASTM International. doi:10.1520/A0370-12a.2.

ASTM Standard A416. 2012. “Standard Specification for Steel Strand, Uncoated Seven-Wire for Prestressed Concrete.” West Conshohocken, PA: ASTM International. doi:10.1520/A0416.

ASTM Standard A615. 2012. “Standard Specification for Deformed and Plain Carbon-Steel Bars for Concrete Reinforcement.” West Conshohocken, PA: ASTM International. doi:10.1520/A0615.

ASTM Standard A881. 2010. “Standard Specification for Steel Wire, Indented, Low-Relaxation for Prestressed Concrete Railroad Ties.” West Conshohocken, PA: ASTM International. doi:10.1520/A0881.

ASTM Standard C31. 2012. “Standard Practice for Making and Curing Concrete Test Specimens in the Field.” West Conshohocken, PA: ASTM International. doi:10.1520/C0031.

ASTM Standard C39. 2012. “Standard Test Method for Compressive Strength of Cylindrical Concrete Specimens.” West Conshohocken, PA: ASTM International. doi:10.1520/C0039.

ASTM Standard C469. 2010. “Standard Test Method for Static Modulus of Elasticity and Poisson’s Ratio of Concrete in Compression.” West Conshohocken, PA: ASTM International. doi:10.1520/C0469.

Jenkins, Ryan W. 2011. “Analytical Investigation of the Stiffness of Non-Sway Eccentrically Loaded Slender Reinforced Concrete Columns.” Purdue University.

Khuntia, Madhu, and S. K. Ghosh. 2004. “Flexural Stiffness of Reinforced Concrete Columns and Beams : Analytical Approach.” *ACI Structural Journal* 101 (3): 351–63.

Lin, T.Y., and Ned H. Burns. 1981. *Design of Prestressed Concrete Structures*. Third Edit. New York, NY: John Wiley & Sons.

Lloyd, Natalie Anne, and B. Vijaya Rangan. 1995. *High Strength Concrete Columns Under Eccentric Compression*. Vol. 3600. Perth, Western Austrailia.

MacGregor, James G., John E. Breen, and Edward O. Pfrang. 1970. “Design of Slender Concrete Columns.” *ACI Journal* 67 (1): 6–28.

Mirza, S. A. 1990. “Flexural Stiffness of Rectangular Reinforced Concrete Columns.” *ACI Structural Journal* 87 (4): 425–35.

Nathan, N D. 1985. “Rational Analysis and Design of Prestressed Concrete Beam Columns and Wall Panels.” *PCI Journal* 30 (3): 82–133.

PCI Committee on Prestressed Concrete Columns. 1988. “Recommended Practice for the Design of Prestressed Concrete Columns and Walls.” *PCI Journal* 33 (4): 56–95.

PCI Industry Handbook Committee. 2010. “PCI Design Handbook (7th Edition).” Chicago, IL: Precast/Prestressed Concrete Institute.

APPENDICES

Appendix A Prestressing Data and Calculations

Column Geometry and Material Properties

Column Geometry

$b = 6.125$ in.

$h = 6.125$ in.

$A_g = 37.52$ in.^{2}

6 prestressing wires

$A_{pw} = 0.0344$ in.^{2}

$A_{ps} = 6A_{pw} = 0.206$ in.^{2}

Stressing Values

$f_{si} = 196.2$ ksi $= 6750$ lbs

$E_{ps} = 29000$ ksi

Concrete Properties

$f_{ci}^{'} = 4070$ psi

$E_{ci} = 3300$ ksi

$n_{ci} = 8.79$

$f_c^{'} = 6570$ psi

$E_c = 3821$ ksi

$n_c = 7.59$

Prestress Loss Calculations

Elastic Shortening

$ES = n_{ci} f_{cir} = 9.1$ ksi

$A_{ti} = A_g + (n_{ci} - 1) A_{ps} = 39.12$ in^2

$F_0 = A_{ps} f_{si} = 40.5$ kip

$f_{cir} = F_0 / A_{ti} = 1035$ psi

Creep of Concrete

$CR = K_{cr}\left(E_{ps} / E_c\right)\left(f_{cir} - f_{cds}\right) = 15.7$ ksi

$K_{cr} = 2.0$ (for normalweight concrete)

$f_{cds} = 0$

Shrinkage of Concrete

$SH = 8.2x10^{-6} * K_{sh} E_{ps}\left(1 - 0.06V / S\right)\left(100 - RH\right) = 10.8$ ksi

$K_{sh} = 1.0$ (for pretensioned members)

$RH = 50\%$

$V / S = bh / \left(2b + 2h\right) = 1.53$

Relaxation of Tendons

$RE = \left[K_{re} - J\left(SH + CR + ES\right)\right]C = 3.6$ ksi

$K_{re} = 5.00$ *ksi*

$J = 0.040$

$C = 1.01$

Calculations Summary

$$TL = ES + CR + SH + RE = 39.2 \text{ ksi}$$

$$f_{se} = f_{si} - TL = 157.0 \text{ ksi}$$

$$f_c = \frac{A_{ps} f_{se}}{\left(A_g - A_{ps}\right)} = 869 \text{ psi}$$

$$\varepsilon_{si} = \frac{f_{se}}{E_s} + \frac{f_c}{E_c} = 5642 \text{ με}$$

*See PCI Design Handbook (2010) for definitions of Equations and Variables

Appendix B Uncorrected Slender Column Tests Results

Table B.1 – Summary of Deflection Corrections

Column ID	Correction, in.	Eccentricity, in.	Ratio
R3-40-10-ST	-0.014	0.6	-2.3%
R3-40-25-ST	-0.015	1.5	-1.0%
R3-70-10-ST	-0.006	0.6	-1.0%
R3-70-25-ST	0.032	1.5	2.1%
R5-40-10-ST	0.005	0.6	0.8%
R5-40-25-ST	-0.012	1.5	-0.8%
R5-70-10-ST	0.031	0.6	5.2%
R5-70-25-ST	0.065	1.5	4.3%
P2-40-10-ST	-0.006	0.6	-1.0%
P2-40-25-ST	0.016	1.5	1.1%
P2-70-10-ST	-0.024	0.6	-4.0%
P2-70-25-ST	-0.054	1.5	-3.6%
P4-40-10-ST	0.017	0.6	2.8%
P4-40-25-ST	0.036	1.5	2.4%
P4-70-10-ST	-0.015	0.6	-2.5%
P4-70-25-ST	-0.033	1.5	-2.2%
P6-40-10-ST	0.003	0.6	0.5%
P6-40-25-ST	0.001	1.5	0.1%
P6-70-10-ST	-0.029	0.6	-4.8%
P6-70-25-ST	-0.033	1.5	-2.2%
R3-40-10-LT	0.005	0.6	0.8%
R3-40-25-LT(1)	-0.007	1.5	-0.5%
R3-40-25-LT(2)	-0.005	1.5	-0.3%
R3-70-10-LT(1)	-0.011	0.6	-1.8%
R3-70-10-LT(2)	-0.004	0.6	-0.7%
R3-70-25-LT	0.008	1.5	0.5%
R5-40-10-LT	-0.021	0.6	-3.5%
R5-40-25-LT(1)	-0.002	1.5	-0.1%
R5-40-25-LT(2)	-0.012	1.5	-0.8%
R5-70-10-LT(1)	-0.025	0.6	-4.2%
R5-70-10-LT(2)	-0.018	0.6	-3.0%
R5-70-25-LT	-0.019	1.5	-1.3%
P4-40-10-LT	-0.013	0.6	-2.2%
P4-40-25-LT	-0.002	1.5	-0.1%
P4-70-10-LT	-0.014	0.6	-2.3%
P4-70-25-LT	-0.015	1.5	-1.0%

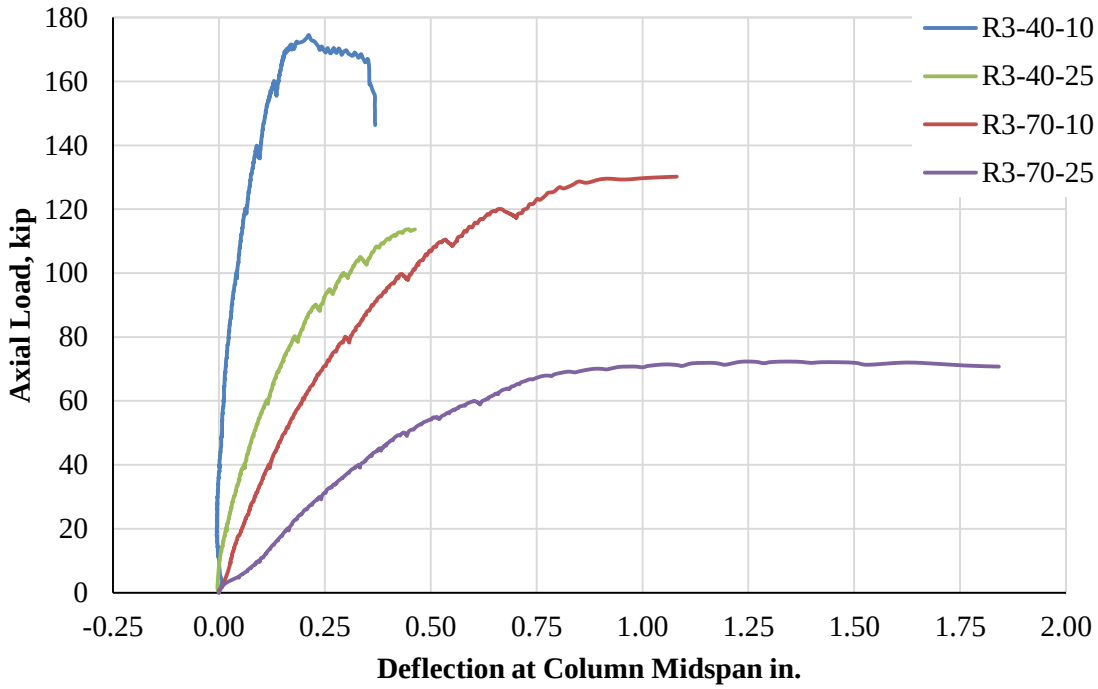

Figure B.1 – Uncorrected Short-Term Tests Results (#3 bars)

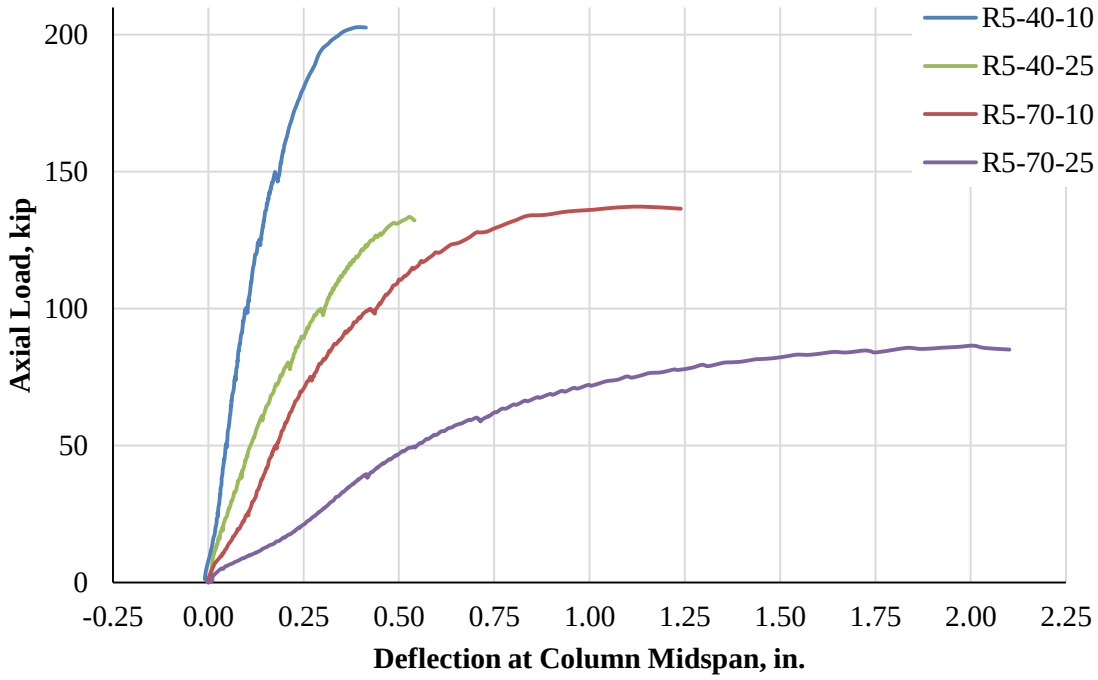

Figure B.2 – Uncorrected Short-Term Tests Results (#5 bars)

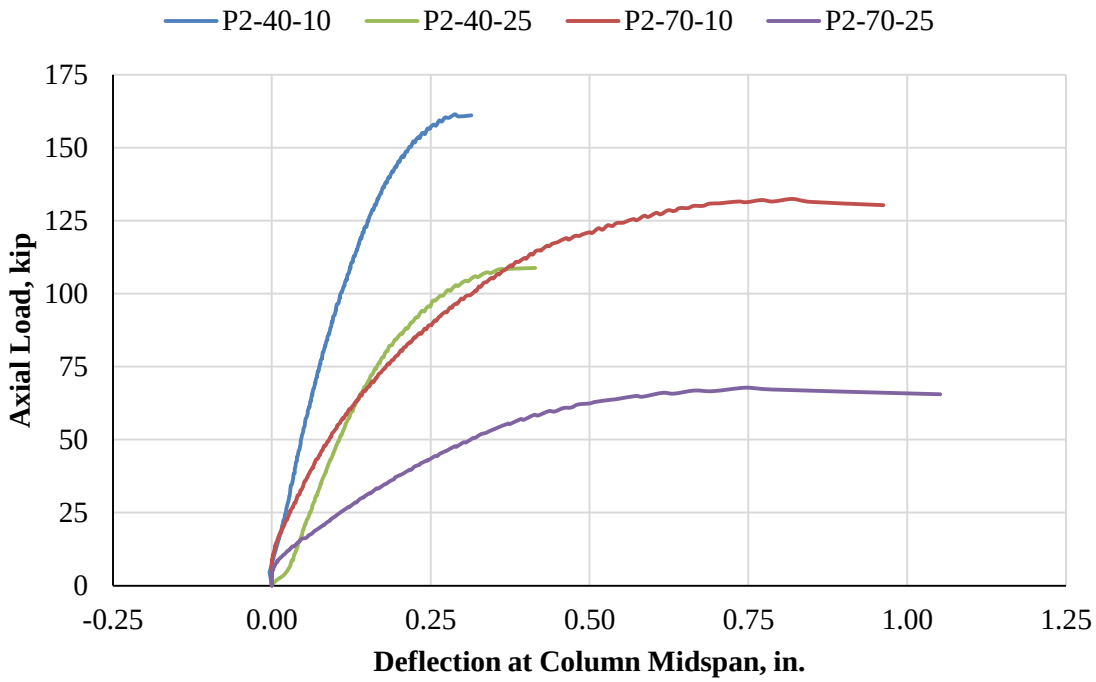

Figure B.3 – Uncorrected Short-Term Tests Results (2 – PS Wires)

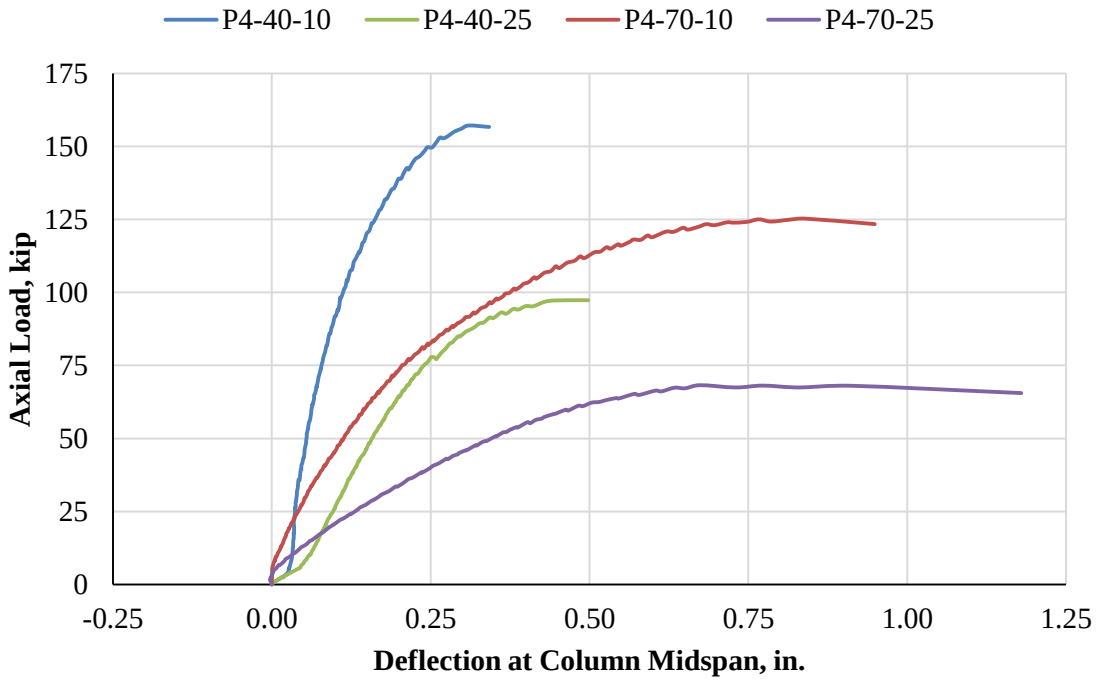

Figure B.4 – Uncorrected Short-Term Tests Results (4 – PS Wires)

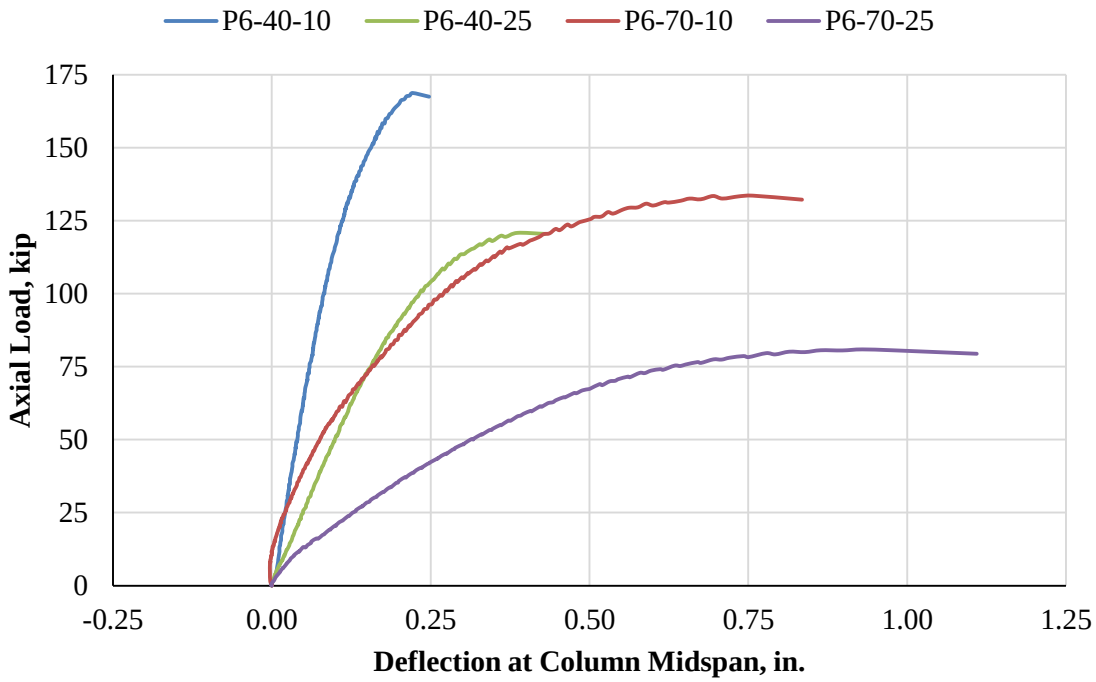

Figure B.5 – Uncorrected Short-Term Tests Results (6 – PS Wires)

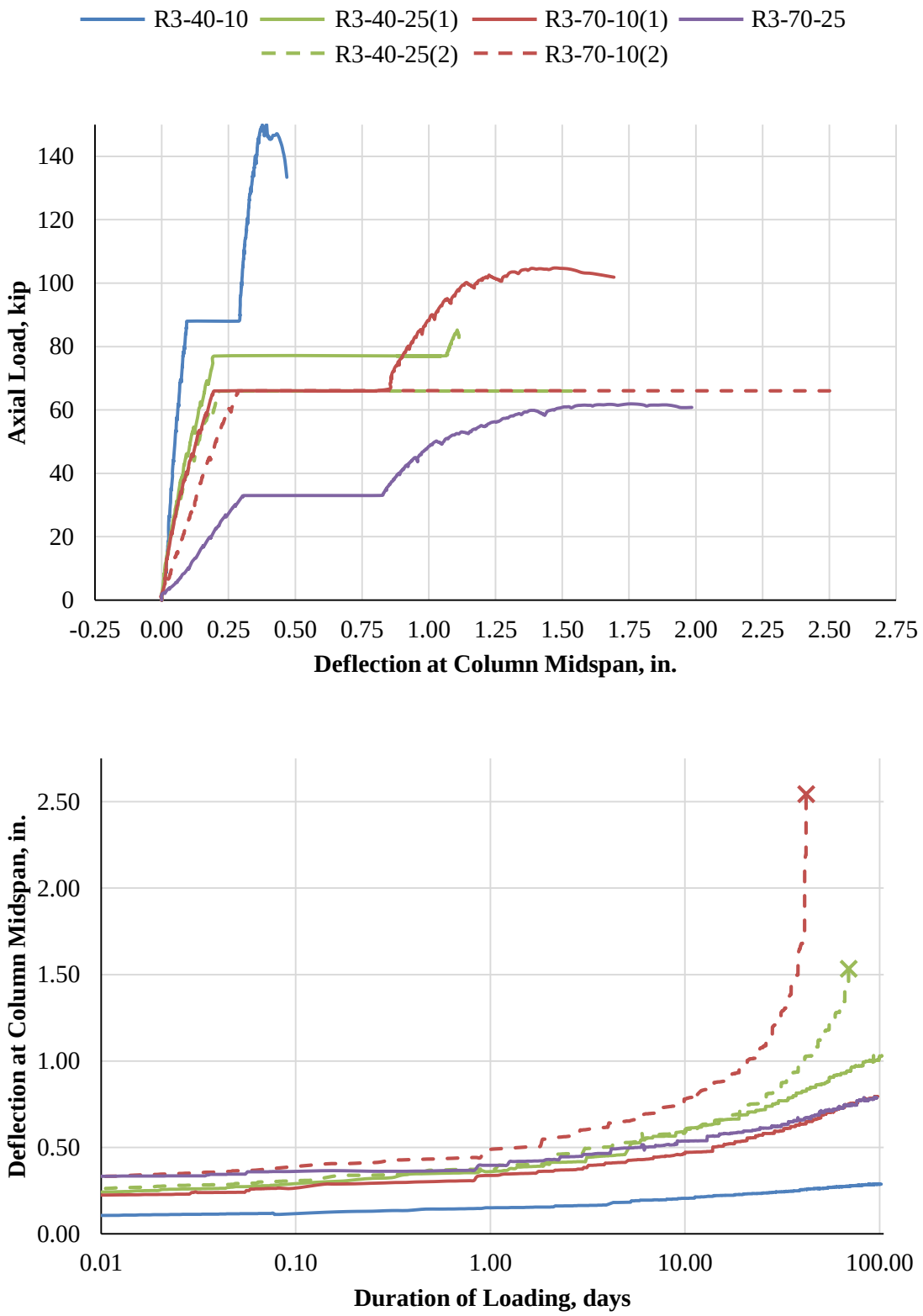

Figure B.6 – Uncorrected Long-Term Tests Results (#3 bars)

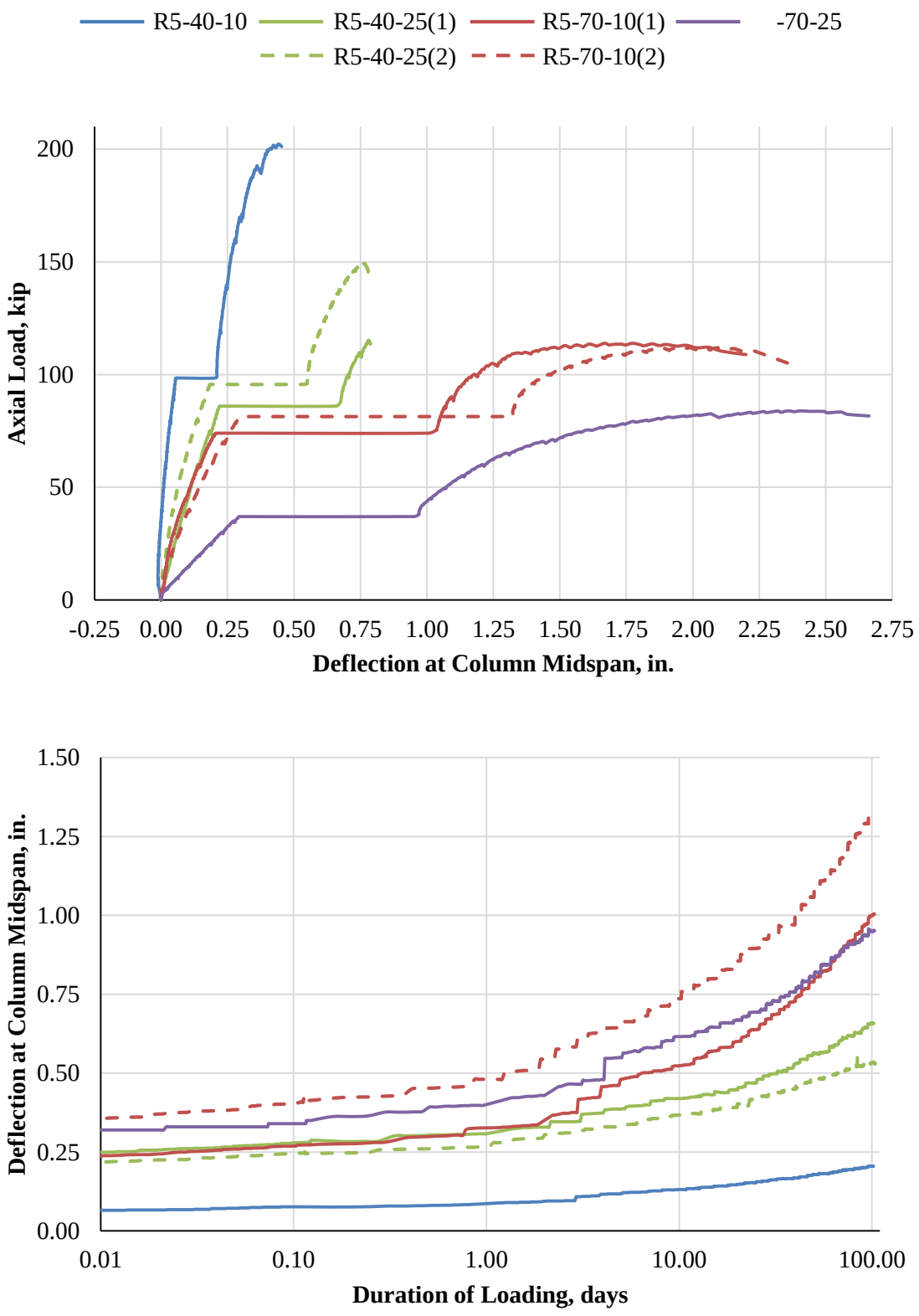

Figure B.7 – Uncorrected Long-Term Tests Results (#5 bars)

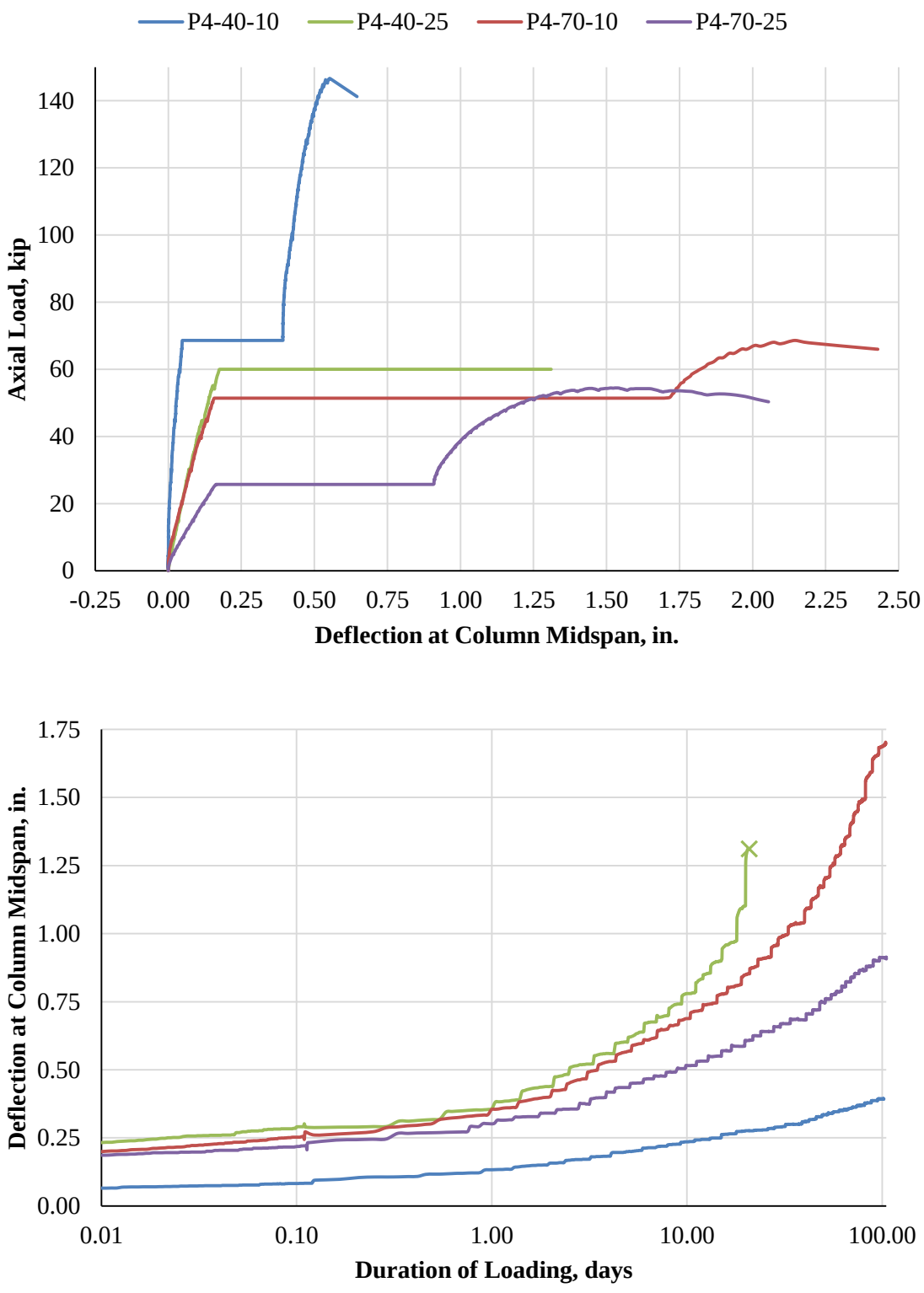

Figure B.8 – Uncorrected Long-Term Tests Results (4 – PS Wire)

Appendix C Column Database Summary and Analysis

Table C.1 – Summary of Column Properties (Lloyd and Rangan)

Column	*b*, in.	*h*, in.	kl_u, in.	Rebar Layout	f_y, ksi	*e*, in.	f_c', psi
I A	6.890	6.890	66.1	6 – 12 mm (125 mm spacing)	62.37	0.591	8410
I B	6.890	6.890	66.1		62.37	1.969	8410
I C	6.890	6.890	66.1		62.37	2.559	8410
II A	11.810	3.940	66.1	6 – 12 mm (50 mm spacing)	62.37	0.394	8410
II B	11.810	3.940	66.1		62.37	1.181	8410
II C	11.810	3.940	66.1		62.37	1.575	8410
III A	6.890	6.890	66.1	4 – 12 mm (125 mm spacing)	62.37	0.591	8410
III B	6.890	6.890	66.1		62.37	1.969	8410
III C	6.890	6.890	66.1		62.37	2.559	8410
IV A	11.810	3.940	66.1	4 – 12 mm (50 mm spacing)	62.37	0.394	8410
IV B	11.810	3.940	66.1		62.37	1.181	8410
IV C	11.810	3.940	66.1		62.37	1.575	8410
V A	6.890	6.890	66.1	6 – 12 mm (125 mm spacing)	62.37	0.591	13340
V B	6.890	6.890	66.1		62.37	1.969	13340
V C	6.890	6.890	66.1		62.37	2.559	13340
VI A	11.810	3.940	66.1	6 – 12 mm (50 mm spacing)	62.37	0.394	13340
VI B	11.810	3.940	66.1		62.37	1.181	13340
VI C	11.810	3.940	66.1		62.37	1.575	13340
VII A	6.890	6.890	66.1	4 – 12 mm (125 mm spacing)	62.37	0.591	13340
VII B	6.890	6.890	66.1		62.37	1.969	13340
VII C	6.890	6.890	66.1		62.37	2.559	13340
VIII A	11.810	3.940	66.1	4 – 12 mm (50 mm spacing)	62.37	0.394	13340
VIII B	11.810	3.940	66.1		62.37	1.181	13340
VIII C	11.810	3.940	66.1		62.37	1.575	13340
IX A	6.890	6.890	66.1	4 –12 mm (125 mm spacing)	62.37	0.591	14904
IX B	6.890	6.890	66.1		62.37	1.969	14904
IX C	6.890	6.890	66.1		62.37	2.559	14904
X A	11.810	3.940	66.1	4 – 12 mm (50 mm spacing)	62.37	0.394	14904
X B	11.810	3.940	66.1		62.37	1.181	14904
X C	11.810	3.940	66.1		62.37	1.575	14904
XI A	6.890	6.890	66.1	4 – 12 mm (125 mm spacing)	62.37	0.591	14904
XI B	6.890	6.890	66.1		62.37	1.969	14904
XII A	11.810	3.940	66.1	4 – 12 mm (50 mm spacing)	62.37	0.394	14904
XII B	11.810	3.940	66.1		62.37	1.181	14904
XII C	11.810	3.940	66.1		62.37	1.575	14904

Table C.2 – Summary of Short-Term Capacities at Nominal Strengths (Lloyd and Rangan)

Column	Computed Axial Capacity, kip					
	Test	**Eq. 4.1**	**Eq. 4.2**	**Eq. 4.3**	**Eq. 4.4**	**Eq. 4.5**
I A	322.0	293.8	296.0	323.2	317.5	313.4
I B	181.1	165.3	166.4	181.9	174.8	172.0
I C	146.7	137.7	138.6	148.0	138.5	138.6
II A	264.7	121.0	152.7	234.7	223.0	214.1
II B	98.9	78.6	94.2	122.2	109.8	106.2
II C	76.3	64.5	75.2	92.4	74.2	75.2
III A	*	269.7	285.2	305.1	303.8	302.3
III B	161.9	147.1	154.7	165.9	162.1	160.5
III C	*	115.1	122.1	130.6	121.9	122.1
IV A	204.6	108.1	149.0	214.5	213.9	209.3
IV B	94.5	67.2	86.3	109.5	100.8	98.1
IV C	60.3	54.1	66.5	77.8	65.2	66.5
V A	*	387.2	405.0	454.2	445.1	441.5
V B	*	211.2	219.1	244.6	233.5	230.1
V C	*	166.2	173.5	194.4	175.2	173.5
VI A	273.1	145.0	195.7	319.5	301.9	292.2
VI B	107.0	92.8	117.0	162.0	141.3	135.9
VI C	94.4	75.6	91.8	115.9	91.4	91.8
VII A	*	356.6	395.8	434.3	432.2	431.4
VII B	*	187.2	206.2	225.8	219.5	217.5
VII C	149.1	139.8	153.9	168.4	155.2	153.9
VIII A	*	130.9	193.0	294.8	294.0	289.1
VIII B	*	80.8	108.5	143.4	130.2	126.8
VIII C	69.0	64.5	82.0	98.3	81.1	82.0
IX A	*	368.0	411.1	452.6	450.4	449.7
IX B	*	192.1	213.2	234.2	227.4	225.4
IX C	166.3	143.0	158.1	173.6	159.7	158.1
X A	347.2	133.9	198.9	305.9	305.2	300.2
X B	95.3	82.6	111.5	148.0	134.2	130.7
X C	75.5	65.8	84.0	101.1	83.2	84.0
XI A	*	368.0	411.1	452.6	450.4	449.7
XI B	*	192.1	213.2	234.2	227.4	225.4
XII A	352.9	133.9	198.9	305.9	305.2	300.2
XII B	114.6	82.6	111.5	148.0	134.2	130.7
XII C	70.7	65.8	84.0	101.1	83.2	84.0

*Test did not reach computed axial strength

Table C.3 – Summary of Short-Term Capacities at Design Strengths (Lloyd and Rangan)

Column	Computed Axial Capacity, kip					
	Test	**Eq. 4.1**	**Eq. 4.2**	**Eq. 4.3**	**Eq. 4.4**	**Eq. 4.5**
I A	220.3	206.6	207.4	220.2	218.6	217.4
I B	126.2	116.6	117.1	125.7	122.3	121.1
I C	102.6	96.1	96.5	101.9	97.3	96.5
II A	200.9	108.1	131.6	180.7	177.1	172.8
II B	83.1	67.0	74.5	90.9	83.7	81.6
II C	64.4	56.8	62.6	70.2	62.4	62.6
III A	205.5	193.6	199.0	209.2	208.9	208.4
III B	116.0	105.2	108.9	115.5	113.6	112.8
III C	92.5	88.2	90.0	92.4	90.4	90.0
IV A	173.2	97.6	128.3	169.7	169.5	167.2
IV B	76.8	61.3	71.1	82.5	78.1	76.7
IV C	58.1	51.3	59.2	64.9	58.7	59.2
V A	309.3	282.4	288.9	311.5	308.9	307.5
V B	171.5	152.2	156.1	170.2	164.8	163.2
V C	133.9	127.1	129.0	134.9	130.0	129.1
VI A	235.1	132.6	172.3	248.0	244.0	238.7
VI B	99.4	85.5	99.2	121.8	111.0	108.3
VI C	86.2	72.0	82.9	95.0	82.9	82.9
VII A	299.9	267.0	281.5	300.4	300.0	299.3
VII B	158.9	138.8	147.2	158.7	155.4	154.3
VII C	124.9	118.9	123.2	127.5	124.0	123.3
VIII A	217.7	121.6	170.1	237.8	237.6	234.7
VIII B	*	77.9	96.2	111.9	106.5	105.1
VIII C	68.1	61.4	77.5	88.8	76.9	77.5
IX A	316.2	277.0	293.1	313.3	312.9	312.2
IX B	165.5	143.3	152.5	164.7	161.2	160.1
IX C	131.4	123.1	127.8	132.4	128.6	128.0
X A	264.4	124.8	175.8	247.3	247.1	244.1
X B	96.4	79.7	99.7	115.9	110.5	109.1
X C	74.3	62.7	79.5	92.1	78.9	79.5
XI A	317.5	277.0	293.1	313.3	312.9	312.2
XI B	165.2	143.3	152.5	164.7	161.2	160.1
XII A	265.2	124.8	175.8	247.3	247.1	244.1
XII B	106.7	79.7	99.7	115.9	110.5	109.1
XII C	70.5	62.7	79.5	92.1	78.9	79.5

*Test did not reach computed axial strength

Appendix D Comparison of Long-Term and Short-Term Tests Results

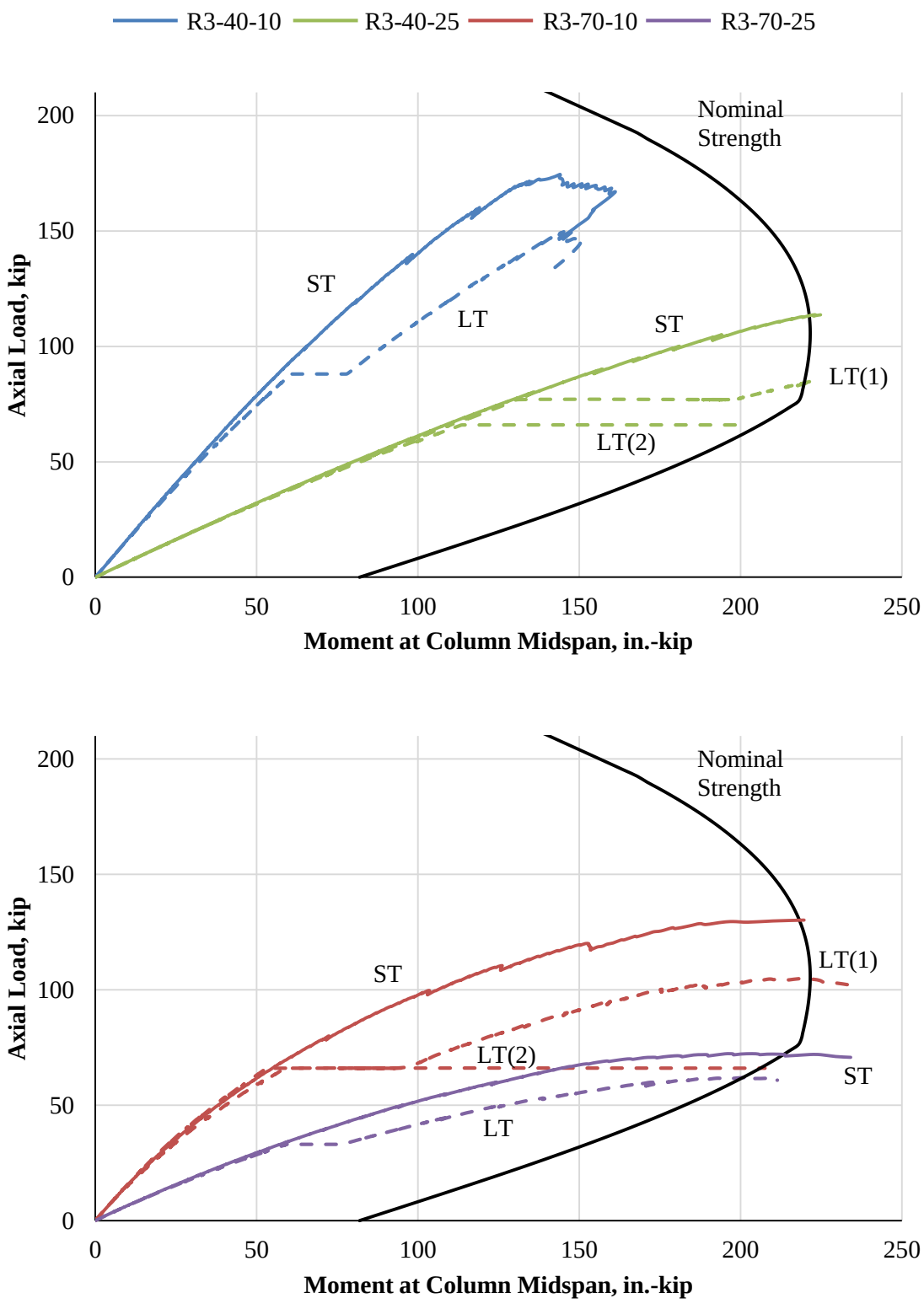

Figure D.1 – Comparison of Long-Term and Short-Term Tests Results (#3 bars)

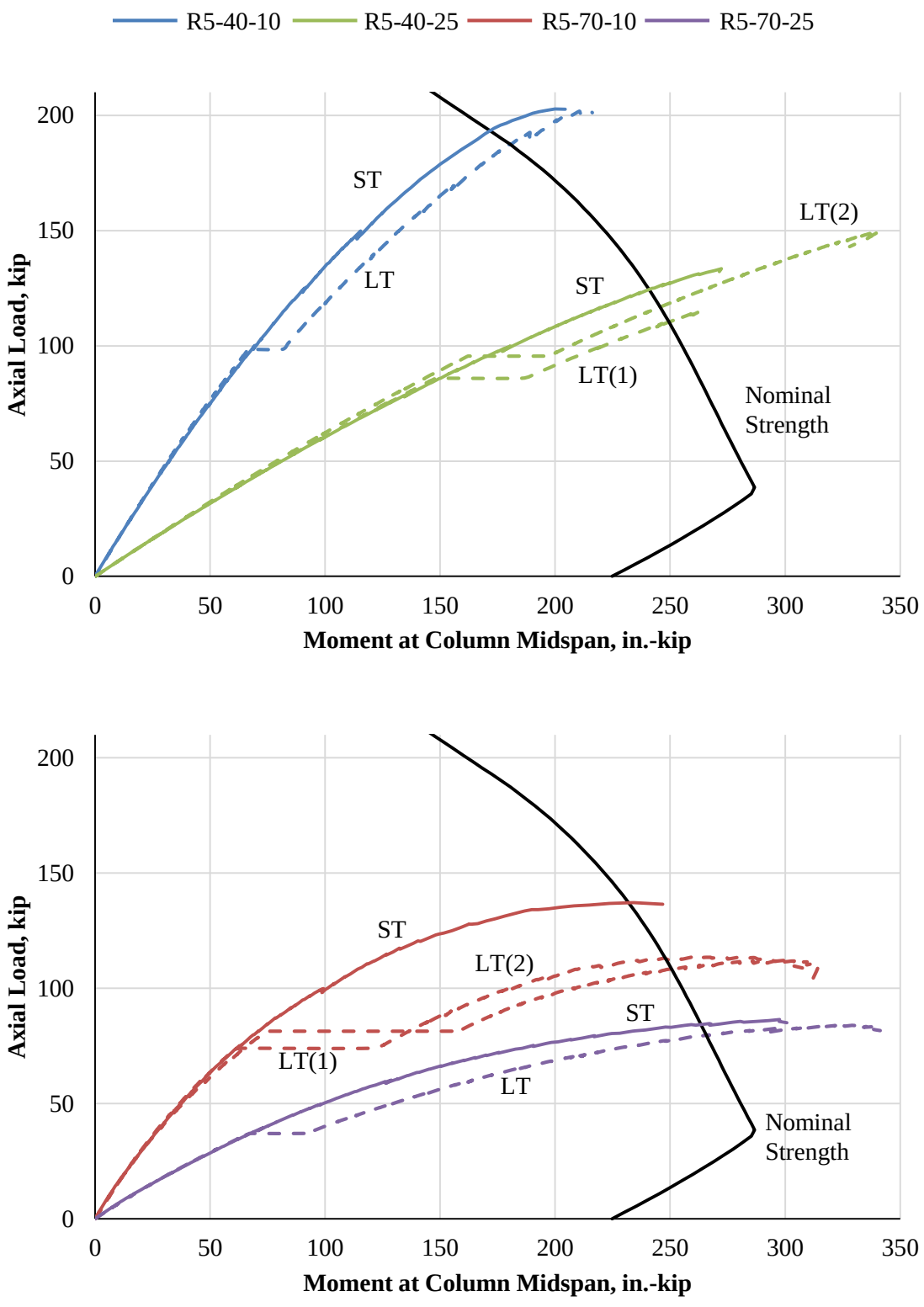

Figure D.2 – Comparison of Long-Term and Short-Term Tests Results (#5 bars)

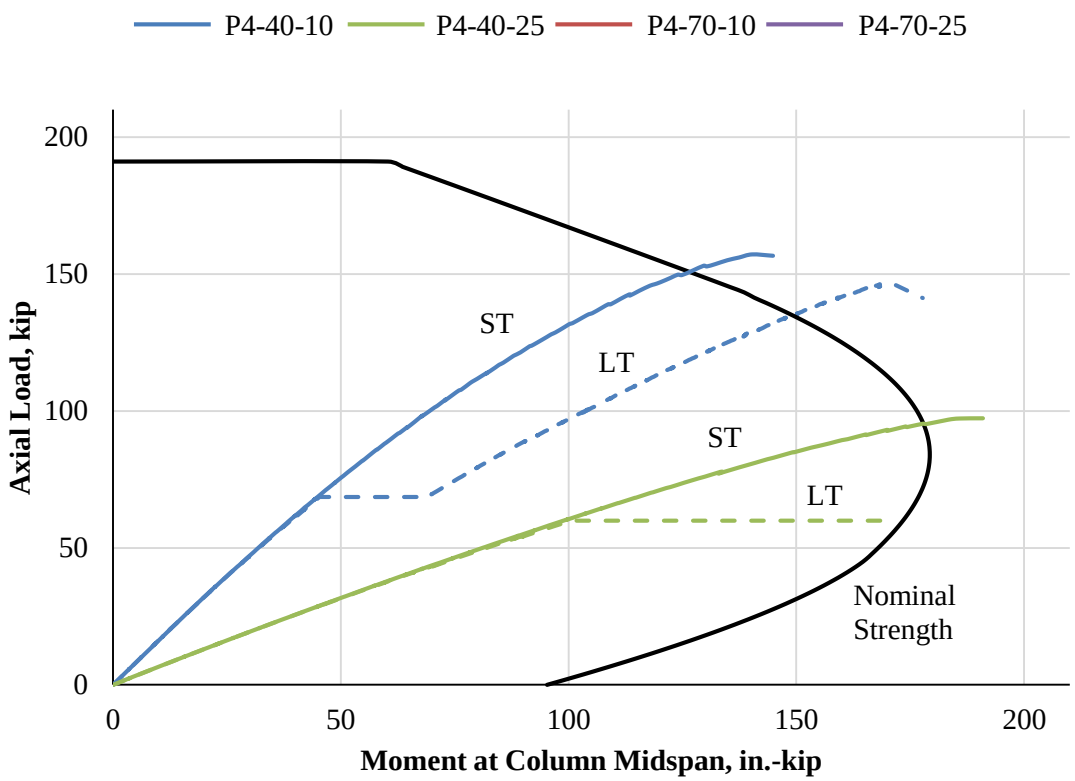

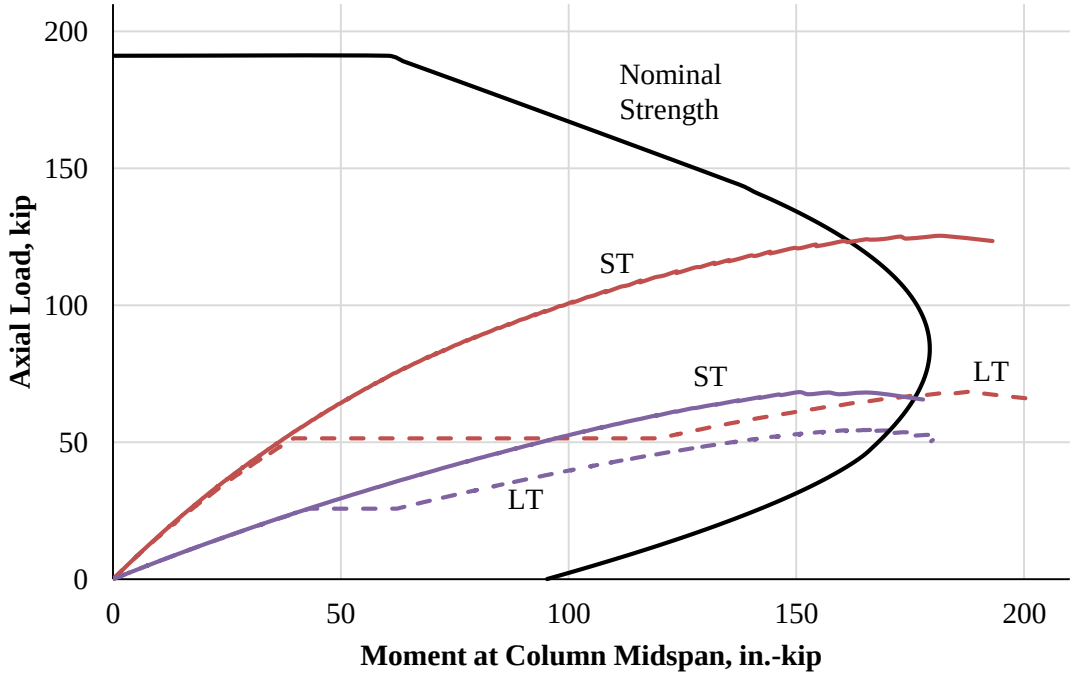

Comparison of Long-Term and Short-Term Tests Results (4 – PS Wires)

Appendix E Evaluation of β_{dns} Method for Long-Term Effects

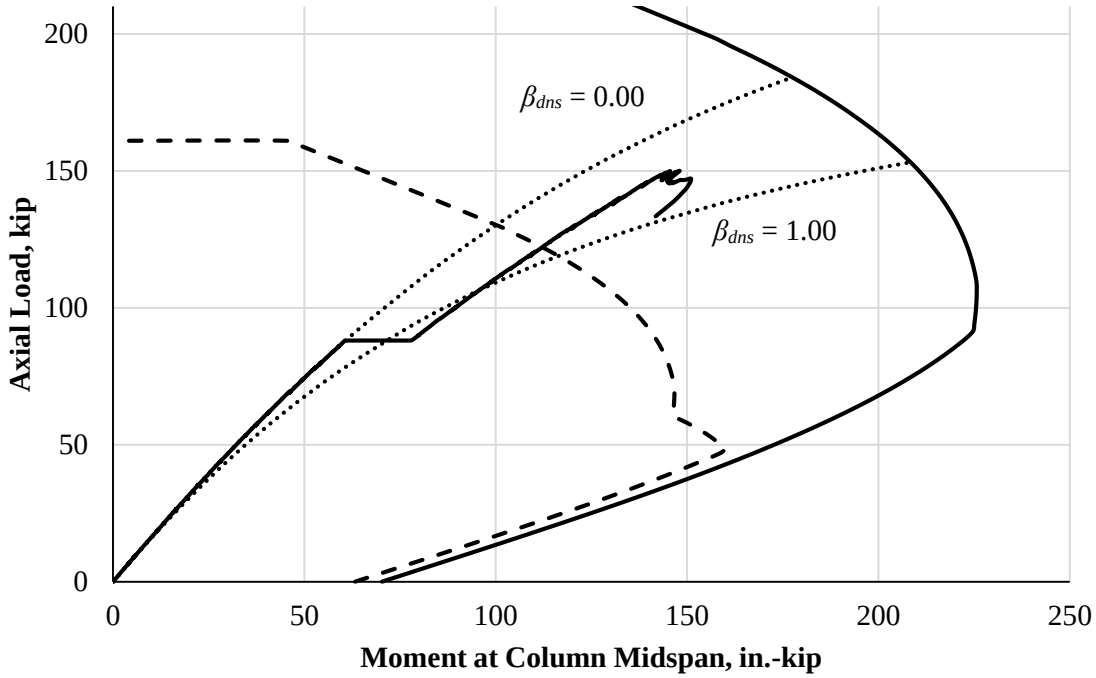

(a) Equation 4.4

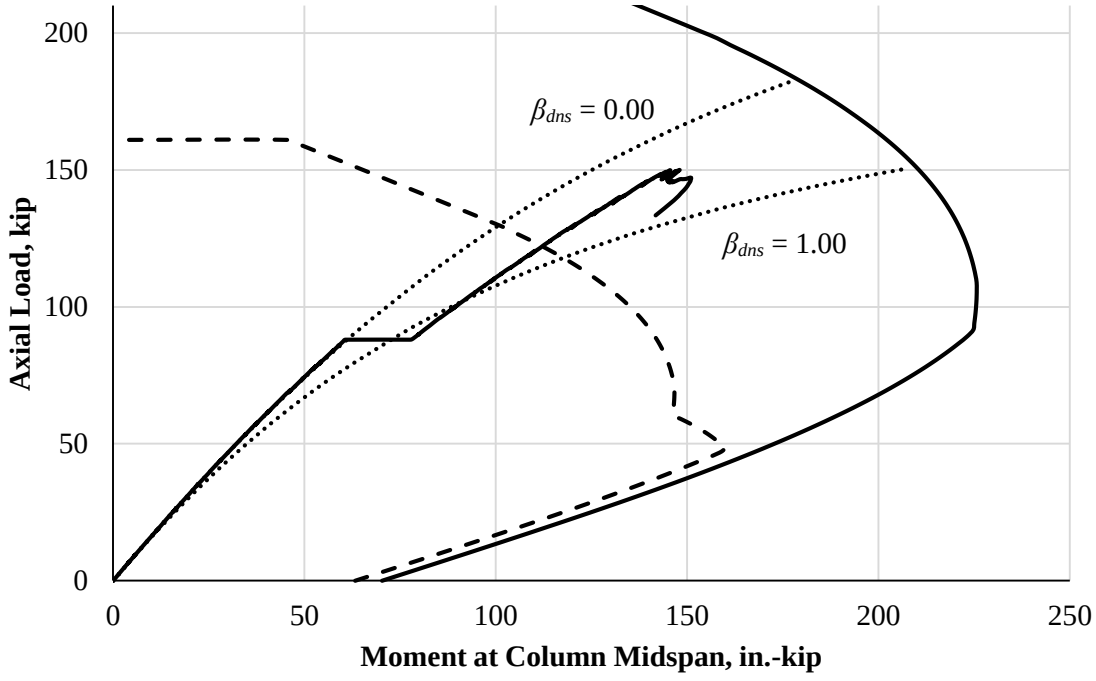

(a) Equation 4.5

Figure E.1 – Evaluation of β_{dns} Method (R3-40-10-LT)

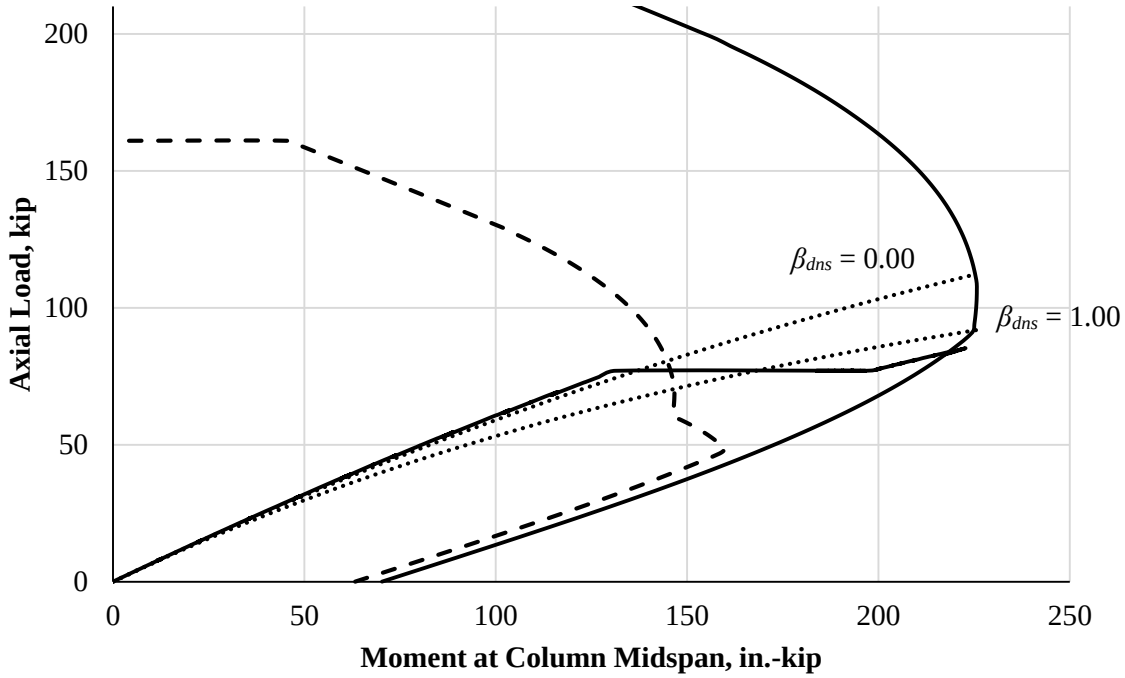

(a) Equation 4.4

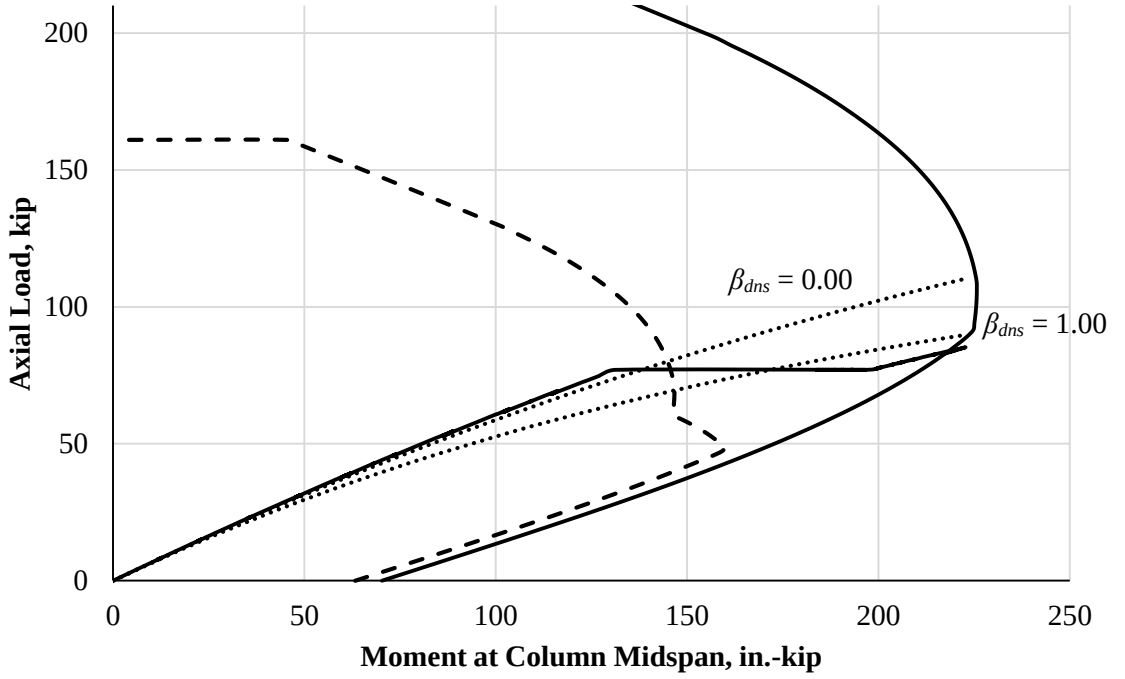

(a) Equation 4.5

Figure E.2 – Evaluation of β_{dns} Method (R3-40-25-LT(1))

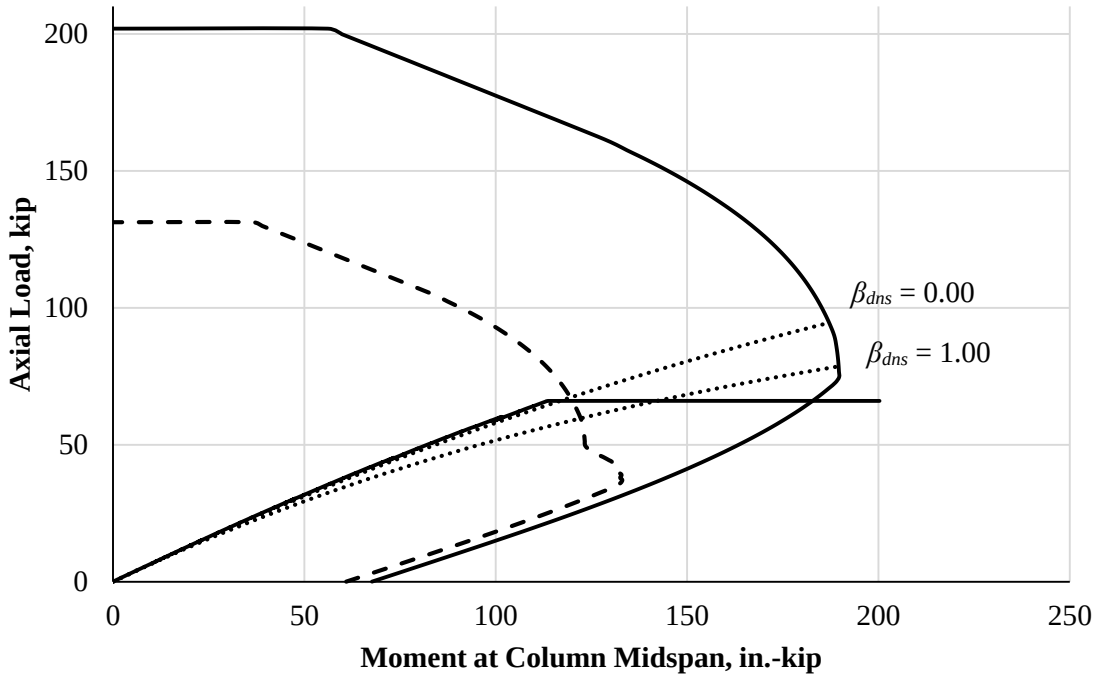

(a) Equation 4.4

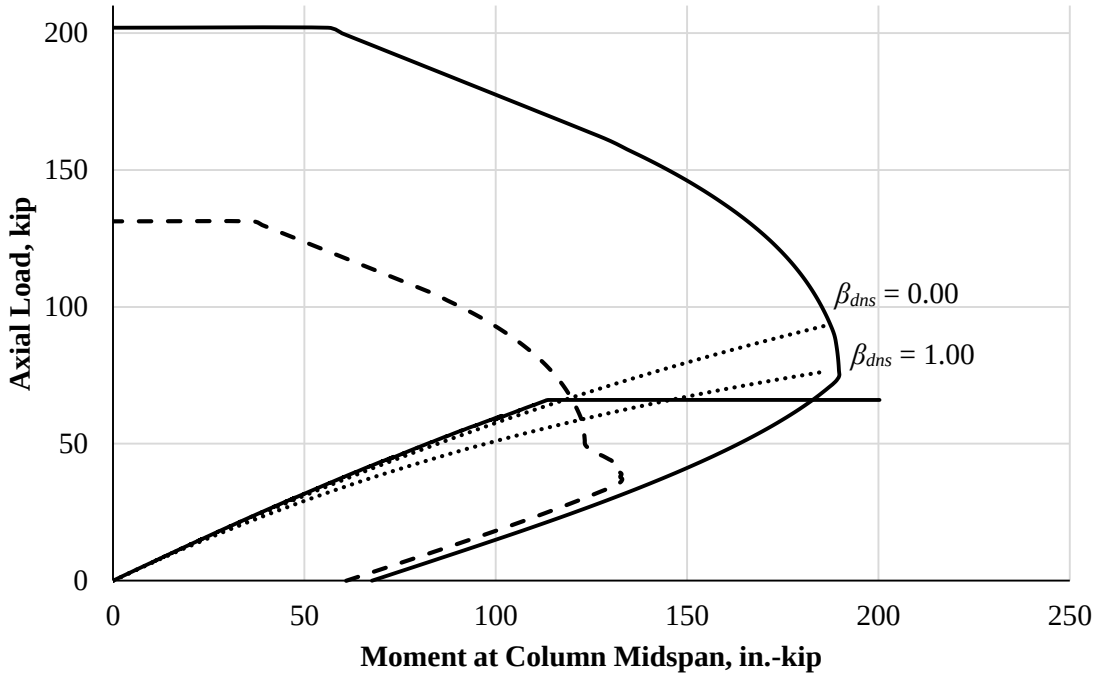

(a) Equation 4.5

Figure E.3 – Evaluation of β_{dns} Method (R3-40-25-LT(2))

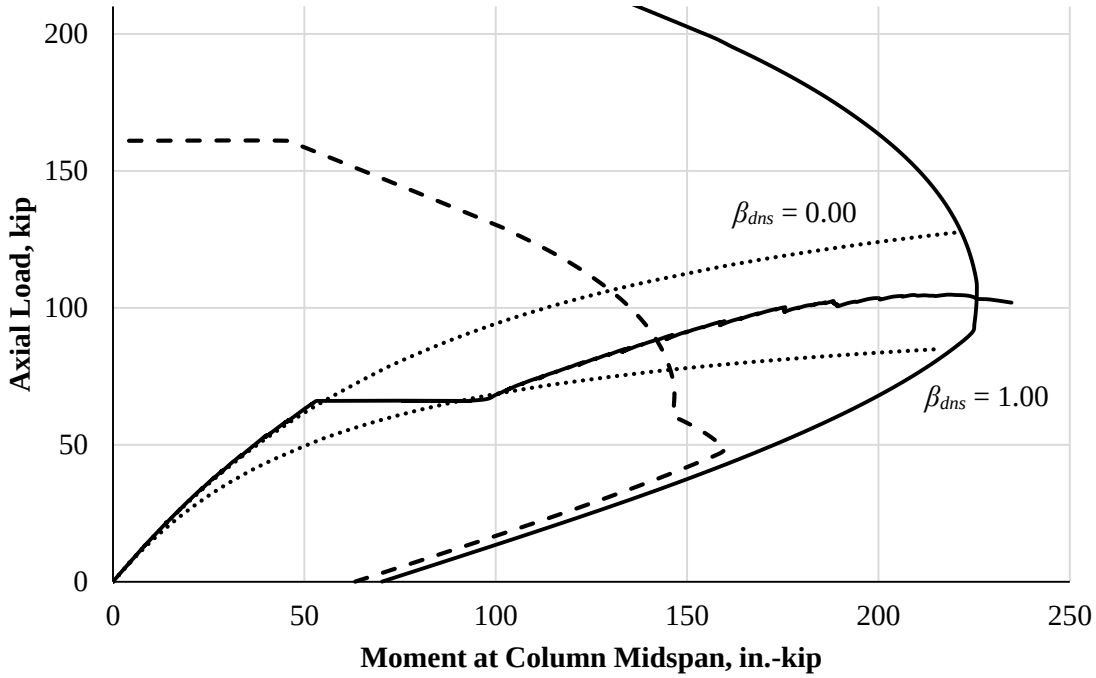

(a) Equation 4.4

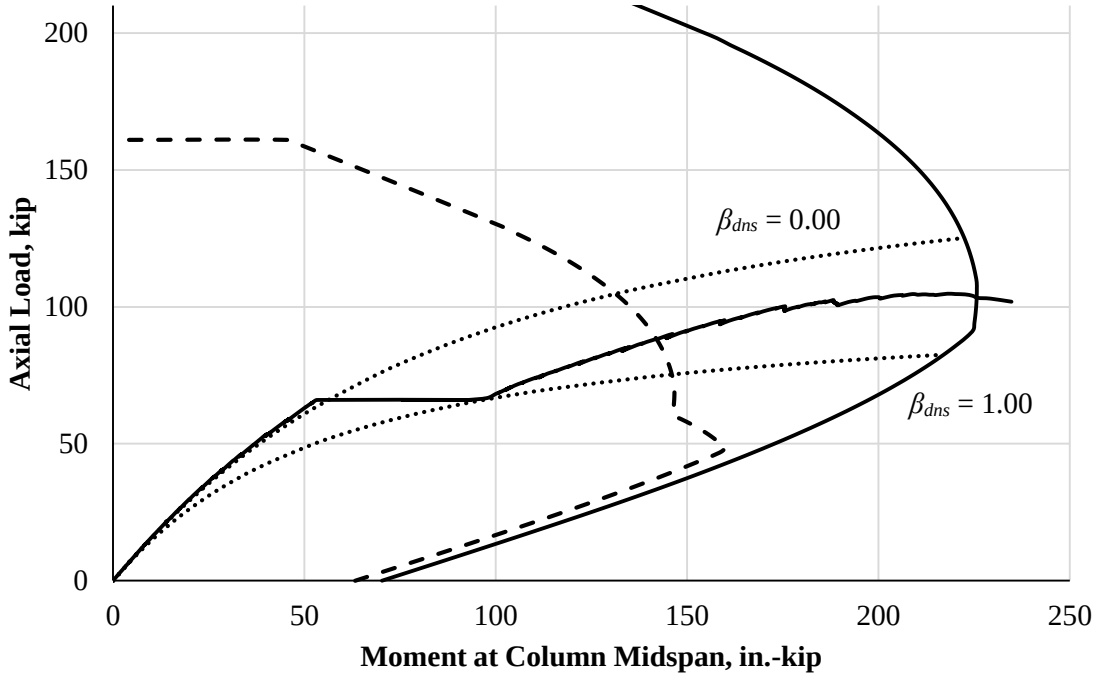

(a) Equation 4.5

Figure E.4 – Evaluation of β_{dns} Method (R3-70-10-LT(1))

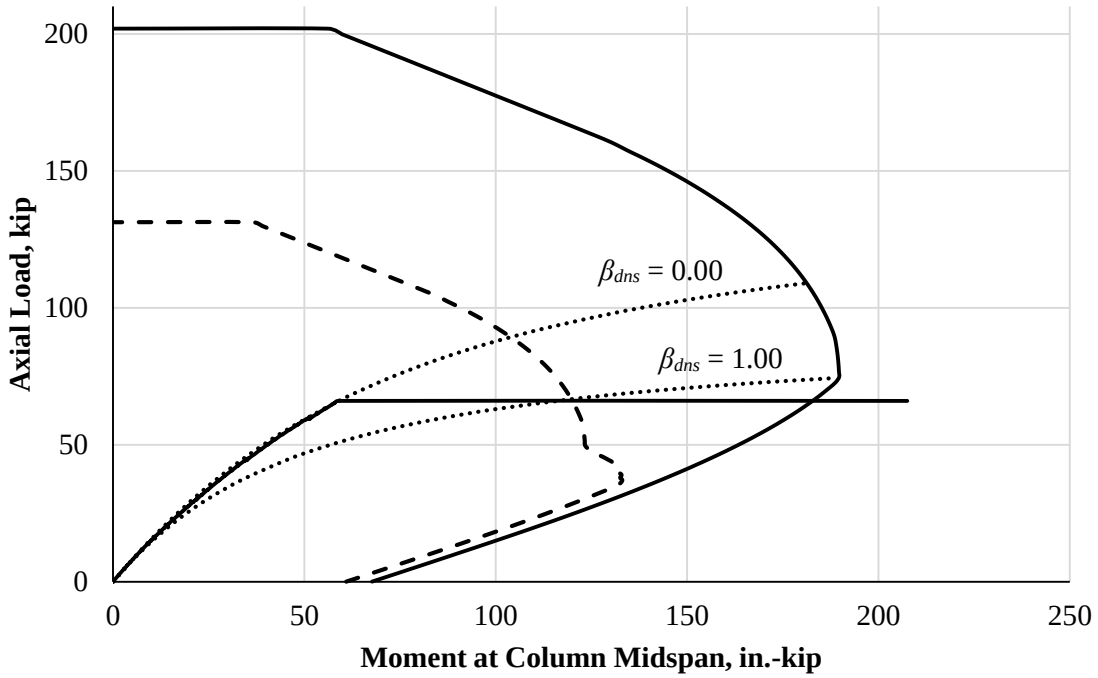

(a) Equation 4.4

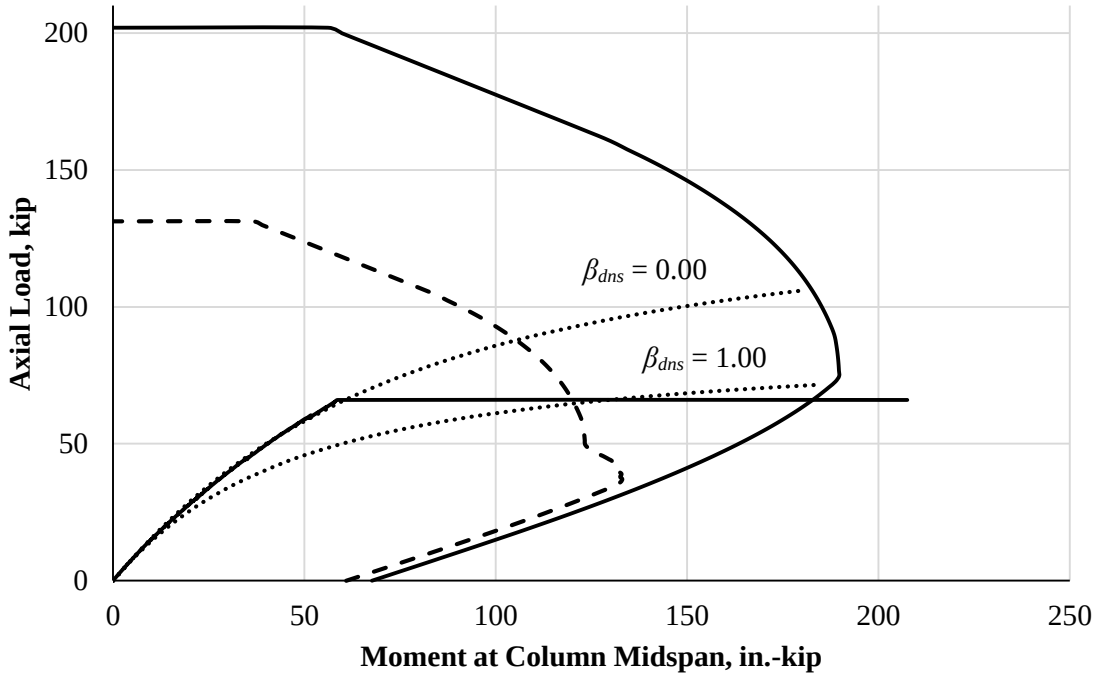

(a) Equation 4.5

Figure E.5 – Evaluation of β_{dns} Method (R3-70-10-LT(2))

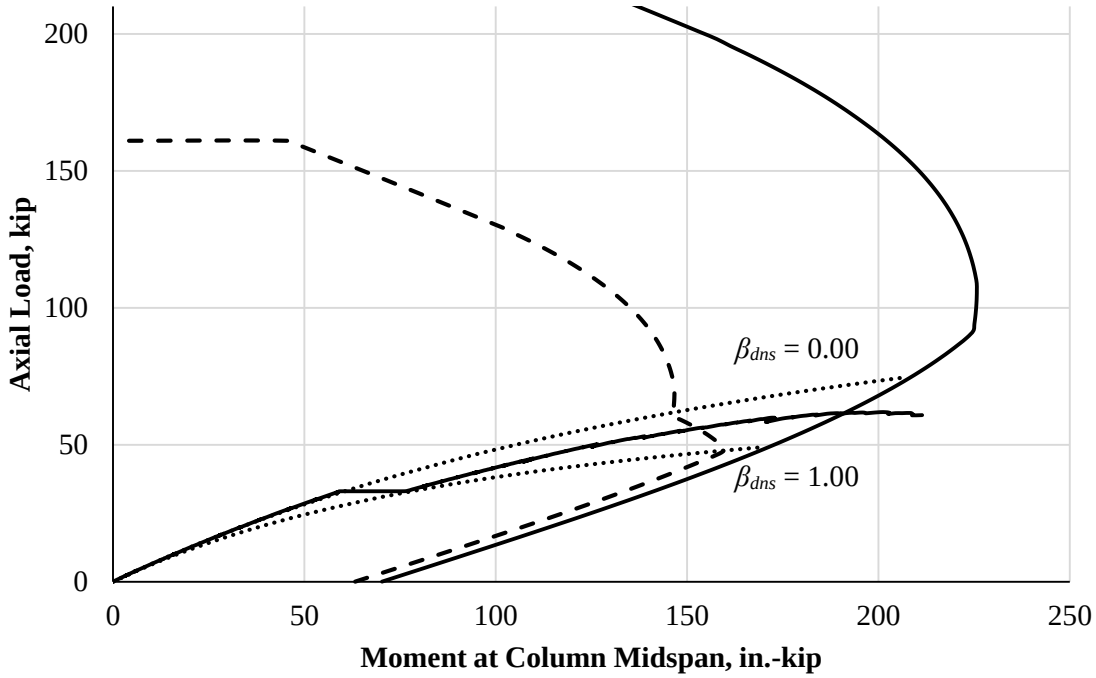

(a) Equation 4.4

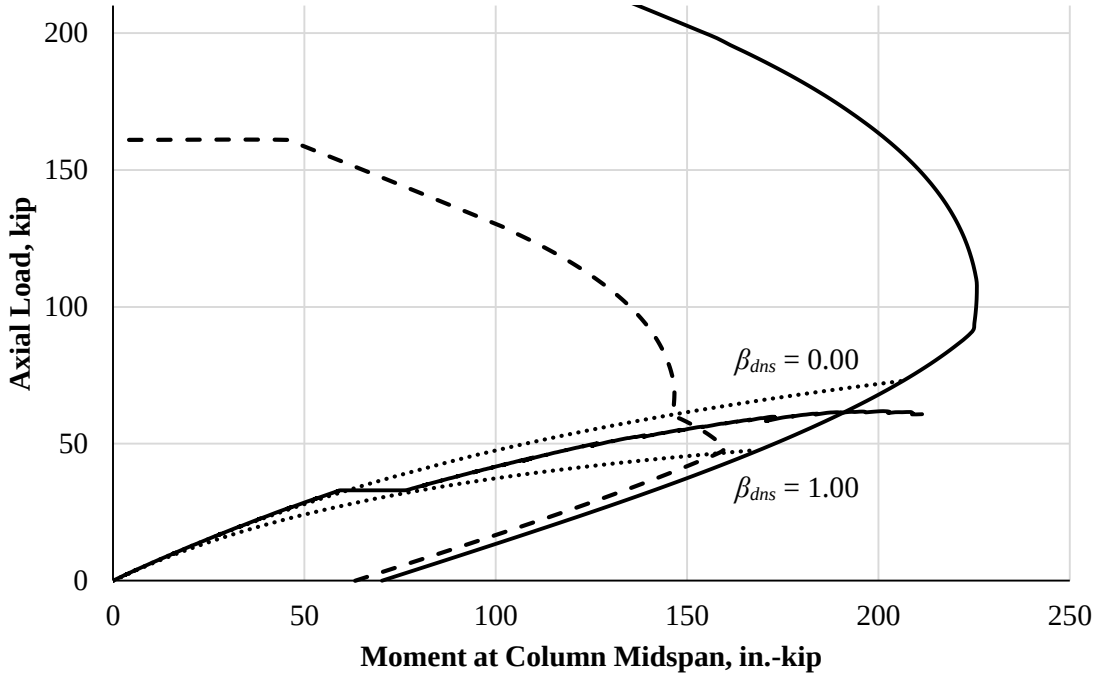

(a) Equation 4.5

Figure E.6 – Evaluation of β_{dns} Method (R3-70-25-LT)

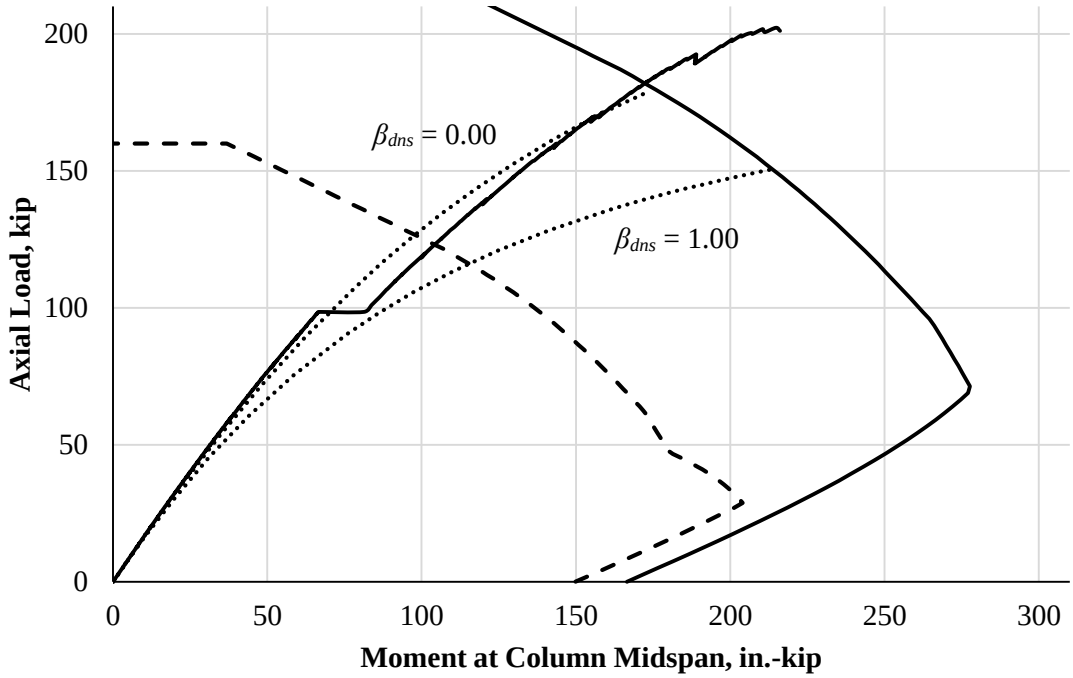

(a) Equation 4.4

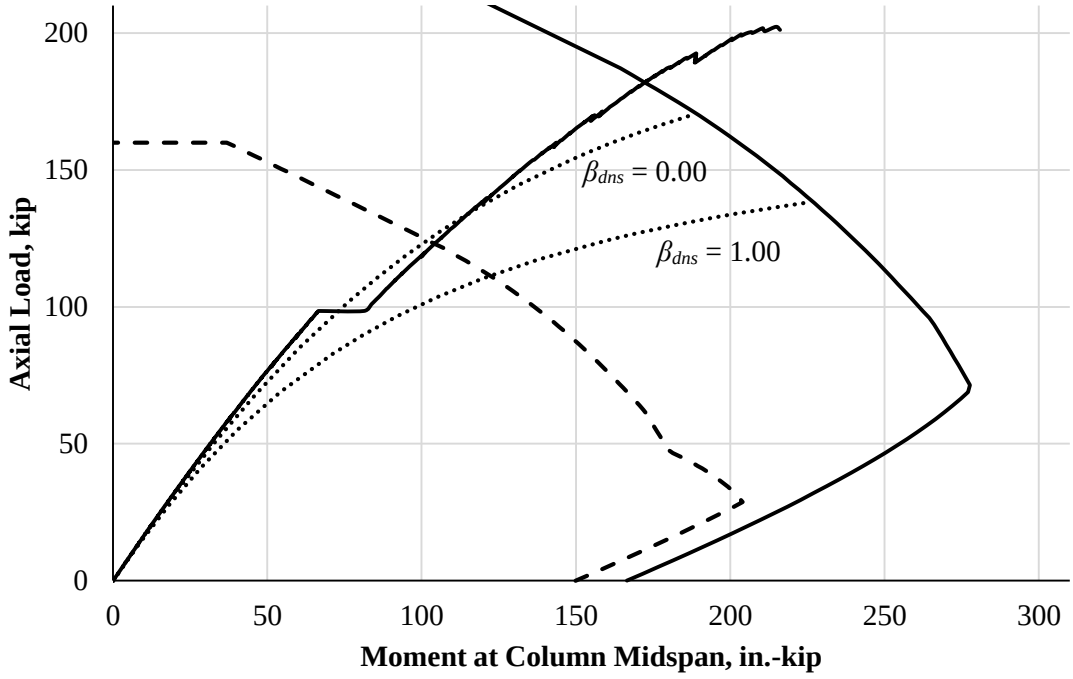

(a) Equation 4.5

Figure E.7 – Evaluation of β_{dns} Method (R5-40-10-LT)

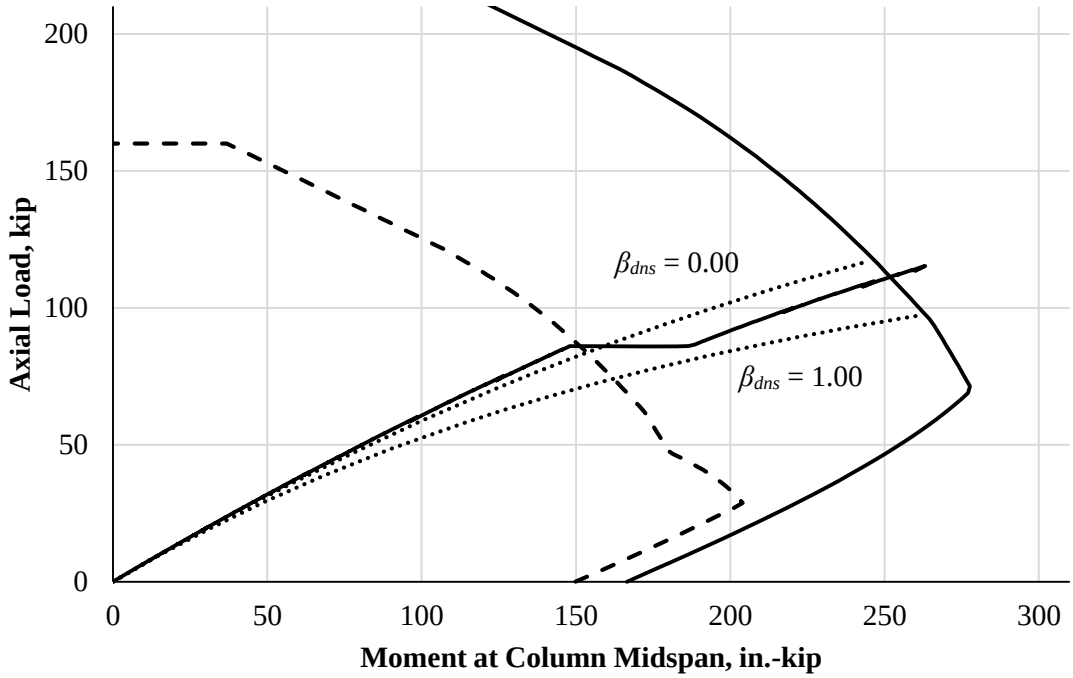

(a) Equation 4.4

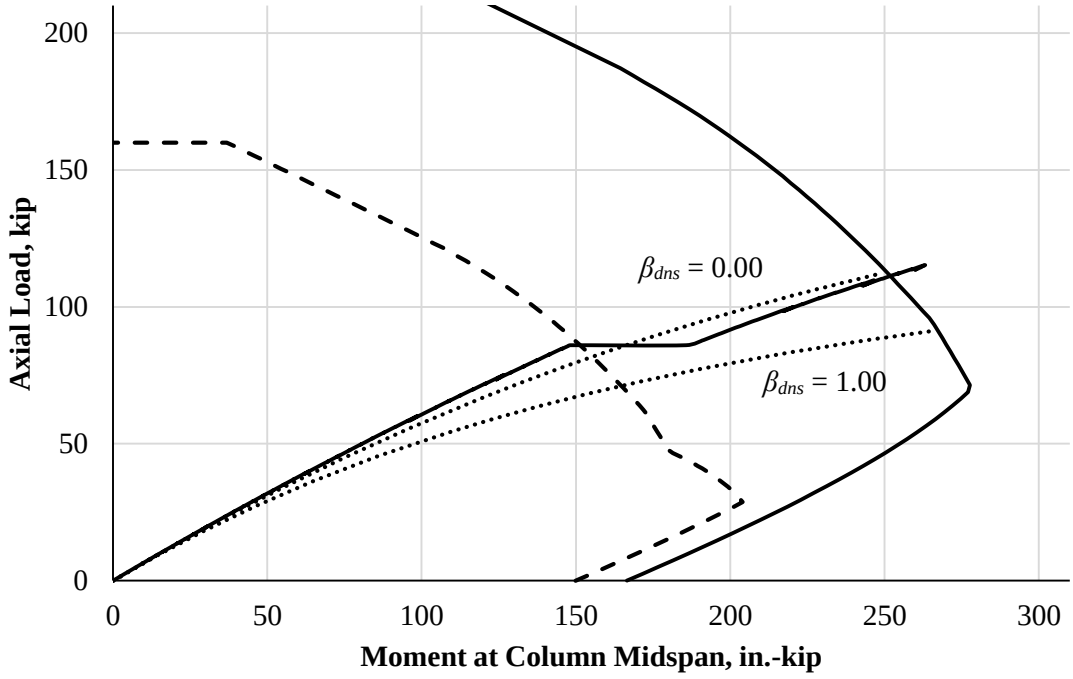

(a) Equation 4.5

Figure E.8 – Evaluation of β_{dns} Method (R5-40-25-LT(1))

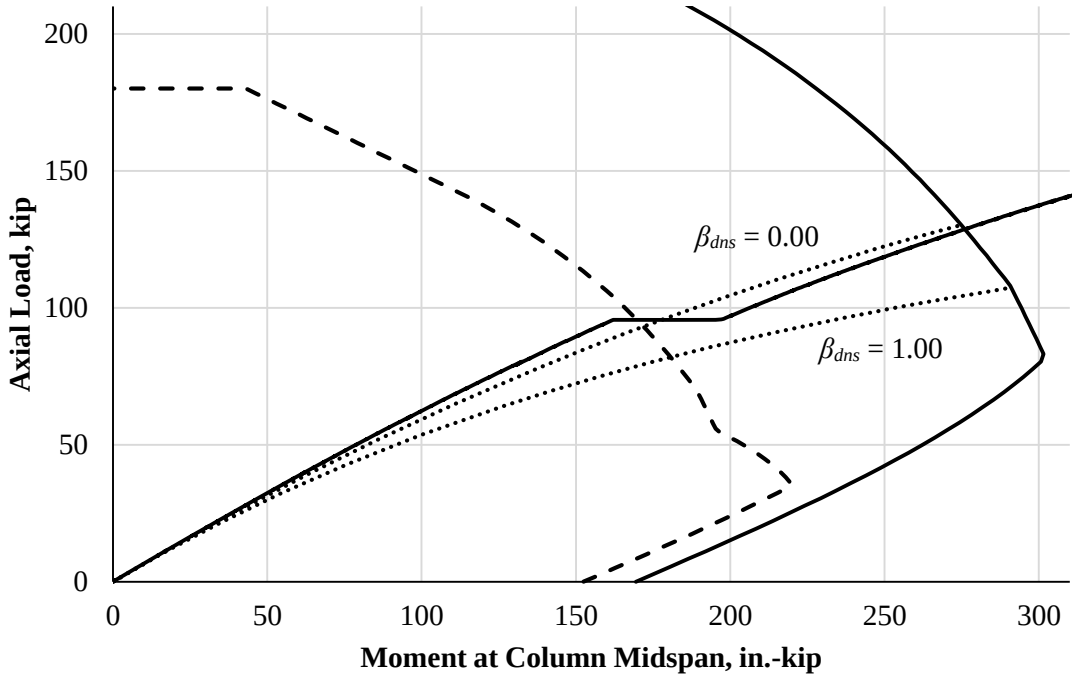

(a) Equation 4.4

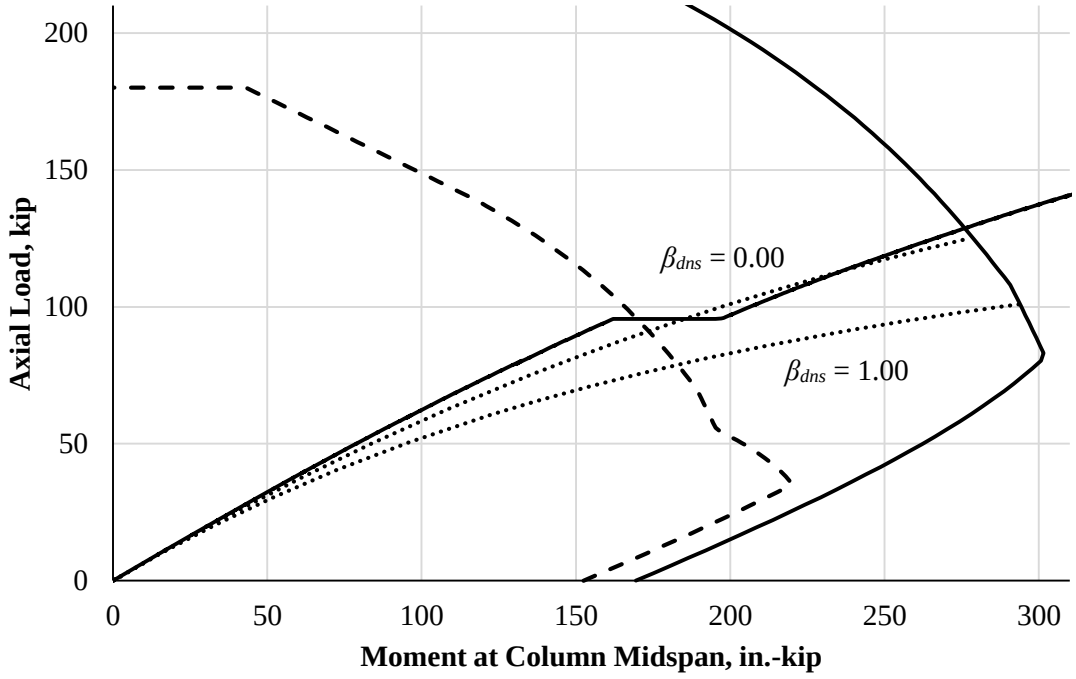

(a) Equation 4.5

Figure E.9 – Evaluation of β_{dns} Method (R5-40-25-LT(2))

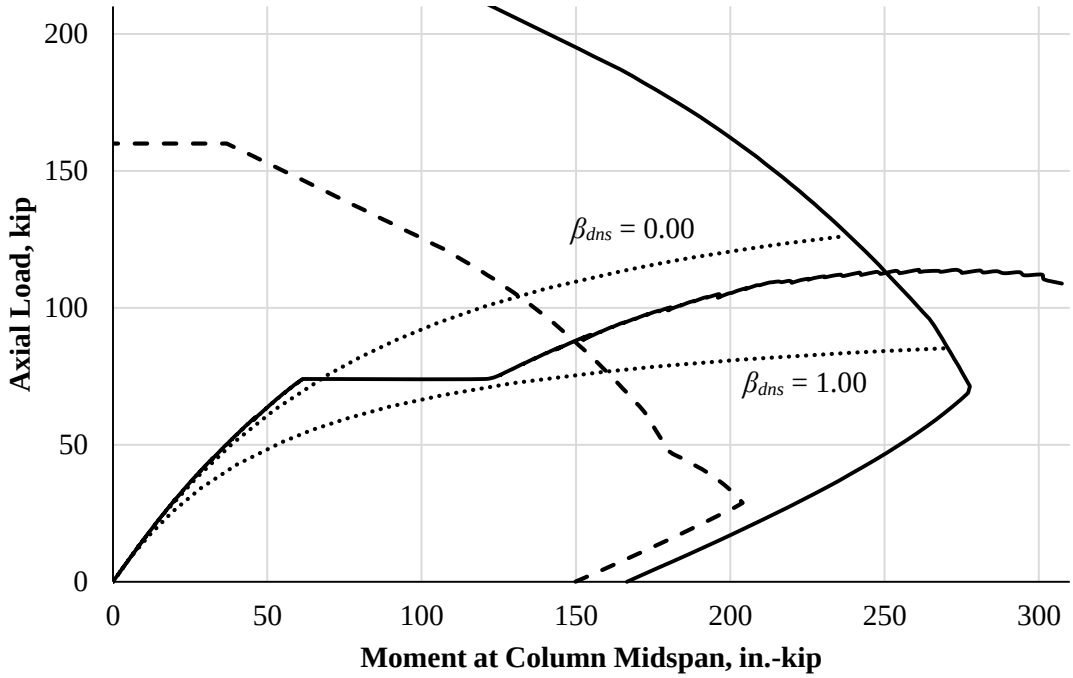

(a) Equation 4.4

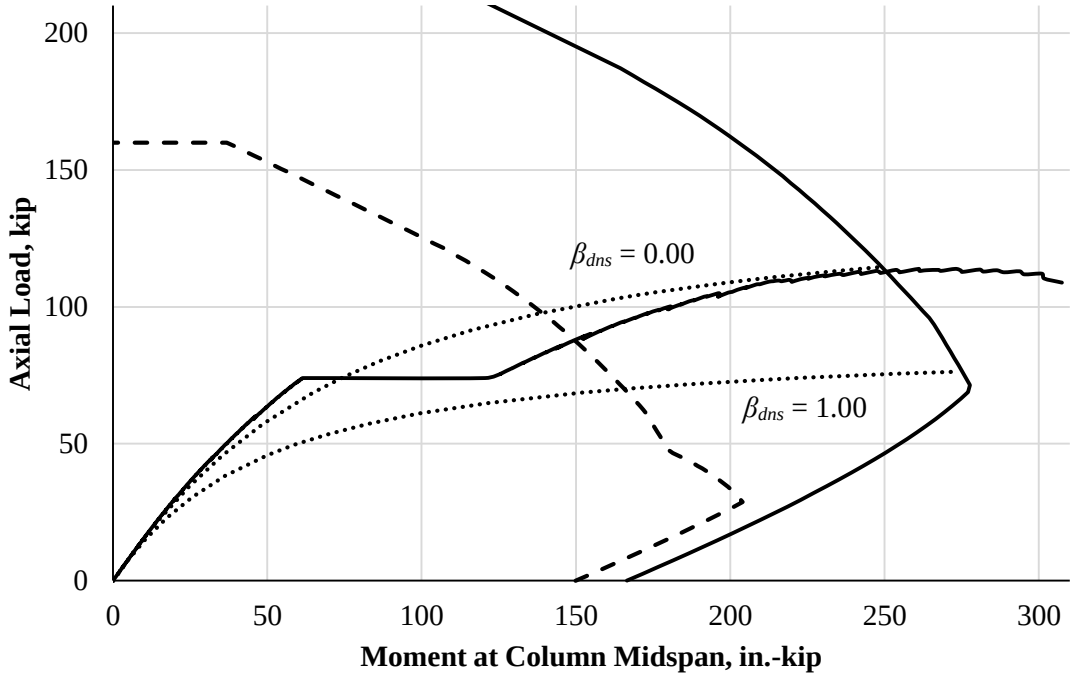

(a) Equation 4.5

Figure E.10 – Evaluation of β_{dns} Method (R5-70-10-LT(1))

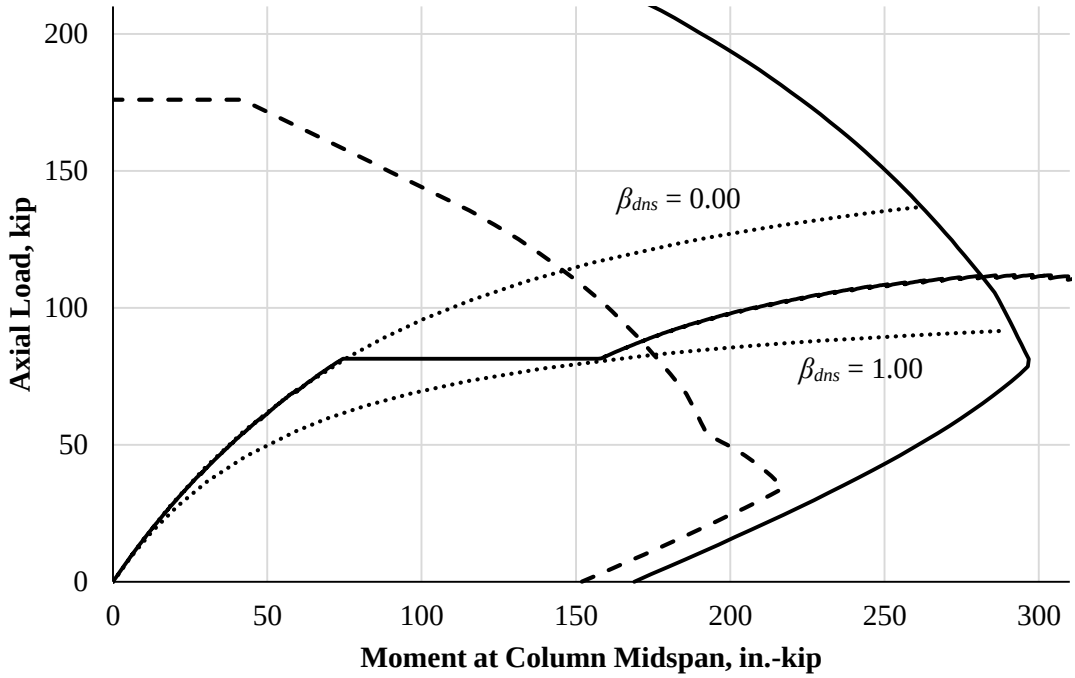

(a) Equation 4.4

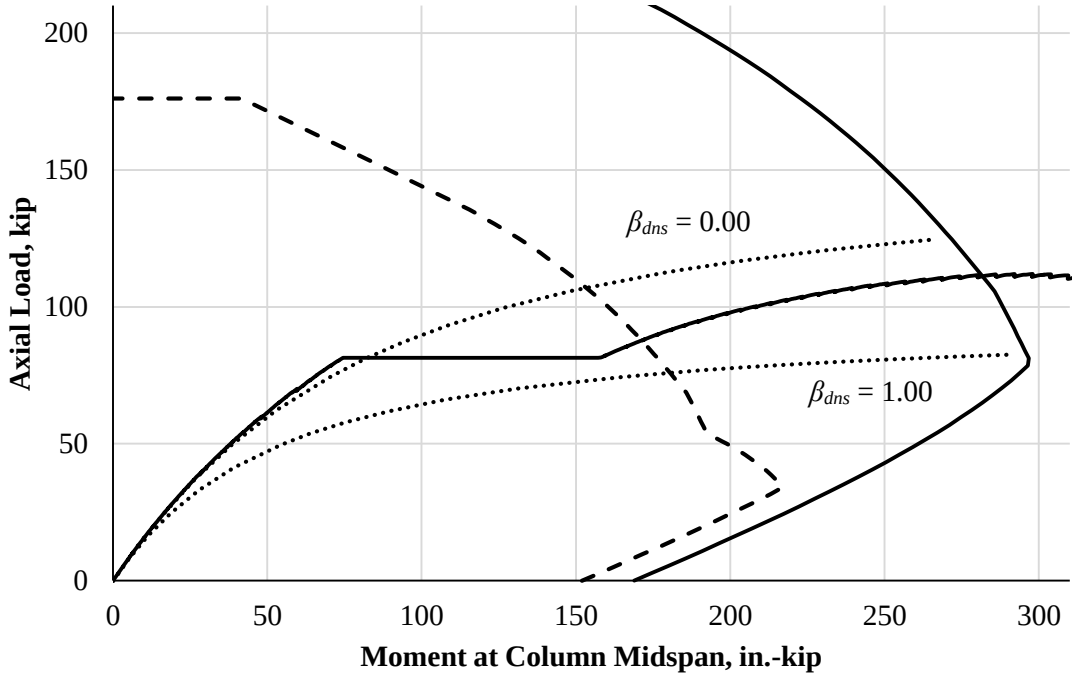

(a) Equation 4.5

Figure E.11 – Evaluation of β_{dns} Method (R5-70-10-LT(2))

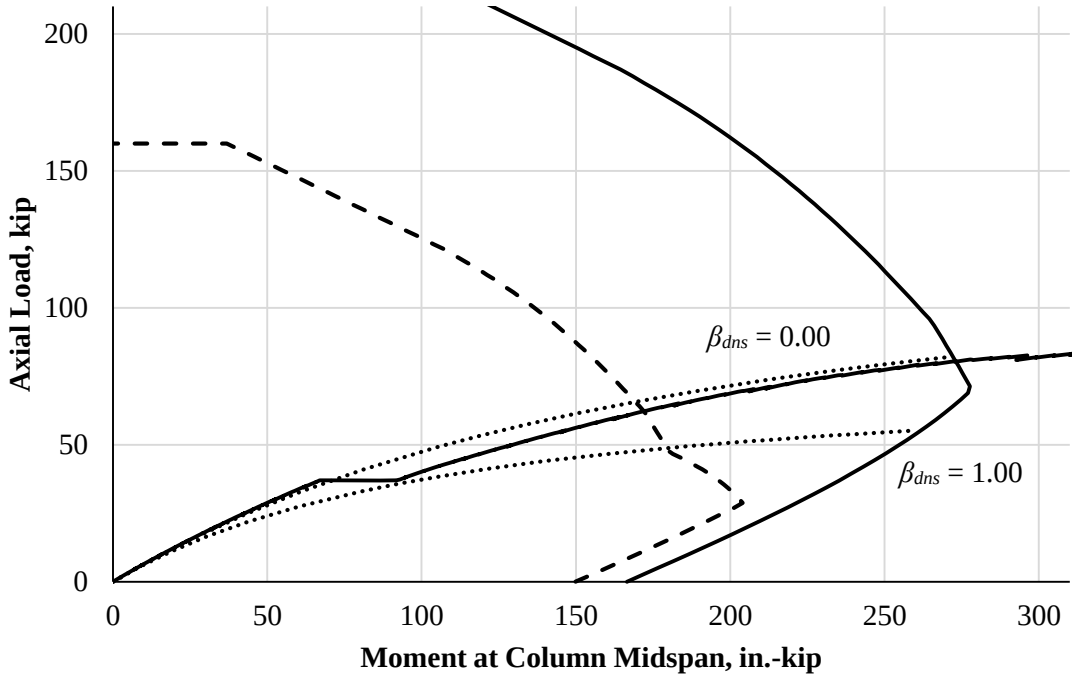

(a) Equation 6.4

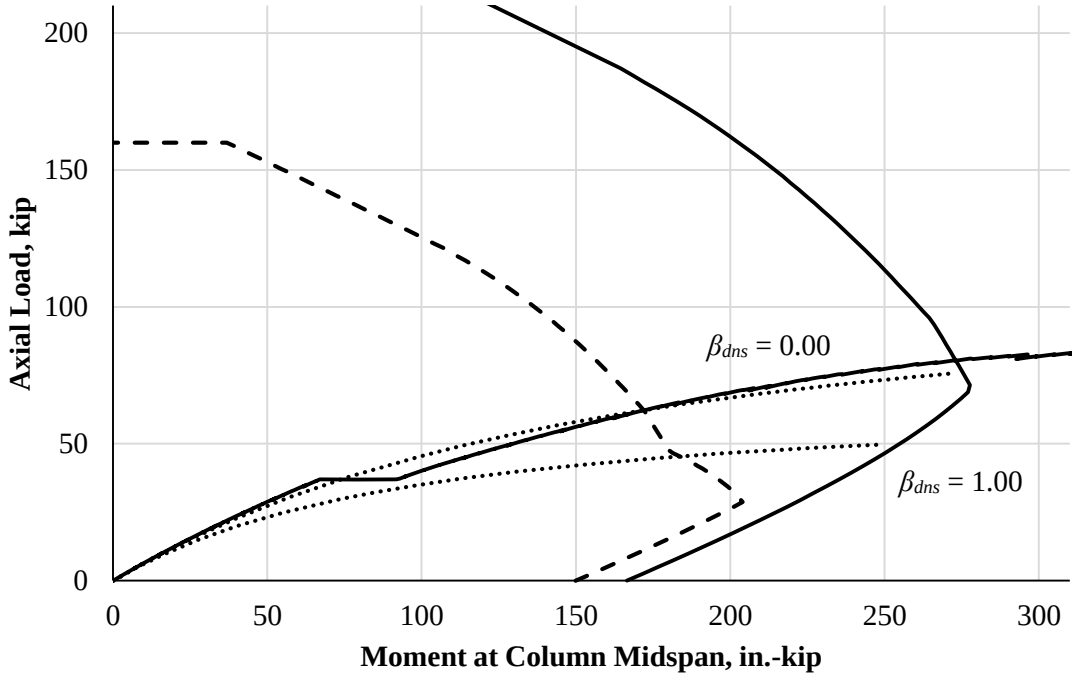

(a) Equation 6.6

Figure E.12 – Evaluation of β_{dns} Method (P4-70-25-LT)

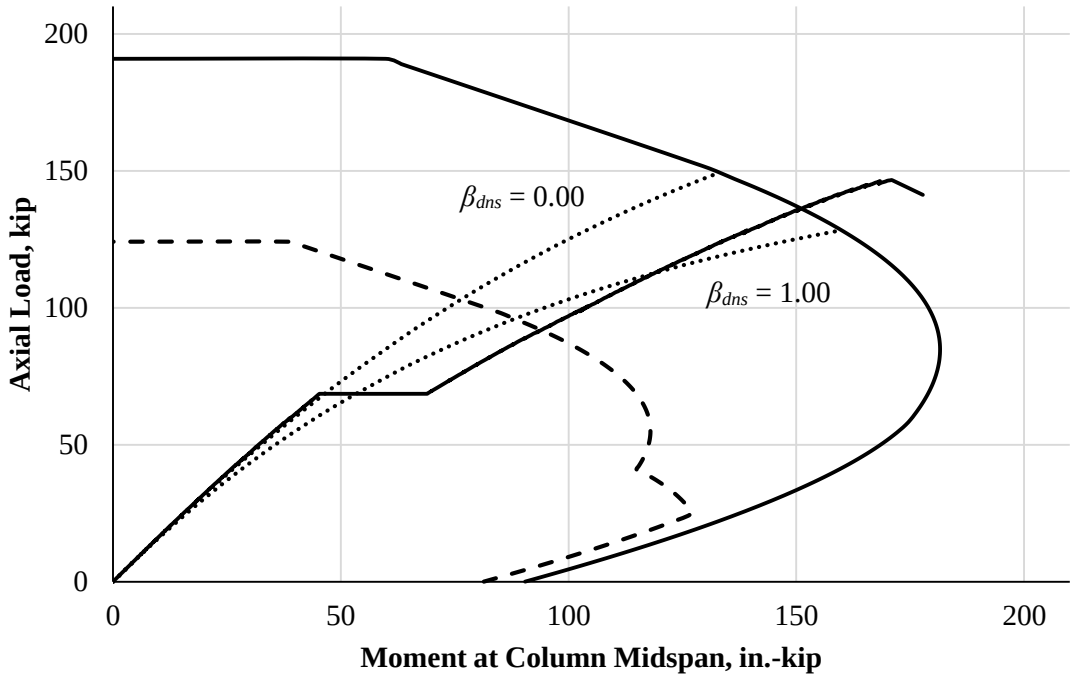

(a) Equation 6.4

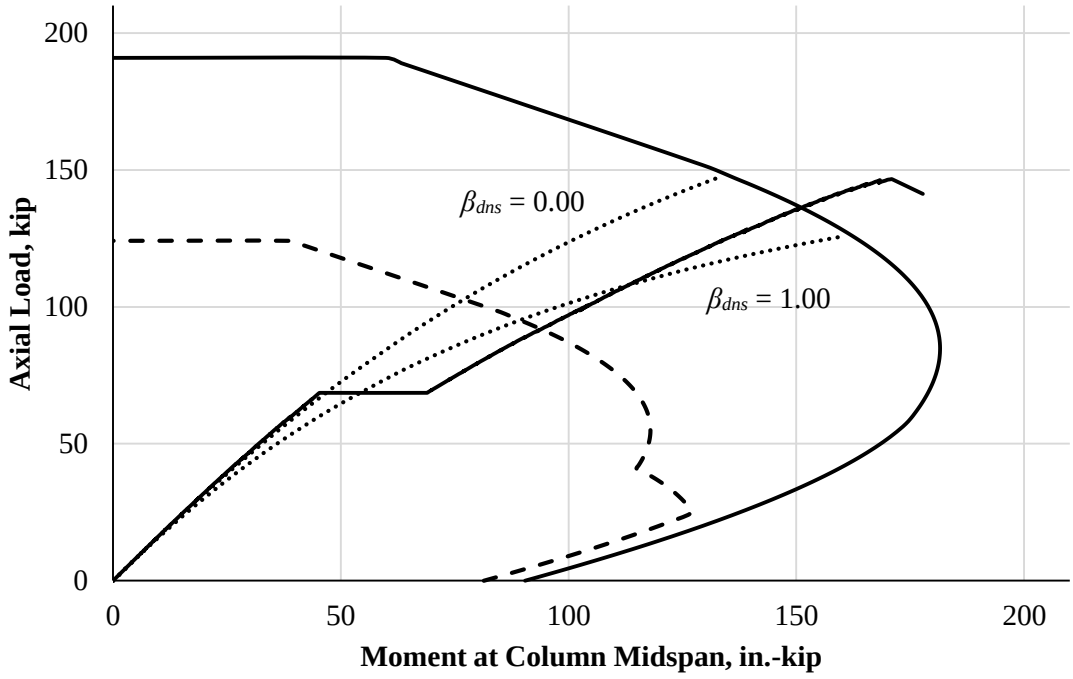

(a) Equation 6.6

Figure E.13 – Evaluation of β_{dns} Method (P4-40-10-LT)

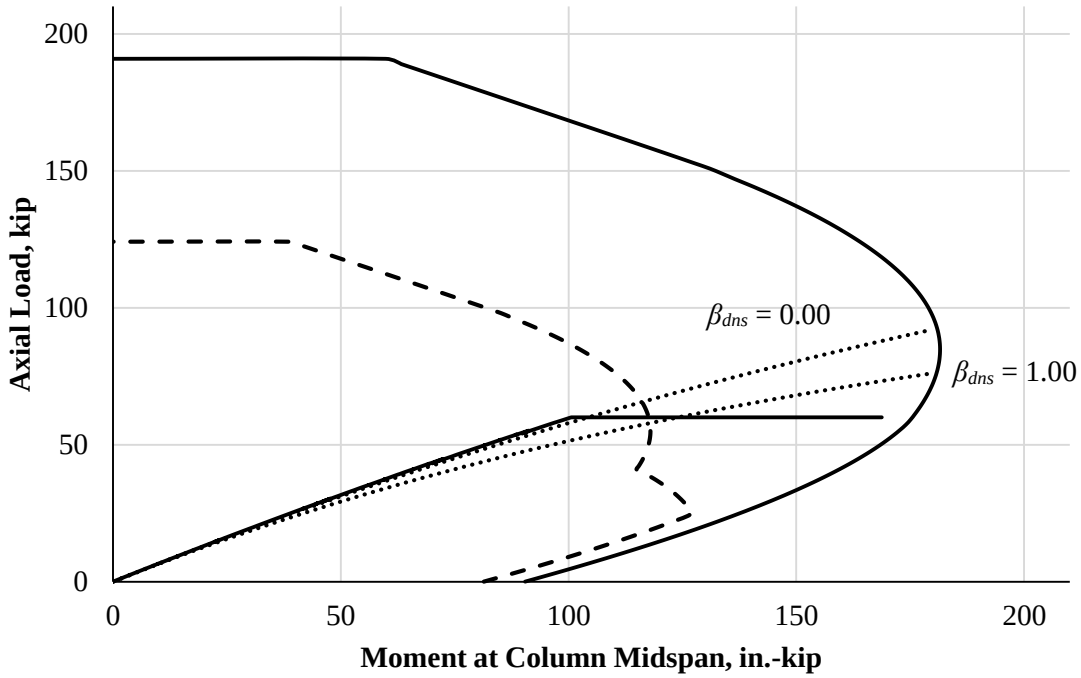

(a) Equation 6.4

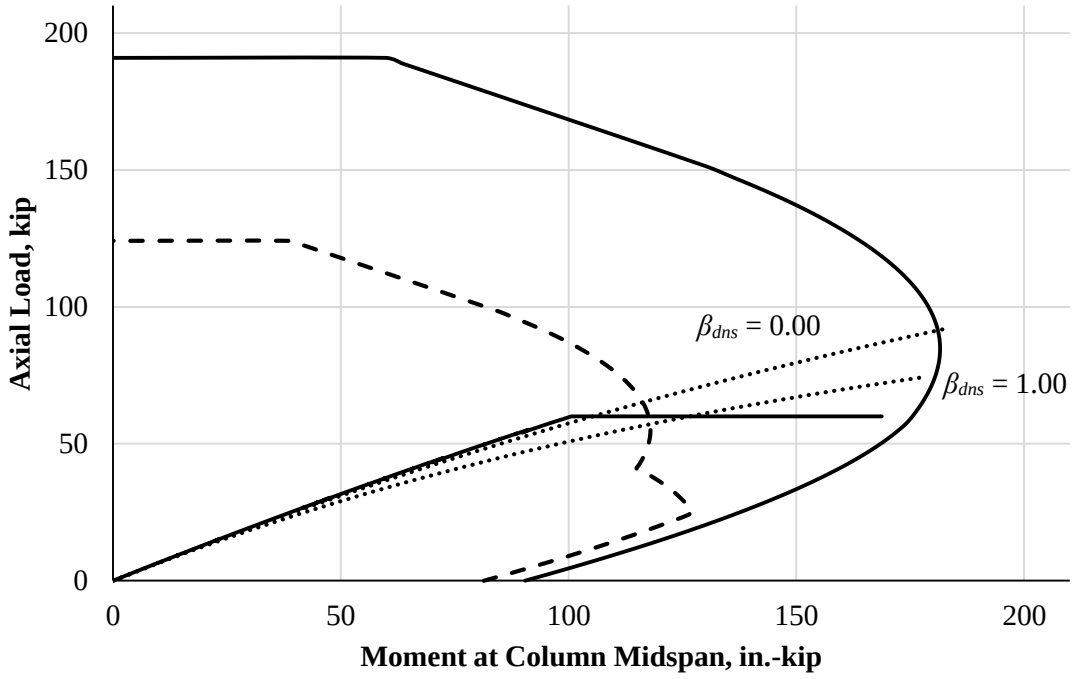

(a) Equation 6.6

Figure E.14 – Evaluation of β_{dns} Method (P4-40-25-LT)

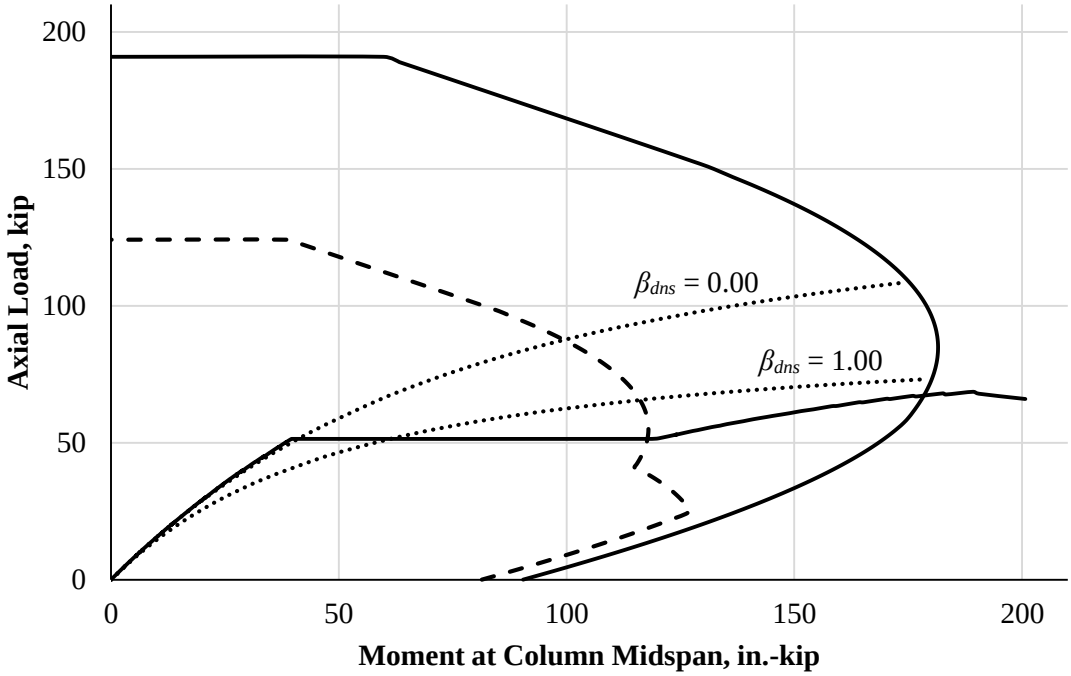

(a) Equation 6.4

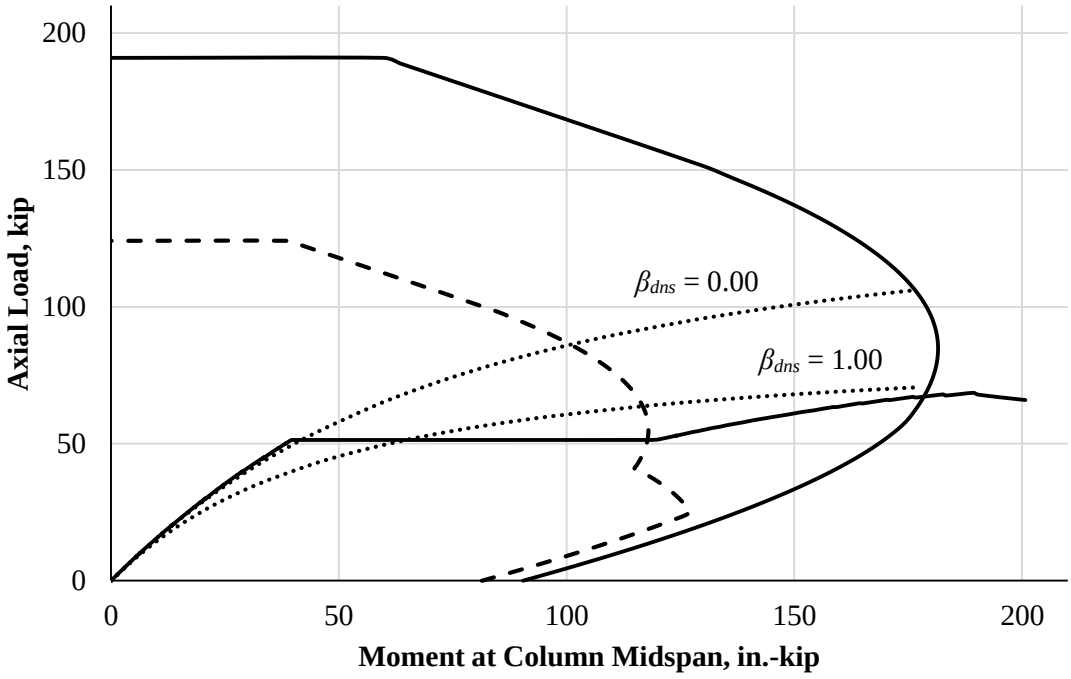

(a) Equation 6.6

Figure E.15 – Evaluation of β_{dns} Method (P4-70-10-LT)

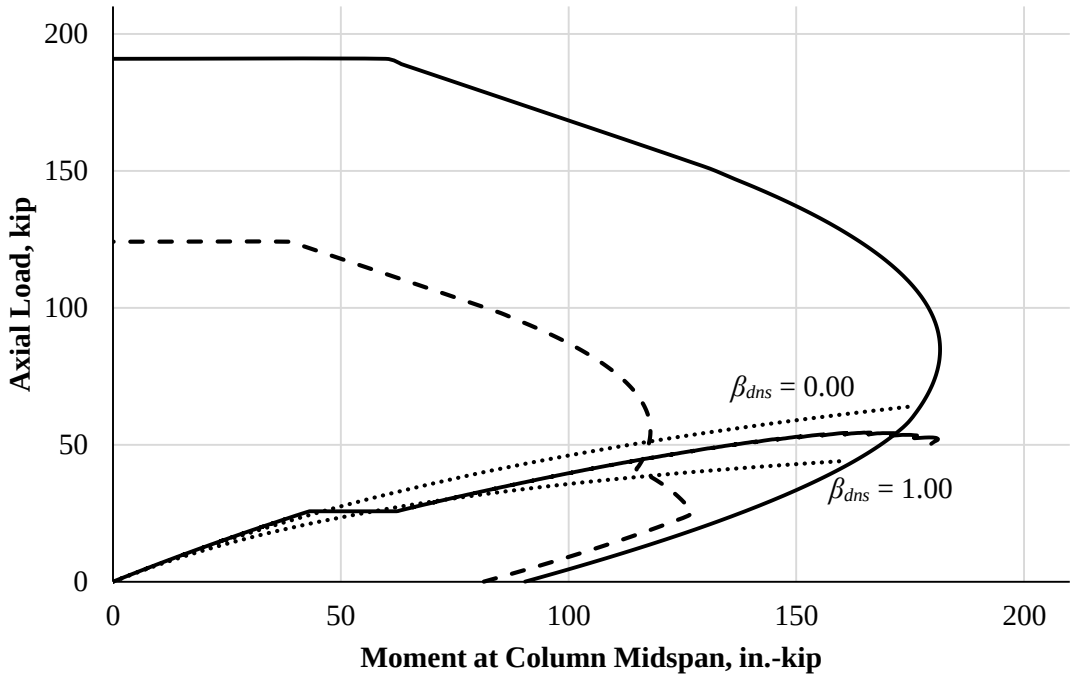

(a) Equation 6.4

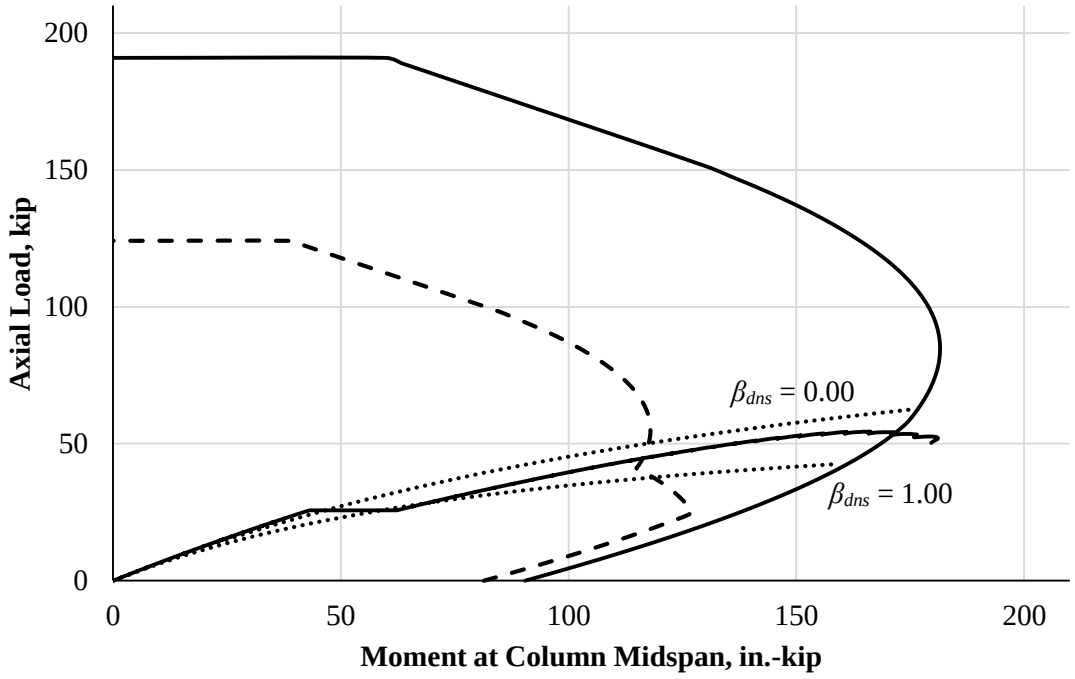

(a) Equation 6.6

Figure E.16 – Evaluation of β_{dns} Method (P4-70-25-LT)